001
Handbook Introduction

Effective November 30, 2000

Document Owner:

Approved by:

R. W. Sniffin   12/11/00

R. W. Sniffin   Date

K. R. Kimball   14 DEC 00

K. R. Kimball   Date
Manager, DSMS Implementation
Engineering

Released by:

[Signature on file in TMOD Library]

TMOD Document Release   Date

Change Log

Rev	Issue Date	Affected Paragraphs	Change Summary
Initial	1/15/2001	All	All

Note to Readers

There are two sets of document histories in the 810-005 document, and these histories are reflected in the header at the top of the page. First, the entire document is periodically released as a revision when major changes affect a majority of the modules. For example, this module is part of 810-005, Revision E. Second, the individual modules also change, starting as an initial issue that has no revision letter. When a module is changed, a change letter is appended to the module number on the second line of the header and a summary of the changes is entered in the module's change log.

This module supersedes module INT-10 in 810-005, Rev. D.

Contents

1   Introduction

1.1   Purpose

This modular handbook has been approved by the Deep Space Mission Systems (DSMS) Engineering Program Office and is published as a source of interface design data for all flight projects using the Deep Space Network (DSN). It provides information useful to flight projects contemplating the design of hardware and software, with reasonable assurance that the resulting project telecommunications interfaces will be compatible with the established or planned DSN configurations.

1.2   Scope

The handbook consists of modules that present technical information applicable to the current DSN configuration and preliminary information applicable to future DSN configurations. These modules will be revised to reflect new capabilities and distributed to all users as these capabilities become approved by the DSMS Engineering Program Office.

This handbook is primarily concerned with performance parameters of equipment that supports the forward and return telecommunications link interfaces between spacecraft and the DSN. Other interfaces, such as ground data interfaces and administrative interfaces, are covered in a companion handbook, the Telecommunications and Mission Operations Directorate (TMOD) Document 810-007, DSMS Mission Interface Design Handbook.

1.3.   *Distribution*

This handbook is published as an electronic document. However, organizations or individuals under contract to, or having received a request for proposal from, the National Aeronautics and Space Administration (NASA) or one of its centers, may receive loose-leaf bound printed copies upon request to the DSMS Engineering Program Office or the editor of this document. Persons receiving printed copies will normally be notified of revisions by electronic mail but may also request delivery of printed revisions.

Persons having no further use for printed copies of the document are requested to return them to the editor of this document. The purpose of this request is to minimize the possibility of documents remaining in circulation if they are not being maintained. Requests for mailing address changes should also be submitted to the editor of this document.

2   *General Information*

2.1   *Constraints*

The disclosure of a capability by this handbook does not ensure that it can be made available to all potential DSN users. Specific support commitments must be negotiated between individual flight projects and the TMOD Plans and Commitments Office. Details about this office, names for personnel to contact, and their electronic addresses are available at the following website: <http://deepspace.jpl.nasa.gov/advmiss/>. Furthermore, this handbook does not relieve projects of the responsibility for obtaining frequency spectrum support for their equipment designs. This spectrum support is obtained through the JPL Frequency Manager, who is resident in the Plans and Commitments Program Office .

In seeking viable solutions to telecommunications or data-processing problems, flight projects are not necessarily constrained by the effective design parameters contained in this handbook. However, flight project requirements that could require DSN interface design beyond what is specified by this handbook are subject to negotiation with the Plans and Commitments Program Office.

The term *user* appears throughout this handbook whenever a mode of operation or parameter must be selected by a flight project. It must be understood that it is only in rare cases that these decisions can be made in real time. All DSN activities are planned well in advance and conducted by highly skilled persons trained in handling contingencies. Changes to planned operations must be made in accordance with DSN procedures that are beyond the scope of this document.

2.2 *Types of Data*

It is the intent of this handbook to provide data verified by measurement and, therefore, representing actual performance. Unless clearly marked to the contrary, data in this handbook should be assumed to comply with this intent.

Sometimes it is necessary to include DSN design performance data that have not been verified by measurement. These data will be clearly identified in the associated text or by appropriate marking.

As hardware and software are tested and evaluated under operational conditions throughout the DSN, performance parameters will be upgraded to represent actual performance and published in the next revision of the appropriate module.

2.3 *Proposed Capabilities*

Whenever sufficient information is known about a capability being implemented in the DSN and having adequate maturity to be considered for spacecraft mission and equipment design, this information will be included in the appropriate modules under the heading of *Proposed Capabilities*. Telecommunications engineers are advised that anything discussed under this heading cannot be committed to except by negotiation with the TMOD Plans and Commitments Program Office.

2.4 *Document Layout*

The modules in this revision of 810-005 have been divided into major sections that can be identified by their module numbers and the color of the tabs in the printed version or the index to the on-line version.

This module is part of an introductory section that may be expanded in the future to include tutorial or summary information. Modules in this section have yellow tabs and numbers starting with 0.

The next section, Space Link Interfaces, contains modules that provide information to those concerned with antenna selection and propagation effects. Modules in this section have blue tabs and numbers starting with 1.

The third section, Station Data Processing, contains modules that provide capabilities and performance of equipment installed in the Signal Processing Center (SPC) portion of each DSN location. This information will be of interest both to telecommunications engineers and spacecraft mission designers. Modules in this section have green tabs and numbers starting with 2.

The fourth section in this revision, Ground Station Properties, contains modules that provide information about the underlying technologies relating to many of the Space Link Interfaces and Station Data Processing modules. These modules have been grouped to consolidate this information in one place. Modules in this section have brown tabs and numbers starting with 3.

2.5 *Module Revision and Control*

The modules contained in this handbook are approved for publication under the authority of the cover page signatories. Revisions are indicated by a revision letter following the module designator.

A summary of the changes and additions to the on-line version of 810-005 can be accessed on the home page of the document, located at the website listed on the cover and title page of this document. Currency of modules in printed copies can be verified against the information in the Table of Contents supplied with each revision or by comparison with the on-line version. Minor corrections or changes to printed copies may be issued in the form of module change pages that will be appropriately marked and recorded in a Change Log near the front of the module.

Persons requesting additions of modules to the handbook should direct their request to the DSMS Engineering Program Office. Persons requesting changes, corrections, or additions to existing modules should direct their comments to either of the cover page signatories or to their functional titles at the DSMS Engineering Program Office. All modules are subject to the review and approval process of TMOD Standard Practice, DSMS Documentation Structure, Standards, and Definitions; TMOD Document 810-001.

2.6 *Abbreviations*

Abbreviations are normally defined after their first textual usage and are compiled in module 901, Handbook Glossary. It should be recognized, however, that certain common abbreviations or acronyms used in this handbook may not defined. External users may refer to any of several compilations of electronic terms for omitted definitions. Users with access to the JPL Intranet can find additional abbreviations in DSMS System Engineering Standard; DSMS Abbreviations and Acronyms, TMOD Document 820-062.

2.7 *Applicable Documents*

The latest issues of the following documents are referenced by modules in this handbook or are the source of requirements for this handbook or the capabilities described herein.

2.7.1 *DSMS External Documents*

The following documents either are public documents or may be made available to organizations or individuals under contract to, or having received a request for a proposal from, NASA or one of its centers.

1. The Telecommunications and Mission Operations Progress Report, On-line document <http://eis.jpl.nasa.gov/tmo/progress_report/>

2. DSMS Standard Practice, DSMS Mission Interface Design Handbook; TMOD Document 810-007

3. DSMS Requirements and Design, DSMS External Interface Specification; TMOD Document 820-013

2.7.2 *DSMS Internal Documents*

The following DSMS internal documents are referenced by, or provide requirements for, this handbook and may be found at the Product Data Management System website <http://pdms.jpl.nasa.gov/Reports/TMOD/m_epub.html>.

1. TMOD Standard Practice, DSMS Documentation Structure, Standards, and Definitions; TMOD Document 810-00l

2. DSMS System Engineering Standard, DSMS Abbreviations and Acronyms; TMOD Document 820-062

3. DSMS Subsystem Requirements and Design; TMOD Document Series 834

101
70-m Subnet
Telecommunications Interfaces

Effective November 30, 2000

Document Owner:

Approved by:

S. D. Slobin   12/11/00

_____   Date

S. D. Slobin
Antenna System Engineer

A. J. Freiley   12-13-00

_____   Date

A. J. Freiley
Antenna Product Domain Service
System Development Engineer

Released by:

[Signature on file in TMOD Library]
_____
TMOD Document Release   Date

Change Log

Rev	Issue Date	Paragraphs Affected	Change Summary
Initial	1/15/2001	All	All

Note to Readers

There are two sets of document histories in the 810-005 document, and these histories are reflected in the header at the top of the page. First, the entire document is periodically released as a revision when major changes affect a majority of the modules. For example, this module is part of 810-005, Revision E. Second, the individual modules also change, starting as an initial issue that has no revision letter. When a module is changed, a change letter is appended to the module number on the second line of the header and a summary of the changes is entered in the module's change log.

This module supersedes TCI-10 in 810-005, Rev. D.

Contents

Illustrations

Tables

1   Introduction

1.1   Purpose

This module provides the performance parameters for the Deep Space Network (DSN) 70-meter antennas that are necessary to perform the nominal design of a telecommunications link. It also summarizes the capabilities of these antennas for mission planning purposes and for comparison with other ground station antennas.

1.2   *Scope*

The scope of this module is limited to providing those parameters that characterize the RF performance of the 70-meter antennas. The parameters do not include effects of weather, such as reduction of system gain and increase in system noise temperature, that are common to all antenna types. These are discussed in module 105, Atmospheric and Environmental Effects. This module also does not discuss mechanical restrictions on antenna performance that are covered in module 302, Antenna Positioning.

2   *General Information*

The DSN 70-m Antenna Subnet contains three 70-meter diameter antennas. One antenna (Deep Space Station [DSS] 14) is located at Goldstone, California; one (DSS 43) is near Canberra, Australia; and one (DSS 63) is near Madrid, Spain. The precise station locations are shown in Module 301, Coverage and Geometry. All antennas support L-, S-, and X-band reception and S-band transmission. In addition, DSS 14 and DSS 43 have an X-band transmission capability.

Figure 1 is a block diagram of the S-band and X-band microwave and transmitter equipment at DSS 14 and DSS 43 that is common to the two stations. The diagram does not show the S-band Ultracone that has been installed at DSS 43 in support of the Galileo S-band mission. A block diagram of the S-band and X-band microwave and transmitter equipment at DSS 63 is shown in Figure 2.

All three stations include the S-band, Polarized, Diplex feedcone (the SPD cone) that contains the feed, the primary low-noise amplifier (LNA) and its support equipment, the diplexer, and the required switches and other waveguide. The backup LNA and S-band transmitters are located in an area beneath the feedcones. Two S-band transmitters are provided for spacecraft communication: a 20-kW S-band transmitter for normal spacecraft communication and a 400-kW transmitter for emergency commanding. The Goldstone site also has a radar transmitter that operates near the normal receive frequency band. The feed employs an orthomode junction that permits simultaneous right-circular polarization (RCP) and left-circular polarization (LCP) to be used. The polarizer may be switched so that either polarization may be directed to the non-diplexed path with the opposite polarization appearing on the diplexed path. The non-diplexed path (orthomode upper arm) is used for listen-only reception or if the spacecraft transmits and receives on opposite polarizations. If the spacecraft receives and transmits simultaneously with the same polarization, the diplexed path must be used, and the noise temperature is higher.

DSS 14 and DSS 43 employ the X-band Transmit-Receive feedcone (the XTR cone). The XTR cone employs a unique feed design that includes a diplexing junction to inject the transmitted signal directly into the feed. This eliminates the need for a waveguide diplexer and a common path for the received and transmitted signals. As a result, much of the received path can be cryogenically cooled with a significant reduction in operating system temperature. The S/X dichroic plate can also be retracted when S-band is not required for a further improvement in X-band performance. The XTR feed includes a fixed circular polarizer, an

orthomode junction, and two identical high-electron-mobility transistor (HEMT) low-noise amplifiers. A separate polarizer is provided for the transmitter so that the transmitted signal can be of either polarization

DSS 63 employs the older X-band receive only feedcone (the XRO cone). The XRO cone includes a switchable polarizer, an orthomode junction, and two maser low-noise amplifiers with their support equipment.

The S- and X-band feeds are provided with phase calibration couplers and comb generators so the stations can be used for very-long baseline interferometry reception in addition to spacecraft tracking.

2.1   Telecommunications Parameters

The significant parameters of the 70-meter antennas that influence telecommunications link design are listed in Tables 1 and 2. Variations in these parameters that are inherent in the design of the antennas are discussed below. Other factors that degrade link performance are discussed in modules 105 (Atmospheric and Environmental Effects) and 106 (Solar Corona and Wind Effects).

2.1.1   Antenna Gain Variation

The antenna gains in Tables 1 and 2 do not include the effect of atmospheric attenuation and should be regarded as vacuum gain at the specified reference point.

2.1.1.1   Frequency Effects

Antenna gains are specified at the indicated frequency (f_0). For operation at higher frequencies in the same band, the gain (dBi) must be increased by $20 \log (f/f_0)$. For operation at lower frequencies in the same band, the gain must be reduced by $20 \log (f/f_0)$.

2.1.1.2   Elevation Angle Effects

Structural deformation causes a reduction in gain when the antenna operates at an elevation angle other than the angle where the reflector panels were aligned. The net gain of the antenna is also reduced by atmospheric attenuation, which is a function of elevation angle and weather condition. These effects are illustrated in Figures 3 through 6, which show the estimated gain versus elevation angle for the hypothetical vacuum condition (structural deformation only) and with 0%, 50%, and 90% weather conditions, designated as CD (cumulative distribution) = 0.00, 0.50, and 0.90. A CD of 0.00 (0%) means the minimum weather effect (exceeded 100% of the time). A CD of 90.0 (90%) means that effect which is exceeded only 10% of the time. Qualitatively, a CD of 0.00 corresponds to the driest condition of the atmosphere; a CD of 0.50 corresponds to humid or very light clouds; and 0.90 corresponds to very cloudy, but with no rain. A CD of 0.25 corresponds to average clear weather and is often used when comparing gains of different antennas. Comprehensive S-band and X-band weather effects models (for weather conditions up to 99% cumulative distribution) are provided in module 105 for detailed design control use.

Figure 3 depicts the S-band (2295 MHz) net gains for all stations as a function of elevation angle and weather condition, including the vacuum condition. Net gain means vacuum-condition gain as reduced by atmosphere attenuation. DSS 43 gain is considered to be identical, using both the SPD cone and the ultracone. The L-band gain curve shapes should be considered identical to the S-band curve shapes, except that they are reduced in value by the difference shown in Table 2. Figures 4 and 5 present the predicted X-band (8420 MHz) net gains of the DSS 14 and DSS 43 antennas as a function of elevation angle and weather condition, including the vacuum condition using the XTR feedcone with the S/X dichroic plate retracted. The gains of the DSS 63 antenna, using the XRO feedcone, are shown for the same conditions in Figure 6. The equations and parameters of these curves are given in Appendix A. The models use a flat-Earth, horizontally stratified atmosphere approximation.

2.1.1.3 *Wind Loading*

The gain reductions at S- and X-band due to wind loading are listed in Table 3. The tabular data are for structural deformation only and presume that the antenna is maintained on-point by conical scan (CONSCAN, discussed in module 302) or an equivalent process. In addition to structural deformation, wind introduces a pointing error that is related to the antenna elevation angle, the angle between the antenna and the wind, and the wind speed. Cumulative probability distributions of wind velocity at Goldstone are given in module 105.

2.1.2 *System Noise Temperature Variation*

The operating system temperature (T_{op}) varies as a function of elevation angle due to changes in the path length through the atmosphere and ground noise received by the sidelobe pattern of the antenna. Figures 7 through 12 show the combined effects of these factors at L-, S-, and X-bands in a hypothetical vacuum (no atmosphere) condition for selected antenna configurations and with the three weather conditions described above. The equations and parameters for these curves are provided in Appendix A of this module. The models use a flat-Earth, horizontally stratified atmosphere approximation.

At S-band (2295 MHz), the clear-sky zenith noise temperatures of each antenna are different; however, their elevation-related effects are considered to be similar. Figure 8 shows S-band noise-temperature curves for DSS 14, LNA-1, non-diplexed. Curves for other antennas and configurations can be calculated by using the noise temperature values or differences shown in Table 2. The L-band system temperature curve (Figure 7) is modeled from the S-band curve so that at zenith the 25%-weather system temperature is 35 K. The X-band (8420 MHz) system temperature curves for three stations are shown in Figures 11 through 13. The figures for DSS 14 and DSS 43 using the XTR feedcone are estimates for X-band only configuration (S/X dichroic plate retracted) based on pre-installation tests. The figure for DSS 63 is for S/X configuration using the XRO feedcone and is derived from measured data and the weather model in module 105.

The system noise temperature values in Table 2 include a contribution due to 25% weather that must be subtracted for comparison with antennas that are specified without atmosphere (hypothetical vacuum). Table 4 provides adjustments to the 25% weather operating system temperatures that were calculated using the weather models in module 105.

Tables 5 through 10 give S-band system noise temperatures to be expected during average clear weather conditions at elevation angles near the horizon, corresponding to rise and set azimuths of spacecraft with declinations of approximately -15° to -25°. These data were gathered specifically to support the Galileo Mission during the 1995 through 1998 period.

Tables 5 and 6 are for rise and set azimuths at DSS 14 (Goldstone) using the S-band SPD cone (the standard S-band receiving system). Tables 7 and 8 are for rise and set azimuths at DSS 43 (Canberra) using the S-band ultracone (an additional, very-low-noise S-band receiving system located on that antenna). Two-way operation (simultaneous transmit and receive) or dual polarization (RCP and LCP) is not possible when the ultracone is being used for reception. The standard SPD cone at DSS 43 is available for diplexed and non-diplexed configuration with a somewhat higher noise temperature, as given in Table 2 and Appendix A, Table A-3. Tables 9 and 10 give rise and set noise temperatures for DSS 63 (Madrid). The elevation dependence of S-band noise temperature for all antennas is considered to be similar to the DSS 14 performance depicted in Figure 8, subject to the low-elevation differences given in Tables 5–10. Figures 9 and 10 show S-band system noise temperatures at a 6° elevation angle for all antennas at the eastern and western horizons for the Galileo range of rise and set azimuths.

2.1.3 Pointing Accuracy

Figure 14 shows the effects of pointing error on effective transmit and receive gain of the antenna (pointing loss) for the S-band transmit and the L- and S-band receive frequencies. The effects of pointing error at the X-band transmit and receive frequencies is shown in Figure 15. These curves are Gaussian approximations based on theoretical antenna beamwidths. Data have been normalized to eliminate elevation and wind-loading effects. The equation used to generate the curves is provided in Appendix A.

2.2 Recommended Minimum Operating Carrier Signal Levels

Table 11 provides the recommended minimum operating carrier-signal levels for selected values of receiver tracking-loop bandwidth (B_l). These levels provide a signal-to-noise ratio of 10 dB in the carrier-tracking loop, based on the nominal zenith system temperatures given in Table 2 and assuming 25% weather.

3 Proposed Capabilities

The following paragraphs discuss capabilities that have not yet been implemented by the DSN but have adequate maturity to be considered for spacecraft mission and equipment design. Telecommunications engineers are advised that any capabilities discussed in this section cannot be committed to except by negotiation with the TMOD Plans and Commitments Program Office.

3.1 70-m X-Band Uplink Implementation

DSS 63 will be equipped with the XTR feedcone and will have the same capabilities as described for DSS 14 and DSS 43 and documented in Tables 1 and 2.

Table 1. S- and X-Band Transmit Characteristics

Parameter	Value	Remarks
ANTENNA		
Gain (dBi)		At gain set elevation angle, referenced to feedhorn aperture for matched polarization; no atmosphere included
S-Band (2115 MHz)	62.7 ±0.2	All stations
X-Band (7145 MHz)	72.9 ±0.2	DSS 14 and DSS 43
Transmitter Waveguide Loss (dB)		
S-Band		All stations
	0.2 ±0.02	400-kW Transmitter output to feedhorn aperture
	0.3 ±0.02	20-kW Transmitter output to feedhorn aperture
X-Band	0.45 ±0.02	20-kW Transmitter output to feedhorn aperture, DSS 14 and DSS 43
Half-Power Beamwidth (deg)		Angular width (2-sided) between half-power points at specified frequency
S-Band	0.128 ±0.014	
X-Band	0.0378 ±0.003	
Polarization	RCP or LCP	One polarization at a time, remotely selected
Ellipticity, RCP or LCP (dB)		Ellipticity is defined as the ratio of peak-to-trough received voltages with a rotating, linearly polarized source and a circularly (elliptically) polarized receiving antenna. Ellipticity (dB) = 20 log (V2/V1)
S-Band	2.2 (max)	All stations
X-Band	≤1.0	DSS 14 and DSS 43

Table 1. S- and X-Band Transmit Characteristics (Continued)

Parameter	Value	Remarks
ANTENNA (Continued)		
Pointing Loss (dB)		
Angular	See module 302	Also, see Figures 14 and 15.
CONSCAN		
S-Band		
	0.1	Recommended value
	0.03	At S-band, using X-band CONSCAN reference set for 0.1-dB loss
X-Band		DSS 14 and DSS 43
	0.1	Recommended value
EXCITER AND TRANSMITTER		
RF Power Output (dBm)		Nominal output power, referenced to transmitter port; settability is limited to 0.25 dB by measurement equipment precision
S-Band		
20-kW Power Amplifier	73.0, +0.0, −1.0	
400-kW Power Amplifier	86.0, +0.0, −1.0	See note at end of Table 1.
X-Band		DSS 14 and DSS 43
20-kW Power Amplifier	73.0, +0.0, −1.0	
Both S-band and X-band transmitters employ variable-beam klystron power amplifiers. The output from this kind of amplifier varies across the bandwidth and may be as much as 1 dB below the nominal rating, as indicated by the tolerance. Performance will also vary from tube to tube. Normal procedure is to run the tubes saturated, but unsaturated operation is also possible. The point at which saturation is achieved depends on drive power and beam voltage. The 20-kW tubes are normally saturated for power levels greater than 60 dBm (1 kW) and the 400-kW tubes are saturated above 83 dBm (200 kW). Minimum power out of the 20-kW tubes is about 53 dBm (200 W) and about 73 dBm (20 kW) for the 400-kW tubes. Efficiency of the tubes drops off rapidly below nominal rated output		

Table 1. S- and X-Band Transmit Characteristics (Continued)

Parameter	Value	Remarks
EXCITER AND TRANSMITTER (Continued)		
EIRP		At gain set elevation angle, referenced to feedhorn aperture
S-Band		
	148.5, +0.0, −1.0	400-kW Transmitter
	135.4, +0.0, −1.0	20-kW Transmitter
X-Band	145.4, +0.0, −1.0	DSS 14 and DSS 43
Frequency Range Covered (MHz)		
S-Band		
1-dB Bandwidth	2110 to 2118	
Coherent with Deep Space S-Band D/L Allocation	2110.2 to 2117.7	240/221 turnaround ratio
Coherent with Deep Space X-Band D/L Allocation	2110.2 to 2119.8	880/221 turnaround ratio
X-Band		DSS 14 and DSS 43
1-dB Bandwidth	7145 to 7190	
Coherent with Deep Space S-Band D/L Allocation	7147.3 to 7177.3	240/749 turnaround ratio
Coherent with Deep Space X-Band D/L Allocation	7149.6 to 7188.9	880/749 turnaround ratio
Tunability		At S-band or X-band transmitter output frequency
Phase Continuous Tuning Range	2.0 MHz	
Maximum Tuning Rate	±12.1 kHz/s	
Frequency Error	0.012 Hz	Average over 100 ms with respect to frequency specified by predicts
Ramp Rate Error	0.001 Hz/s	Average over 4.5 s with respect to rate calculated from frequency predicts

Table 1. S- and X-Band Transmit Characteristics (Continued)

Parameter	Value	Remarks
EXCITER AND TRANSMITTER (Continued)		
S-Band Stability		At transmitter output frequency
Output Power Stability (dB)		12-h period
Saturated Drive	±0.25	20-kW Transmitter
Saturated Drive	±0.5	400-kW Transmitter
Unsaturated Drive	±1.0	20-kW and 400-kW transmitters
Frequency ($\Delta f/f$), 1000-s Averaging	5×10^{-15}	Allan deviation
Phase Stability (dBc)		In 1-Hz bandwidth
1–10 Hz Offset	−60	Below carrier
10 Hz–1 kHz Offset	−70	Below carrier
Group Delay Stability (ns)	≤3.3	Ranging modulation signal path over 12-h period (see module 203)
Spurious Output		
2nd Harmonic (dB)	−85	Below Carrier
3rd Harmonic (dB)	−85	Below Carrier
4th Harmonic (dBm)		
	−140 dBm	20-kW Transmitter
	TBD	400-kW Transmitter
X-Band Stability		DSS 14 and DSS 43 at transmitter output frequency
Output Power Stability (dB)		12-h period
Saturated Drive	±0.25	
Unsaturated Drive	±1.0	
Frequency ($\Delta f/f$), 1000-s Averaging	2.3×10^{-15}	Allan deviation

Table 1. S- and X-Band Transmit Characteristics (Continued)

Parameter	Value	Remarks
EXCITER AND TRANSMITTER		
X-Band Stability (Continued)		At transmitter output frequency
Phase Stability (dBc)		In 1-Hz bandwidth
1–10 Hz Offset	−50	Below carrier
10 Hz–1 kHz Offset	−60	Below carrier
Group Delay Stability (ns)	≤1.0	Ranging modulation signal path over 12 h period (see module 203)
Spurious Output		
2nd Harmonic (dB)	−75	Below carrier
3rd, 4th & 5th Harmonics	−60	Below carrier

Note: 400-kW power amplifier cannot be used below 10° elevation at all stations and between 300° and 360° azimuth at DSS 63.

Table 2. L-, S-, and X-Band Receive Characteristics

Parameter	Value	Remarks
ANTENNA		
Gain (dBi)		At gain set elevation angle for matched polarization, no atmosphere included Note: Favorable (+) and adverse (–) tolerances have a triangular PDF. See Figures 3–6 for elevation dependency.
L-Band (1668 MHz)	60.17 ±0.3	Referenced to LNA-1 or LNA-2 input terminal (includes feedline loss)
S-Band (2295 MHz), All Stations	63.34 ±0.10	Referenced to LNA-1 input terminal (includes feedline loss)
	63.28 ±0.10	Referenced to LNA-2 input terminal (includes feedline loss)
X-Band (8420 MHz), S/X Configuration		Referenced to LNA-1 or LNA-2 input terminal (includes feedline loss). S/X dichroic is in place.
DSS 14 and DSS 43	74.1 ±0.10	XTR Feedcone
DSS 63	74.28 ±0.10	XRO Feedcone
X-Band (8420 MHz), X-Only Configuration	74.3 ±0.10	DSS 14 and DSS 43, referenced to LNA-1 or LNA-2 input terminal (includes feedline loss). S/X dichroic is retracted.
Half-Power Beamwidth (deg.)		Angular width (2-sided) between half-power points at specified frequency
L- Band (1668 MHz)	0.162 ±0.010	
S- Band (2295 MHz)	0.118 ±0.02	
X-Band (8420 MHz)	0.0320 ±0.003	
Polarization		
L-Band, All Stations	LCP	RCP available by changing mechanical configuration of feed
S-Band, All Stations	RCP and LCP	Both polarizations available simultaneously. Choice of diplexed or non-diplexed path is remotely selectable.

Table 2. L-, S-, and X-Band Receive Characteristics (Continued)

Parameter	Value	Remarks
ANTENNA		
Polarization (Continued)		
X-Band		
DSS 14 and DSS 43	RCP and LCP	Both polarizations available simultaneously.
DSS 63	RCP and LCP	Both polarizations available simultaneously. Choice of diplexed or non-diplexed path is remotely selectable.
Ellipticity (dB)		See definition in Table 1.
L-Band	2.0 (max)	
S-Band	0.6 (max)	
X-Band	0.8 (max)	
Pointing Loss (dB, 3 sigma)		
Angular	See module 302	Also, see Figures 14 and 15.
CONSCAN		
S-Band	0.03	At S-band using X-band CONSCAN reference set for 0.1 dB loss at X-band
	0.1	Recommended value when using S-band CONSCAN reference
X-Band	0.1	Recommended value when using X-band CONSCAN reference
LOW NOISE AMPLIFIERS AND RECEIVERS		Only two tracking receiver channels are available that may be operated as two receivers with any pair or combination of L-, S-, and X-band frequencies and polarizations, for example, one S and one X or X-RCP and X-LCP. Both receivers also may be operated in the same band and polarization.

Table 2. L-, S-, and X-Band Receive Characteristics (Continued)

Parameter	Value	Remarks
LOW NOISE AMPLIFIERS AND RECEIVERS (Continued)		
Frequency Ranges Covered (MHz))		1 dB bandwidth
L-Band	1628 to 1708	
S-Band	2270 to 2300	
X-Band	8400–8500	
Recommended Maximum Signal Power (dBm)	-90.0	At LNA input terminal
Recommended Minimum Signal Power (dBm)	See Table 11	
System Noise Temperature (K)		For average clear weather (25% weather condition) near zenith (see Table 4 for adjustments to remove atmospheric contribution); favorable (–) and adverse (+) tolerances have a triangular PDF
L-Band (1628–1708 MHz)	21 ±2	With respect to LNA 1 or 2 input terminal (see Figure 7 for elevation dependency)
S-Band (2270–2300 MHz)		See Figure 8 for representative elevation dependency
DSS 14	15.2, +1.3, –0.7	SPD cone, with respect to LNA-1 input terminal, non-diplexed path
DSS 43	15.6, +1.4, –1.1	
DSS 63	16.9, +1.7, –1.1	
DSS 43	11.7, +1.0, –0.0	Ultracone with respect to LNA input terminal
DSS 14	19.5, +1.3, –0.7	SPD cone, with respect to LNA-1 input terminal, diplexed path
DSS 43	19.9, +1.4, –1.1	
DSS 63	21.2, +1.7, –1.1	
Adjustment for LNA-2 (All DSS)	5 ±1	Add to diplexed or non-diplexed values shown above to obtain performance with LNA-2; tolerances to be RSS'd with tolerances shown above

Table 2. L-, S- and X-Band Receive Characteristics (Continued)

Parameter	Value	Remarks
LOW NOISE AMPLIFIERS AND RECEIVERS		
System Noise Temperature (K) (Continued)		
X-Band (8400–8500 MHz), S/X Configuration		Referenced to LNA-1 or LNA-2 input terminal; S/X dichroic in place
DSS 14	17.4 ±0.3	XTR Feedcone
DSS 43	17.8 ±0.3	XTR Feedcone
DSS 63	21.0 ±2	XRO Feedcone (see Figure 13 for elevation dependency)
X-Band (8420 MHz), X-Only Configuration		DSS 14 and DSS 43, referenced to LNA-1 or LNA-2 input terminal; S/X dichroic retracted (see Figures 11 and 12 for elevation dependency)
DSS 14	16.5 ±0.3	XTR Feedcone
DSS 43	16.9 ±0.3	XTR Feedcone
DSS 63	N/A	XRO dichroic not retractable
Carrier Tracking Loop Noise B/W (Hz)	0.25 – 200	Effective one-sided, noise-equivalent carrier loop bandwidth (B_L)

Table 3. Gain Reduction Due to Wind Loading, 70-m Antenna

Wind Speed		Gain Reduction (dB)*	
km/h	mph	S-band	X-band
32	20	Negligible	0.1
48	30	Negligible	0.3
72	45	0.15	1.5

* Assumes antenna is maintained on-point using CONSCAN or an equivalent.
L-band gain reduction is negligible for wind speeds up to 72 km/h (45 mph).
Worst case with antenna in most adverse orientation for wind.

Table 4. System Noise Temperature Contributions due to 25% Weather

Location	Noise Temperature Contribution (K)*	
	L-band and S-band	X-band
Goldstone (DSS 14)	1.929	2.292
Canberra (DSS 43)	2.109	2.654
Madrid (DSS 63)	2.031	2.545

* From Table 1 in module 105.

Table 5. DSS 14 Eastern Horizon S-Band T_{op} (K) with SPD Cone

ELEV, deg	AZIMUTH, deg																				
	110	111	112	113	114	115	116	117	118	119	120	121	122	123	124	125	126	127	128	129	130
20.0	21.0	21.1	21.0	21.0	21.0	21.1	21.0	21.0	21.0	21.1	21.1	21.2	21.1	21.1	21.1	21.1	21.1	21.1	21.1	21.1	21.1
19.0	21.5	21.5	21.5	21.5	21.5	21.5	21.6	21.7	21.7	21.7	21.6	21.6	21.7	21.7	21.7	21.8	21.8	21.7	21.6	21.6	21.6
18.0	22.1	22.0	22.0	22.0	22.0	21.9	21.9	22.0	22.0	22.0	22.1	22.0	22.0	22.0	22.1	22.1	22.0	22.0	22.0	21.9	22.0
17.0	22.3	22.2	22.2	22.2	22.1	22.2	22.2	22.3	22.2	22.2	22.2	22.2	22.2	22.2	22.2	22.2	22.3	22.2	22.2	22.3	22.3
16.0	22.7	22.7	22.7	22.6	22.7	22.6	22.6	22.6	22.7	22.7	22.6	22.7	22.7	22.7	22.6	22.7	22.7	22.7	22.7	22.9	23.0
15.0	23.2	23.2	23.2	23.2	23.2	23.2	23.3	23.3	23.2	23.3	23.4	23.5	23.5	23.5	23.5	23.5	23.6	23.6	23.6	23.6	23.7
14.0	23.7	23.7	23.7	23.8	23.8	23.8	23.9	23.9	23.9	24.0	24.1	24.1	24.0	24.0	24.0	24.0	24.1	24.3	24.3	24.2	24.2
13.0	24.6	24.5	24.5	24.6	24.6	24.5	24.5	24.6	24.6	24.6	24.6	24.7	24.7	24.7	24.8	24.8	24.7	24.8	24.8	24.9	24.9
12.0	25.2	25.2	25.2	25.2	25.2	25.2	25.3	25.3	25.3	25.4	25.4	25.3	25.4	25.4	25.3	25.3	25.4	25.4	25.4	25.5	25.5
11.0	26.0	26.1	26.1	26.1	26.0	26.1	26.1	26.1	26.1	26.1	26.2	26.2	26.2	26.2	26.2	26.2	26.3	26.3	26.3	26.4	26.5
10.0	27.1	27.2	27.2	27.1	27.2	27.1	27.2	27.2	27.1	27.2	27.2	27.3	27.3	27.3	27.4	27.3	27.3	27.4	27.4	27.5	27.4
9.5	27.4	27.5	27.5	27.6	27.5	27.6	27.6	27.6	27.6	27.6	27.6	27.7	27.8	27.6	27.7	27.7	27.8	27.9	28.0	27.9	28.0
9.0	27.9	27.8	28.2	28.2	27.8	27.8	27.8	27.8	27.8	27.9	27.9	28.0	28.0	28.0	28.0	28.1	28.1	28.5	28.5	28.2	28.2
8.5	29.2	29.2	29.1	29.1	29.2	29.1	29.0	29.0	29.1	29.1	29.1	29.1	29.2	29.3	29.5	29.5	29.4	29.3	29.4	29.5	29.5
8.0	29.6	29.6	29.7	29.7	29.9	29.9	29.8	29.7	29.8	29.8	29.8	30.0	30.0	29.9	29.9	29.9	29.9	30.0	30.0	30.1	30.1
7.5	30.4	30.3	30.3	30.4	30.4	30.4	30.5	30.4	30.4	30.5	30.4	30.5	30.8	30.6	30.6	30.7	30.7	30.7	30.8	30.8	30.9
7.0	31.1	31.2	31.2	31.2	31.2	31.4	31.4	31.2	31.3	31.3	31.3	31.3	31.3	31.4	31.4	31.4	31.5	31.5	31.5	31.6	31.7
6.5	32.1	32.2	32.5	32.3	32.3	32.6	32.4	32.4	32.4	32.5	32.5	32.6	32.5	32.5	32.5	32.6	32.7	32.6	32.7	32.8	32.8
6.0	32.3	32.8	33.0	33.0	33.0	33.0	33.1	33.2	33.2	33.2	33.3	33.3	33.3	33.3	33.3	33.4	33.5	33.6	33.6	33.6	33.8

ELEV, deg	AZIMUTH, deg																				
	130	131	132	133	134	135	136	137	138	139	140	141	142	143	144	145	146	147	148	149	150
20.0	21.1	21.1	21.1	21.1	21.1	21.2	21.2	21.7	21.6	21.1	21.2	21.2	21.2	21.2	21.1	21.1	21.2	21.2	21.2	21.2	21.2
19.0	21.6	21.6	21.6	21.6	21.6	21.6	21.5	21.7	22.1	21.8	21.6	21.8	22.0	21.6	21.6	22.1	21.9	21.6	21.6	21.6	21.6
18.0	22.0	22.0	21.9	21.9	21.9	22.0	22.0	21.9	22.0	22.1	22.1	22.1	22.5	22.6	22.1	22.2	22.8	22.5	22.1	22.3	22.8
17.0	22.3	22.4	22.5	22.6	22.5	22.5	22.5	22.4	22.5	22.5	22.6	22.6	22.6	22.6	22.5	22.5	22.5	22.6	22.5	22.6	22.7
16.0	23.0	22.8	22.8	22.9	22.9	22.9	23.0	23.0	23.1	23.1	23.1	23.2	23.3	23.2	23.1	23.3	23.3	23.1	23.1	23.2	23.2
15.0	23.7	23.6	23.6	23.7	23.6	23.6	23.6	23.7	23.7	23.7	23.8	23.8	23.8	23.8	23.8	23.7	23.7	23.8	23.8	23.7	23.7
14.0	24.2	24.2	24.2	24.2	24.5	24.9	24.6	24.5	24.5	24.5	24.5	24.4	24.4	24.5	24.5	24.5	24.5	24.7	25.0	24.6	24.6
13.0	24.9	24.9	25.0	25.0	25.1	25.2	25.0	24.8	25.0	25.1	25.2	25.2	25.3	25.3	25.3	25.3	25.3	25.5	25.5	25.5	25.5
12.0	25.5	25.5	25.5	25.6	25.6	25.6	25.6	25.6	25.7	25.7	25.7	25.8	25.8	25.9	25.9	25.9	25.9	26.0	26.0	26.0	26.1
11.0	26.5	26.5	26.5	26.9	27.5	26.8	26.8	27.3	26.8	26.6	26.6	26.7	26.6	26.7	26.7	26.7	26.7	26.8	26.9	26.9	26.9
10.0	27.4	27.5	27.5	27.7	27.7	27.6	27.7	27.7	27.7	27.8	27.8	27.9	27.8	27.8	27.7	27.9	27.9	27.9	27.9	28.0	28.1
9.5	28.0	28.0	28.1	28.1	28.2	28.1	28.1	28.1	28.1	28.2	28.2	28.3	28.3	28.3	28.4	28.4	28.4	28.5	28.4	28.4	28.4
9.0	28.2	28.3	28.3	28.4	28.4	28.4	28.5	28.5	28.6	28.6	28.5	28.6	28.7	28.8	28.7	28.8	28.8	28.9	28.9	28.9	28.9
8.5	29.5	29.6	29.7	29.6	29.7	29.9	29.9	29.9	30.0	29.6	29.9	30.1	29.8	29.8	30.0	30.0	29.9	29.9	30.0	30.0	30.0
8.0	30.1	30.1	30.2	30.2	30.3	30.5	30.4	30.3	30.4	30.5	30.4	30.5	30.4	30.3	30.5	30.6	30.6	30.6	30.6	30.7	30.8
7.5	30.9	30.9	30.9	31.1	31.2	31.2	31.2	31.2	31.3	31.4	31.5	31.4	31.4	31.4	31.5	31.5	31.5	31.5	31.6	31.7	31.8
7.0	31.7	31.8	31.9	31.8	32.0	32.1	32.1	32.2	32.1	32.0	32.1	32.2	32.2	32.2	32.2	32.2	32.3	32.4	32.5	32.8	32.9
6.5	32.8	32.9	32.9	33.0	33.1	33.2	33.2	33.2	33.2	33.3	33.6	33.5	33.4	33.4	33.4	33.5	33.6	33.7	33.9	34.1	34.2
6.0	33.8	33.8	33.8	34.0	34.0	34.0	34.1	34.1	34.1	34.3	34.3	34.4	34.4	34.5	34.6	34.6	34.7	34.8	35.0	35.2	35.4

Table 6. DSS 14 Western Horizon S-Band T$_{op}$ (K) with SPD Cone

ELEV, deg	AZIMUTH, deg																				
	210	211	212	213	214	215	216	217	218	219	220	221	222	223	224	225	226	227	228	229	230
9.0	29.7	30.0	31.0	32.0	31.5	30.6	30.0	29.6	29.3	29.3	29.2	29.1	29.0	29.0	28.8	29.0	29.0	29.1	29.0	29.0	29.0
8.5	31.0	31.3	32.3	32.3	31.2	30.6	30.3	30.0	29.9	29.7	29.7	29.7	29.6	29.6	29.5	29.5	29.5	29.5	29.5	29.5	29.5
8.0	27.2	31.5	31.9	33.1	33.8	32.4	31.3	31.1	31.0	30.7	30.6	30.5	30.5	30.8	30.4	30.3	30.4	30.7	30.5	30.4	30.5
7.5	34.7	34.9	34.9	34.9	34.5	33.3	32.3	32.0	31.7	31.4	31.3	31.2	31.2	31.2	31.2	31.2	31.1	31.0	30.9	31.0	31.1
7.0	34.3	34.3	34.3	34.2	34.2	34.2	33.8	33.0	32.5	32.2	32.1	31.7	31.9	31.9	31.9	31.8	31.8	31.8	31.7	31.7	31.8
6.5	34.4	34.3	34.2	34.3	34.2	33.8	33.4	33.0	32.9	33.0	32.8	32.8	32.8	32.8	33.0	32.8	32.8	32.7	32.7	32.7	32.7
6.0	34.6	34.1	34.7	34.8	34.8	34.7	34.4	34.0	33.8	33.7	33.7	33.7	33.7	33.7	33.6	33.6	33.6	33.5	33.6	33.5	33.6
	AZIMUTH, deg																				
	230	231	232	233	234	235	236	237	238	239	240	241	242	243	244	245	246	247	248	249	250
9.0	29.0	28.9	28.9	28.9	29.1	29.1	28.9	29.1	29.4	28.9	28.8	28.8	28.8	28.7	28.8	28.8	28.7	28.7	28.8	28.9	29.0
8.5	29.5	29.4	29.4	29.4	29.5	29.7	29.5	29.5	29.4	29.3	29.4	29.4	29.4	29.4	29.4	29.4	29.4	29.5	29.5	29.5	29.5
8.0	30.5	30.3	30.2	30.2	30.1	30.2	30.2	29.9	30.0	30.1	30.2	30.2	30.2	30.1	30.1	30.1	30.0	30.1	30.2	30.2	30.3
7.5	31.1	31.0	31.0	31.0	30.9	30.9	30.9	31.0	31.0	30.9	30.6	30.9	31.1	31.0	31.0	31.1	30.9	30.9	30.9	30.7	30.5
7.0	31.8	31.8	31.7	31.7	31.8	31.8	31.7	31.7	31.7	31.7	31.7	31.7	31.6	31.6	31.6	31.4	31.6	31.7	31.7	31.6	31.7
6.5	32.7	32.6	32.6	32.6	32.6	32.6	32.6	32.6	32.6	32.6	32.6	32.6	32.5	32.5	32.6	32.6	32.5	32.5	32.5	32.6	32.5	32.5
6.0	33.6	33.7	33.6	33.7	33.9	33.9	33.8	33.8	33.9	33.8	33.8	33.8	33.8	33.7	33.7	33.7	33.7	33.7	33.8	33.8	33.8

Table 7. DSS 43 Eastern Horizon S-Band T_{op} (K) with Ultracone

ELEV, deg	AZIMUTH, deg																				
	90	91	92	93	94	95	96	97	98	99	100	101	102	103	104	105	106	107	108	109	110
20.0	19.0	18.7	18.2	18.9	18.4	18.7	19.0	18.8	18.4	18.7	18.8	18.5	18.2	18.9	18.6	18.7	18.3	19.0	18.3	18.1	18.7
19.0	19.4	19.5	19.3	19.2	19.5	20.1	19.6	19.4	19.3	19.3	18.9	18.7	19.2	19.4	18.8	19.4	19.0	19.0	18.9	19.1	18.8
18.0	20.3	20.0	20.2	19.6	19.7	19.9	20.1	20.2	20.1	19.9	20.2	19.6	20.2	20.1	19.9	19.8	19.6	19.5	20.0	19.6	19.4
17.0	21.1	21.2	20.4	20.6	20.9	20.4	21.2	20.8	21.2	21.1	20.7	20.9	20.8	20.4	20.4	20.9	20.9	20.3	20.2	20.3	20.7
16.0	21.5	21.5	21.1	21.7	21.3	21.5	21.4	21.6	21.4	21.1	21.6	21.3	21.6	21.3	21.4	21.5	21.5	21.2	21.2	20.7	21.0
15.0	22.8	22.7	22.0	22.4	22.2	22.3	22.0	22.7	22.1	22.7	22.3	22.2	22.4	22.3	21.6	22.1	22.3	22.3	22.0	21.8	21.8
14.0	23.3	23.6	23.2	23.5	23.5	23.0	23.3	23.1	23.1	23.2	23.2	23.5	23.3	23.3	22.8	22.9	23.0	23.1	22.4	22.8	22.4
13.0	24.3	23.7	24.0	24.3	23.8	24.6	24.1	23.7	24.0	24.3	23.7	23.9	23.9	24.1	23.8	23.8	23.7	23.8	24.0	23.5	23.6
12.0	25.1	25.3	25.2	25.7	25.2	25.5	25.4	25.4	25.2	25.6	25.1	25.3	25.0	25.0	24.9	25.0	25.1	24.9	24.4	24.8	24.6
11.0	26.5	26.9	26.4	26.0	26.1	26.7	26.3	26.9	27.5	26.8	27.1	27.5	26.9	26.8	27.0	26.0	26.0	26.1	26.0	25.9	25.8
10.0	33.6	32.8	30.6	29.7	29.4	29.4	30.1	33.3	39.9	51.4	58.3	59.1	56.1	48.6	37.1	30.7	28.7	27.8	28.0	27.3	27.2
9.5	50.5	50.1	46.9	41.7	38.5	39.2	45.0	53.9	67.5	82.2	94.3	98.1	94.0	82.4	67.3	53.3	40.3	31.7	29.9	29.0	27.7
9.0	77.0	76.1	71.6	66.6	65.0	69.7	80.5	96.0	114	131	141	142	133	116	96.4	77.9	60.4	45.8	38.6	34.1	31.3
8.5	111	112	111	107	104	104	112	125	143	161	177	187	184	173	155	134	111	90.9	75.1	64.4	54.6
8.0	151	150	148	145	146	151	161	177	195	211	222	223	215	201	182	160	141	124	109	96.9	82.2
7.5	190	191	191	188	185	187	195	207	222	234	240	240	238	236	227	211	195	178	165	153	134
7.0	219	220	220	218	216	220	227	236	240	242	242	241	240	240	238	232	222	212	203	190	171
6.5	235	236	237	237	236	236	239	240	243	244	244	243	242	241	241	242	241	238	236	230	220
6.0	239	240	239	239	240	240	241	242	243	243	243	243	242	241	242	242	242	241	241	239	233

ELEV, deg	AZIMUTH, deg																				
	110	111	112	113	114	115	116	117	118	119	120	121	122	123	124	125	126	127	128	129	130
20.0	18.7	18.3	18.3	17.7	18.1	17.4	17.9	17.7	18.1	17.6	18.0	17.6	17.4	17.5	17.5	18.0	17.9	17.9	17.2	17.5	17.7
19.0	18.8	18.7	18.9	18.9	19.0	18.3	18.8	18.4	18.5	18.7	18.4	17.8	18.3	17.9	18.6	18.0	18.1	17.9	18.0	18.2	17.8
18.0	19.4	19.8	19.5	19.7	19.2	19.5	19.0	18.8	19.2	18.8	18.9	18.9	18.8	18.9	18.9	18.7	18.5	18.9	18.5	18.7	18.9
17.0	20.7	20.1	20.3	19.9	20.3	19.6	20.5	19.6	19.6	19.6	19.8	19.8	19.5	19.5	19.6	19.5	19.4	19.3	19.5	19.0	18.7
16.0	21.0	20.8	21.3	20.9	20.8	20.9	20.7	20.1	20.4	20.8	20.3	19.8	20.4	19.8	20.2	19.8	19.9	20.1	19.7	20.0	20.9
15.0	21.8	21.6	21.6	21.5	21.5	21.5	21.3	21.5	21.3	21.0	21.3	21.3	20.9	20.9	21.3	20.9	20.9	20.6	20.8	20.7	20.3
14.0	22.4	22.4	22.4	22.7	22.4	22.4	22.2	22.2	22.3	22.1	22.1	21.6	21.9	21.7	21.8	21.7	21.9	21.7	21.1	21.3	21.1
13.0	23.6	24.0	23.2	23.3	23.3	23.2	23.1	22.9	23.0	23.0	23.0	23.7	22.7	22.5	23.2	22.4	22.3	22.2	22.6	22.8	22.1
12.0	24.6	24.3	23.8	24.3	24.3	24.2	24.1	23.9	24.2	23.4	23.8	23.3	23.7	24.0	23.8	23.8	23.5	23.6	23.5	23.3	23.3
11.0	25.8	25.8	25.5	25.5	25.3	24.9	25.1	25.2	25.3	24.6	25.0	24.9	24.6	25.3	24.9	25.2	24.6	24.8	24.3	24.8	25.1
10.0	27.2	27.3	27.1	26.3	26.5	26.4	26.2	26.8	26.1	26.1	26.0	26.3	26.2	26.4	26.3	27.3	28.0	27.3	26.4	26.2	26.2
9.5	27.7	28.5	28.4	27.1	27.8	27.2	27.0	27.0	26.7	26.6	27.0	26.4	26.7	27.2	26.6	26.9	26.5	26.9	26.8	26.5	26.5
9.0	31.3	29.7	28.8	28.8	28.6	28.2	28.2	27.9	28.0	27.9	27.7	27.2	27.5	27.5	27.4	27.5	27.2	27.5	27.5	27.5	26.7
8.5	54.6	41.6	33.6	30.0	29.7	29.0	28.8	29.1	29.2	28.7	28.5	28.5	28.4	28.7	28.6	28.4	28.9	28.5	28.9	28.4	28.2
8.0	82.2	63.6	46.3	36.1	31.6	30.5	29.8	29.5	30.0	29.7	29.5	29.3	29.5	29.6	29.6	29.4	30.4	30.0	30.4	29.6	29.9
7.5	134	113	89.0	68.0	50.8	38.0	33.1	31.4	31.1	31.5	31.4	30.8	31.3	31.5	31.5	31.4	31.4	31.3	31.8	31.4	31.5
7.0	171	147	122	96.9	74.1	52.7	37.1	34.0	33.2	33.8	33.5	33.3	34.1	33.8	33.9	34.3	34.0	33.4	33.8	33.6	32.7
6.5	220	200	178	153	126	99.5	72.0	48.4	38.2	36.2	36.9	37.4	37.6	39.6	41.2	42.5	41.4	38.5	37.2	36.0	36.7
6.0	233	219	199	175	148	116	85.7	61.1	46.9	42.7	42.8	46.3	52.5	60.2	64.6	63.4	56.7	48.6	43.0	40.0	39.4

Table 8. DSS 43 Western Horizon S-Band T_{op} (K) with Ultracone

ELEV, deg	AZIMUTH, deg																				
	230	231	232	233	234	235	236	237	238	239	240	241	242	243	244	245	246	247	248	249	250
20.0	17.4	17.3	17.4	17.5	17.3	17.6	17.4	17.5	17.7	17.5	17.5	17.5	17.4	17.6	17.7	17.4	17.6	17.6	17.5	17.6	17.5
19.0	18.0	18.0	18.2	18.1	18.2	18.2	18.1	18.2	18.1	18.3	18.3	18.2	18.3	18.5	18.3	18.2	18.1	18.2	18.3	18.3	18.2
18.0	18.7	18.6	18.7	18.7	18.8	19.0	18.8	18.7	18.9	19.0	19.0	18.9	18.9	19.0	18.8	18.9	18.9	18.8	18.9	18.9	18.7
17.0	19.4	19.3	19.5	19.4	19.4	19.4	19.4	19.6	19.5	19.4	19.6	19.5	19.6	19.4	19.5	19.4	19.4	19.5	19.3	19.5	19.5
16.0	20.0	20.1	20.0	20.2	20.4	20.2	20.2	20.3	20.3	20.2	20.3	20.3	20.2	20.1	20.2	20.2	20.4	20.1	20.2	20.1	20.3
15.0	20.9	20.9	21.0	20.9	21.0	21.0	21.0	21.0	21.1	21.1	21.0	21.1	21.1	21.1	21.0	21.0	21.0	20.9	21.1	21.2	20.9
14.0	21.9	21.7	21.6	21.6	21.6	21.7	21.9	21.8	21.9	21.8	21.9	21.9	22.0	21.9	21.9	21.9	21.9	21.8	21.8	21.7	21.7
13.0	22.5	22.5	22.7	22.6	22.6	22.6	22.6	22.7	22.6	22.7	22.7	22.8	22.8	22.6	22.8	22.7	22.7	22.7	22.8	22.7	22.5
12.0	23.5	23.4	23.4	23.5	23.5	23.6	23.7	23.6	23.7	23.6	23.9	23.7	23.8	23.9	23.8	23.9	23.8	23.7	23.7	23.7	23.7
11.0	24.9	25.0	25.1	25.2	25.1	25.2	25.3	25.4	25.3	25.4	25.2	25.3	25.4	25.4	25.5	25.5	25.4	25.3	25.3	25.2	25.0
10.5	25.1	25.2	25.1	25.4	25.4	25.7	25.6	26.1	26.8	26.8	26.4	26.0	26.5	27.1	26.5	26.7	27.5	27.3	26.0	25.6	25.7
10.0	25.9	26.0	26.6	27.4	27.4	27.4	28.8	31.4	32.0	31.4	29.7	29.5	32.1	31.2	29.8	32.8	32.7	29.0	27.4	27.1	27.1
9.5	27.7	28.0	28.0	30.3	32.8	32.6	33.0	35.3	38.6	39.3	39.6	37.0	36.8	38.5	37.9	37.4	39.3	37.8	34.2	31.4	30.4
9.0	34.0	34.4	36.4	39.4	41.2	43.7	44.5	48.0	48.5	50.3	51.3	50.0	48.5	49.1	50.2	49.5	47.8	45.0	42.6	38.6	39.7
8.5	40.4	42.8	46.5	49.5	50.5	55.0	58.7	61.3	62.0	61.9	66.7	66.1	64.4	62.8	65.7	65.2	62.0	58.4	57.6	55.5	51.1
8.0	54.6	59.7	64.4	63.2	69.2	74.6	77.7	78.2	78.3	83.9	85.0	83.5	80.8	83.2	84.1	80.1	74.8	73.4	73.7	68.4	64.1
7.5	68.6	70.0	78.1	81.7	80.5	88.8	94.6	97.3	96.4	98.6	104	106	103	101	104	104	96.4	92.0	92.6	92.1	85.5
7.0	86.7	92.7	101	98.8	103	112	118	116	118	121	128	125	123	124	127	120	112	113	113	110	103
6.5	106	111	120	120	121	130	138	137	138	141	145	149	145	144	147	146	138	133	135	133	127
6.0	129	136	143	141	144	154	159	159	161	164	170	168	166	168	169	166	159	155	156	152	145

ELEV, deg	AZIMUTH, deg																				
	250	251	252	253	254	255	256	257	258	259	260	261	262	263	264	265	266	267	268	269	270
20.0	17.5	17.6	17.3	17.6	17.3	17.4	17.4	17.5	17.4	17.4	17.4	17.4	17.4	17.4	17.3	17.5	17.5	17.4	17.3	17.4	17.6
19.0	18.2	18.2	18.2	18.1	18.1	18.2	18.0	18.1	18.0	18.0	18.0	18.1	18.1	18.0	18.0	17.9	17.9	17.9	17.9	17.8	18.0
18.0	18.7	18.9	18.8	18.8	18.9	18.8	18.8	18.7	18.6	18.6	18.6	18.6	18.6	18.6	18.5	18.6	18.5	18.6	18.5	18.5	18.6
17.0	19.5	19.3	19.1	19.5	19.4	19.3	19.2	19.2	19.1	19.2	19.3	19.2	19.2	19.2	18.9	19.0	19.1	19.2	19.0	19.0	19.0
16.0	20.3	20.3	20.2	20.2	20.0	20.1	20.1	20.1	20.0	20.0	20.0	19.9	20.0	19.9	19.9	19.8	19.9	19.8	19.7	19.8	19.4
15.0	20.9	20.8	21.0	21.0	20.9	20.9	20.9	20.8	20.8	20.9	20.9	20.9	20.9	20.8	20.6	20.7	20.7	20.5	20.5	20.6	20.4
14.0	21.7	21.8	21.9	21.6	21.8	21.7	21.7	21.7	21.7	21.8	21.5	21.7	21.7	21.7	21.5	21.4	21.5	21.4	21.5	21.4	21.5
13.0	22.5	22.7	22.6	22.6	22.6	22.6	22.6	22.6	22.6	22.5	22.6	22.6	22.6	22.5	22.4	22.4	22.3	22.3	22.5	22.2	22.5
12.0	23.7	23.8	23.7	23.8	23.6	23.6	23.7	23.6	23.6	23.5	23.5	23.6	23.5	23.6	23.5	23.4	23.4	23.3	23.4	23.3	23.0
11.0	25.0	25.1	25.1	24.9	24.9	24.8	24.8	24.8	24.6	24.7	24.7	24.4	24.6	24.5	24.5	24.4	24.5	24.4	24.3	24.3	24.3
10.5	25.7	25.7	25.7	25.6	25.5	25.3	25.4	25.3	25.2	25.3	25.1	25.2	25.0	25.0	24.9	24.9	25.0	24.9	24.9	24.8	24.7
10.0	27.1	27.5	27.4	26.5	26.7	26.5	26.1	25.9	25.9	25.8	25.7	25.8	25.7	25.7	25.6	25.6	25.8	25.6	25.5	25.4	25.3
9.5	30.4	32.1	33.2	30.6	29.3	30.2	28.6	27.2	26.7	26.7	26.6	26.4	26.4	26.5	26.3	26.2	26.3	26.2	26.2	26.1	25.8
9.0	39.7	41.0	38.4	35.8	35.6	33.3	30.1	28.3	27.8	27.5	27.4	27.3	27.3	27.1	27.0	26.9	27.1	27.0	26.9	26.9	27.0
8.5	51.1	50.5	48.8	48.4	46.3	40.9	36.3	35.3	31.3	29.2	28.4	28.3	28.1	28.0	27.8	27.8	27.8	27.8	27.7	27.7	27.5
8.0	64.1	62.9	64.0	61.1	55.9	48.5	47.5	43.9	37.2	31.9	29.7	29.2	29.1	28.8	29.1	28.7	28.8	28.6	28.8	28.6	28.5
7.5	85.5	81.1	80.2	80.4	76.0	68.0	63.1	59.9	51.8	43.3	36.1	32.1	30.6	30.4	30.2	30.1	30.2	30.0	30.2	29.8	30.0
7.0	103	98.4	98.6	97.8	91.3	82.9	79.6	71.7	61.1	52.0	43.8	36.9	33.9	32.5	31.6	31.3	31.3	31.2	31.1	31.2	31.2
6.5	127	119	118	119	115	105	101	93.9	81.0	71.1	61.7	52.4	44.8	40.8	35.9	33.9	33.3	32.9	32.8	32.8	32.8
6.0	145	140	140	141	132	125	120	109	96.1	86.0	76.4	65.8	57.0	52.2	45.1	39.0	37.2	37.5	36.9	35.7	35.4

Table 9. DSS 63 Eastern Horizon S-Band T_{op} (K) with SPD Cone

ELEV, deg	AZIMUTH, deg																			
	110	111	112	113	114	115	116	117	118	119	120	121	122	123	124	125	126	127	128	129	130
40.0	18.4	18.6	18.5	18.4	18.5	18.3	18.1	18.1	18.1	18.1	18.1	18.3	18.3	18.4	18.2	18.1	18.2	18.2	18.2	18.2	18.2
35.0	18.7	18.7	18.8	18.7	18.7	18.7	18.6	18.6	18.6	18.6	18.5	18.5	18.5	18.5	18.5	18.4	18.5	18.5	18.5	18.5	18.6
30.0	18.9	19.0	19.1	19.0	19.0	19.0	18.9	19.1	19.0	19.0	19.0	19.1	19.0	19.0	19.2	19.1	19.1	19.1	19.3	19.2	19.1
25.0	20.0	19.9	20.1	20.1	20.1	20.1	20.1	20.0	20.0	20.0	19.9	19.9	20.0	19.9	19.8	19.7	19.8	19.8	19.8	19.8	19.9
20.0	21.5	21.5	21.6	21.7	21.6	21.7	21.7	21.8	21.7	21.6	21.4	21.4	21.4	21.5	21.7	21.8	21.8	21.7	21.5	21.5	21.6
19.0	21.8	21.8	21.9	21.9	21.9	21.9	21.9	21.9	21.9	22.0	22.1	22.1	22.3	22.0	22.1	21.9	21.9	21.8	21.7	21.9	21.9
18.0	22.8	22.9	22.9	23.2	23.3	23.0	23.1	23.0	22.9	23.0	22.8	23.0	22.9	23.0	23.0	22.9	22.8	22.9	22.7	22.7	22.6
17.0	22.8	22.8	22.8	23.0	22.8	22.7	22.9	22.9	22.8	23.0	23.0	22.9	23.1	23.0	22.9	23.0	23.1	22.9	22.8	23.0	23.0
16.0	23.9	24.1	24.2	24.1	23.8	24.0	24.0	23.9	23.7	23.6	23.7	23.5	23.5	23.7	23.6	23.5	23.6	23.5	23.4	23.4	23.6
15.0	24.4	24.4	24.4	24.4	24.5	24.4	24.4	24.3	24.4	24.2	24.5	24.4	24.5	24.6	24.7	24.7	24.7	24.7	24.7	24.8	24.7
14.0	25.0	24.9	25.1	25.1	25.1	25.1	25.3	25.3	25.2	25.3	25.3	25.3	25.3	25.3	25.2	25.2	25.3	25.2	25.3	25.3	25.3
13.0	26.2	26.2	26.2	26.2	26.2	26.3	26.2	26.3	26.3	26.4	26.3	26.2	26.3	26.4	26.3	26.3	26.0	26.0	26.1	26.2	26.2
12.0	27.4	27.5	27.6	27.4	27.3	27.4	27.3	27.4	27.3	27.1	27.3	27.1	27.1	27.2	27.2	27.2	27.3	27.4	27.5	27.5	27.4
11.0	28.1	28.2	28.1	28.1	27.9	27.9	28.0	28.0	27.9	28.0	28.1	28.0	27.9	28.0	27.7	28.0	28.1	28.2	28.0	28.0	27.7
10.0	30.2	30.1	29.9	30.0	29.8	29.9	29.7	29.8	29.6	29.4	29.3	29.3	29.2	29.1	29.0	29.0	29.2	29.1	29.2	29.3	29.2
9.5	30.3	30.3	30.3	30.2	30.2	30.0	30.2	30.0	30.1	30.1	29.8	29.7	29.5	29.5	29.4	29.4	29.6	29.5	29.4	29.5	29.5
9.0	30.3	30.3	30.6	30.1	30.1	30.3	30.2	30.3	30.4	30.2	30.0	30.0	29.8	29.8	29.8	29.8	29.9	29.8	30.0	30.1	30.1
8.5	31.1	31.3	31.1	30.9	30.8	30.7	30.8	30.9	31.1	31.1	31.3	31.2	31.1	31.1	31.1	31.1	31.2	31.0	31.0	31.0	31.2
8.0	32.2	32.5	32.6	32.4	32.6	32.4	32.6	32.3	32.6	32.4	32.3	32.3	32.5	32.5	32.6	32.5	32.5	32.4	32.4	32.3	32.2
7.5	33.2	33.4	33.4	33.2	33.2	33.3	33.5	33.5	33.6	33.5	33.4	33.3	33.4	33.6	33.5	33.5	33.4	33.4	33.4	33.4	33.3
7.0	34.6	34.6	34.5	34.3	34.4	34.4	34.5	34.4	34.6	34.6	34.6	34.7	34.6	34.8	34.7	34.3	34.6	34.6	34.5	34.7	34.8
6.5	35.8	36.3	36.0	36.2	35.9	36.0	36.0	35.8	35.9	35.9	35.9	35.9	35.8	35.7	36.1	35.8	35.6	35.7	35.6	35.8	35.8
6.0	37.5	37.6	37.6	37.5	37.6	37.5	37.5	37.3	37.2	37.2	37.3	37.4	37.2	37.2	37.3	37.2	37.1	37.0	37.2	37.0	37.1

ELEV, deg	AZIMUTH, deg																			
	130	131	132	133	134	135	136	137	138	139	140	141	142	143	144	145	146	147	148	149	150
40.0	18.2	18.3	18.3	18.3	18.3	18.3	18.3	18.4	18.4	18.4	18.1	18.0	18.1	18.1	18.2	18.2	18.4	18.5	18.5	18.3	18.3
35.0	18.6	18.5	18.5	18.7	18.7	18.7	18.9	18.9	18.9	18.8	18.7	18.6	18.5	18.4	18.5	18.5	18.6	18.7	18.7	18.8	18.8
30.0	19.1	19.2	19.1	19.3	19.1	19.2	19.3	19.3	19.2	19.3	19.1	19.1	19.0	19.2	19.1	19.0	19.2	19.1	19.2	19.2	19.1
25.0	19.9	19.9	20.0	20.0	20.1	20.1	20.2	20.1	20.0	20.0	20.0	19.9	19.9	19.9	19.9	19.9	19.7	19.8	20.1	20.1	20.0
20.0	21.6	21.6	21.7	21.6	21.7	21.8	21.8	21.8	21.9	21.6	21.7	21.8	21.7	21.7	21.6	21.6	21.7	21.9	21.8	21.7	21.7
19.0	21.9	22.0	22.0	22.0	21.9	22.0	22.3	22.1	22.2	22.1	22.0	22.0	22.0	22.1	22.1	22.3	22.3	22.2	22.3	22.2	22.1
18.0	22.6	22.6	22.7	22.4	22.7	22.7	22.6	22.7	22.8	22.8	22.8	22.8	22.8	22.6	22.6	22.5	22.4	22.6	22.7	22.7	22.6
17.0	23.0	22.9	22.9	22.8	22.9	22.9	22.9	22.8	22.9	22.9	23.1	23.2	23.4	23.5	23.5	23.5	23.5	23.4	23.4	23.5	23.5
16.0	23.6	23.5	23.5	23.3	23.2	23.3	23.4	23.7	23.6	23.7	23.8	23.8	23.7	23.7	23.8	24.0	23.8	23.9	24.1	24.3	24.1
15.0	24.7	24.6	24.5	24.7	24.8	24.7	24.6	24.6	24.6	24.5	24.3	24.2	24.1	24.4	24.6	24.4	24.5	24.4	24.3	24.3	24.3
14.0	25.3	25.3	25.4	25.5	25.3	25.2	25.4	25.3	25.2	25.3	25.3	25.4	25.4	25.4	25.6	25.5	25.5	25.6	25.3	25.3	25.2
13.0	26.2	26.1	26.1	26.3	26.4	26.3	26.2	26.4	26.3	26.3	26.3	26.4	26.2	26.1	26.1	26.1	26.2	26.4	26.3	26.3	26.3
12.0	27.4	27.3	27.4	27.5	27.2	27.4	27.2	27.4	27.1	27.2	27.0	27.0	26.9	27.1	26.9	27.1	26.8	26.9	26.8	27.0	27.2
11.0	27.7	28.0	28.1	27.9	27.8	27.9	28.1	28.2	28.6	28.7	28.6	28.7	28.8	28.9	28.9	28.8	28.8	28.7	28.9	28.8	28.7
10.0	29.2	29.3	29.1	29.2	29.3	29.2	29.3	29.4	29.3	29.3	29.2	29.1	29.2	29.2	29.1	29.1	29.1	29.2	29.3	29.3	29.4
9.5	29.5	29.3	29.5	29.5	29.2	29.5	29.4	29.2	29.5	29.5	29.2	29.1	29.4	29.2	29.2	29.4	29.3	29.4	29.4	29.3	29.4
9.0	30.1	30.2	30.3	30.3	30.6	30.4	30.4	30.6	30.6	30.6	30.4	30.4	30.6	30.6	30.5	30.4	30.5	30.4	30.1	30.3	30.1
8.5	31.2	31.1	30.9	31.0	30.9	30.7	30.6	30.4	30.3	30.2	30.5	30.5	30.6	30.5	30.3	30.2	30.2	30.3	30.4	30.5	30.7
8.0	32.2	31.9	31.7	31.9	31.8	31.9	31.8	31.7	31.6	31.5	31.5	32.0	31.6	31.5	31.3	31.8	31.8	31.4	31.5	31.3	31.1
7.5	33.3	33.4	33.3	33.1	33.1	33.0	32.9	32.5	32.8	32.6	32.8	32.7	32.8	32.9	32.8	32.8	32.7	32.6	32.7	32.7	32.7
7.0	34.8	34.6	34.7	34.6	34.5	34.3	34.3	34.1	34.1	34.1	33.9	33.8	33.8	33.8	34.2	33.8	33.8	33.6	33.6	33.3	33.3
6.5	35.8	35.8	35.7	35.7	35.8	35.6	35.7	35.6	35.7	35.5	35.4	35.5	35.4	35.6	35.6	35.4	35.4	35.3	35.2	35.2	35.2
6.0	37.1	37.0	37.1	37.1	37.1	36.8	36.8	36.7	36.8	36.7	36.9	36.8	36.6	36.7	36.7	36.5	36.7	36.2	36.2	36.1	36.1

Table 10. DSS 63 Western Horizon S-Band T_{op} (K) with SPD Cone

ELEV, deg	AZIMUTH, deg																				
	210	211	212	213	214	215	216	217	218	219	220	221	222	223	224	225	226	227	228	229	230
40.0	26.2	20.4	19.6	19.7	19.4	19.6	20.2	20.5	21.6	26.6	22.3	20.2	19.6	19.5	19.1	19.1	19.2	19.2	19.3	19.2	19.1
35.0	19.5	19.5	19.9	19.8	20.0	20.2	20.4	20.7	22.0	25.8	21.6	20.6	20.3	20.1	19.9	19.8	19.7	19.7	19.6	19.7	19.7
30.0	20.4	20.6	20.7	20.9	21.0	21.8	24.2	22.9	21.9	21.5	21.0	20.8	20.8	20.7	20.6	20.5	20.5	20.5	20.4	20.4	20.2
25.0	21.2	21.3	21.2	21.5	21.7	23.0	26.6	24.4	22.6	22.1	21.8	21.5	21.3	21.4	21.2	21.1	21.1	21.1	21.1	21.1	20.9
20.0	22.9	23.4	23.7	24.0	25.5	26.4	24.6	23.8	23.5	23.1	23.0	22.7	22.8	22.7	22.6	22.4	22.4	22.4	22.6	22.7	22.5
19.0	23.5	23.6	23.8	24.3	25.7	27.4	25.5	24.6	24.0	23.6	23.3	23.2	23.4	23.0	23.2	23.0	23.0	22.9	22.9	23.0	22.9
18.0	24.3	25.0	28.2	30.5	26.1	25.3	24.5	24.2	23.8	23.7	23.6	23.6	23.5	23.6	23.4	23.4	23.4	23.4	23.4	23.4	23.5
17.0	24.8	25.0	27.3	27.3	26.8	25.7	24.9	24.7	24.5	24.2	24.2	24.1	24.0	24.0	24.0	24.0	24.0	24.0	23.9	24.0	23.9
16.0	25.8	27.2	28.0	26.6	25.7	25.4	24.9	24.7	24.6	24.6	24.5	24.8	24.8	24.8	24.6	24.7	24.6	24.6	24.7	24.7	24.5
15.0	27.1	27.8	29.8	27.6	27.3	26.4	25.7	25.5	25.6	25.4	25.3	25.6	25.3	25.3	25.3	26.0	27.6	25.5	25.1	25.2	25.0
14.0	29.5	35.3	28.7	26.9	26.6	26.3	26.3	26.0	26.2	26.0	26.1	26.1	26.0	26.1	26.2	26.0	26.0	26.0	26.1	26.0	26.1
13.0	35.0	42.1	30.3	28.1	27.5	27.4	27.0	26.8	27.0	26.8	26.8	26.9	26.7	26.8	26.9	27.0	26.9	26.8	26.9	26.8	26.8
12.0	30.7	29.6	28.6	28.2	27.9	27.9	27.7	27.5	27.7	27.5	27.5	27.5	27.5	27.5	27.5	27.6	27.7	27.8	27.7	27.8	27.8
11.0	31.3	30.8	29.8	29.2	28.9	28.7	28.4	28.4	28.6	28.5	28.5	28.6	28.5	28.5	28.5	28.4	28.4	28.7	28.6	28.6	28.6
10.0	29.8	29.9	29.8	29.6	29.5	29.4	29.3	29.4	29.3	29.4	29.5	29.4	29.3	29.7	29.5	29.5	29.4	29.5	29.5	29.7	29.7
9.5	30.6	30.4	30.2	30.3	30.1	30.1	30.1	30.1	30.2	30.1	30.3	30.3	30.0	30.0	30.6	30.3	30.1	30.3	30.4	30.2	30.2
9.0	30.9	30.9	30.8	30.7	30.9	30.6	30.8	30.7	30.8	30.7	31.1	30.8	30.7	30.7	30.9	30.8	30.9	30.7	31.1	30.8	31.0
8.5	31.5	31.5	31.4	31.6	31.7	31.5	31.4	31.5	31.4	31.4	31.3	31.3	31.2	31.2	31.3	31.3	31.2	31.4	31.3	31.3	31.3
8.0	32.3	32.1	31.9	32.3	32.1	32.1	32.2	31.9	32.4	32.2	32.3	32.2	32.4	32.3	32.0	32.2	32.4	32.4	32.4	32.5	32.5
7.5	33.1	33.2	32.9	33.5	33.0	33.0	33.3	33.0	32.9	33.4	33.2	33.3	33.2	33.1	33.4	33.5	33.2	33.3	33.2	33.2	33.5
7.0	33.9	34.5	33.8	34.3	34.3	34.1	34.0	34.0	34.3	34.3	34.6	34.3	34.3	34.5	34.7	34.8	34.6	34.7	34.7	34.5	34.5
6.5	34.4	34.2	34.7	34.8	34.7	34.8	34.4	34.5	34.4	34.8	34.5	34.9	34.8	34.7	35.0	35.2	35.2	35.3	35.2	35.2	35.4
6.0	35.4	35.3	35.7	36.2	35.5	35.9	35.8	35.8	36.1	36.6	36.7	36.3	36.8	36.9	36.9	37.0	37.1	36.9	37.2	37.3	37.1

ELEV, deg	AZIMUTH, deg																				
	230	231	232	233	234	235	236	237	238	239	240	241	242	243	244	245	246	247	248	249	250
40.0	19.1	19.0	18.9	18.9	18.9	18.8	18.8	18.8	18.9	18.8	18.8	18.9	18.9	18.9	18.9	18.9	18.9	18.9	18.9	18.9	19.0
35.0	19.7	19.5	19.6	19.4	19.3	19.5	19.4	19.3	19.5	19.4	19.2	19.2	19.4	19.4	19.2	19.1	19.2	19.3	19.4	19.2	19.2
30.0	20.2	20.3	20.2	20.2	20.3	20.2	20.2	20.1	20.1	20.0	20.1	20.0	19.9	20.0	20.0	20.1	20.1	20.0	20.2	20.2	20.2
25.0	20.9	20.9	21.2	21.1	20.8	20.9	20.9	20.9	20.9	20.9	21.0	21.0	21.0	21.0	21.1	21.1	21.1	21.1	21.1	21.1	21.0
20.0	22.5	22.6	22.7	22.5	22.6	22.6	22.5	22.9	22.7	22.7	22.6	22.5	22.5	22.5	22.6	22.6	22.6	22.6	22.6	22.7	22.8
19.0	22.9	23.0	23.0	23.0	23.0	23.0	23.0	23.0	23.0	23.2	23.1	23.2	23.2	23.1	23.1	23.1	23.1	23.1	23.2	23.2	23.2
18.0	23.5	23.5	23.5	23.5	23.6	23.6	23.7	23.7	23.7	23.8	23.8	23.9	23.8	23.7	23.7	23.7	23.7	23.7	23.8	23.8	23.8
17.0	23.9	23.9	24.1	24.1	24.1	24.1	24.1	24.1	24.3	24.3	24.3	24.3	24.2	24.2	24.2	24.2	24.2	24.2	24.2	24.3	24.3
16.0	24.5	24.6	24.7	24.7	24.7	24.8	24.8	24.8	24.8	24.9	24.7	24.7	24.6	24.6	24.7	24.8	24.9	24.8	24.9	24.9	24.9
15.0	25.0	25.2	25.2	25.2	25.1	25.3	25.2	25.3	25.3	25.3	25.6	25.4	25.5	25.5	25.5	25.6	25.6	25.6	25.5	25.7	25.6
14.0	26.1	26.0	26.1	26.1	26.2	26.2	26.2	26.3	26.2	26.3	26.4	26.3	26.3	26.3	26.4	26.4	26.4	26.5	26.6	26.5	26.6
13.0	26.8	26.9	26.8	26.8	26.8	26.9	26.9	26.9	26.9	27.0	27.0	27.0	27.1	27.1	27.1	27.1	27.1	27.1	27.2	27.2	27.3
12.0	27.8	27.6	27.7	27.7	27.8	27.8	27.8	27.8	27.9	28.0	27.9	27.9	27.9	27.9	28.0	28.0	28.0	28.1	28.1	28.2	28.2
11.0	28.6	28.6	28.5	28.5	28.6	28.5	28.6	28.8	28.7	28.7	28.9	28.8	28.8	28.8	28.8	28.9	28.9	28.9	28.9	29.0	29.0
10.0	29.7	29.5	29.5	29.5	29.6	29.6	29.6	29.7	29.8	29.9	29.8	29.8	29.9	29.9	30.0	30.0	30.0	30.0	30.1	30.1	30.1
9.5	30.2	30.4	30.3	30.3	30.3	30.3	30.2	30.5	30.4	30.4	30.6	30.5	30.6	30.6	30.6	30.7	30.8	30.7	30.6	30.7	30.7
9.0	31.0	30.8	31.0	30.9	31.1	31.0	31.0	31.1	31.1	31.3	31.2	31.3	31.4	31.3	31.4	31.4	31.4	31.4	31.4	31.5	31.6
8.5	31.3	31.3	31.5	31.5	31.4	31.5	31.6	31.7	31.6	31.8	31.8	32.0	31.8	31.9	32.1	32.0	32.2	32.2	32.3	32.3	32.4
8.0	32.5	32.4	32.5	32.4	32.3	32.5	32.7	32.7	32.8	32.9	32.8	32.9	32.9	33.0	32.9	33.0	33.1	33.2	33.3	33.3	33.5
7.5	33.5	33.3	33.1	33.3	33.4	33.5	33.6	33.6	33.8	33.9	34.0	33.9	34.1	34.3	34.2	34.7	34.5	34.6	34.5	34.6	34.7
7.0	34.5	34.6	34.5	34.5	34.5	34.7	34.5	34.6	34.7	34.9	35.1	35.4	35.4	35.5	35.6	35.8	36.1	36.3	36.5	36.4	36.5
6.5	35.4	35.4	35.4	35.7	36.0	35.9	36.0	35.8	35.3	35.7	35.8	36.2	36.5	36.8	37.2	37.9	39.0	42.3	45.9	44.5	39.2
6.0	37.1	37.2	37.1	37.0	37.3	37.3	37.2	37.5	37.5	37.9	38.4	39.2	41.6	47.5	49.4	57.4	89.6	113	122	118	105

Table 11. Recommended Minimum Operating Carrier Signal Levels (dBm)†

Band, LNA, and Configuration	Receiver Effective Noise Bandwidth (B_L) (Hz)*				
	0.25	1.0	2.0	20.0	200
L-Band					
LNA-1 or 2	−181.4	−175.4	−172.3	−162.3	−152.3
S-Band Ultracone					
DSS 43	−183.9	−177.9	−174.9	−164.9	−154.9
S-Band LNA-1, Non-diplexed					
DSS 14	−182.8	−176.8	−173.8	−163.8	−153.8
DSS 43	−182.7	−176.7	−173.7	−163.7	−153.7
DSS 63	−182.3	−176.3	−173.3	−163.3	−153.3
S-Band LNA-1, Diplexed					
DSS 14	−181.7	−175.7	−172.7	−162.7	−152.7
DSS 43	−181.6	−175.6	−172.6	−162.6	−152.6
DSS 63	−181.4	−175.3	−172.3	−162.3	−152.3
S-Band LNA-2, Non-diplexed					
DSS 14	−181.6	−175.5	−172.5	−162.5	−152.5
DSS 43	−181.5	−175.5	−172.5	−162.5	−152.5
DSS 63	−181.2	−175.2	−172.2	−162.2	−152.2
S-Band LNA-2, Diplexed					
DSS 14	−180.7	−174.7	−171.7	−161.7	−151.7
DSS 43	−180.7	−174.6	−171.6	−161.6	−151.6
DSS 63	−180.4	−174.4	−171.4	−161.4	−151.4
X-Band LNA-1 and LNA 2, S/X Dichroic In-place					
DSS 14 (XTR feedcone)	−182.2	−176.2	−173.2	−163.2	−153.2
DSS 43 (XTR feedcone)	−182.1	−176.1	−173.1	−163.1	−153.1
DSS 63 (XRO feedcone)	−181.4	−175.4	−172.4	−162.4	−152.4
X-Band LNA-1 and LNA 2, S/X Dichroic Retracted					
DSS 14	−182.4	−176.4	−173.4	−163.4	−153.4
DSS 43	−182.3	−176.3	−173.3	−163.3	−153.3

† Levels are referenced to LNA input terminals with nominal zenith system noise, including 25% weather.

* Bandwidths are centered about the received carrier.
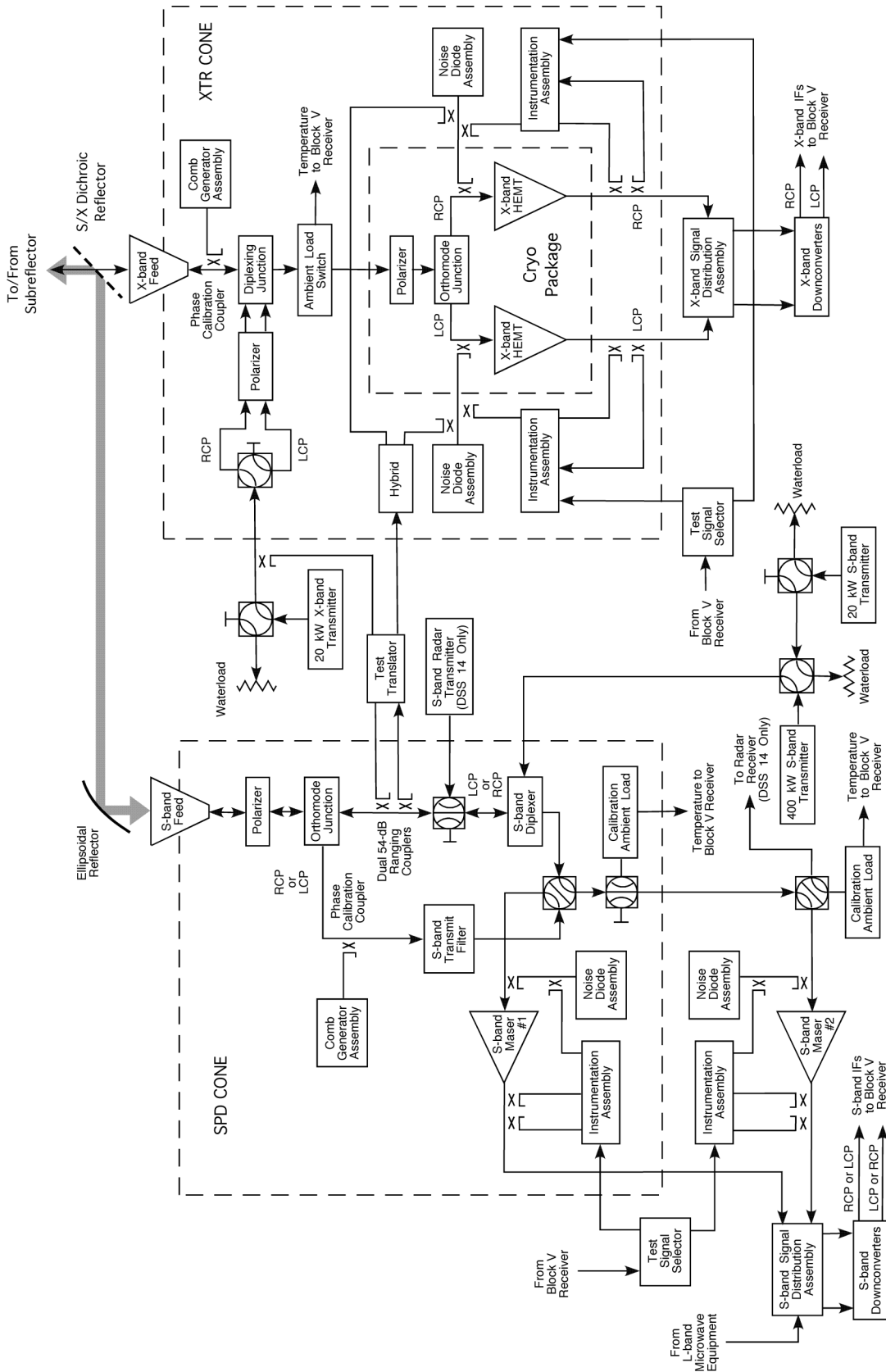
Figure 1.   Functional Block Diagram of DSS 14 and DSS 43 Microwave and Transmitter Equipment
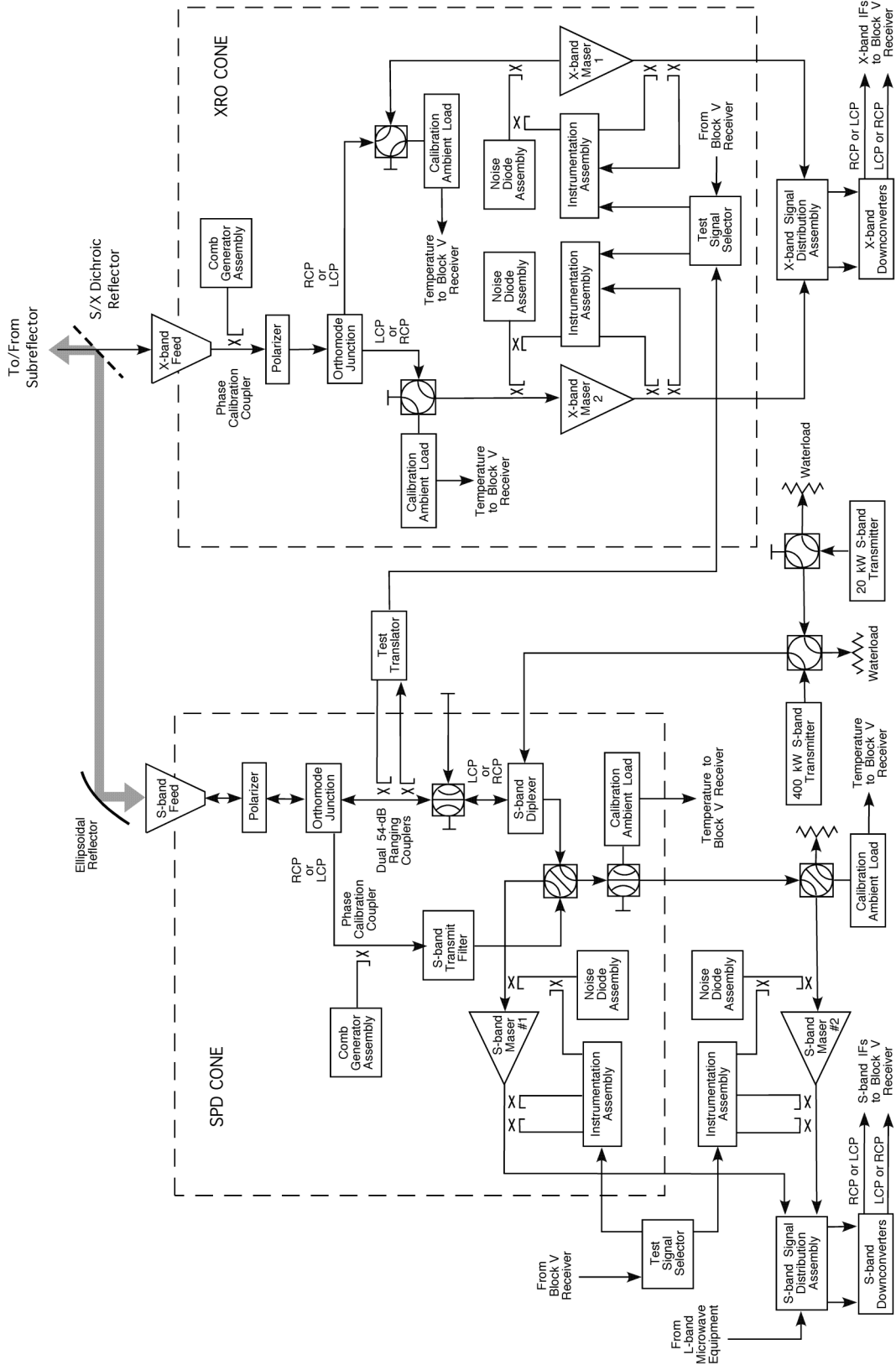
Figure 2.   Functional Block Diagram of DSS 63 Microwave and Transmitter Equipment
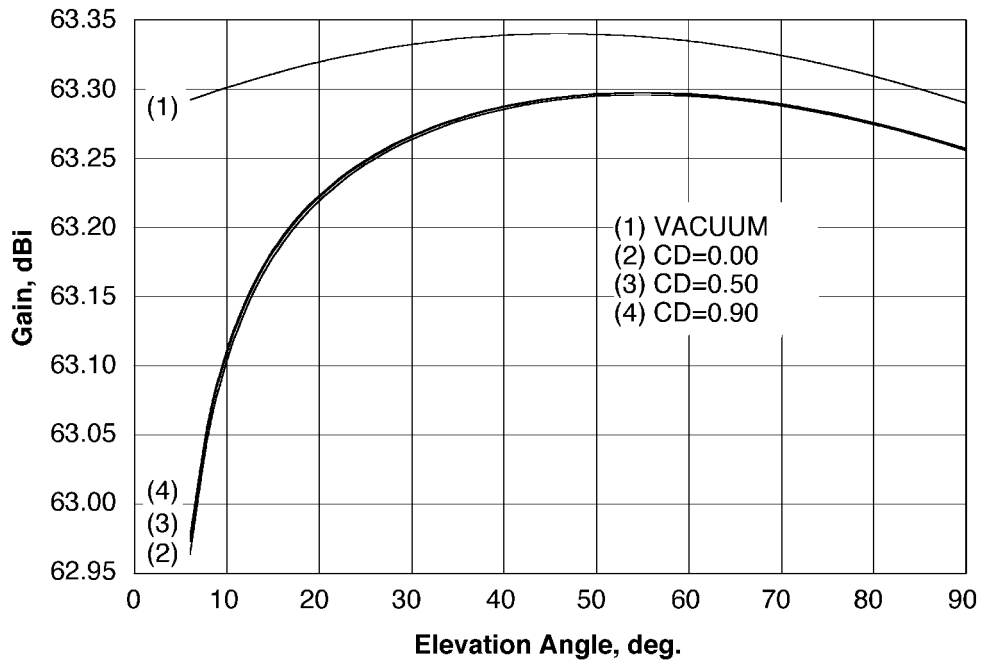
Figure 3. S-Band Receive Gain Versus Elevation Angle, All Stations
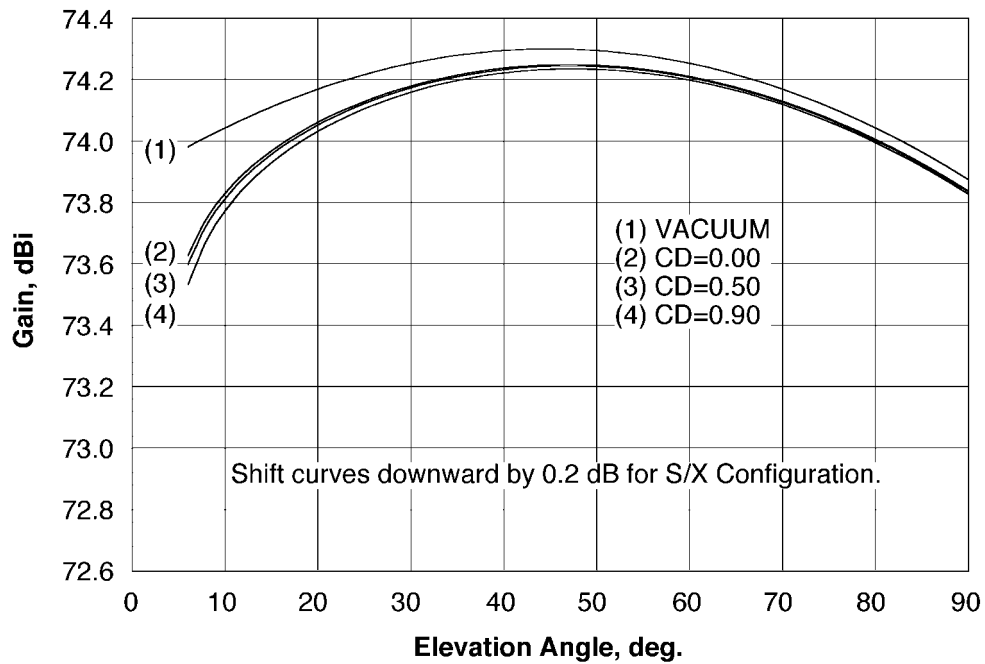
Figure 4. Predicted X-Band Receive Gain Versus Elevation Angle, DSS 14
Antenna, X-Only Configuration (S/X Dichroic Retracted)
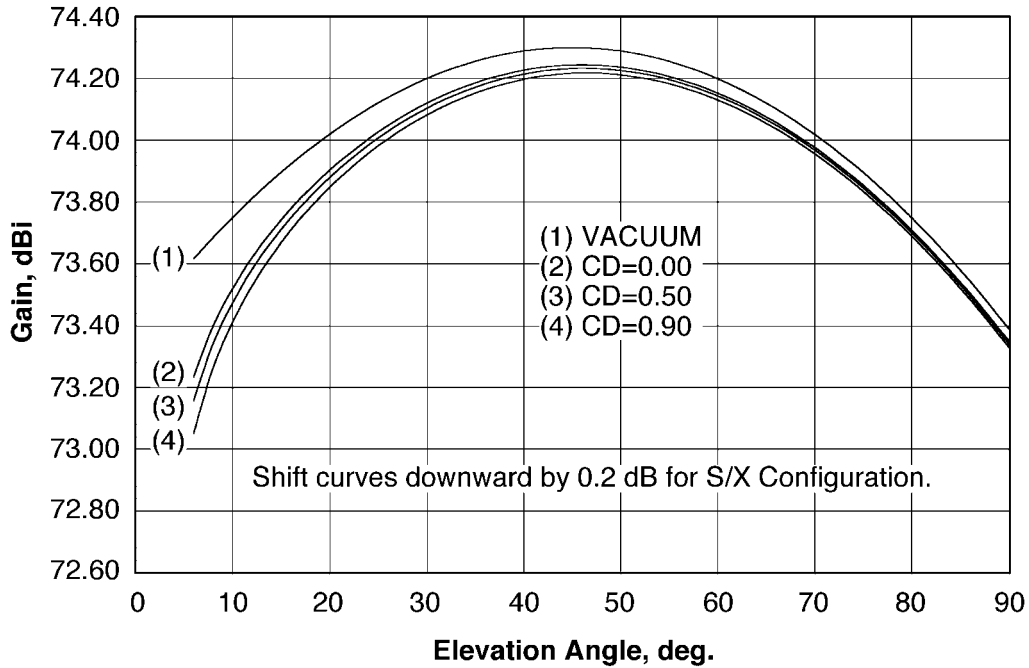
Figure 5. Predicted X-Band Receive Gain Versus Elevation Angle, DSS 43 Antenna, X-Only Configuration (S/X Dichroic Retracted)
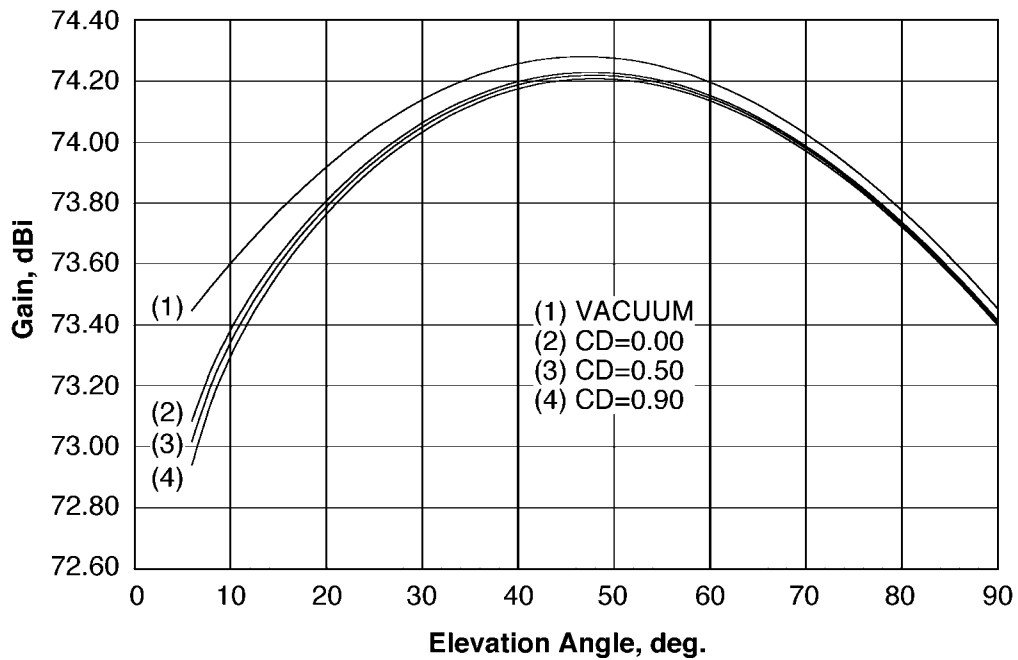
Figure 6.   X-Band Receive Gain Versus Elevation Angle, DSS 63 Antenna
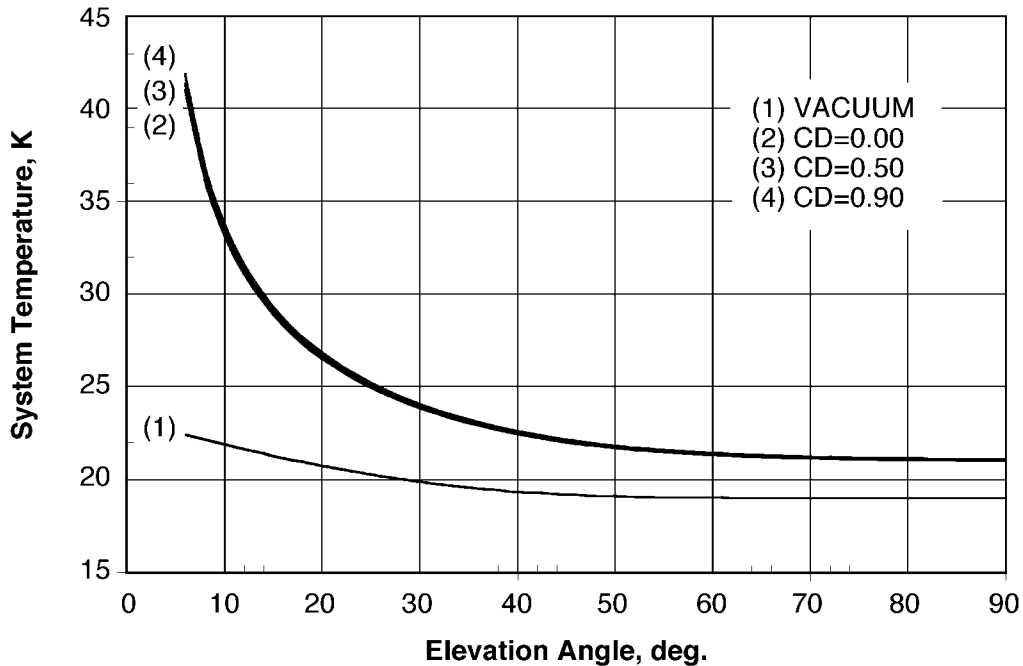
Figure 7. L-Band System Noise Temperature, All Stations
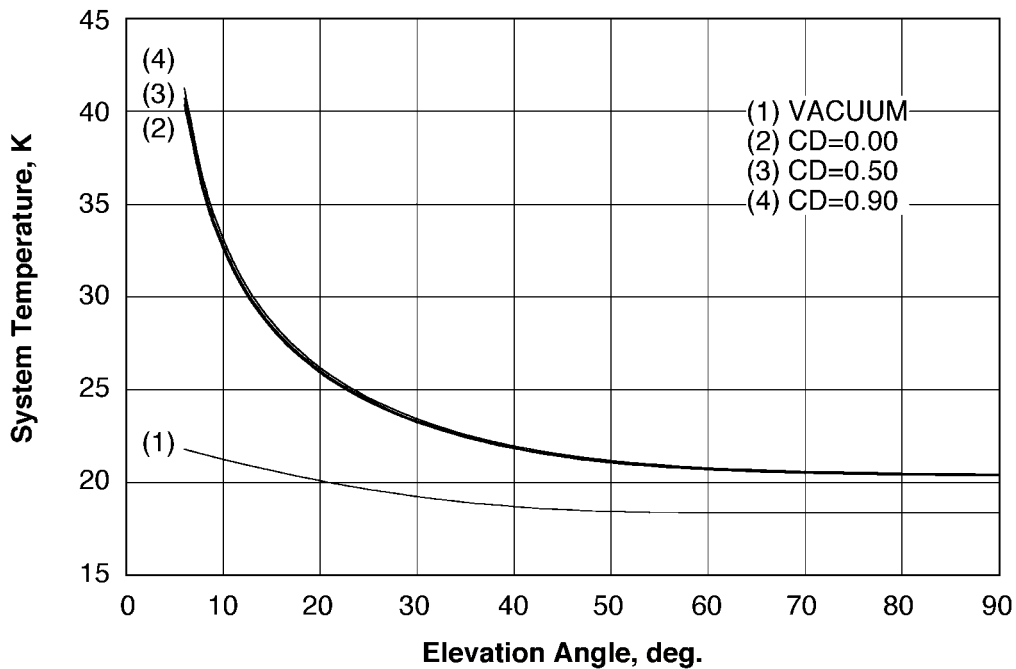
Figure 8. S-Band System Noise Temperature Versus Elevation Angle, DSS 14,
LNA-1, Non-diplexed (See Appendix A for DSS 43 and 63)
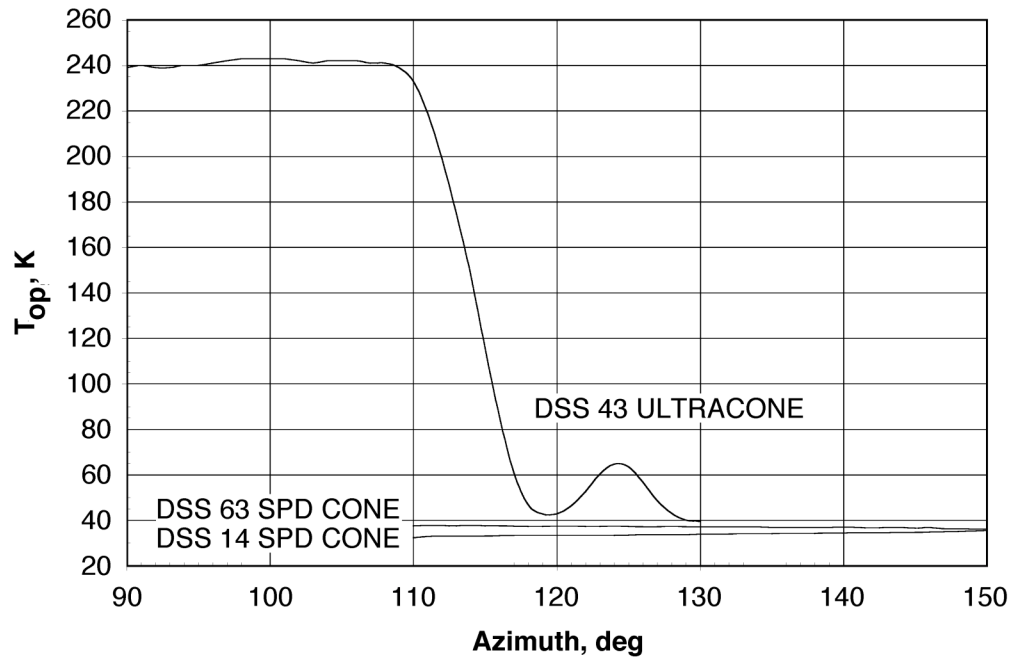
Figure 9.   Eastern Horizon S-Band System Noise Temperature at 6° Elevation Angle
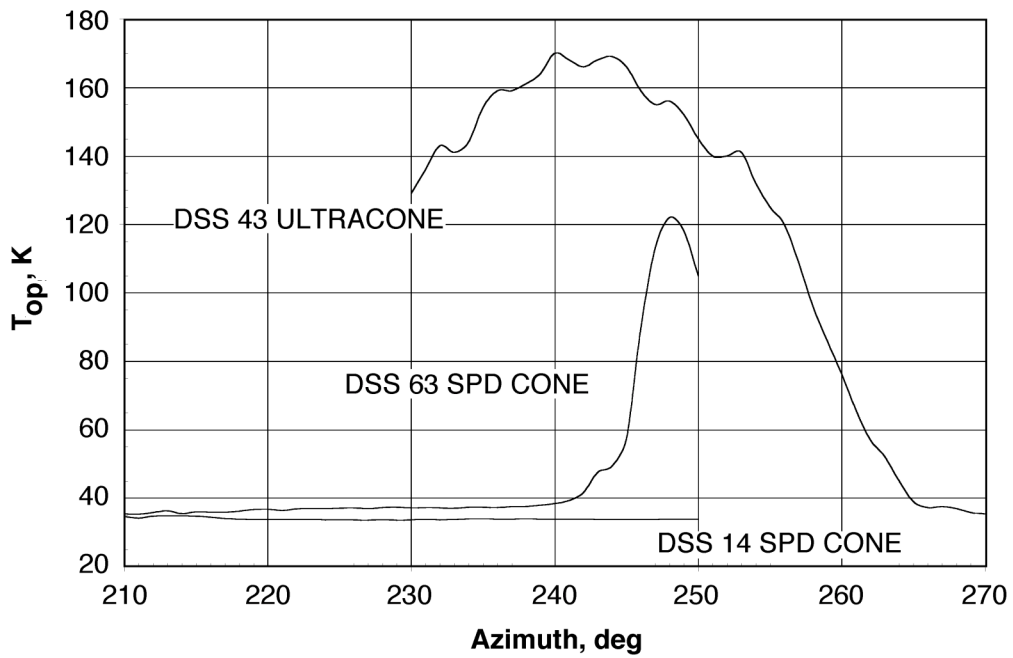
Figure 10. Western Horizon S-Band System Noise Temperature at 6° Elevation Angle
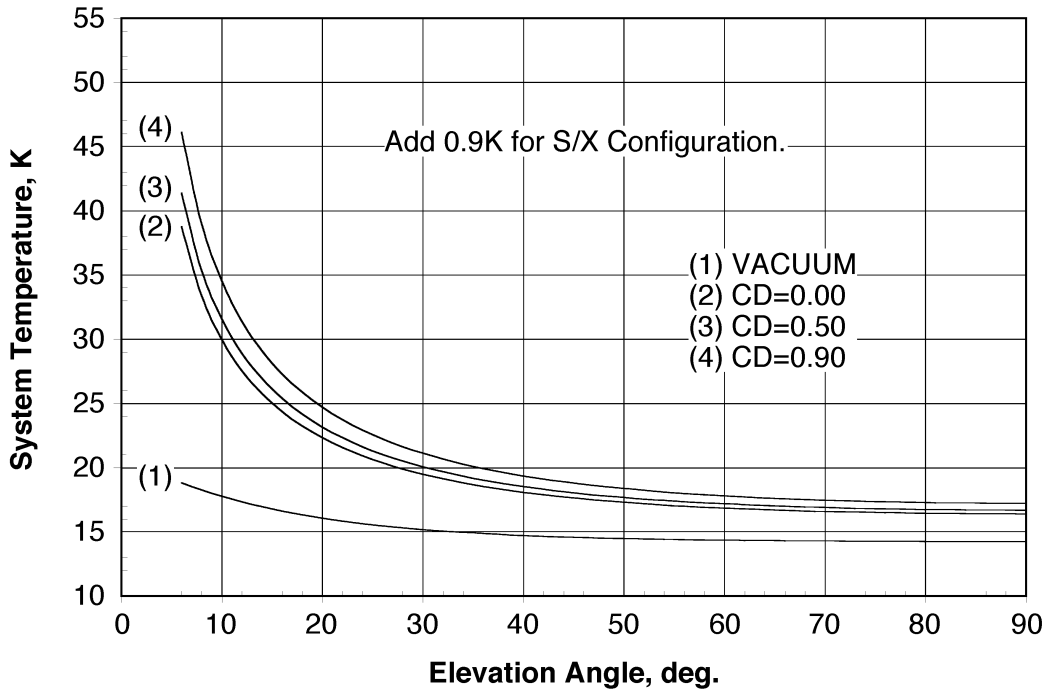
Figure 11. Predicted X-Band System Noise Temperature Versus Elevation Angle,
DSS 14, X-Only Configuration (S/X Dichroic Retracted)
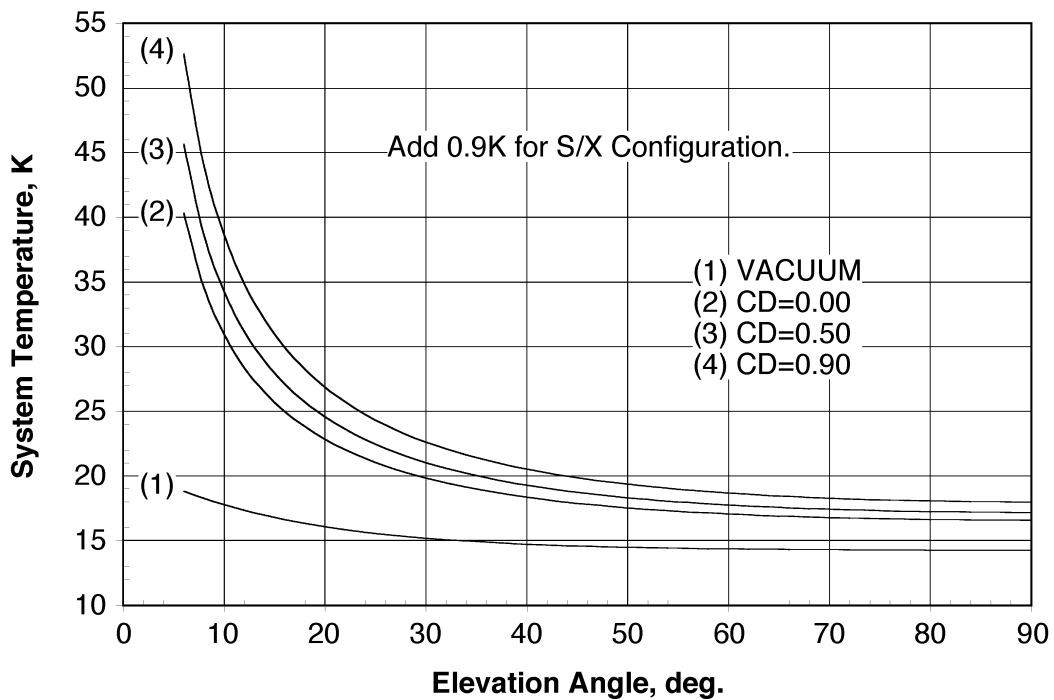
Figure 12. Predicted X-Band System Noise Temperature Versus Elevation Angle,
DSS 43, X-Only Configuration (S/X Dichroic Retracted)
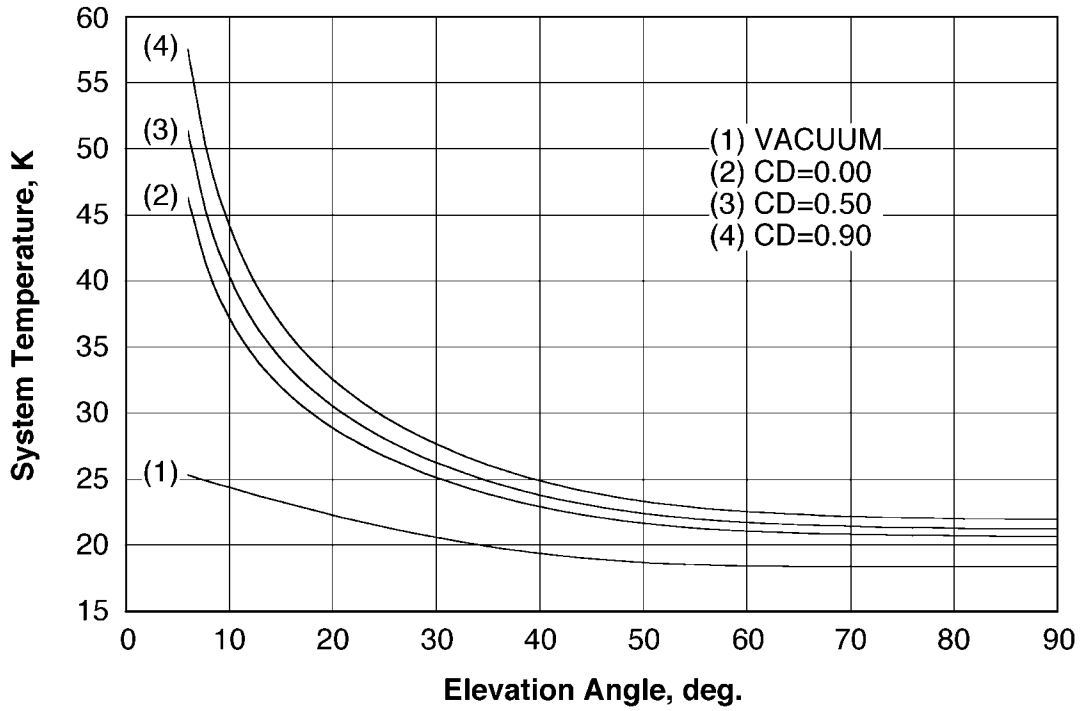
Figure 13. X-Band System Noise Temperature Versus Elevation Angle, DSS 63
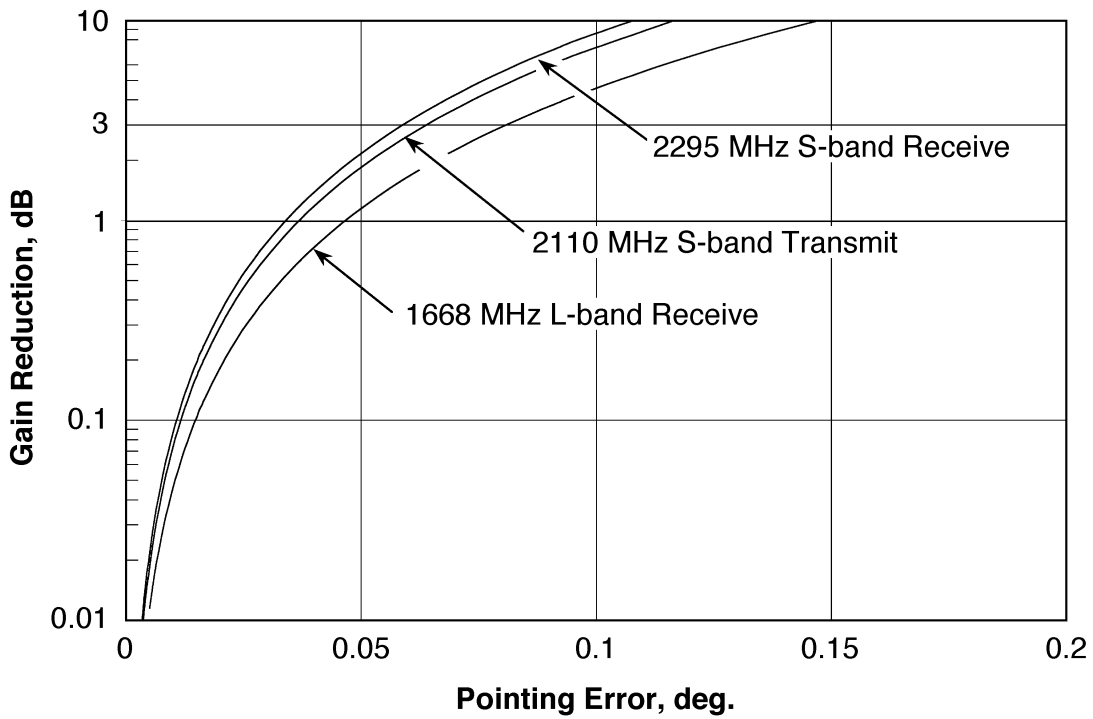
Figure 14. L-Band and S-Band Pointing Loss Versus Pointing Error
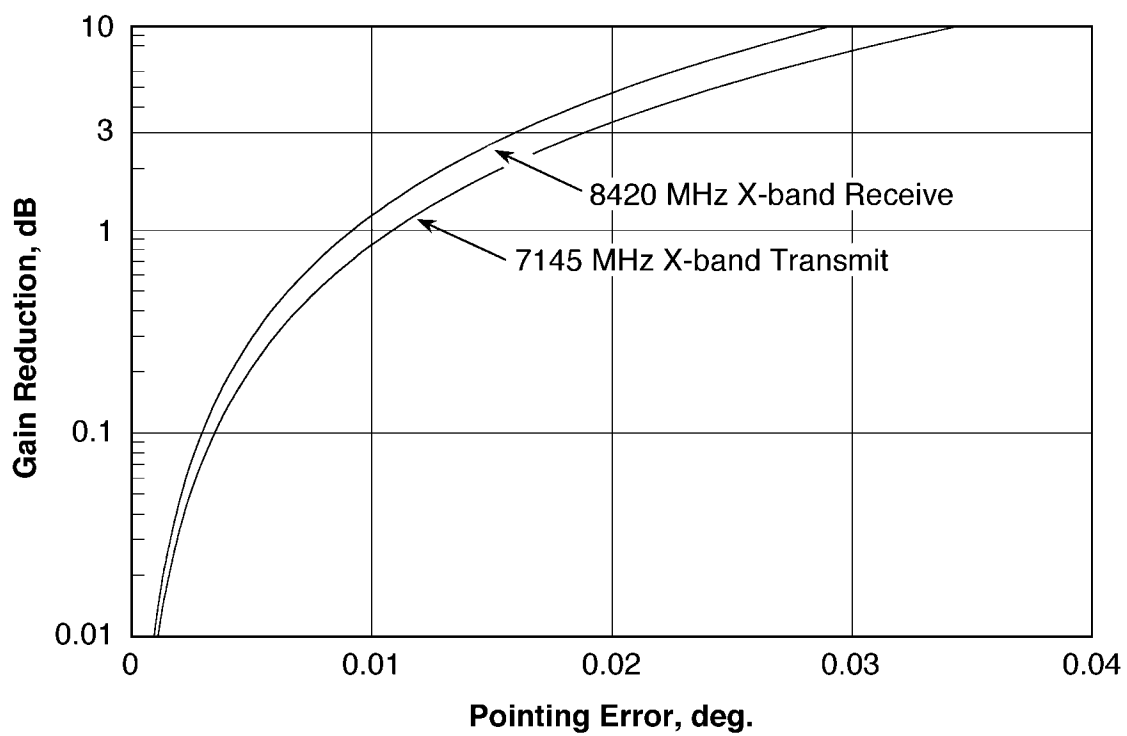
Figure 15. X-Band Pointing Loss Versus Pointing Error

Appendix A
Equations for Modeling

A.1   Equations for Gain Versus Elevation Angle

The following equation can be used to generate L-band receive, S-band transmit, and S-band receive gain versus elevation angle curves for all stations and X-band receive gain versus elevation angle curves for DSS 63. Examples of these curves are shown in Figures 3 and 6. See paragraph 2.1.1.1 for frequency effect modeling and module 105 for atmospheric attenuation at weather conditions other than 0%, 50%, and 90% cumulative distribution.

$$G(\theta) = G_0 - G_1 \left(\cos\gamma - \cos\theta\right)^2 - G_2 \left(\sin\gamma - \sin\theta\right)^2 - \frac{A_{ZEN}}{\sin\theta}, \ \ \text{dBi} \tag{1}$$

where

θ	=	antenna elevation angle (deg.) $6 \le \theta \le 90$
G_0, G_1, G_2, γ	=	parameters from Table A-1
A_{ZEN}	=	zenith atmospheric attenuation, dB, from Table A-2 or from Table 2 in module 105.

The following equation can be used to generate X-band transmit and receive gain versus elevation curves for DSS 14 and DSS 43. Examples of these curves are shown in Figures 4 and 5. See paragraph 2.1.1.1 for frequency effect modeling and module 105 for atmospheric attenuation at weather conditions other than 0%, 50%, and 90% cumulative distribution.

$$G(\theta) = G_0 - G_1 \left(\theta - \gamma\right)^2 - \frac{A_{ZEN}}{\sin\theta}, \ \ \text{dBi} \tag{2}$$

where

θ	=	antenna elevation angle (deg.) $6 \le \theta \le 90$
G_0, G_1, γ	=	parameters from Table A-1
A_{ZEN}	=	zenith atmospheric attenuation from Table A-2 or from Table 2 in module 105, dB.

A.2   *Equations for System Temperature Versus Elevation Angle*

The following equation can be used to generate L-band and S-band system temperature versus elevation angle curves for all stations and X- band system temperature versus elevation angle for DSS 63. Examples of these curves are shown in Figures 7, 8, and 13. See module 105 for atmospheric attenuation at weather conditions other than 0%, 50%, and 90% cumulative distribution.

$$T_{op}(\theta) = T_1 + T_2 e^{\frac{-a}{(90.001-\theta)}} + (255 + 25\,\text{CD})\left(1 - \frac{1}{10^{\frac{A_{ZEN}}{10\sin\theta}}}\right),\ \text{K} \tag{3}$$

where

θ =   antenna elevation angle (deg.), $6 \le \theta \le 90$

T_1, T_2, a =   parameters from Table A-3

CD   =   cumulative distribution used to select A_{ZEN} from Table A-2 or from Table 2 in module 105, $0 \le CD \le 0.99$

A_{ZEN} =   zenith atmospheric attenuation for selected CD from Table A-2 or from Table 2 in module 105, dB.

The following equation can be used to generate X-band system temperature versus elevation curves for DSS 14 and DSS 43. Examples of these curves were shown in Figures 11 and 12. See module 105 for atmospheric attenuation at weather conditions other than 0%, 50%, and 90% cumulative distribution.

$$T_{op}(\theta) = T_1 + T_2 e^{-a\theta} + (255 + 25\,\text{CD})\left(1 - \frac{1}{10^{\frac{A_{ZEN}}{10\sin\theta}}}\right),\ \text{K} \tag{4}$$

where

θ =   antenna elevation angle (deg.), $6 \le \theta \le 90$

T_1, T_2, a =   parameters from A-3

CD   =   cumulative distribution used to select A_{ZEN} from Table A-2 or from Table 2 in module 105, $0 \le CD \le 0.99$

A_{ZEN} =   zenith atmospheric attenuation for selected CD from Table A-2 or from Table 2 in module 105, dB.

A.3 Equation for Gain Reduction Versus Pointing Error

The following equation can be used to generate gain-reduction versus pointing error curves, examples of which are depicted in Figures 14 and 15.

$$\Delta G(\theta) = 10\log\left(e^{\frac{2.773\theta^2}{HPBW^2}} \right), \text{ dBi} \tag{5}$$

where

θ = pointing error (deg.)

$HPBW$ = half-power beamwidth in degrees (from Tables 1 or 2).

Table A-1. Vacuum Component of Gain Parameters

Configuration and Stations	Parameters†				
	G_0 (Transmit)	G_0 (Receive)	G_1	G_2	γ
L-Band, All Stations	—	60.01	0.088	0.104	46.27
S-Band, All Stations	62.7	63.34	0.088	0.104	46.27
X-Band, S/X Configuration*					
DSS 14	72.9	74.1	0.00021	—	45.0
DSS 43	72.9	74.1	0.00045	—	45.0
DSS 63	—	74.28	1.49	1.766	46.83
X-Band, X-Only Configuration*					
DSS 14	72.9	74.3	0.00021	—	45.0
DSS 43	72.9	74.3	0.00045	—	45.0

Notes:

* DSS 14 and DSS 43 X-band parameters are for predicted performance. Model for DSS 14 and DSS 43 X-band performance is different from model used for other frequency bands and for DSS 63. See Equations (1) and (2).

† G_0 values are nominal at the frequency specified in Table 1 or Table 2. Other parameters apply to all frequencies within the same band.

Table A-2. Zenith Atmosphere Attenuation Above Vacuum (A_{ZEN})

Weather Condition†	A_{ZEN}, dB*				
	L-Band	S-Band	X-Band		
	All Stations	All Stations	DSS 14	DSS 43	DSS 63
Vacuum	0.000	0.000	0.000	0.000	0.000
CD = 0.00	0.034	0.034	0.037	0.040	0.038
CD = 0.50	0.033	0.033	0.040	0.048	0.045
CD = 0.90	0.033	0.033	0.047	0.059	0.053

Notes:

* From Table 2 in module 105, L- and S-band values are average for all stations.

† CD = cumulative distribution.

Table A-3. Vacuum Component of System Noise Temperature Parameters

Configuration and Stations	Parameters*		
	T_1	T_2	a
L-Band, All Stations	19.0	101.95	285
S-Band, DSS 14, SPD Cone, Non-diplexed†	13.35	101.95	285
S-Band, DSS 43, SPD Cone, Non-diplexed†	13.75	101.95	285
S-Band, DSS 63, SPD Cone, Non-diplexed†	15.05	101.95	285
S-Band, DSS 14, SPD Cone, Diplexed†	17.65	101.95	285
S-Band, DSS 43, SPD Cone, Diplexed†	14.05	101.95	285
S-Band, DSS 63, SPD Cone, Diplexed†	19.35	101.95	285
S-Band, DSS 43, Ultracone	9.78	101.95	285
X-Band, DSS 14, X-Only Configuration	14.2	6.8	0.065
X-Band, DSS 14, S/X Configuration	15.1	6.8	0.065
X-Band, DSS 43, X-Only Configuration	14.56	6.4	0.07
X-Band, DSS 43, S/X Configuration	15.78	10.0	0.10
X-Band, DSS 63, S/X Configuration	18.39	122.43	241.5

Notes:

- Model for DSS 14 and DSS 43 X-band System Noise Temperature, Equation (4), is different from model used at other frequency bands and for DSS 63, Equation (3).

† S-band noise temperature parameters are for LNA 1. Increase T_1 by 5.0 K for LNA-2.

103
34-m HEF Subnet
Telecommunications Interfaces

Effective November 30, 2000

Document Owner:

Approved by:

S.D.Slobin   12/11/00

_____   _____
S. D. Slobin   Date
Antenna System Engineer

A.J.Freiley   12-13-06

_____   _____
A. J. Freiley   Date
Antenna Product Domain Service
System Development Engineer

Released by:

[Signature on file in TMOD Library]
_____
TMOD Document Release   Date

Change Log

Rev	Issue Date	Affected Paragraphs	Change Summary
Initial	1/15/2001	All	All

Note to Readers

There are two sets of document histories in the 810-005 document, and these histories are reflected in the header at the top of the page. First, the entire document is periodically released as a revision when major changes affect a majority of the modules. For example, this module is part of 810-005, Revision E. Second, the individual modules also change, starting as an initial issue that has no revision letter. When a module is changed, a change letter is appended to the module number on the second line of the header and a summary of the changes is entered in the module's change log.

This module supersedes TCI-30 in 810-005, Rev. D.

Contents

Illustrations

Tables

1   Introduction

1.1   Purpose

This module provides the performance parameters for the Deep Space Network (DSN) high-efficiency (HEF) 34-meter antennas that are necessary to perform the nominal design of a telecommunications link. It also summarizes the capabilities of these antennas for mission planning purposes and for comparison with other ground station antennas.

1.2   Scope

The scope of this module is limited to providing those parameters that characterize the RF performance of the 34-meter HEF antennas. The parameters do not include effects of weather, such as reduction of system gain and increase in system noise temperature, that are common to all antenna types. These are discussed in module 105, Atmospheric and

Environmental Effects. This module also does not discuss mechanical restrictions on antenna performance that are covered in module 302, Antenna Positioning.

2 General Information

The DSN 34-m Antenna Subnet contains three 34-meter diameter HEF antennas. These antennas employ an elevation over azimuth (AZ-EL) axis configuration, a single dual-frequency feedhorn, and a dual-shaped reflector design. One antenna (DSS 15) is located at Goldstone, California; one (DSS 45) near Canberra, Australia; and one (DSS 65) near Madrid, Spain. The precise station locations are shown in Module 301, Coverage and Geometry.

A block diagram of the 34-meter HEF microwave and transmitter equipment is shown in Figure 1. An orthomode junction for X-band is employed that permits simultaneous right-circular polarization (RCP) or left-circular polarization (LCP) operation. For listen-only operation or when transmitting and receiving on opposite polarizations, the low-noise path (orthomode upper arm) is used for reception. If the spacecraft receives and transmits simultaneously with the same polarization, the diplexed path must be used and the noise temperature is higher. The labyrinth used to extract the S-band signal from the feed also provides simultaneous RCP and LCP operation; however, the presence of only one S-band low noise amplifier (LNA) and receiver channel limits the use to selectable RCP or LCP.

In addition to spacecraft tracking, the DSN 34-m Antenna Subnet is also used for very-long baseline interferometry and radio-source catalog maintenance.

2.1 Telecommunications Parameters

The significant parameters of the 34-meter HEF antennas that influence telecommunications link design are listed in Tables 1 and 2. Variations in these parameters that are inherent in the design of the antennas are discussed below. Other factors that degrade link performance are discussed in modules 105 (Atmospheric and Environmental Effects) and 106 (Solar Corona and Wind Effects).

2.1.1 Antenna Gain Variation

The antenna gains in Tables 1 and 2 do not include the effect of atmospheric attenuation and should be regarded as vacuum gain at the specified reference point.

2.1.1.1 Frequency Effects

Antenna gains are specified at the indicated frequency (f_0). For operation at higher frequencies in the same band, the gain (dBi) must be increased by $20 \log (f/f_0)$. For operation at lower frequencies in the same band, the gain must be reduced by $20 \log (f/f_0)$.

2.1.1.2 Elevation Angle Effects

Structural deformation causes a reduction in gain whenever the antenna is operated at an elevation angle other than the angle where the reflector panels were aligned. The

effective gain of the antenna is reduced also by atmospheric attenuation, which is a function of elevation. Figures 2 through 5 show the estimated gain versus elevation angle for the hypothetical vacuum condition (structural deformation only) and with 0%, 50%, and 90% weather conditions, designated as CD (cumulative distribution) = 0.00, 0.50, and 0.90. A CD of 0.00 (0%) means the minimum weather effect (exceeded 100% of the time). A CD of 90.0 (90%) means that effect which is exceeded only 10% of the time. Qualitatively, a CD of 0.00 corresponds to the driest condition of the atmosphere; a CD of 0.50 corresponds to humid or very light clouds; and 0.90 corresponds to very cloudy, but with no rain. A CD of 0.25 corresponds to average clear weather and often is used when comparing gains of different antennas. Comprehensive S-band and X-band weather-effects models (for weather conditions up to 99% cumulative distribution) are provided in module 105 for detailed design control table use. Equations and parameters for the curves in Figures 2 through 5 are provided in Appendix A.

2.1.1.3 *Wind Loading*

The gain reduction at X-band due to wind loading is listed in Table 3. The tabular data are for structural deformation only and presume that the antenna is maintained on-point by conical scan (CONSCAN, discussed in module 302) or an equivalent process. In addition to structural deformation, wind introduces a pointing error that is related to the antenna elevation angle, the angle between the antenna and the wind, and the wind speed. The effects of pointing error are discussed below. Cumulative probability distributions of wind velocity at Goldstone are given in module 105.

2.1.2 *System Noise Temperature Variation*

The operating system temperature (T_{op}) varies as a function of elevation angle due to changes in the path length through the atmosphere and ground noise received by the sidelobe pattern of the antenna. Figures 6 through 10 show the combined effects of these factors in a hypothetical vacuum (no atmosphere) condition and with the three weather conditions described above. The equations and parameters for these curves are provided in Appendix A of this module.

The system noise temperature values in Table 2 include a contribution due to 25% weather that must be subtracted for comparison with antennas that are specified without atmosphere (hypothetical vacuum). Table 4 provides adjustments to the 25% weather operating system temperature that were calculated using the weather models in module 105.

When two low-noise amplifiers (LNAs) are available for use, the amplifier in the lowest noise configuration is designated as LNA-1. Under some conditions, LNA-2 may be used, and the higher noise temperature values apply.

2.1.3 *Pointing Accuracy*

Figures 11 and 12 show the effects of pointing error on effective transmit and receive gain of the antenna. These curves are Gaussian approximations based on measured and predicted antenna beamwidths. Data have been normalized to eliminate elevation and wind-loading effects. The equations used to derive the curves are provided in Appendix A.

2.2 *Recommended Minimum Operating Carrier Signal Levels*

Table 5 provides the recommended minimum operating carrier-signal levels for selected values of receiver tracking-loop bandwidth (B_l). These levels provide a signal-to-noise ratio of 10 dB in the carrier-tracking loop, based on the nominal zenith system temperatures given in Table 2 and assuming 25% weather.

3 *Proposed Capabilities*

The following paragraph discusses capabilities that have not yet been implemented by the DSN but have adequate maturity to be considered for spacecraft mission and equipment design. Telecommunications engineers are advised that any capabilities discussed in this section cannot be committed to except by negotiation with the Telecommunications and Mission Operations Directorate (TMOD) Plans and Commitments Program Office.

3.1 *S-Band LNA Enhancement*

The existing S-band high-electron-mobility transistor (HEMT) LNAs at DSS 15 and DSS 45 and the cooled field-effect transistor (FET) LNA at DSS 65 are in the process of being replaced with HEMT amplifiers incorporating a cryogenically cooled input filter. The result will be a reduction in S-band system temperature (T_{op}) at all HEF stations to 26 ± 2 K near zenith, assuming a 25% average clear atmosphere.

Table 1. X-Band Transmit Characteristics

Parameter	Value	Remarks
ANTENNA		
Gain at 7145 MHz (dBi)	67.1 ±0.2	At gain set elevation angle, referenced to feedhorn aperture for matched polarization; no atmosphere included
Transmitter Waveguide Loss (dB)	0.25 ±0.05	20-kW transmitter output terminal (waterload switch) to feedhorn aperture
Half-Power Beamwidth (deg)	0.0777 ±0.004	Angular width (2-sided) between half-power points at specified frequency
Polarization	RCP or LCP	One polarization at a time, remotely selected
Ellipticity (dB)	1.0 (max)	Peak-to-peak axial ratio defined as the ratio of peak-to-trough received voltages with a rotating linearly polarized source and the feed configured as a circularly (elliptically) polarized receiving antenna
Pointing Loss (dB)		
Angular	See module 302	Also see Figure 12
CONSCAN	0.1	X-band CONSCAN reference set for 0.1 dB loss
EXCITER AND TRANSMITTER		
RF Power Output (dBm)	73.0, +0.0, −1.0	Referenced to 20-kW transmitter output terminal (waterload switch). Settability is limited to 0.25 dB by measurement equipment precision
Power output varies across the bandwidth and may be as much as 1 dB below nominal rating. Performance will also vary from tube to tube. Normal procedure is to run the tubes saturated, but unsaturated operation is also possible. The point at which saturation is achieved depends on drive power and beam voltage. The 20-kW tubes are normally saturated for power levels greater than 60 dBm (1 kW). Minimum power out of the 20-kW tubes is about 53 dBm (200 W). Efficiency of the tubes drops off rapidly below nominal rated output.		
EIRP (dBm)	139.9, +0.2, −1.0	

Table 1. X-Band Transmit Characteristics (Continued)

Parameter	Value	Remarks
EXCITER AND TRANSMITTER (Continued)		
Frequency Range Covered (MHz)	7145 to 7190	
Instantaneous 1-dB Bandwidth (MHz)	45	
Coherent with Deep Space S-Band D/L Allocation	7151.9–7177.3	240/749 turnaround ratio
Coherent with Deep Space S-Band D/L Allocation	7151.9–7188.9	880/749 turnaround ratio
Tunability (Hz)		At transmitter output frequency
Phase Continuous Tuning Range	2.0 MHz	
Maximum Tuning Rate	±12.1 kHz/s	
Frequency Error	0.012 Hz	Average over 100 ms with respect to frequency specified by predicts
Ramp Rate Error	0.001 Hz/s	Average over 4.5 s with respect to rate calculated from frequency predicts
Stability		At transmitter output frequency
Output Power Variation (dB)		Across frequency band over 12-h period
Saturated Drive	0.25	
Unsaturated Drive	≤1.0	
Group Delay Stability (ns)	≤1.0	Ranging modulation signal path over 12-h period (see module 203)
Frequency Stability		Allan deviation
1 s	3.3×10^{-13}	
10 s	5.2×10^{-14}	
1000–3600 s	3.1×10^{-15}	

Table 1. X-Band Transmit Characteristics (Continued)

Parameter	Value	Remarks
Spurious Output (dB)		Below carrier
1–10 Hz	−50	
10 Hz–1.5 MHz	−60	
1.5 MHz–8 MHz	−45	
2nd Harmonic	−75	
3rd, 4th & 5th Harmonics	−60	

Table 2. S- and X-Band Receive Characteristics

Parameter	Value	Remarks
ANTENNA		
Gain (dBi)		At gain set point (peak of gain versus elevation curve). See Figures 2–5 for elevation dependency. Tolerances have triangular PDF.
S-Band (2295 MHz)	56.0 ±0.25	Referenced to LNA input terminal (includes feedline loss) for matched polarization, no atmosphere included
X-Band (8420 MHz)	68.3 ±0.2	Referenced to maser LNA input terminal (includes feedline loss), non-diplexed (low noise) path, for matched polarization, no atmosphere included
	68.1 ±0.2	Referenced to maser LNA input terminal (includes feedline loss), diplexed path, for matched polarization, no atmosphere included
	68.2 ±0.2	Referenced to wideband HEMT input terminal (includes feedline loss), non-diplexed path, for matched polarization, no atmosphere included
	68.0 ±0.2	Referenced to wideband HEMT input terminal (includes feedline loss), diplexed path, for matched polarization, no atmosphere included

Table 2. S- and X-Band Receive Characteristics (Continued)

Parameter	Value	Remarks
ANTENNA (Continued)		
Half-Power Beamwidth (deg.)		Angular width (2-sided) between half-power points at specified frequency
S-Band	0.242 ±0.020	
X-Band	0.0660 ±0.004	
Polarization		Remotely selected
S-Band	RCP or LCP	
X-Band	RCP or LCP	Same or opposite from transmit polarization
Ellipticity (dB)	0.7	Peak-to-peak voltage axial ratio, RCP and LCP. See definition in Table 1.
S-Band	≤1.0	
X-Band	≤0.8	
Pointing Loss (dB, 3 sigma)		
Angular	See module 302	Also see Figures 11 and 12
CONSCAN		
S-Band	0.03	Loss at S-band when using X-band CONSCAN reference set for 0.1 dB loss at X-band
	0.1	Recommended value when using S-band CONSCAN reference
X-Band	0.1	Recommended value when using X-band CONSCAN reference
RECEIVER		
Frequency Ranges Covered (MHz))		
S-Band	2200–2300 MHz	
X-Band		
Telemetry	8400–8500 MHz	
VLBI	8200–8600 MHz	Wideband HEMT LNA

Table 2. S- and X-Band Receive Characteristics (Continued)

Parameter	Value	Remarks
RECEIVER (contd)		
Recommended Maximum Signal Power (dBm)	-90.0	At LNA input terminal
Recommended Minimum Signal Power (dBm)	See Table 5	
System Noise Temperature (K)		For average clear weather (25% weather condition) near zenith. See Figures 6–9 for elevation dependency. See Table 4 for adjustments to remove atmospheric contribution.
S-Band (2200–2300 MHz)	38.1 (DSS 15, 45) 44.1 (DSS 65)	With respect to LNA input terminal.
X-Band (8400–8600 MHz)		
DSS 15	19.8 ±2	With respect to maser input terminal, non-diplexed path.
DSS 45	20.2 ±2	
DSS 65	20.1 ±2	
DSS 15	28.9 ±2	With respect to maser input terminal, diplexed path.
DSS 45	29.3 ±2	
DSS 65	29.2 ±2	
DSS 15	44.8 ±2	With respect to wideband HEMT input terminal, diplexed path.
DSS 45	45.2 ±2	
DSS 65	45.1 ±2	
(8200–8600 MHz)		
DSS 15	35.7 ±2	With respect to wideband HEMT input terminal, non-diplexed path.
DSS 45	36.1 ±2	
DSS 65	36.0 ±2	
Carrier Tracking Loop Noise B/W (Hz)	0.25–200	Effective one-sided, noise-equivalent carrier loop bandwidth (B_L)

Table 3. Gain Reduction Due to Wind Loading, 34-m HEF Antennas

Wind Speed		X-Band Gain Reduction (dB)*
(km/hr)	(mph)	
16	10	0.2
48	30	0.3
72	45	0.4

* Assumes antenna is maintained on-point using CONSCAN or equivalent
closed-loop pointing technique.
S-band gain reduction is negligible for wind speeds up to 72 km/hr (45 mph).
Worst case, with most adverse wind orientation.

Table 4. System Noise Temperature Contributions due to 25% Weather

Location	Noise Temperature Contribution (K)†	
	S-band	X-band
Goldstone (DSS 15)	1.929	2.292
Canberra (DSS 45)	2.109	2.654
Madrid (DSS 65)	2.031	2.545

† Calculated using weather model in module 105.

Table 5. Recommended Minimum Operating Carrier Signal Levels (dBm)†

Band, LNA, and Configuration	Receiver Effective Noise Bandwidth (B_L) (Hz)				
	0.25	1.0	2.0	20.0	200
S-Band LNA					
DSS 15 and DSS 45 (HEMT)	−178.8	−172.8	−169.8	−159.8	−149.8
DSS 65 (Cooled FET)	−178.2	−172.2	−169.1	−159.1	−149.1
X-Band Primary LNA (MASER)					
DSS 15 Non-Diplexed	−181.7	−175.6	−172.6	−162.6	−152.6
DSS 45 Non-Diplexed	−181.6	−175.5	−172.5	−162.5	−152.5
DSS 65 Non-Diplexed	−181.6	−175.6	−172.6	−162.6	−152.6
DSS 15 Diplexed	−180.0	−174.0	−171.0	−161.0	−151.0
DSS 45 Diplexed	−180.0	−173.9	−170.9	−160.9	−150.9
DSS 65 Diplexed	−180.0	−173.9	−170.9	−160.9	−150.9
X-Band Backup LNA (W/B HEMT)					
DSS 15 Non-Diplexed	−179.1	−173.1	−170.1	−160.1	−150.1
DSS 45 Non-Diplexed	−179.0	−173.0	−170.0	−160.0	−150.0
DSS 65 Non-Diplexed	−179.1	−173.0	−170.0	−160.0	−150.0
DSS 15 Diplexed	−178.1	−172.1	−169.1	−159.1	−149.1
DSS 45 Diplexed	−178.1	−172.0	−169.0	−159.0	−149.0
DSS 65 Diplexed	−178.1	−172.1	−169.0	−159.0	−149.0

†   Levels are referenced to LNA input terminals with nominal zenith system noise including 25% weather.

*   Bandwidths are centered about the received carrier.
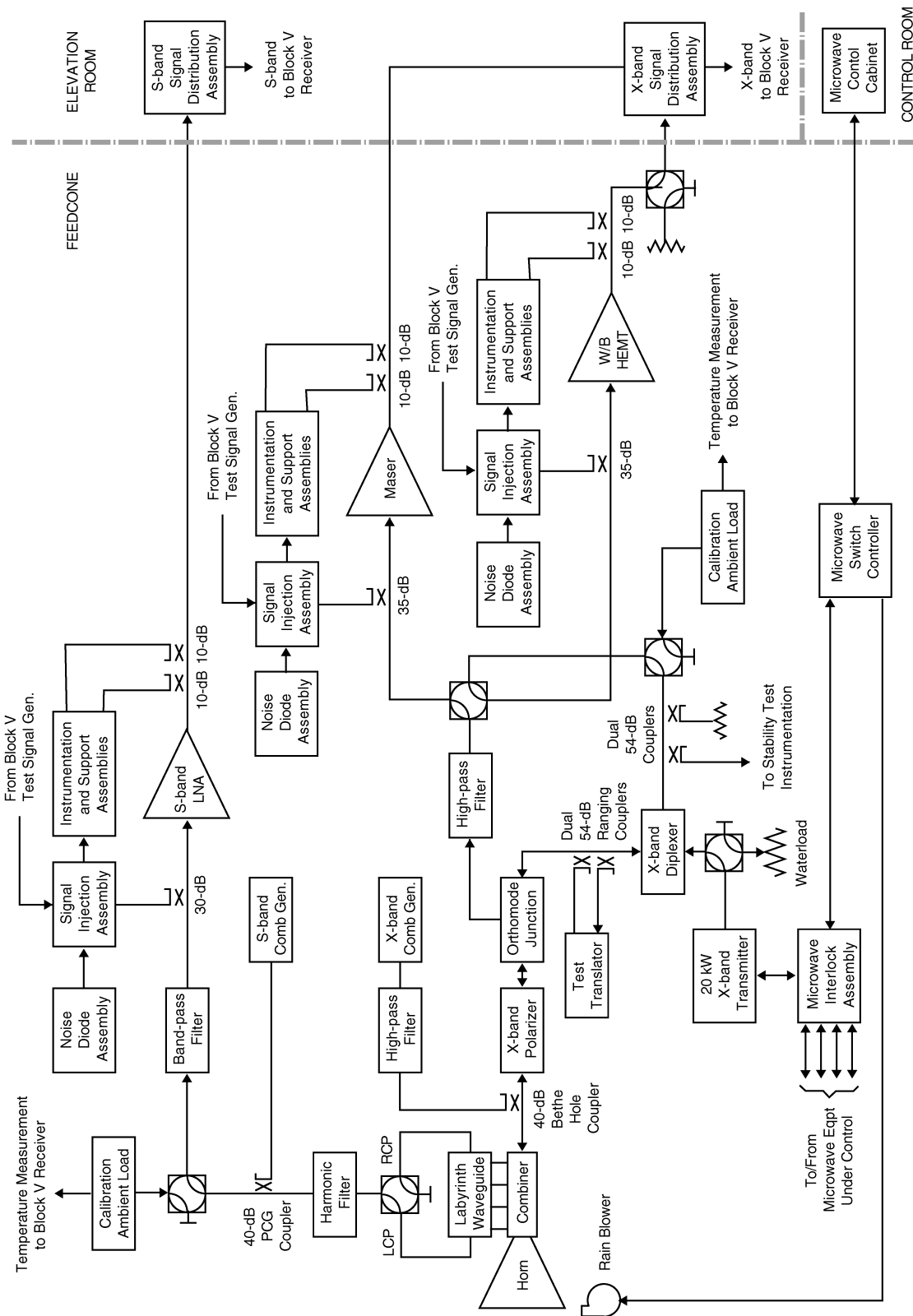
Figure 1. Functional Block Diagram of Microwave and Transmitter Subsystem
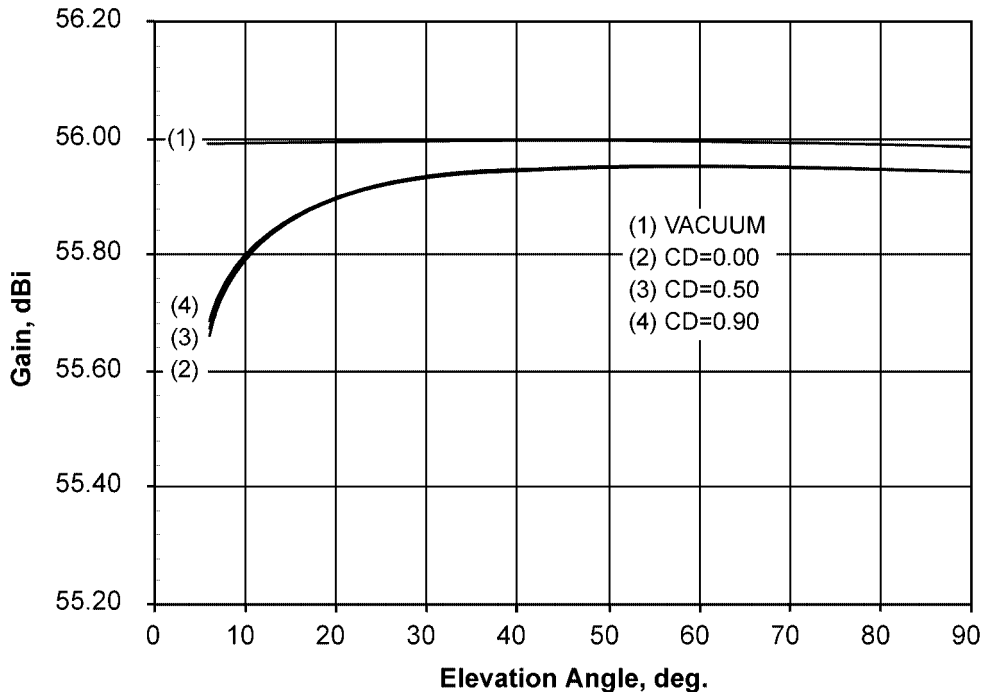
Figure 2.   S-Band Receive Gain Versus Elevation Angle, All HEF Antennas
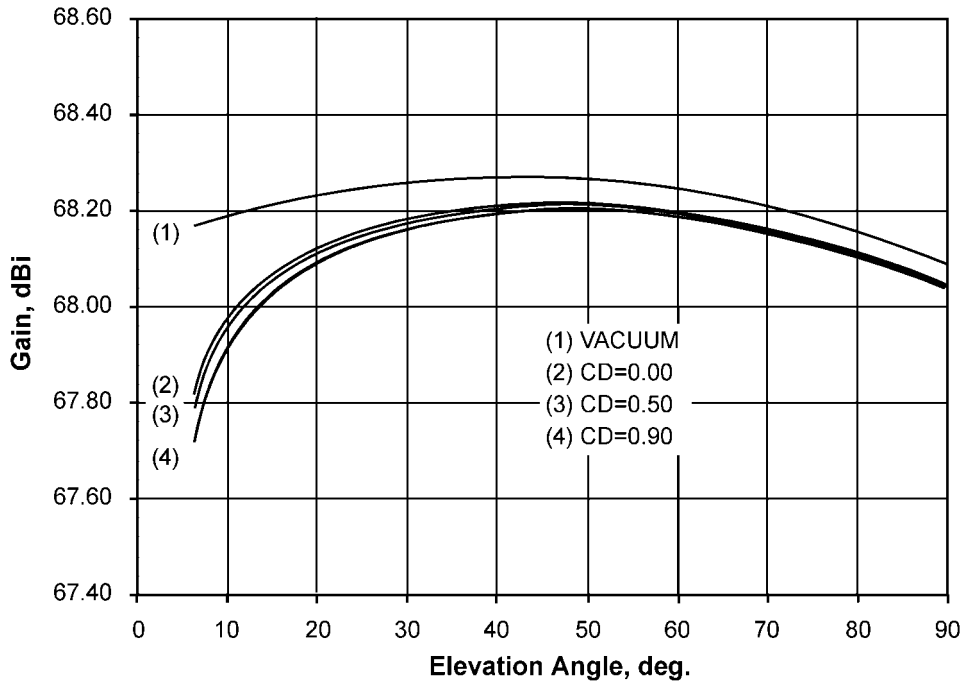
Figure 3.   X-Band Receive Gain Versus Elevation Angle, DSS 15 Antenna,
Non-Diplexed Path, Maser LNA Input
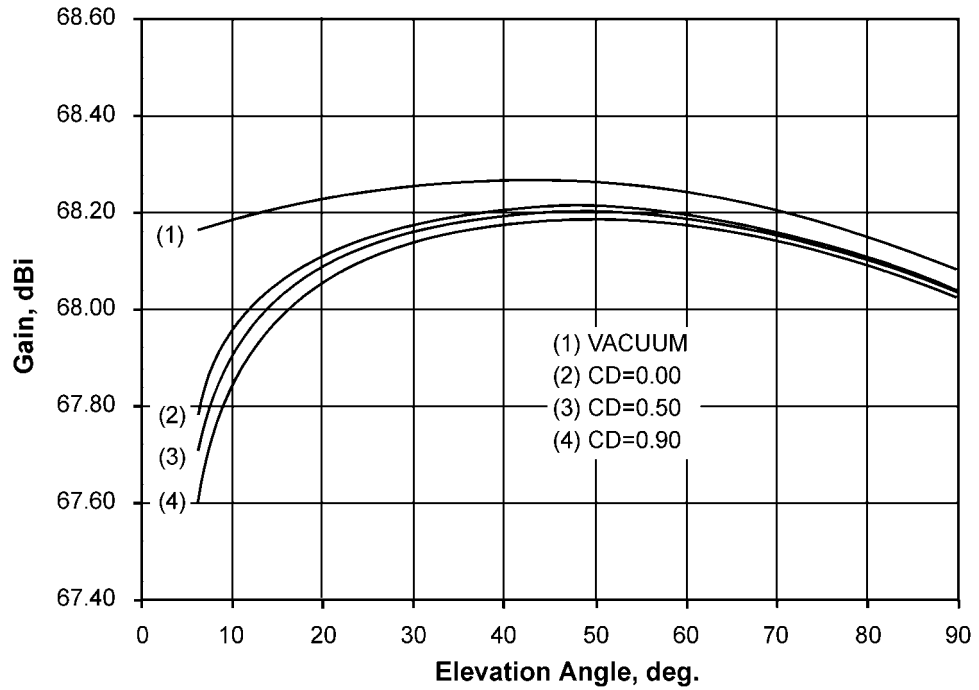
Figure 4.   X-Band Receive Gain Versus Elevation Angle, DSS 45 Antenna, Non-Diplexed Path, Maser LNA Input
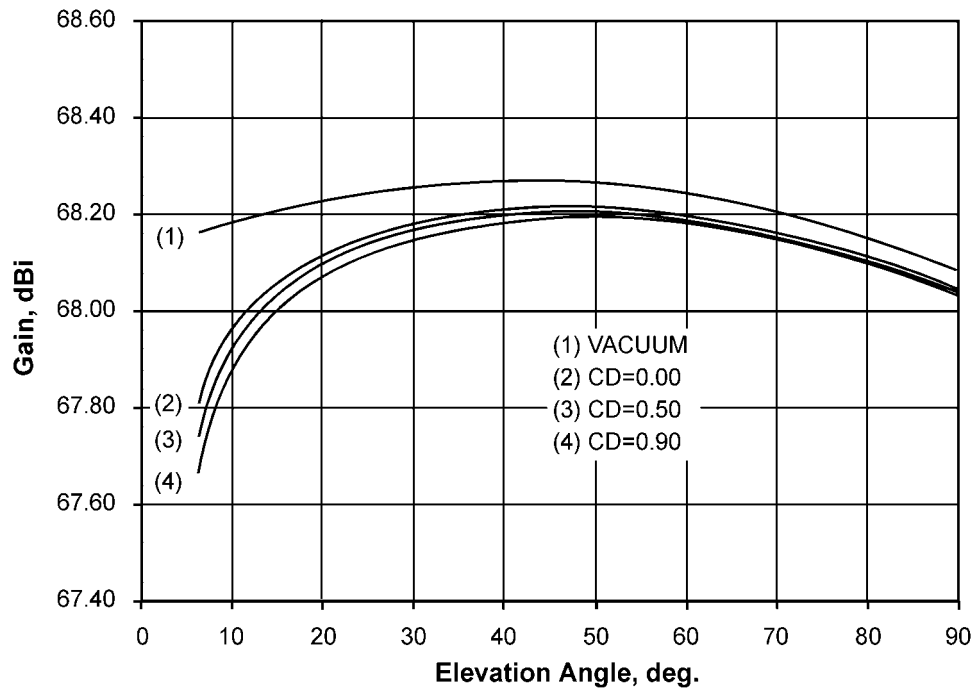
Figure 5.   X-Band Receive Gain Versus Elevation Angle, DSS 65 Antenna, Non-Diplexed Path, Maser LNA Input
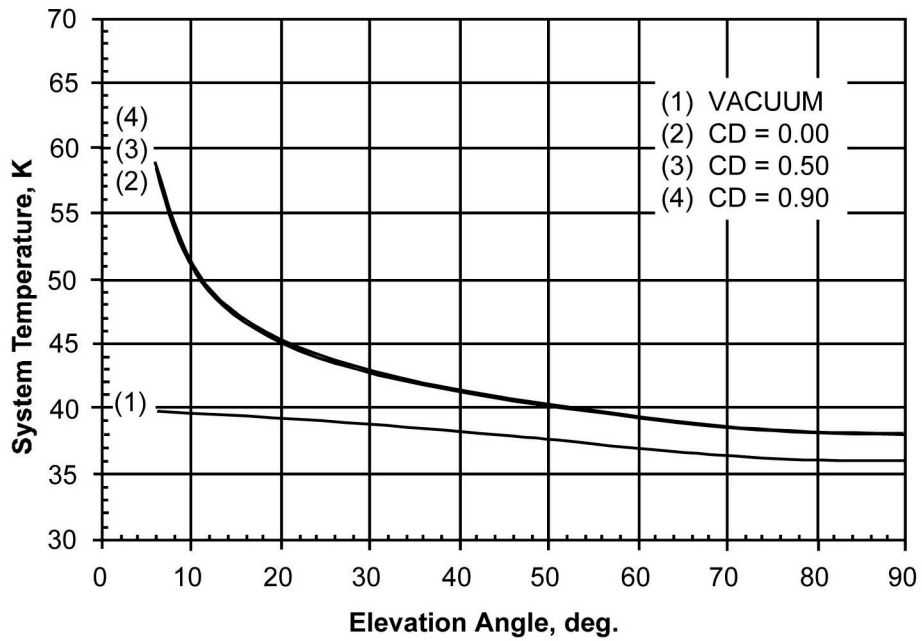
Figure 6.   S-Band System Temperature Versus Elevation Angle, Average
for DSS 15 and DSS 45 Antennas at LNA Input
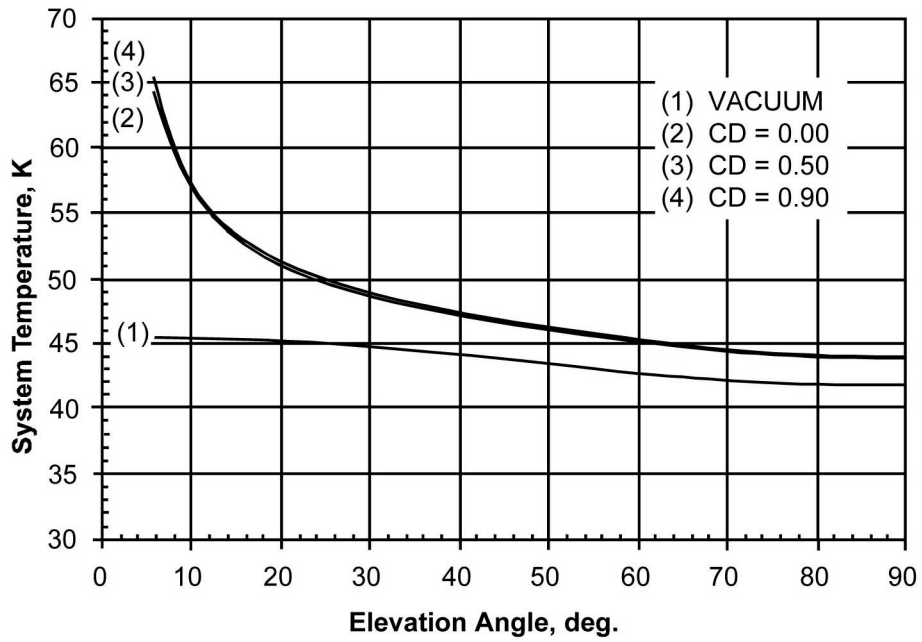
Figure 7.   S-Band System Temperature Versus Elevation Angle, DSS 65
at LNA Input
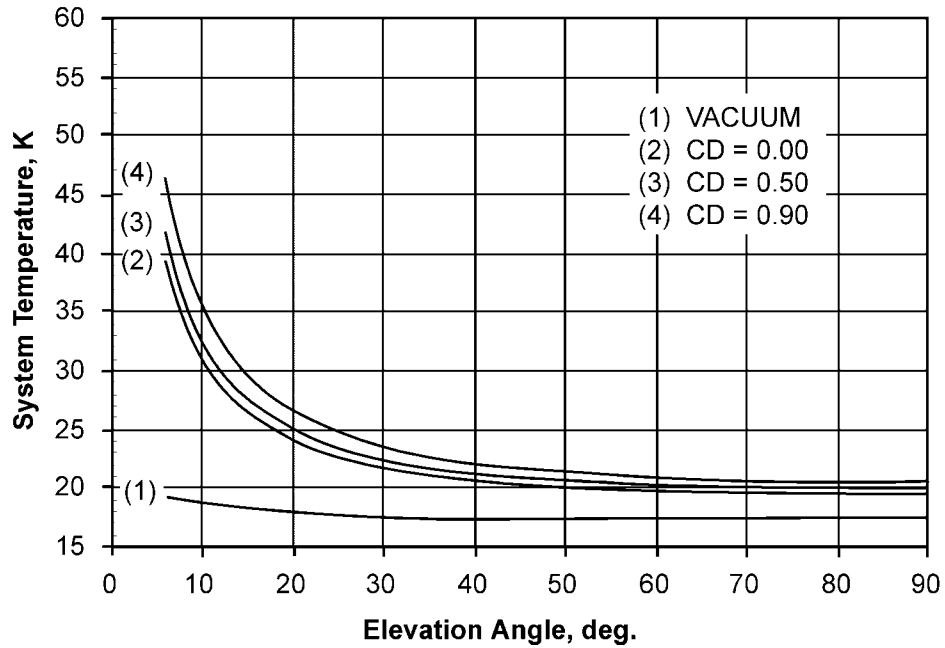
Figure 8.   X-Band System Temperature Versus Elevation Angle, DSS 15
Antenna, Non-Diplexed Path, Maser LNA Input
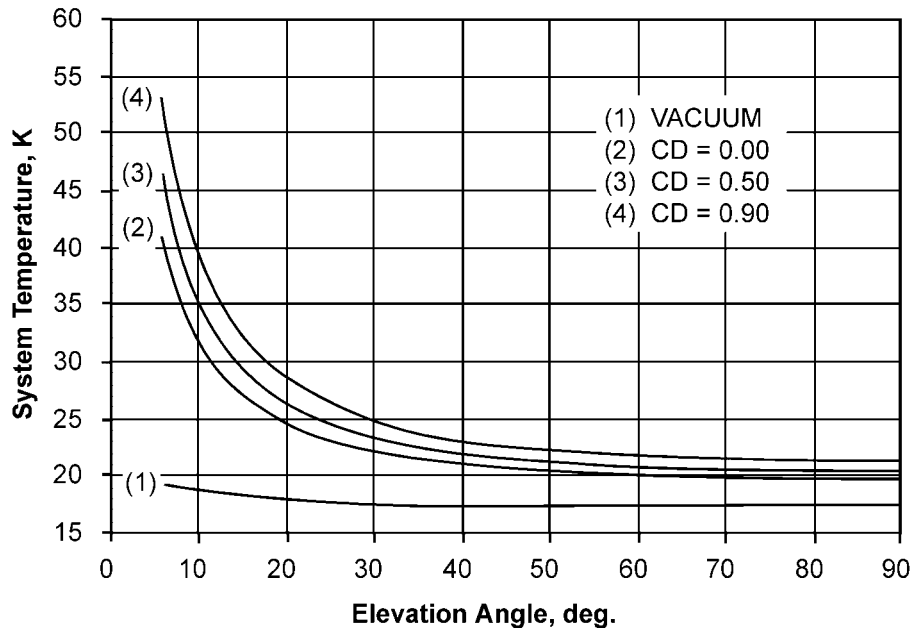
Figure 9.   X-Band System Temperature Versus Elevation Angle, DSS 45
Antenna, Non-Diplexed Path, Maser LNA Input

19
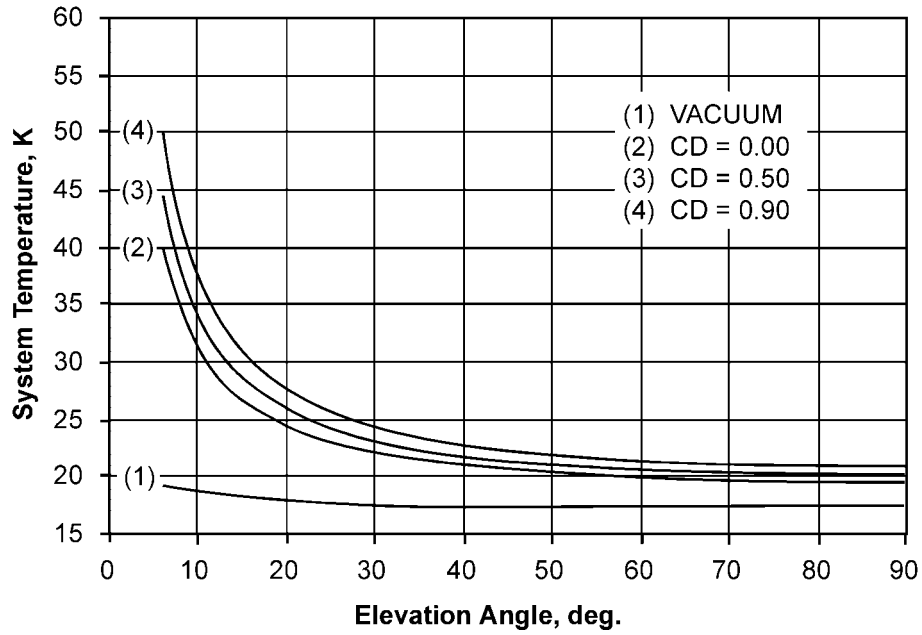
Figure 10. X-Band System Temperature Versus Elevation Angle, DSS 65
Antenna, Non-Diplexed Path, Maser LNA Input
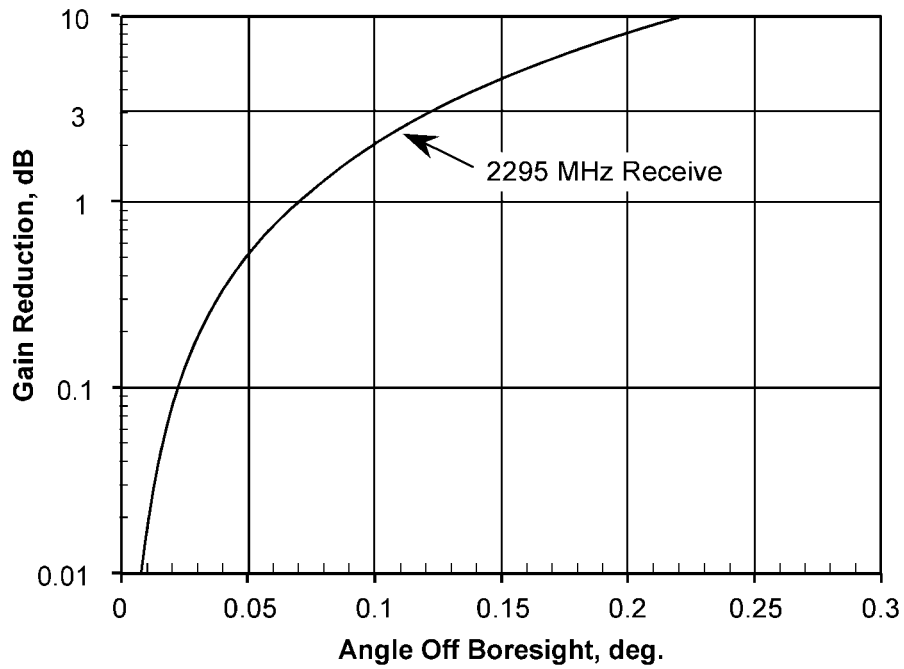
Figure 11. S-Band Gain Reduction Versus Angle Off Boresight
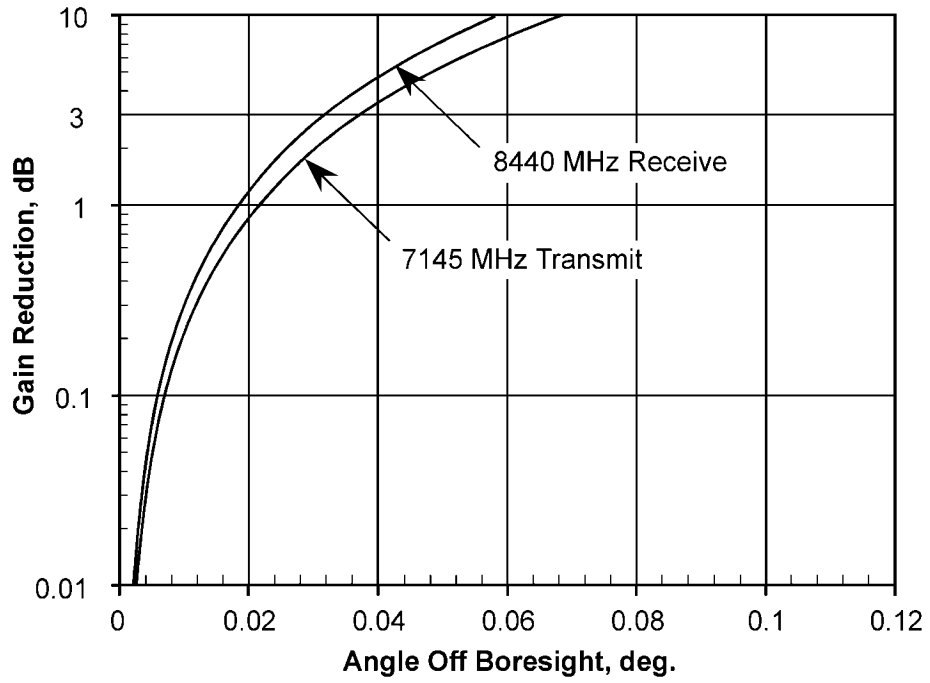
Figure 12. X-Band Gain Reduction Versus Angle Off Boresight

Appendix A
Equations for Modeling

A.1   Equation for Gain Versus Elevation Angle

The following equation can be used to generate S-band receive and X-band transmit and receive gain versus elevation angle curves. Examples of these curves are depicted in Figures 2–5. See paragraph 2.1.1.1 for frequency effect modeling and module 105 for atmospheric attenuation at weather conditions other than 0%, 50%, and 90% cumulative distribution.

$$G(\theta) = G_0 - G_1(\theta - \gamma)^2 - \frac{A_{ZEN}}{\sin\theta} \ , \ \ \text{dBi} \tag{1}$$

where

θ = antenna elevation angle (deg.) $6 \leq \theta \leq 90$

$G_0, G_1, \ \gamma$ = parameters from Table A-1

A_{ZEN} = zenith atmospheric attenuation from Table A-2 or from Table 2 in module 105, dB.

A.2   Equation for System Temperature Versus Elevation Angle

The following equation can be used to generate S- and X-band system temperature versus elevation angle curves. Examples of these curves are depicted in Figures 6–10. See module 105 for atmospheric attenuation at weather conditions other than 0%, 50%, and 90% cumulative distribution.

$$T_{op}(\theta) = T_1 + T_2 e^{\frac{-a}{(90.001-\theta)}} + (255 + 25\,\text{CD})\left(1 - \frac{1}{10^{\frac{A_{ZEN}}{10\sin\theta}}}\right), \ \ \text{K} \tag{2}$$

where

θ = antenna elevation angle (deg.), $6 \leq \theta \leq 90$

T_1, T_2, a = parameters from Table A-3

CD = cumulative distribution used to select A_{ZEN} from Table A-2 or from Table 2 in module 105, $0 \leq CD \leq 0.99$

A_{ZEN} = zenith atmospheric attenuation for selected CD from Table A-2 or from Table 2 in module 105, dB.

A.3   *Equation for Gain Reduction Versus Pointing Error*

The following equation can be used to generate gain-reduction versus pointing error curves, examples of which are depicted in Figures 10 and 11.

$$\Delta G(\theta) = 10\log\left(e^{\frac{2.773\theta^2}{HPBW^2}} \right), \ \ dB \tag{3}$$

where

θ = pointing error (deg.)

$HPBW$ = half-power beamwidth in degrees (from Tables 1 or 2).

Table A-1. Vacuum Component of Gain Parameters

Configuration and Stations	Parameters†			
	$G_0{}^*$ (Transmit)	$G_0{}^*$ (Receive)	G_1	γ
S-band, All Stations (Figure 2)	—	56.00	0.000006	42.0
X-band, All Stations (Figures 3—5)	67.1	68.27	0.00008	42.0

Notes:
   † G0 values are nominal at the frequency specified in Table 1 or Table 2. Other parameters apply to all frequencies within the same band.
   * Favorable tolerance = +0.5 dB, adverse tolerance = –0.5 dB, with a triangular PDF.

Table A-2. S- and X-Band Zenith Atmosphere Attenuation Above Vacuum (A_{ZEN})

Weather Condition†	A_{ZEN}, dB*					
	S-band			X-band		
	DSS 15	DSS 45	DSS 65	DSS 15	DSS 45	DSS 65
Vacuum	0.000	0.000	0.000	0.000	0.000	0.000
CD = 0.00	0.033	0.036	0.034	0.037	0.040	0.038
CD = 0.50	0.032	0.035	0.033	0.040	0.048	0.045
CD = 0.90	0.031	0.034	0.033	0.047	0.059	0.053

Notes:

   *   From Table 2 in module 105

   †   CD = cumulative distribution.

Table A-3. Vacuum Component of System Noise Temperature Parameters

Configuration and Stations	Parameters		
	T_1*	T_2	a
S-Band, DSS 15 and DSS 45	36.1	8.063	63.45
S-Band, DSS 65	42.1	8.063	63.45
X-Band, All Stations, Maser Non-diplexed	17.55	1742	573.6
X-Band, All Stations, Maser Diplexed	26.65	1742	573.6
X-Band, All Stations, W/B HEMT, Non-diplexed	33.4.	1742	573.6
X-Band, All Stations, W/B HEMT, Diplexed	42.3	1742	573.6

Note:

   *   Favorable tolerance = –2 K, adverse tolerance = +2 K, with a triangular PDF.

104
34-m BWG Stations
Telecommunications Interfaces

Effective November 30, 2000

Document Owner:

S. D. Slobin   12/11/00
S. D. Slobin   Date
Antenna System Engineer

Approved by:

A. J. Freiley   12-13-00
A. J. Freiley   Date
Antenna Product Domain Service
System Development Engineer

Released by:

[Signature on file in TMOD Library]
TMOD Document Release   Date

Change Log

Rev	Issue Date	Affected Paragraphs	Change Summary
Initial	1/15/2001	All	All

Note to Readers

There are two sets of document histories in the 810-005 document, and these histories are reflected in the header at the top of the page. First, the entire document is periodically released as a revision when major changes affect a majority of the modules. For example, this module is part of 810-005, Revision E. Second, the individual modules also change, starting as an initial issue that has no revision letter. When a module is changed, a change letter is appended to the module number on the second line of the header and a summary of the changes is entered in the module's change log.

This module supersedes TCI-31 in 810-005, Rev. D.

Contents

Illustrations

Tables

1 Introduction

1.1 Purpose

This module provides the performance parameters for the Deep Space Network (DSN) 34-m Beam Waveguide (BWG) antennas and the 34-m High-Speed BWG (HSB) antenna that are necessary to perform the nominal design of a telecommunications link. It also summarizes the capabilities of these antennas for mission planning purposes and for comparison with other ground station antennas.

1.2 Scope

The scope of this module is limited to providing those parameters that characterize the RF performance of the 34-meter BWG and HSB antennas, including the effects of weather that are unique to these types of antennas. Unless otherwise specified, the parameters do not include weather effects, such as reduction of system gain and increase in system noise temperature, that are common to all antenna types. These are discussed in module 105, Atmospheric and Environmental Effects. This module also does not discuss mechanical restrictions on antenna performance that are covered in module 302, Antenna Positioning.

2 General Information

The 34-meter diameter BWG and HSB antennas are the new generation of antennas being built for use in the DSN. These antennas differ from more conventional antennas (for example, the 34-meter HEF antennas; refer to module 103) in the fact that a series of small

mirrors (approximately 2.5 meters diameter) direct microwave energy from the region above the main reflector to a location at the base of the antenna, typically in a pedestal room, which may be located below ground level. The pedestal room is located below the azimuth track of the antenna, although other beam-waveguide designs (not utilized by the DSN) locate the microwave equipment in an "alidade room" above the azimuth track, but below the main reflector. All antennas described in this module are of the pedestal room design.

In this configuration, numerous "stations" of microwave equipment, contained in the pedestal room, can be accessed by rotation of an ellipsoidal mirror located on the pedestal room floor. This enables great versatility of design and allows tracking using equipment at one station while equipment installation or maintenance is carried out at the other stations. Since cryogenic low-noise amplifiers (LNAs) do not tip (as they do when located in a cone or room above the elevation axis), certain state-of-the-art ultra-low-noise amplifier (ULNA) and feed designs can be implemented.

The HSB antenna differs from the BWG antennas in that the pedestal room is above ground level, the optics design is different, and the subreflector does not focus automatically for the purpose of maintaining gain as the elevation angle of the antenna changes. The HSB antenna has higher tracking rates than do the BWG antennas; thus, it is the appropriate antenna to use when tracking Earth-orbiting satellites.

The capabilities of each antenna are significantly different depending on the microwave, transmitting, and receiving equipment installed. A summary of these differences is provided in Table 1. Functional block diagrams for each antenna are provided in Figures 1–5. In general, each antenna has two LNAs for telemetry reception or radio science (although the HSB antenna only has one and DSS 25 has three). Each antenna also has at least one transmitter. Antennas with more than one transmitter can operate only one of them at a time. Once again, DSS 25 is an exception and has a Ka-band transmitter that can be operated at the same time as its X-band transmitter.

All feeds provide selectable right-circular polarization (RCP) or left-circular polarization (LCP) with the exception of the Ka-band feeds at DSS 25 that operate only with RCP. The transmitter is coupled into the microwave path using a frequency-selective diplexer. Because the diplexer increases the operating system temperature, a non-diplexed path is also provided at all antennas (except the HSB antenna) for receive-only operation.

Stations with X-band transmitters can transmit with either the same or the opposite polarization from that being received, whereas S-band transmission must be the same polarization as is being received. If the uplink and downlink are of the same polarization, reception must be through the diplexer with increased noise and lower gain than the non-diplexed path. DSS 25 and DSS 26 have two X-band LNAs and can receive simultaneous RCP and LCP (although one of the signals will be via the non-diplexed path and the other will be via the diplexed path). The two LNAs at DSS 25 and DSS 26 can also be interchanged between the diplexed and non-diplexed paths. Thus, there are four possible ways a single X-band signal can be received at these stations.

2.1 *Telecommunications Parameters*

The significant parameters of the 34-meter BWG and HSB antennas that influence the design of the telecommunications uplink are listed in Tables 2 through 8. Variations in these parameters, which are inherent in the design of the antennas, are discussed below. Other factors that degrade link performance are discussed in modules 105 (Atmospheric and Environmental Effects) and 106 (Solar Corona and Solar Wind Effects).

The values in these tables do not include the effects of the atmosphere. However, the attenuation and noise-temperature effects of weather for three specific weather conditions are included in the figures at the end of the module so that they may be used for a quick estimate of telecommunications link performance for those specific conditions without reference to module 105. For detailed design control table use, the more comprehensive and detailed S-, X-, and Ka-band weather effects models (for weather conditions up to 99% cumulative distribution) in module 105 should be used.

2.1.1 *Antenna Gain Variation*

Because the gain is referenced to the feedhorn aperture, such items as diplexers and waveguide runs to alternate LNAs that are "downstream" (below or toward the LNA) do not affect the gain at the reference plane. Dichroic plates that are "upstream" of the feedhorn aperture cause a reduction in gain.

2.1.1.1 *Frequency Effects*

Antenna gains are specified at the indicated frequency (f_0). For operation at higher frequencies in the same band, the gain (dBi) must be increased by 20 log (f/f_0). For operation at lower frequencies in the same band, the gain must be reduced by 20 log (f/f_0).

2.1.1.2 *Elevation Angle Effects*

Structural deformation causes a reduction in gain when the antenna is operated at an elevation angle other than where the reflector panels were aligned. The effective gain of the antenna also is reduced by atmospheric attenuation, which is a function of elevation. Figures 6 through 11 show representative curves of gain versus elevation angle for selected stations and configurations. The curves show the hypothetical vacuum (no atmosphere) condition and the gain with 0%, 50%, and 90% weather conditions, designated as CD (cumulative distribution) = 0.00, 0.50, and 0.90. 0% means minimum weather effect (exceeded 100% of the time); 90% means that effect which is exceeded only 10% of the time. Qualitatively, 0% corresponds to the driest condition of the atmosphere; 25% corresponds to average clear; 50% corresponds to humid or very light clouds; and 90% corresponds to very cloudy, but with no rain. Appendix A provides the complete set of parameters from which these curves were created. These parameters, in combination with the weather-effects parameters from module 105, can be used to calculate the gain versus elevation angle curve for any antenna, in any configuration, for weather conditions up to 99% CD.

2.1.1.3 *Wind Loading*

The gain reduction at X-band due to wind loading is listed in Table 9. The tabular data are for structural deformation only and presume that the antenna is maintained on-point by

conical scan (CONSCAN) or Monopulse, discussed in module 302, Antenna Positioning. In addition to structural deformation, wind introduces a pointing error, which is related to the antenna elevation angle, the angle between the antenna and the wind, and the wind speed. The effects of pointing error are discussed below. Cumulative probability distributions of wind velocity at Goldstone are given in module 105.

2.1.2 *System Noise Temperature Variation*

The operating system temperature (T_{op}) varies as a function of elevation angle due to changes in the path length through the atmosphere and ground noise received by the sidelobe pattern of the antenna. Figures 12 through 17 show the combined effects of these factors for the same set of stations and configurations selected above. The figures show the hypothetical vacuum and the 0%, 50%, and 90% weather conditions. The equations and parameters for these curves are provided in Appendix A and can be used, in combination with the weather-effects parameters from module 105, to calculate the system temperature versus elevation curve for any antenna, in any configuration, for weather conditions up to 99% CD.

When two LNAs are available for use, the amplifier in the lowest loss (lowest noise) configuration is considered prime and is designated LNA-1. Under some conditions, LNA-2 may be used; in these instances, the higher noise-temperature values apply.

The system temperature values in Tables 6–8 do not include any atmospheric contribution and must be increased for comparison with antennas that are specified with 25% weather. Table 10 provides adjustments to the hypothetical no-atmosphere (vacuum) operating system temperature ($T_{op, vac}$) that were calculated using the weather models in module 105.

2.1.3 *Antenna Pointing*

2.1.3.1 *Pointing Accuracy*

The pointing accuracy of an antenna, often referred to as its *blind-pointing* performance, is the difference between the calculated beam direction and the actual beam direction. The error is random and can be divided into two major categories. The first of these includes the computational errors and uncertainties associated with the radio sources used to calibrate the antenna and the location of the spacecraft provided by its navigation team. The second has many components associated with converting a calculated beam direction to the physical positioning of a large mechanical structure. Included are such things as atmospheric instability, servo and encoder errors, thermally and gravitationally induced structural deformation, azimuth track leveling (for an azimuth-elevation antenna), and both seismic and diurnal ground tilt.

Blind pointing is modeled by assuming equal pointing performance in the elevation (EL) and cross-elevation (X-EL) directions. That is, the random pointing errors in each direction have uncorrelated Gaussian distributions with the same standard deviation. This results in a Rayleigh distribution for pointing error where the mean radial error is 1.253 times the standard deviation of the EL and X-EL components. For a Rayleigh distribution, the probability that the pointing error will be less than the mean radial error is 54.4%. Conversely, the probability that the mean radial error will be exceeded is 45.6%.

Table 11 provides the modeled blind-pointing performance and the resulting gain reductions in various wind conditions for the BWG antennas. In addition to the mean radial error (CD = 54.4%), pointing errors for the 90%, 95%, and 99% points on the Rayleigh distribution curve are also provided. A CD of 90% implies that 90% of the time, the pointing error or pointing loss will be less than the value shown, and so forth.

2.1.3.2   Pointing Loss

Figures 18 through 20 show the effects of pointing error on effective transmit and receive gain of the antenna. These curves are Gaussian approximations based on measured and predicted antenna beamwidths. Data have been normalized to eliminate elevation and wind-loading effects. The equations used to derive the curves are provided in Appendix A.

2.1.3.3   Ka-Band Aberration Correction

The extremely narrow beamwidth at Ka-band requires that a Ka-band uplink signal be aimed at where the spacecraft will be when the signal arrives, while simultaneously receiving a signal that left the spacecraft one light-time previously. This is accomplished by mounting the Ka-band transmit feed on a movable X-Y platform that can displace the transmitted beam as much as 30 millidegrees from the received beam. The fact that the transmit feed is displaced from its optimum focus causes the gain reduction depicted in Figure 21. The equation used to generate this curve is provided in Appendix A.

2.2   Recommended Minimum Operating Carrier Signal Levels

Table 12 provides the recommended minimum operating carrier-signal levels for selected values of receiver tracking-loop bandwidth (B_l) when using the Block V Receiver (BVR). These levels provide a signal-to-noise ratio of 10 dB in the carrier tracking loop, based on the nominal zenith system temperatures given in Tables 5–8 adjusted for an average clear atmosphere, CD=0.25. Use of loop bandwidths less than 1 Hz are not recommended for the HSB antenna due to phase noise introduced by its long distance (approximately 30 km) between the antenna and its BVR.

The HSB antenna has an additional receiver, the Multifunction Receiver (MFR), that provides wider loop bandwidths for high-Doppler Earth-orbiter spacecraft. The recommended minimum operating carrier signal levels for the available MFR tracking loop bandwidths are provided in Table 13. These values also provide a tracking loop signal-to-noise ratio of 10 dB based on the nominal zenith system temperature given in Table 8 and an average clear atmosphere.

3 Proposed Capabilities

The following paragraphs discuss capabilities that have not yet been implemented by the DSN but have adequate maturity to be considered for spacecraft mission and equipment design. Telecommunications engineers are advised that any capabilities discussed in this section cannot be committed to except by negotiation with the Telecommunications and Mission Operations Directorate (TMOD) Plans and Commitments Program Office.

3.1 34-m BWG Ka-Band Implementation

All DSN BWG antennas except DSS 27 are being equipped with a Ka-band receive-only capability by replacing the existing X-band feed and microwave components with an X/X/Ka-band feed that includes the X-band diplexing function. The 34-m BWG Ka-band implementation will eliminate the need to run transmitted power through the feed's receive port and allows the entire receive portion to be cryogenically cooled.

3.1.1 X-Band Uplink Performance

The X-band uplink performance will be as described in Table 4 (with the exception of X-band effective isotropic radiated power [EIRP] that may be reduced approximately 0.1 dB due to increased loss in the waveguide that couples the transmitter to the feed). An X-band transmitter will be added to DSS 24 so that all BWG antennas (except DSS 27) will have X-band uplink and simultaneous X- and Ka-band downlink capability.

3.1.2 X-Band Downlink Performance

The combination of the cryogenically cooled feed, better amplifiers, and reduced microwave complexity is expected to provide a peak vacuum gain over temperature (G/T) of 56 dB at all stations. This G/T will be independent of whether the transmitter is in operation and will apply when the polarization is the same as the transmitter or opposite to the transmitter. Uplink and downlink polarization will be independent, and DSS 25 and 26 will be able to provide simultaneous RCP and LCP because they have two X-band downconverters. The remaining stations will provide selectable RCP or LCP. Other receive characteristics will be as described in Tables 6 and 7.

3.1.3 Ka-Band Downlink Performance

The same technology used at X-band is expected to provide a peak vacuum Ka-band G/T of at least 63.6 dB at all stations. Selectable RCP or LCP will be available, however monopulse tracking will only be available for RCP. Other receive characteristics will be as described in Table 7.

Table 1.   Capabilities of DSN BWG and HSB Antennas

Antenna	Type	S-band		X-band		Ka-band	
		Uplink*	Downlink†	Uplink*	Downlink†	Uplink*	Downlink†
DSS 24	BWG	20 kW	1	—	1	—	—
DSS 25	BWG	—	—	4 kW	1	800 W	1
DSS 25	BWG	—	—	4 kW	2	—	—
DSS 27	HSB	200 W	1	—	—	—	—
DSS 34	BWG	20 kW	1	4 kW	1	—	—
DSS 54	BWG	20 kW	1	4 kW	1	—	—

Notes:

*   An entry in this column refers to the maximum available uplink power. A dash means that no capability is available.

†   An entry in this column refers to the maximum number of Low Noise Amplifiers and receiver front-ends that are available for this band. A dash mean that no capability is available.

Table 2.   S-Band Transmit Characteristics, DSS 24, 34, and 54

Parameter	Value	Remarks
ANTENNA		
Gain at 2115 MHz (dBi)	56.1, +0.2, –0.3 dB	At peak of gain versus elevation curve, referenced to feedhorn aperture for matched polarization; no atmosphere included; triangular probability density function (PDF) tolerance.
Transmitter Waveguide Loss (dB)	0.6 ±0.1	20-kW transmitter output terminal (waterload switch) to feedhorn aperture
Half-Power Beamwidth (deg)	0.263 ±0.020	Angular width (2-sided) between half-power points at specified frequency
Polarization	RCP or LCP	One polarization at a time, remotely selected. Polarization must be the same as received polarization.
Ellipticity (dB)	1.0 (max)	Peak-to-peak axial ratio defined as the ratio of peak-to-trough received voltages with a rotating linearly polarized source and the feed configured as a circularly (elliptically) polarized receiving antenna

Table 2.   S-Band Transmit Characteristics, DSS 24, 34, and 54 (Continued)

Parameter	Value	Remarks
ANTENNA (Continued)		
Pointing Loss (dB)		
Angular	See module 302	Also see Figure 18
CONSCAN	0.01	X-band CONSCAN reference set for 0.1 dB loss
	0.1	S-band CONSCAN reference set for 0.1 dB loss
EXCITER AND TRANSMITTER		
Frequency Range Covered (MHz)	2025–2120	Power amplifier is step-tunable over the specified range in six 20-MHz segments, with 5-MHz overlap between segments. Tuning between segments can be accomplished in 30 seconds.
Instantaneous 1-dB Bandwidth (MHz)	20	
Coherent with Earth Orbiter S-Band D/L Allocation	2028.8–2108.7	240/221 turnaround ratio
Coherent with deep space S-Band D/L channels	2110.2–2117.7	240/221 turnaround ratio
Coherent with deep space X-Band D/L channels	2110.2–2119.8	880/221 turnaround ratio
RF Power Output (dBm)		Referenced to 20-kW transmitter output terminal (waterload switch). Settability is limited to 0.25 dB by measurement equipment precision.
2025–2070 MHz	53.0–73.0, +0.0, −1.0	
2070–2090 MHz	53.0–67.0, +0.0, −1.0	S-band uplink is restricted to 5 kW over 2070–2090 frequency range
2060–2120 MHz	53.0–73.0, +0.0, −1.0	

Table 2.   S-Band Transmit Characteristics, DSS 24, 34, and 54 (Continued)

Parameter	Value	Remarks
EXCITER AND TRANSMITTER (Continued)		
Power output varies across the bandwidth and may be as much as 1 dB below nominal rating. Performance will also vary from tube to tube. Normal procedure is to run the tubes saturated, but unsaturated operation is also possible. The point at which saturation is achieved depends on drive power and beam voltage. The 20-kW tubes are normally saturated for power levels greater than 60 dBm (1 kW). Minimum power out of the 20-kW tubes is about 53 dBm (200 W). Efficiency of the tubes drops off rapidly below nominal rated output.		
EIRP (dBm)	128.5, +0.2, –1.0 dB	At gain set elevation angle, referenced to feedhorn aperture
Tunability		At transmitter output frequency
Phase Continuous Tuning Range (MHz)	2.0	
Maximum Tuning Rate (kHz/s)	±12.1	
Frequency Error (Hz)	0.012	Average over 100 ms with respect to frequency specified by predicts
Ramp Rate Error (Hz/s)	0.001	Average over 4.5 s with respect to rate calculated from frequency predicts
Stability		At transmitter output frequency
Output Power Stability (dB)		Over 12-h period
Saturated Drive	0.5	
Unsaturated Drive	1.0	
Incidental AM (dB)	60	Below carrier
Group Delay Stability (ns)	≤3.3	Ranging modulation signal path (see module 203) over 12-h period
Frequency Stability		Allan deviation
1000 s	5.0×10^{-14}	
Spurious Output (dB)		Below carrier
2nd Harmonic	–85	
3rd Harmonic	–85	
4th Harmonic	–140	At input to X-band horn, with transmitter set for 20-kW output

Table 3.   S-Band Transmit Characteristics, DSS 27

Parameter	Value	Remarks
ANTENNA		
Gain at 2115 MHz (dBi)	54.4, +0.2, –0.3 dB	At peak of gain versus elevation angle curve, referenced to feedhorn aperture for matched polarization; no atmosphere included; triangular PDF tolerance.
Transmitter Waveguide Loss (dB)	0.6 ±0.1	20-kW transmitter output terminal (waterload switch) to feedhorn aperture
Half-Power Beamwidth (deg)	0.263 ±0.020	Angular width (2-sided) between half-power points at specified frequency
Polarization	RCP or LCP	One polarization at a time, remotely selected. Polarization must be the same as received polarization.
Ellipticity (dB)	1.0 (max)	Peak-to-peak axial ratio defined as the ratio of peak-to-trough received voltages with a rotating linearly polarized source and the feed configured as a circularly (elliptically) polarized receiving antenna
Pointing Loss		
Angular	See module 302	Also see Figure 18
EXCITER AND TRANSMITTER		
Frequency range covered (MHz)	2025–2120	
Coherent with Earth orbiter S-Band D/L allocation	2028.8–2108.7	240/221 turnaround ratio
Coherent with deep space S-Band D/L channels	2110.2–2117.7	240/221 turnaround ratio
Coherent with deep space X-Band D/L channels	2110.2–2119.8	880/221 turnaround ratio. No X-band receiver is available at DSS 27
RF Power Output (dBm)	47.0–53.0, ±0.5 dB	Referenced to 200 W transmitter output terminal (power load switch). Settability is limited to 0.25 dB by measurement equipment precision.

Table 3.   S-Band Transmit Characteristics, DSS 27 (Continued)

Parameter	Value	Remarks
EXCITER AND TRANSMITTER (Continued) Power output varies across the bandwidth and may be as much as 1 dB below nominal rating. The 200 W tube is a fixed beam klystron designed to saturate at its rated power. Operation at less than the nominal 200 W is accomplished by operating the tube unsaturated. Minimum power out of is about 47 dBm (50 W).		
EIRP (dBm)	106.8 ±0.6 dB	At gain set elevation angle, referenced to feedhorn aperture
Tunability (Hz)	100	At transmitter output frequency
Output Power Stability (dB)	±0.25	Worst case over 8-h period using 30-m sample intervals
Spurious Output (dB)		Below carrier
2025–2120 MHz	−88	
2200–2300 MHz	−94	
2nd Harmonic	−60	
3rd Harmonic	−60	
8400–8500 MHz	−94	

Table 4.   X-Band Transmit Characteristics, DSS 25, 26, 34, and 54

Parameter	Value	Remarks
ANTENNA		
Gain at 7145 MHz (dBi)	67.1, +0.2, −0.3 dB	At peak of gain versus elevation angle curve, referenced to feedhorn aperture for matched polarization; no atmosphere included; triangular PDF tolerance.
Transmitter Waveguide Loss (dB)	0.4 ±0.1	4-kW transmitter output terminal (waterload switch) to feedhorn aperture
Half-Power Beamwidth (deg)	0.0777 ±0.0040	Angular width (2-sided) between half-power points at specified frequency
Polarization	RCP or LCP	One polarization at a time, remotely selected, independent of received polarization.

Table 4.   X-Band Transmit Characteristics, DSS 25, 26, 34, and 54 (Continued)

Parameter	Value	Remarks
ANTENNA (Continued)		
Ellipticity (dB)	1.0 (max)	Peak-to-peak axial. See Table 2 for definition.
Pointing Loss (dB)		
Angular	See module 302	Also see Figure 19
CONSCAN	0.1	X-band CONSCAN reference set for 0.1 dB loss
EXCITER AND TRANSMITTER		
Frequency range covered (MHz)	7145–7190	
Coherent with deep space S-Band D/L channels	7147.3–7177.3	240/749 turnaround ratio
Coherent with deep space X-Band D/L channels	7149.6–7188.9	880/749 turnaround ratio
RF Power Output (dBm)	47.0–66.0, ±0.5 dB	Referenced to 4-kW transmitter output terminal (waterload switch). Settability is limited to 0.25 dB by measurement equipment precision.
Power output varies across the bandwidth and may be as much as 1 dB below nominal rating. The 4 kW tubes are fixed beam klystrons designed to saturate at their rated power however performance varies from tube to tube. Operation at less than the nominal 4.0 kW is unsaturated. Minimum power output is about 47 dBm (50 W). Efficiency of the tubes drops off rapidly below nominal rated output.		
EIRP (dBm)	133.1 ±0.7 dB	At gain set elevation angle, referenced to feedhorn aperture
Tunability		At transmitter output frequency
Phase Continuous Tuning Range (MHz)	2.0 MHz	
Maximum Tuning Rate (kHz/s)	±12.1	

Table 4.   X-Band Transmit Characteristics, DSS 25, 26, 34, and 54 (Continued)

Parameter	Value	Remarks
EXCITER AND TRANSMITTER (Continued)		
Tunability (Continued)		
Frequency Error (Hz)	0.012	Average over 100 ms with respect to frequency specified by predicts
Ramp Rate Error (Hz/s)	0.001	Average over 4.5 s with respect to rate calculated from frequency predicts
Stability		At transmitter output frequency
Output Power Stability (dB)	0.2	First Differences, 10–1000 s intervals over 12-h period
Output Power Variation (dB)		Across frequency band over 12-h period
Saturated Drive	0.25	
Unsaturated Drive	1.0	
Group Delay Stability (ns)	≤1.0	Ranging modulation signal path over 12-h period (see module 203)
Frequency Stability		Allan deviation
1 s	3.3×10^{-13}	
10 s	5.0×10^{-14}	
1000–3600 s	2.7×10^{-15}	
Spurious Output (dB)		Below carrier
1–10 Hz	−50	
10 Hz–1.5 MHz	−60	
1.5 MHz–8 MHz	−45	
2nd Harmonic	−75	
3rd, 4th & 5th Harmonics	−60	

Table 5. Ka-Band Transmit Characteristics, DSS 25

Parameter	Value	Remarks
ANTENNA		
Gain at 34200 MHz (dBi)	79.5, +0.2, −0.3 dB	At peak of gain versus elevation angle curve, referenced to feedhorn aperture for matched polarization; no atmosphere included; triangular PDF tolerance.
Transmitter Waveguide Loss (dB)	0.25 ±0.1	800W transmitter output terminal (waterload switch) to feedhorn aperture
Half-Power Beamwidth (deg)	0.0162 ±0.0010	Angular width (2-sided) between half-power points at specified frequency
Polarization	RCP	
Ellipticity (dB)	1.0 (max)	Peak-to-peak axial. See Table 2 for definition.
Pointing Loss		CONSCAN is not available.
Angular	See module 302	Also see Figure 20
EXCITER AND TRANSMITTER		
Frequency range covered (MHz)	34200–34700	
Coherent with deep space Ka-Band D/L channels	34343.2–34570.9	3344/3599 turnaround ratio
Coherent with deep space X-Band D/L channels	34354.3–34554.2	880/3599 turnaround ratio
RF Power Output (dBm)	47.0–59.0, ±0.5 dB	Referenced to 800 W transmitter output terminal (waterload switch). Settability is limited to 0.25 dB by measurement equipment precision.
Power output varies across the bandwidth and may be as much as 1 dB below nominal rating. The 800 W tube is a fixed beam klystron designed to saturate at its rated power. Operation at less than the nominal 800 W is unsaturated. Minimum power output is about 47 dBm (50 W).		
EIRP (dBm)	138.2, +0.6, −0.5 dB	At gain set elevation angle, referenced to feedhorn aperture
Stability		At transmitter output frequency
Output Power Variation (dB)		Across frequency band over 12 h

Table 5. Ka-Band Transmit Characteristics, DSS 25 (Continued)

Parameter	Value	Remarks
EXCITER AND TRANSMITTER (Continued)		
Coherent with deep space X-Band D/L channels	34354.3–34554.2	880/3599 turnaround ratio
RF Power Output (dBm)	47.0–59.0, ±0.5 dB	Referenced to 800 W transmitter output terminal (waterload switch). Settability is limited to 0.25 dB by measurement equipment precision.
Power output varies across the bandwidth and may be as much as 1 dB below nominal rating. The 800 W tube is a fixed beam klystron designed to saturate at its rated power. Operation at less than the nominal 800 W is unsaturated. Minimum power output is about 47 dBm (50 W).		
EIRP (dBm)	138.2, +0.6, –0.5 dB	Referenced to feed
Stability		At transmitter output frequency
Output Power Variation (dB)		Across frequency band over 12 h
Saturated Drive	0.25	
Unsaturated Drive	≤1.0	
Frequency Stability		Allan deviation
1 s	3.3×10^{-13}	
10 s	5.2×10^{-14}	
1000–3600 s	3.1×10^{-15}	
1000–3600 s	3.1×10^{-15}	
Spurious Output (dB)		Below carrier
1–10 Hz	–50	
10 Hz–1.5 MHz	–60	
1.5 MHz–8 MHz	–45	

Table 6.   S- and X-Band Receive Characteristics, DSS 24, 34, and 54

Parameter	Value	Remarks
ANTENNA		
Gain (dBi)		At peak of gain versus elevation angle curve, referenced to feedhorn aperture (feed and feedline losses are accounted for in system temperature), for matched polarization; no atmosphere included; triangular PDF tolerance. See Figures 6, 8, and 9 for representative gain versus elevation curves.
S-Band (2295 MHz)	56.8, +0.1, –0.2 dB	
X-Band (8420 MHz)	68.2, +0.1, –0.2 dB	
Half-Power Beamwidth (deg.)		Angular width (2-sided) between half-power points at specified frequency
S-Band	0.242 ±0.020	
X-Band	0.0660 ±0.0040	
Polarization		Remotely selected
S-Band	RCP or LCP	Same as transmit polarization
X-Band	RCP or LCP	Same as or opposite from transmit polarization
Ellipticity (dB)		Peak-to-peak voltage axial ratio, RCP and LCP. See definition in Table 2.
S-Band	≤1.0	
X-Band	≤0.7	
Pointing Loss (dB, 3 sigma)		
Angular	See module 302	Also see Figures 18 and 19
CONSCAN		
S-Band	0.03	Loss at S-band when using X-band CONSCAN reference set for 0.1 dB loss at X-band
	0.1	Recommended value when using S-band CONSCAN reference
X-Band	0.1	Recommended value when using X-band CONSCAN reference

Table 6.   S- and X-Band Receive Characteristics, DSS 24, 34, and 54 (Continued)

Parameter	Value	Remarks
RECEIVER		
Frequency Ranges Covered (MHz))		
S-Band	2200–2300	
X-Band	8400–8500	
Recommended Maximum Signal Power (dBm)	-90.0	At LNA input terminal
Recommended Minimum Signal Power (dBm)	See Table 12	
System Noise Temperature (K)		Near zenith, no atmosphere included. See Figures 12, 14, and 15 for representative system temperature versus elevation curves. Tolerances have a triangular PDF.
S-Band (2200–2300 MHz) Non-Diplexed Path		Referenced to feedhorn aperture.
DSS 24	28.3, −1.0, +2.0 K	
DSS 34	30.7, −1.0, +2.0 K	
DSS 54	28.9, −1.0, +2.0 K	
S-Band (2200–2300 MHz) Diplexed Path		Referenced to feedhorn aperture.
DSS 24	34.8, −1.0, +2.0 K	
DSS 34	39.3, −1.0, +2.0 K	
DSS 54	37.5, −1.0, +2.0 K	
X-Band (8400–8500 MHz) Non-Diplexed Path		X-band only operation (S/X-band dichroic plate retracted). Referenced to feedhorn aperture.
DSS 24	23.2, −1.0, +2.0 K	LNA = MASER
DSS 34	28.0, −1.0, +2.0 K	LNA = HEMT
DSS 54	21.1, −1.0, +2.0 K	LNA = MASER

Table 6.   S- and X-Band Receive Characteristics, DSS 24, 34, and 54 (Continued)

Parameter	Value	Remarks
RECEIVER (Continued)		
System Noise Temperature (K), (Continued)		
X-Band (8400–8500 MHz) Diplexed Path		X-band only operation (dichroic plate retracted). Referenced to feedhorn aperture.
DSS 34	35.5, −1.0, +2.0 K	LNA = HEMT
DSS 54	28.6, −1.0, +2.0 K	LNA = MASER
X-Band (8400–8500 MHz) Non-Diplexed Path		S/X-band operation. Referenced to feedhorn aperture.
DSS 24	24.6, −1.0, +2.0 K	LNA = MASER
DSS 34	29.7, −1.0, +2.0 K	LNA = HEMT
DSS 54	22.8, −1.0, +2.0 K	LNA = MASER
X-Band (8400–8500 MHz) Diplexed Path		S/X-band operation. Referenced to feedhorn aperture.
DSS 34	37.2, −1.0, +2.0 K	LNA = HEMT
DSS 54	30.2, −1.0, +2.0 K	LNA = MASER
Carrier Tracking Loop Noise B/W (Hz)	0.25–200	Effective one-sided, noise-equivalent carrier loop bandwidth (B_L)

Table 7.   X- and Ka-Band Receive Characteristics, DSS 25 and 26

Parameter	Value	Remarks
ANTENNA		
Gain (dBi)		At peak of gain versus elevation angle curve, referenced to feedhorn aperture (feed and feedline losses are accounted for in system temperature), for matched polarization; no atmosphere included; triangular PDF tolerance. See Figures 10 and 11 for representative DSS 25 gain versus elevation curves.
X-Band (8420 MHz)	68.4, +0.1, –0.2 dB	DSS 25
	68.3, +0.1, –0.2 dB	DSS 26
Ka-Band (32000 MHz)		DSS 25 only
	79.0, +0.3, –0.3 dB	Ka-band only operation (X-Ka dichroic plate retracted).
	78.8, +0.2, –0.3 dB	X/Ka-band operation
Half-Power Beamwidth (deg.)		Angular width (2-sided) between half-power points at specified frequency
X-Band	0.0660 ±0.0040	
Ka-Band	0.0174 ±0.0020	DSS 25 only
Polarization		
X-Band DSS 25	RCP and LCP	Both polarizations simultaneously available; polarization using diplexed path is remotely selected
X-Band DSS 26	RCP or LCP	One polarization at a time
Ka-Band	RCP	DSS 25 only
Ellipticity (dB)		Peak-to-peak voltage axial ratio. See definition in Table 2.
X-Band	≤0.7	RCP and LCP
Ka-Band	≤1.0	
Pointing Loss (dB, 3 sigma)		
Angular	See module 302	Also see Figures 19 and 20
CONSCAN		(Not available at Ka-band)

Table 7. X- and Ka-Band Receive Characteristics, DSS 25 and 26 (Continued)

Parameter	Value	Remarks
ANTENNA (Continued)		
Pointing Loss (dB, 3 sigma) (Continued)		
X-Band	0.1	Recommended value when using X-band CONSCAN reference
Monopulse		DSS 25 only. Receiver loop SNR ≥35 dB
X-Band	0.007	Using Ka-band monopulse reference
Ka-Band	0.1	
RECEIVER		
Frequency Ranges (MHz)		
X-Band	8400–8500	
Ka-Band	31800–32300	
Recommended Maximum Signal Power (dBm)	-90.0	At LNA input terminal
Recommended Minimum Signal Power (dBm)	See Table 12	
System Noise Temperature (K)		Near zenith, no atmosphere included. See Figures 16 and 17 for DSS 25 system temperature versus elevation curves. Tolerances have a triangular PDF.
X-Band (8400–8500 MHz) Non-Diplexed Path		Referenced to feedhorn aperture.
DSS 25, LNA 1	22.1, –1.0, +2.0 K	LNA = MASER
DSS 25, LNA 2	35.9, –1.0, +2.0 K	LNA = HEMT
DSS 26	N/A	
X-Band (8400–8500 MHz) Diplexed Path		Referenced to feedhorn aperture.
DSS 25, LNA 1	29.6, –1.0, +2.0 K	LNA = MASER
DSS 25, LNA 2	43.4, –1.0, +2.0 K	LNA = HEMT
DSS 26, LNA 1 (RCP)	25.8 –1.0, +2.0 K	LNA = HEMT
DSS 26, LNA 2 (LCP)	26.5 –1.0, +2.0 K	LNA = HEMT

Table 7. X- and Ka-Band Receive Characteristics, DSS 25 and 26 (Continued)

Parameter	Value	Remarks
RECEIVER (Continued)		
System Noise Temperature (K) (Continued)		
DSS 26, LNA 1 & 2	26.2 –1.0, +2.0 K	LNA = HEMT
Ka-Band (31800–32300 MHz)		Ka-band only operation (X/Ka-band dichroic plate retracted), referenced to feedhorn aperture.
DSS 25	29.3, –1.0, +2.0	LNA = HEMT
DSS 26	N/A	
Ka-Band (31800–32300 MHz)		X/Ka-band operation, referenced to feedhorn aperture.
DSS 25	32.8, –1.0, +2.0	LNA = HEMT
DSS 26	N/A	
Carrier Tracking Loop Noise B/W (Hz)	0.25–200	Effective one-sided, noise-equivalent carrier loop bandwidth (B_L)

Table 8. S-Band Receive Characteristics, DSS 27

Parameter	Value	Remarks
ANTENNA		
Gain (dBi)		At peak of gain versus elevation angle curve, referenced to feedhorn aperture (feed and feedline losses are accounted for in system temperature), for matched polarization; no atmosphere included; triangular PDF tolerance. See Figures for elevation dependency.
S-Band	55.1, +0.1, –0.2 dB	
Half-Power Beamwidth (deg)		Angular width (2-sided) between half-power points at specified frequency
S-Band	0.242 ±0.020	
Polarization		Remotely selected
S-Band	RCP or LCP	Same as transmit polarization

Table 8.   S-Band Receive Characteristics, DSS 27 (continued)

Parameter	Value	Remarks
ANTENNA (Continued)		
Ellipticity (dB)		Peak-to-peak voltage axial ratio, RCP and LCP. See definition in Table 2.
S-Band	≤1.0	
Pointing Loss (dB, 3-sigma)		
Angular	See module 302	Also see Figure 18
RECEIVER		
Frequency Ranges Covered (MHz))		
S-Band	2200–2300	
Recommended Maximum Signal Power (dBm)	–90.0	At LNA input terminal
Recommended Minimum Signal Power (dBm)	See Table 12	
S-Band System Noise Temperature (K) (2200–2300 MHz)		With respect to feedhorn aperture, near zenith, no atmosphere included. See Figure 13 for elevation dependency. Tolerances have a triangular PDF.
DSS 27	101, –1.0, +2.0 K	LNA = Room temperature HEMT
Incremental Tunability (kHz)	10	Continuously variable tuning around center frequency available in ±15 kHz and ±300 kHz ranges
Carrier Tracking Loop Noise B/W (Hz)	1.0–200	Effective one-sided, noise-equivalent carrier loop bandwidth (B_L) when using Block V Receiver
Noise Bandwidth (Hz)	10 ±10%	Effective one-sided threshold noise bandwidth (B_{LO}) when using Multifunction Receiver
	30 ±10%	
	100 ±10%	
	300 ±10%	
	1000 ±10%	
	3000 ±10%	

Table 9.   Gain Reduction Due to Wind Loading, 34-m BWG Antennas

Wind Speed		X-Band Gain Reduction (dB)*
(km/hr)	(mph)	
16	10	0.2
48	30	0.3
72	45	0.4

* Assumes antenna is maintained on-point using CONSCAN or an equivalent.
  S-band gain reduction is negligible for wind speeds up to 72 km/h (45 mph).
  Worst case with antenna in most adverse orientation for wind.

Table 10.   System Noise Temperature Contributions due to 25% Weather

Location	Noise Temperature Contribution (K)*		
	S-band	X-band	Ka-band
Goldstone (DSS 24, 25, 26 & 27)	1.929	2.292	9.116
Canberra (DSS 34)	2.109	2.654	11.331
Madrid (DSS 54)	2.031	2.545	10.797

* From Table 1 in module 105.

Table 11.   Pointing Accuracy and Pointing Loss in Various Wind Conditions

Wind Speed < 4.5 km/s (<10 mph)				
Cumulative Distribution (CD)	Pointing Error, mdeg	Pointing Loss, dB		
		S-band	X-band	Ka-band
Mean (54.4%)	1.670	0.001	0.008	0.111
90%	2.825	0.002	0.022	0.319
95%	3.251	0.002	0.029	0.422
99%	3.997	0.003	0.044	0.639
Wind Speed < 8.9 km/s (<20 mph)				
Cumulative Distribution (CD)	Pointing Error, mdeg	Pointing Loss, dB		
		S-band	X-band	Ka-band
Mean (54.4%)	3.330	0.002	0.031	0.443
90%	5.633	0.007	0.088	1.268
95%	6.483	0.009	0.116	1.679
99%	7.971	0.013	0.176	2.539
Wind Speed < 13.4 km/s (<30 mph)				
Cumulative Distribution (CD)	Pointing Error, mdeg	Pointing Loss, dB		
		S-band	X-band	Ka-band
Mean (54.4%)	5.000	0.005	0.069	0.999
90%	8.458	0.015	0.198	2.858
95%	9.734	0.019	0.262	3.786
99%	11.968	0.029	0.396	5.724

Table 12.   Recommended Minimum Operating Carrier Signal Levels (dBm)
for BWG Antennas Using the Block V Receiver (BVR)*

Band, LNA, and Configuration	Receiver Effective Noise Bandwidth (B$_L$) (Hz) [†]				
	0.25	1.0	2.0	20.0	200
S-Band					
DSS 24 Non-Diplexed	−179.8	−173.8	−170.8	−160.8	−150.8
DSS 34 Non-Diplexed	−179.5	−173.4	−170.4	−160.4	−150.4
DSS 54 Non-Diplexed	−179.7	−173.7	−170.7	−160.7	−150.7
DSS 24 S-Diplexed	−179.0	−173.0	−169.9	−159.9	−149.9
DSS 34 S-Diplexed	−178.5	−172.4	−169.4	−159.4	−149.4
DSS 54 S-Diplexed	−178.7	−172.6	−169.6	−159.6	−149.6
DSS 27 Diplexed		−168.5	−165.5	−155.5	−145.5
X-Band Only					
DSS 24 Non-Diplexed	−180.6	−174.5	−171.5	−161.5	−151.5
DSS 34 Non-Diplexed	−179.8	−173.7	−170.7	−160.7	−150.7
DSS 54 Non-Diplexed	−180.9	−174.9	−171.8	−161.8	−151.8
DSS 34 X-Diplexed	−178.8	−172.8	−169.8	−159.8	−149.8
DSS 54 X-Diplexed	−179.7	−173.7	−170.7	−160.7	−150.7
S/X-band					
DSS 24 Non-Diplexed	−180.3	−174.3	−171.3	−161.3	−151.3
DSS 34 Non-Diplexed	−179.5	−173.5	−170.5	−160.5	−150.5
DSS 54 Non-Diplexed	−180.6	−174.6	−171.5	−161.5	−151.5
DSS 34 Diplexed	−178.6	−172.6	−169.6	−159.6	−149.6
DSS 54 Diplexed	−179.5	−173.4	−170.4	−160.4	−150.4
X-Band LNA-1					
DSS 25 Non-Diplexed	−180.8	−174.7	−171.7	−161.7	−151.7
DSS 25 Diplexed	−179.6	−173.6	−170.6	−160.6	−150.6
DSS 26 Diplexed	−180.1	−174.0	−171.0	−161.0	−151.0

*   Levels are referenced to LNA input terminals with nominal zenith system noise
temperature and average clear weather (CD=0.25).
[†]   Bandwidth is centered about the received carrier.

Table 13.   Recommended Minimum Operating Carrier Signal Levels (dBm)
for BWG Antennas Using the Block V Receiver (BVR)*

Band, LNA, and Configuration	Receiver Effective Noise Bandwidth (B_L) (Hz) [†]				
	0.25	1.0	2.0	20.0	200
X-Band LNA-2					
DSS 25 Non-Diplexed	−178.8	−172.8	−169.8	−159.8	−149.8
DSS 25 Diplexed	−178.0	−172.0	−169.0	−159.0	−149.0
DSS 26 Diplexed	−180.1	−174.0	−171.0	−161.0	−151.0
Ka-Band Only					
DSS 25	−178.8	−172.8	−169.7	−159.7	−149.7
X/Ka-Band					
DSS 25	−178.4	−172.4	−169.4	−159.4	−149.4

*   Levels are referenced to LNA input terminals with nominal zenith system noise temperature
    and average clear weather (CD=0.25).
[†]   Bandwidth is centered about the received carrier.

Table 14.   Recommended Minimum Operating Carrier Signal Levels (dBm)
for DSS 27 HSB Antenna Using the Multifunction Receiver (MFR)*

Band, LNA, and Configuration	Receiver Effective Noise Bandwidth (B_L) (Hz) [†]					
	10	30	100	300	1000	3000
S-Band						
DSS 27 Diplexed	−155.5	−150.7	−145.5	−140.7	−135.5	−130.7

*   Levels are referenced to LNA input terminals with nominal zenith system noise temperature
    and average clear weather (CD=0.25).
[†]   Indicated bandwidths are one-sided. That is, a value such as "30 Hz" means 30 Hz on each
    side of the carrier frequency for a total bandwidth of 60 Hz, and so forth
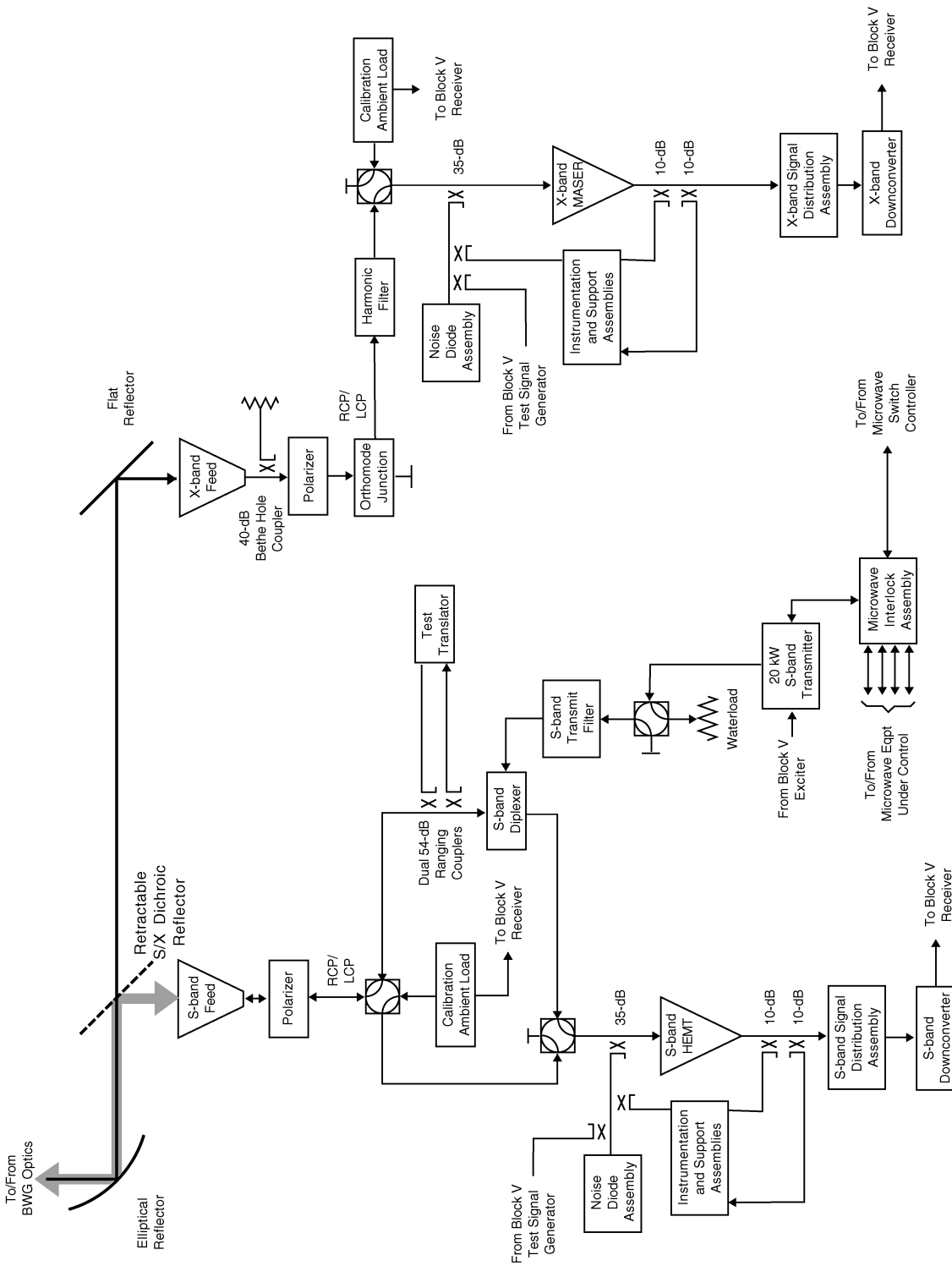
Figure 1. Functional Block Diagram of DSS 24 Antenna
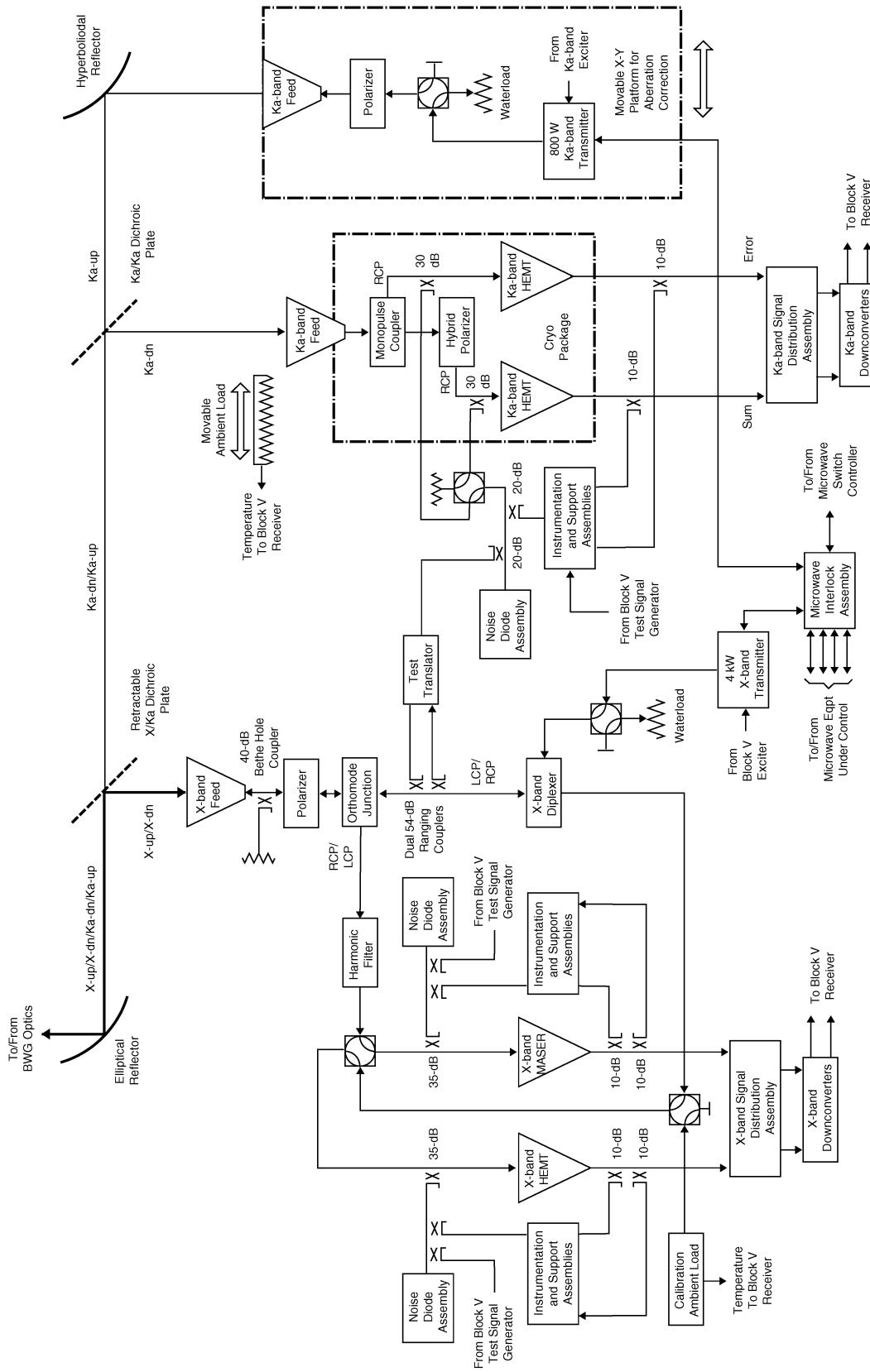
Figure 2.   Functional Block Diagram of DSS 25 Antenna
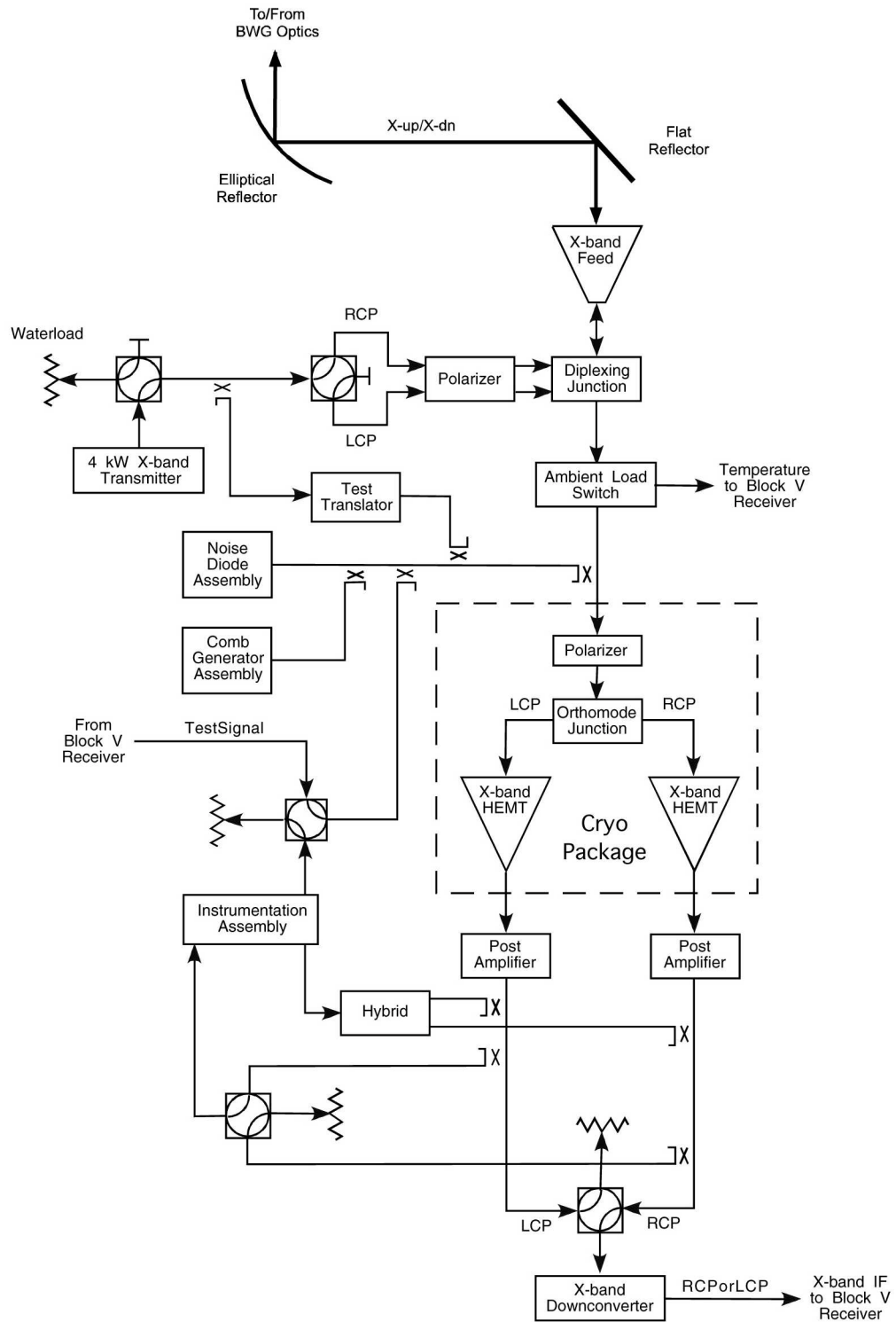
Figure 3.   Functional Block Diagram of DSS 26 Antenna

Figure 4. Functional Block Diagram of DSS 34 and DSS 54 Antennas
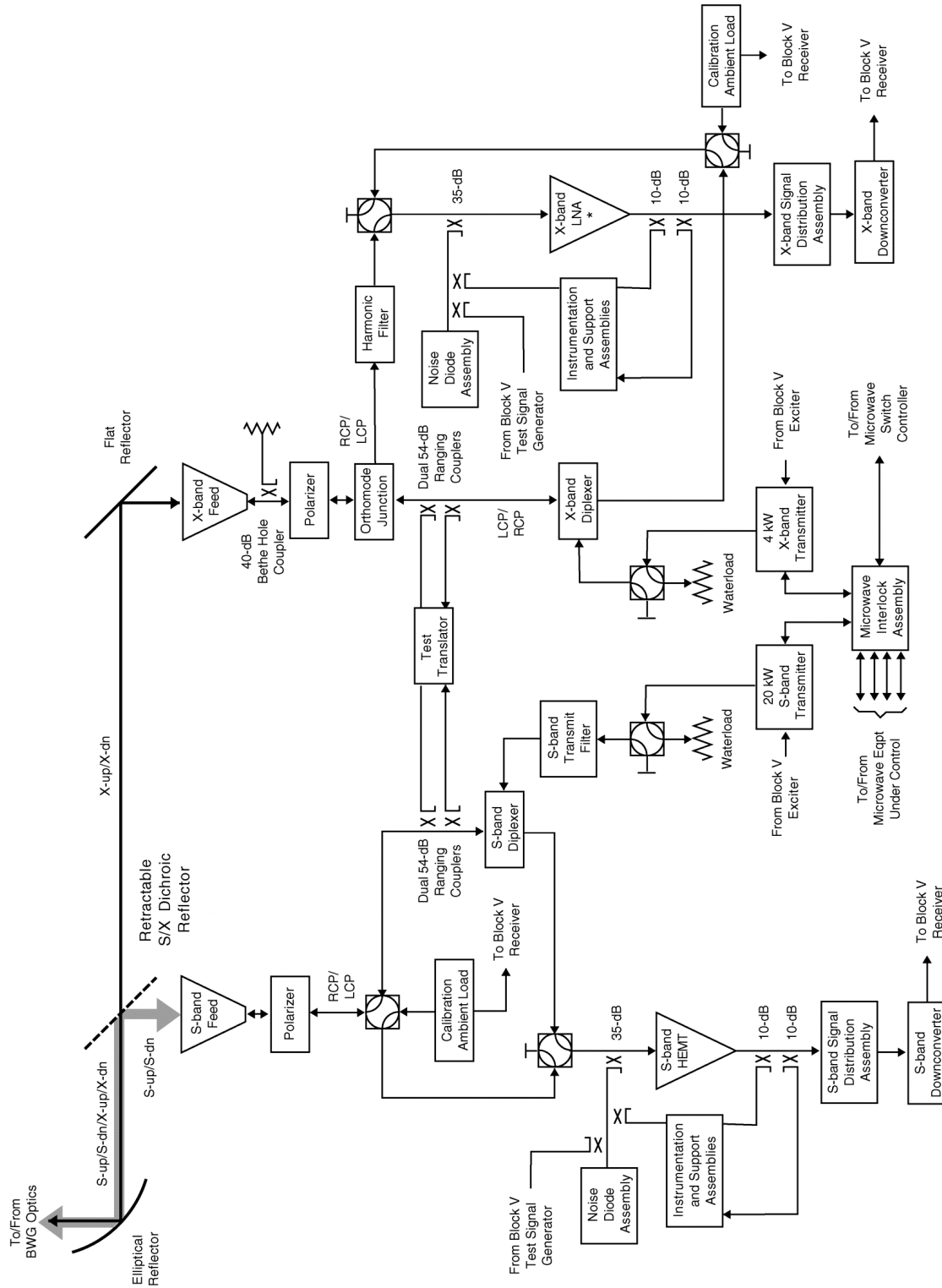
NOTE: * X-band LNA is HEMT at DSS 34 and MASER at DSS 54.

34
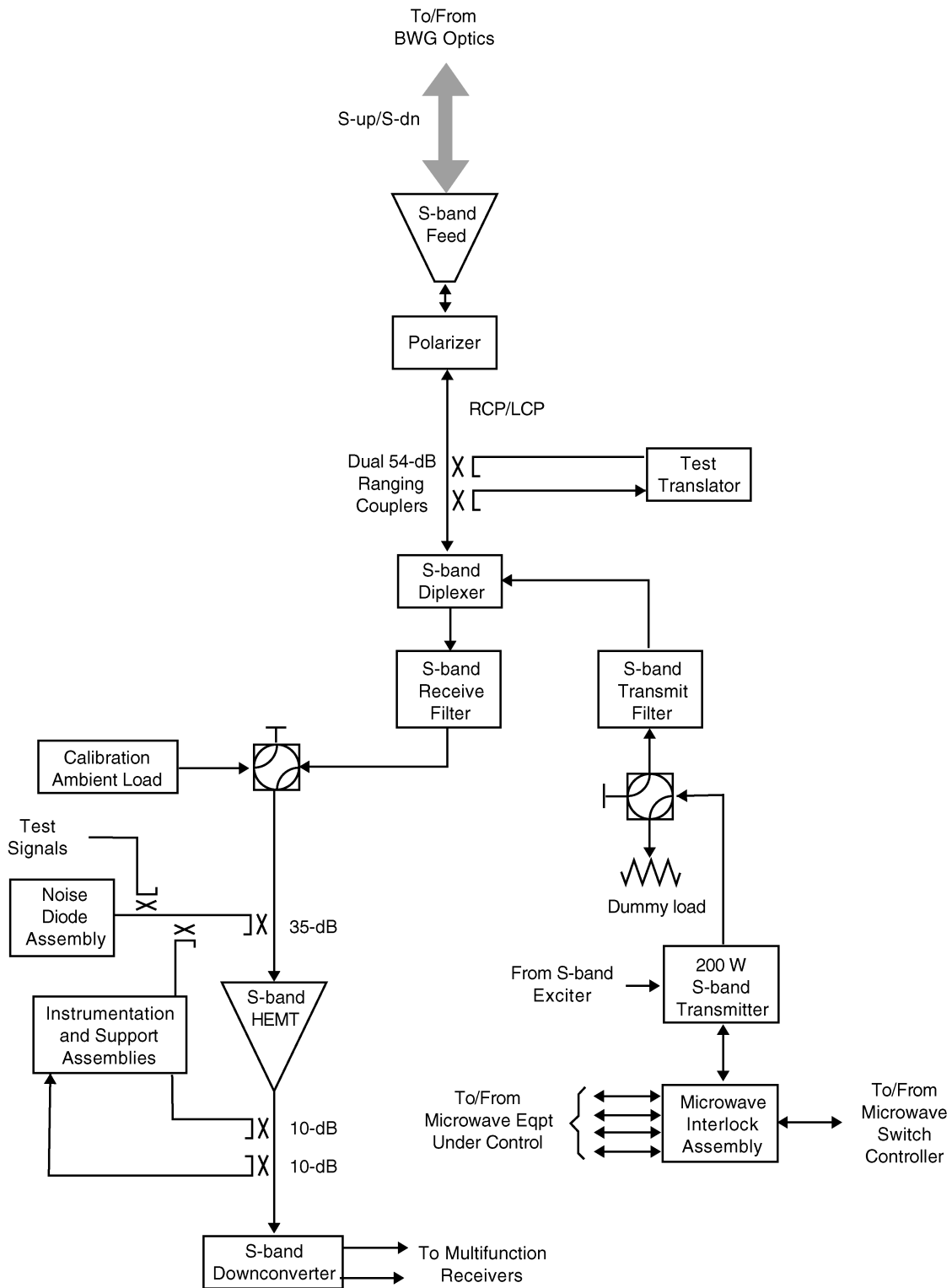
Figure 5.   Functional Block Diagram of DSS 27 Antenna
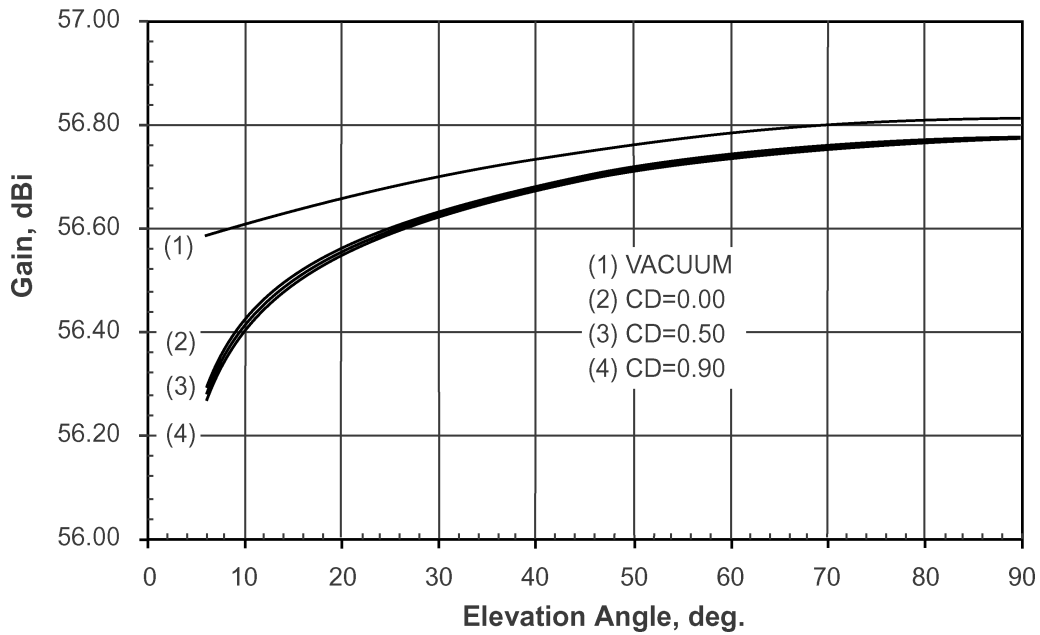
Figure 6. DSS 24 (Goldstone) S-Band Receive Gain Versus Elevation Angle, S/X Mode, 2295 MHz
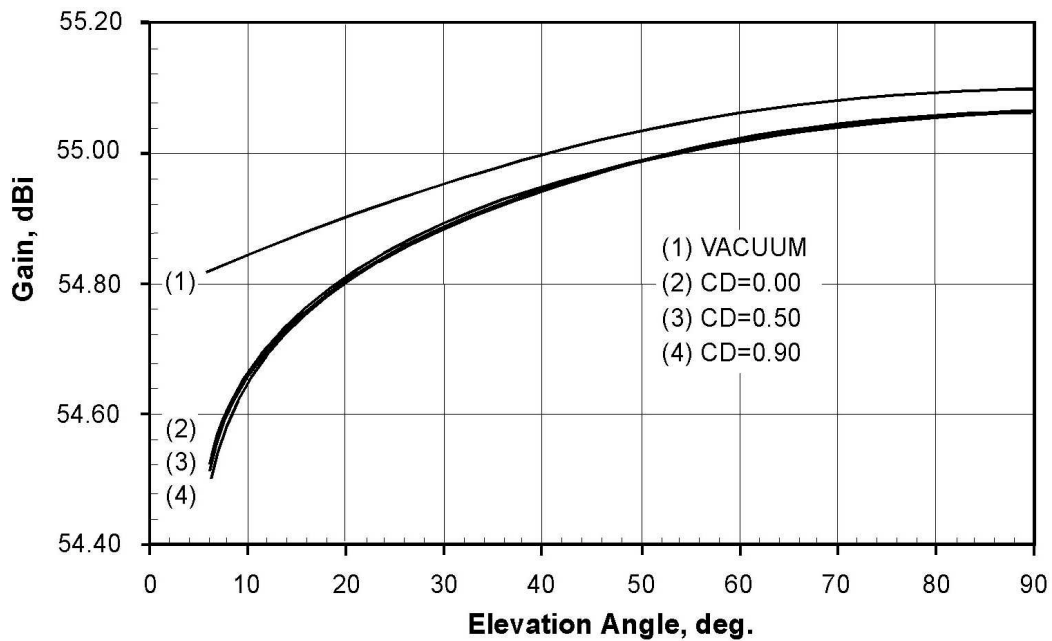
Figure 7. DSS 27 (Goldstone) S-Band Receive Gain Versus Elevation Angle, 2295 MHz
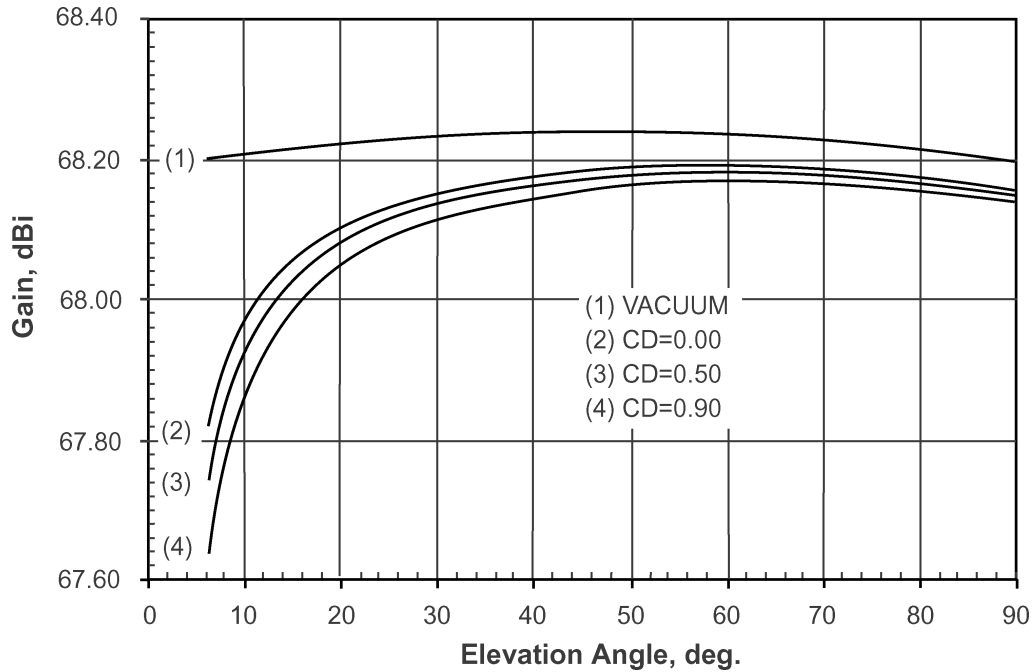
Figure 8. DSS 34 (Canberra) X-Band Receive Gain Versus Elevation Angle, S/X Mode, 8420 MHz
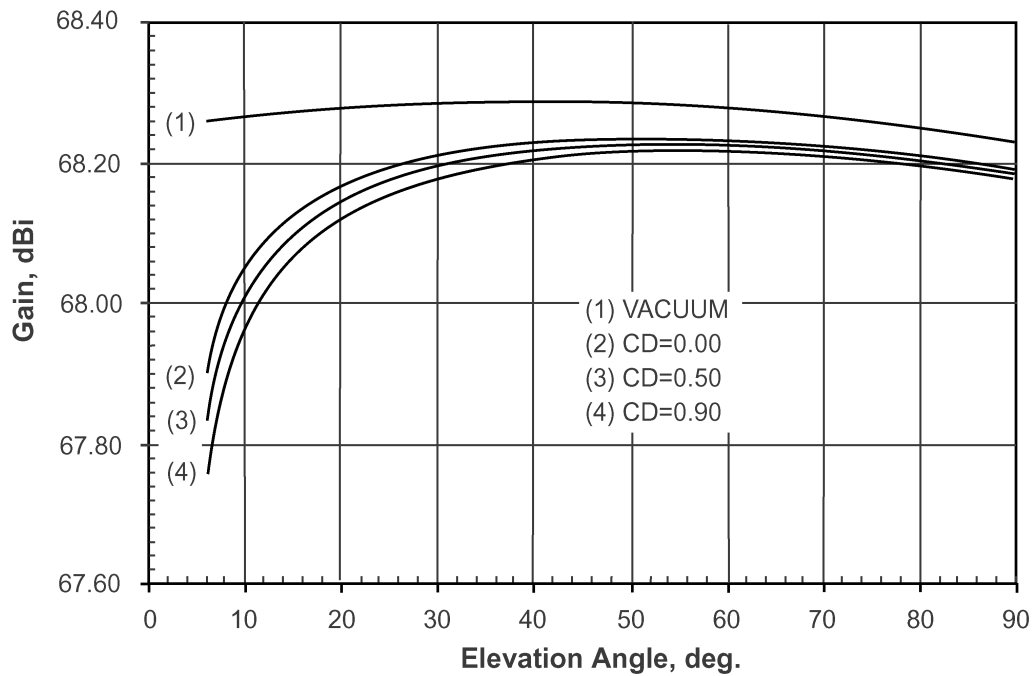
Figure 9. DSS 54 (Madrid) X-Band Receive Gain Versus Elevation Angle, X-Only Mode (S/X Dichroic Retracted), 8420 MHz
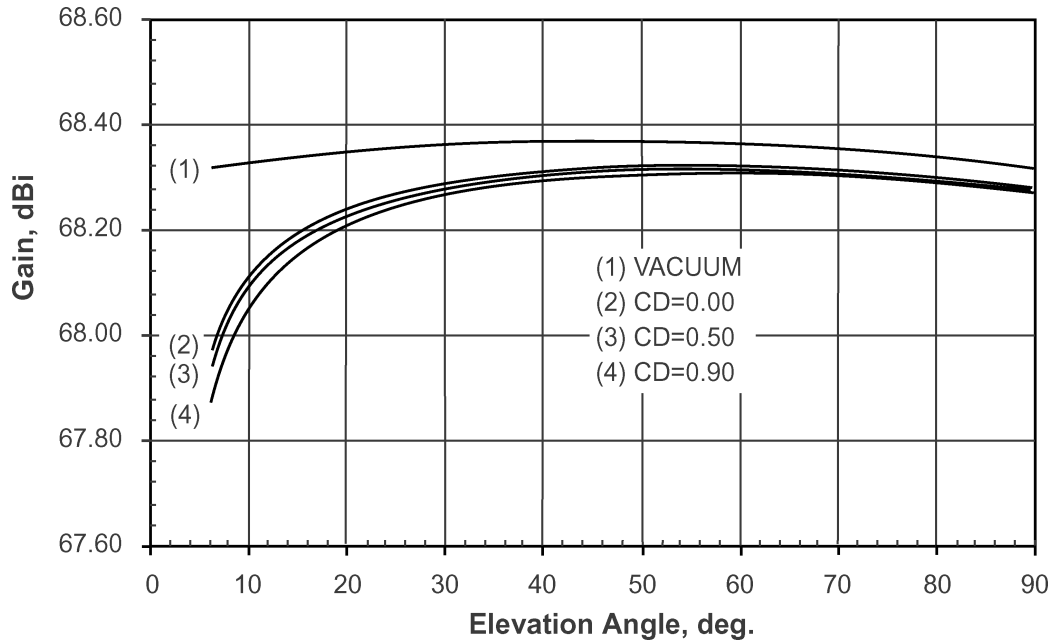
Figure 10.DSS 25 (Goldstone) X-Band Receive Gain Versus Elevation Angle, 8420 MHz
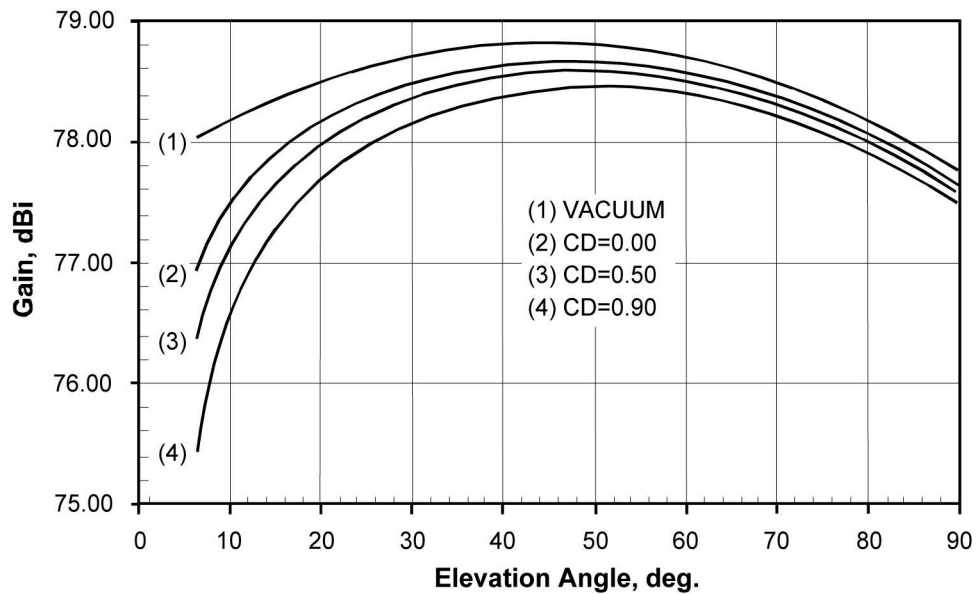
Figure 11. DSS 25 (Goldstone) Ka-Band Receive Gain Versus Elevation Angle, X/Ka Mode (X/Ka Dichroic In-Place), 32000 MHz
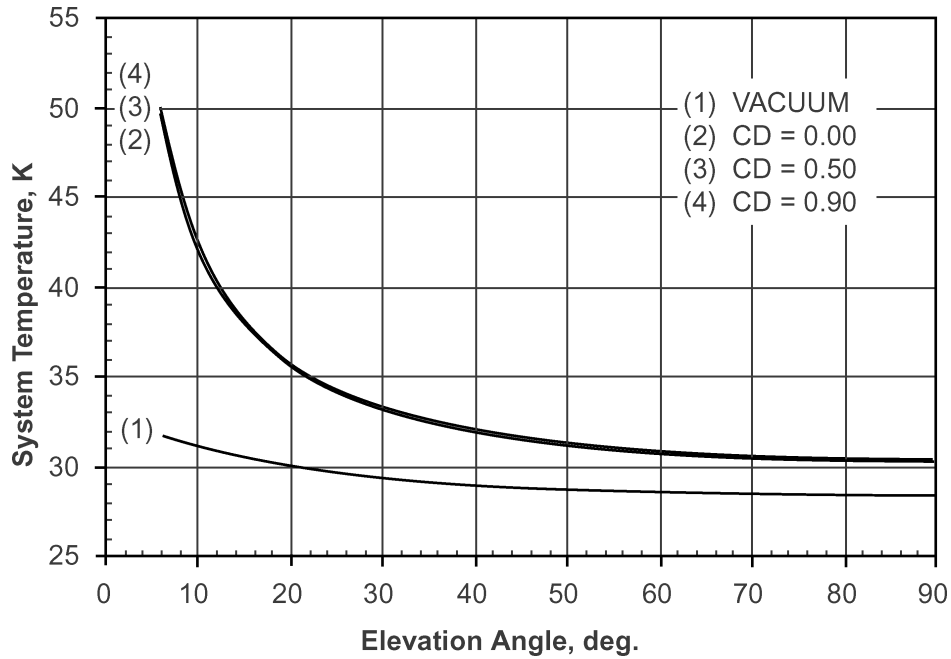
Figure 12. DSS 24 (Goldstone) S-Band System Temperature Versus Elevation Angle, S/X Mode, Non-Diplexed Path, 2295 MHz
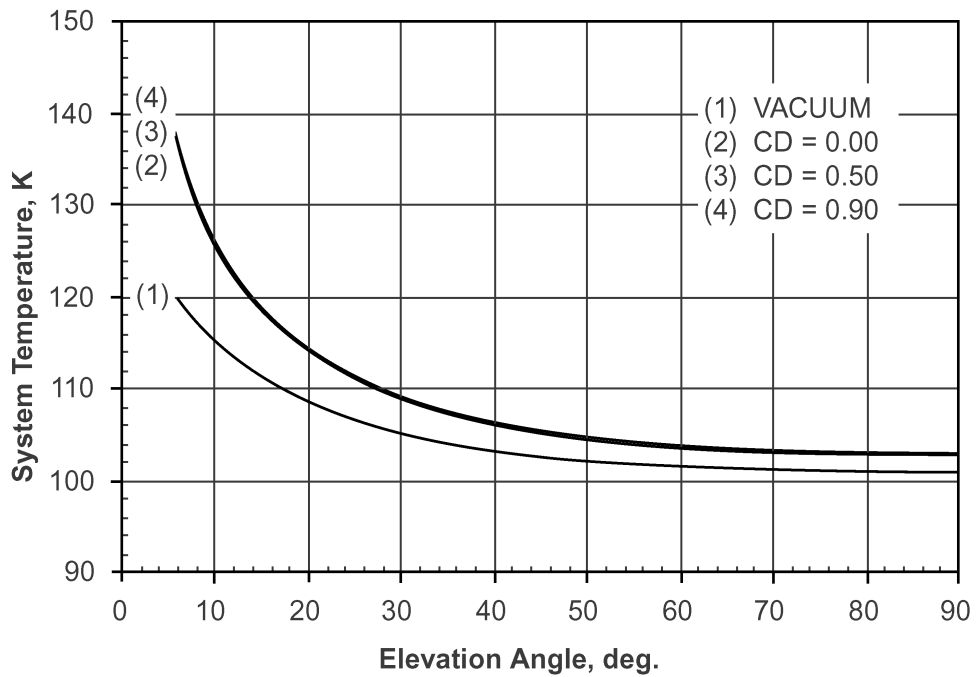
Figure 13. DSS 27 (Goldstone) S-Band System Temperature Versus Elevation Angle, Diplexed Path, 2295 MHz
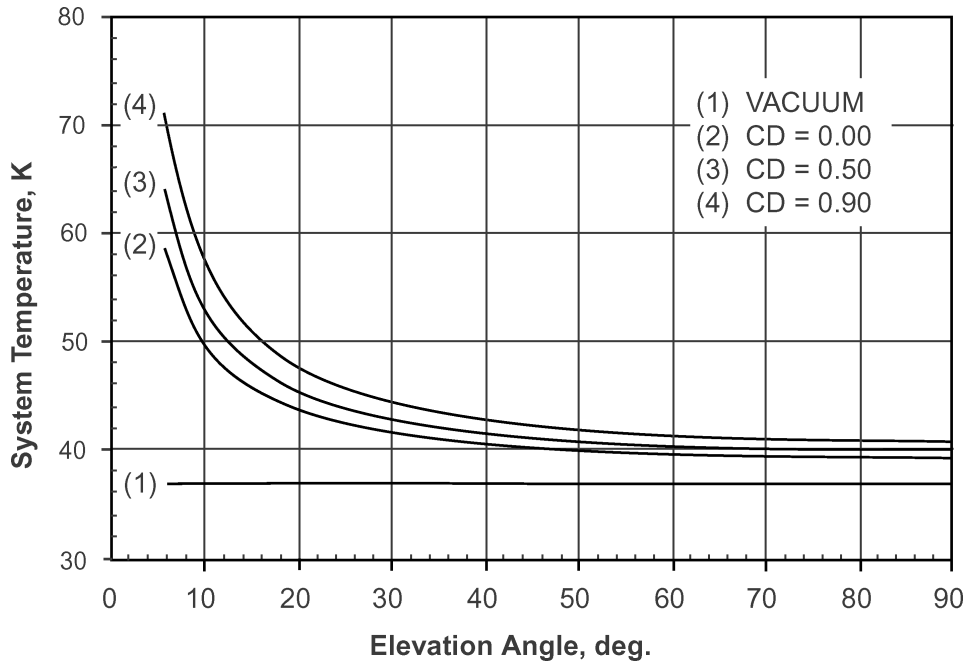
Figure 14. DSS 34 (Canberra) X-Band System Temperature Versus Elevation Angle,
S/X Mode, Diplexed Path, 8420 MHz
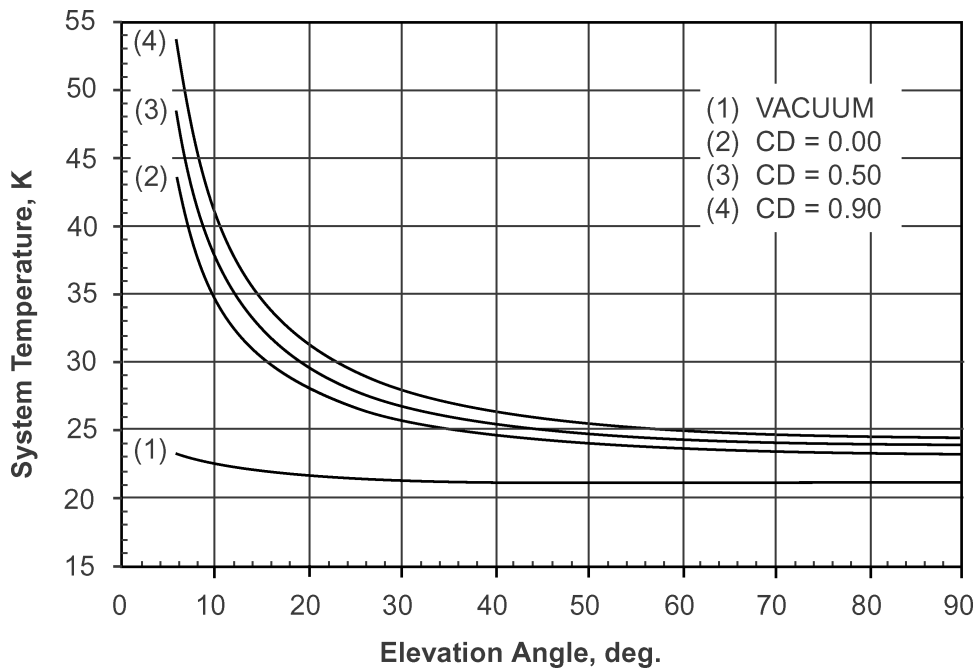
Figure 15. DSS 54 (Madrid) X-Band System Temperature Versus Elevation Angle,
X-Only Mode (S/X Dichroic Retracted), Non-Diplexed Path, 8420 MHz
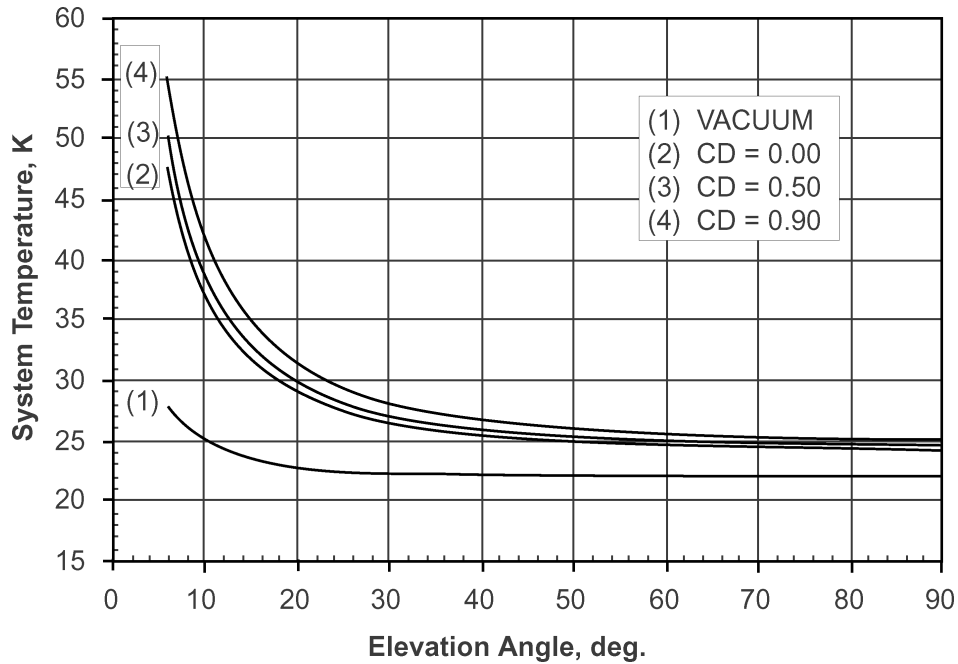
Figure 16. DSS 25 (Goldstone) X-Band System Temperature Versus Elevation Angle, Non-Diplexed Path, 8420 MHz
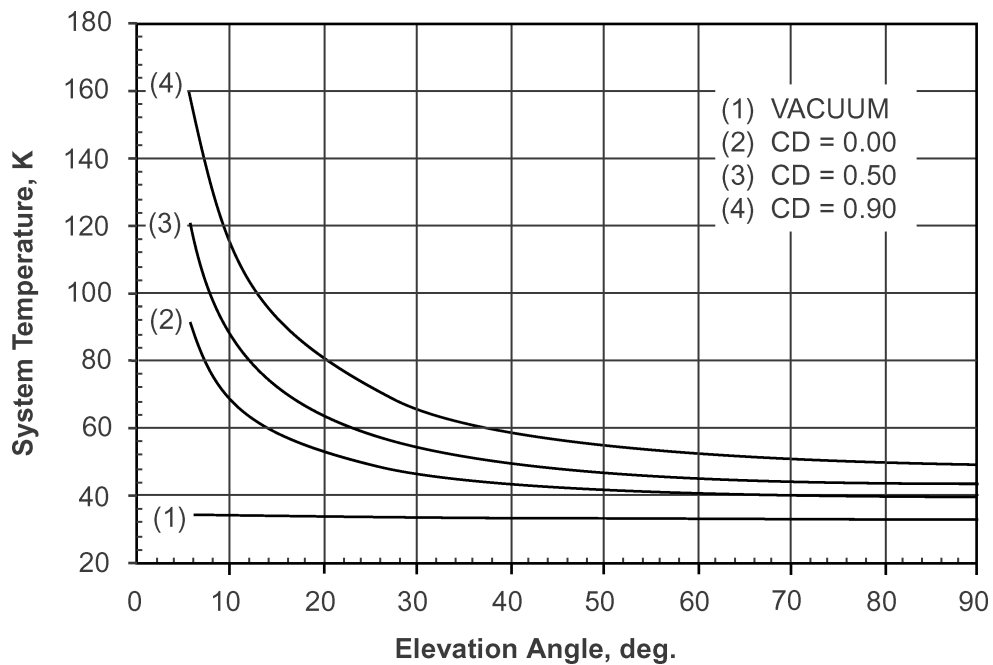
Figure 17. DSS 25 (Goldstone) Ka-Band System Temperature Versus Elevation Angle, X/Ka Mode (X/Ka Dichroic in Place), 32000 MHz
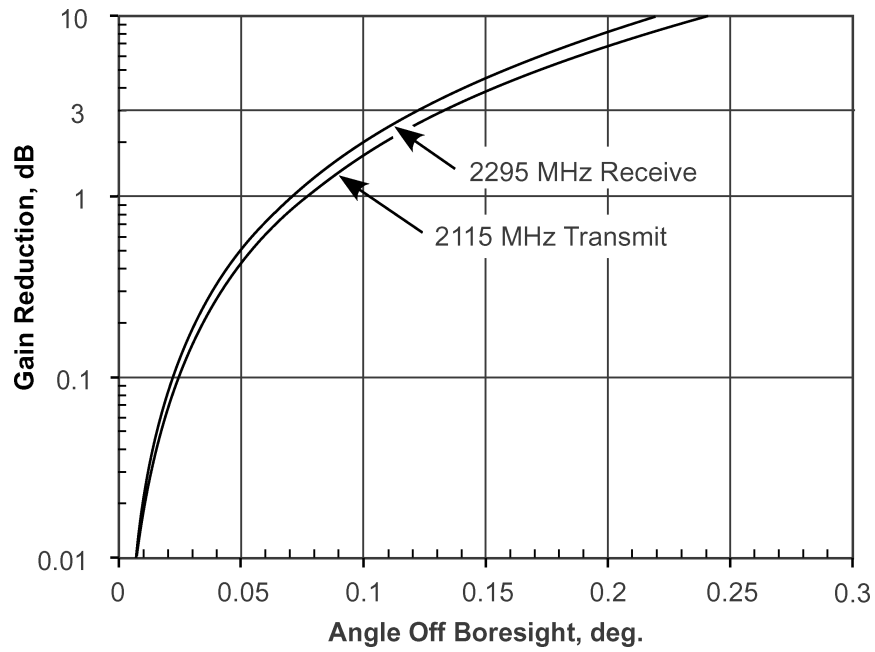
Figure 18. S-Band Gain Reduction Versus Angle off Boresight
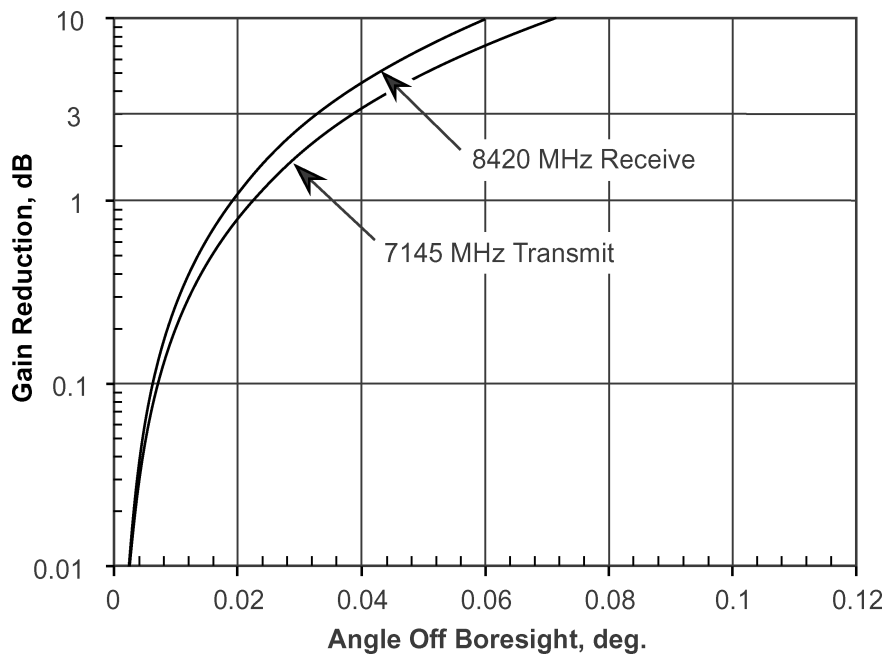
Figure 19. X-Band Gain Reduction Versus Angle off Boresight
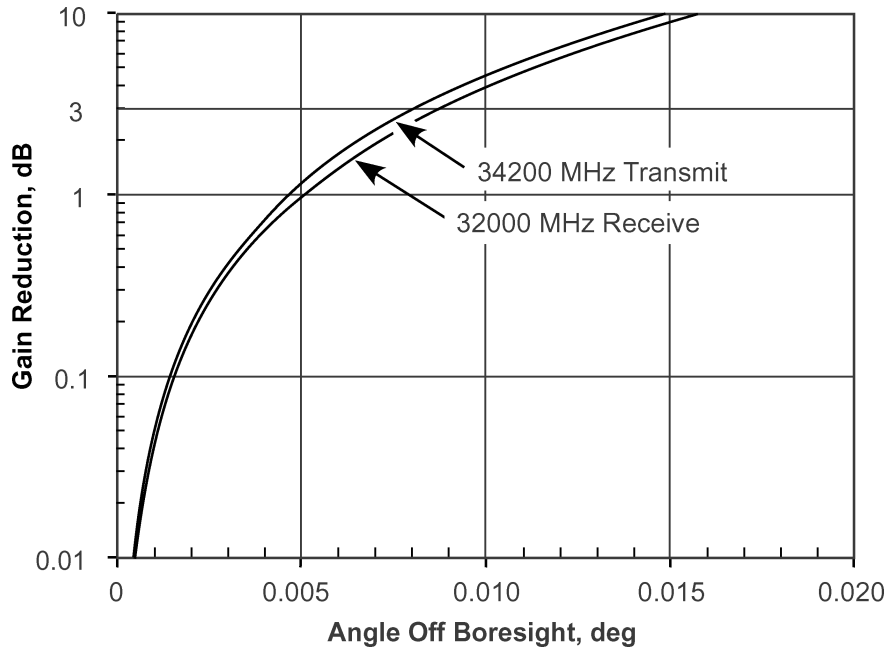
Figure 20.   Ka-Band Gain Reduction Versus Angle off Boresight
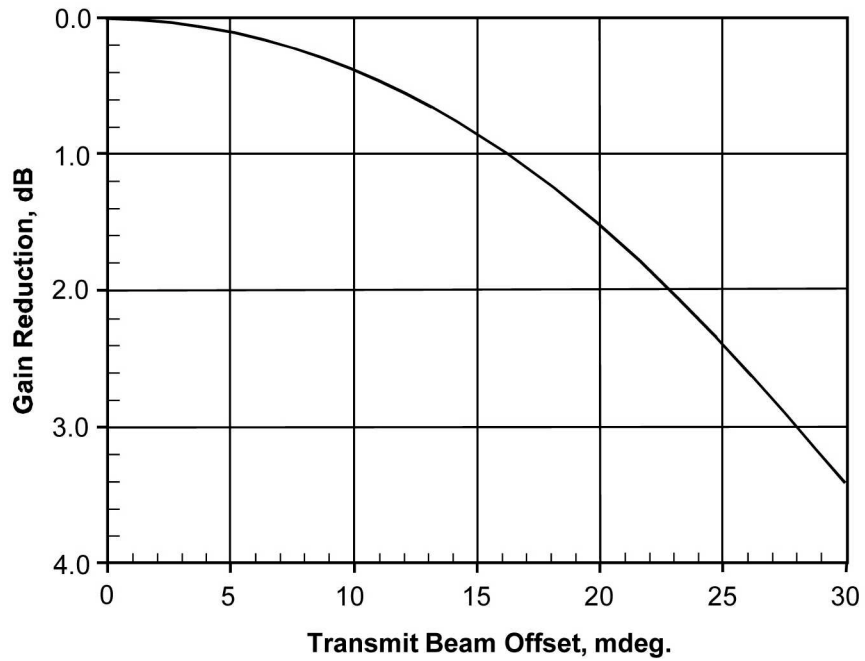
Figure 21. Ka-Band Transmit Gain Reduction Due to Aberration Correction

Appendix A
Equations for Modeling

A.1 *Equations for Gain Versus Elevation Angle*

The following equation can be used to generate S-, X-, and Ka-band transmit and receive gain versus elevation angle curves. Examples of these curves for selected stations and configurations are shown in Figures 6–11. See paragraph 2.1.1.1 for frequency effect modeling and module 105 for atmospheric attenuation at weather conditions other than 0%, 50%, and 90% cumulative distribution.

$$G(\theta) = G_0 - G_1(\theta - \gamma)^2 - \frac{A_{ZEN}}{\sin\theta}, \quad \text{dBi} \tag{A-1}$$

where

θ $=$ antenna elevation angle (deg.) $6 \leq \theta \leq 90$

G_0, G_1, γ $=$ parameters from Tables A1, A2, and A3

A_{ZEN} $=$ zenith atmospheric attenuation from Table A-4 or from Table 2 in module 105, dB.

A.2 *Equations for System Temperature Versus Elevation Angle*

The following equation can be used to generate S-, X, and Ka-band system temperature versus elevation angle curves. Examples of these curves are shown in Figures 12–17. See module 105 for atmospheric attenuation at weather conditions other than 0%, 50%, and 90% cumulative distribution..

$$T_{op}(\theta) = T_1 + T_2 e^{-a\theta} + (255 + 25CD)\left(1 - \frac{1}{10^{\frac{A_{ZEN}}{10\sin\theta}}}\right), \quad \text{K} \tag{A-2}$$

where

θ $=$ antenna elevation angle (deg), $6 \leq \theta \leq 90$

T_1, T_2, a $=$ parameters from Tables A-1, A-2, or A-3

CD $=$ cumulative distribution used to select A_{ZEN} from Table A-4 or from Table 2 in module 105, $0 \leq CD \leq 0.99$

A_{ZEN} $=$ zenith atmospheric attenuation from Table A-4 or from Table 2 in module 105, dB.

A.3   *Equation for Gain Reduction Versus Pointing Error*

The following equation can be used to generate gain reduction versus pointing error curves, examples of which are depicted in Figures 18, 19, and 20.

$$\Delta G(\theta) = 10 \log \left(e^{-\frac{2.773\,\theta^2}{HPBW^2}} \right), \text{dB} \tag{A-3}$$

where

θ =   pointing error, deg

$HPBW$ =   half-power beamwidth (from Tables 2 through 8).

A.4   *Equation for Transmit Aberration Gain Reduction*

The following equation can be used to generate the Ka-band transmit gain reduction curve depicted in Figure 21.

$$\Delta G(\phi) = -0.0038\phi^2, \text{dB} \tag{A-4}$$

where

ϕ =   transmit beam offset, mdeg.

Table A-1. S-Band Vacuum Gain and System Noise Temperature Parameters

Station and Configuration	Vacuum Gain Parameters				Vacuum System Noise Temperature Parameters			Figures
	G_0† Transmit	G_0† Receive	G_1	γ	T_1	T_2	a	
DSS 24 (Goldstone)								
S/X, Non-Diplexed (HEMT)	—	56.81	0.000032	90.0	28.34	4.7	0.05	6, 12
S/X, Diplexed (HEMT)	56.1	56.81	0.000032	90.0	34.79	4.7	0.05	
DSS 27 (Goldstone)								
S-Only, Diplexed (R/T HEMT)	54.4	55.10	0.00004	90.0	101.00	27.0	0.061	7, 13
DSS 34 (Canberra)								
S/X, Non-Diplexed (HEMT)	—	56.75	0.000037	52.5	30.68	0.0	0.0	
S/X, Diplexed (HEMT)	56.1	56.75	0.000037	52.5	39.28	0.0	0.0	
DSS 54 (Madrid)								
S/X, Non-Diplexed (HEMT)	—	56.75	0.000037	45.0	28.88	0.0	0.0	
S/X, Diplexed (HEMT)	56.1	56.75	0.000037	45.0	37.48	0.0	0.0	

Notes:
† G_0 values are nominal at the frequency specified in Tables 2, 3, 6, or 8. Other parameters apply to all frequencies within the same band.

Table A-2. X-Band Vacuum Gain and System Noise Temperature Parameters

Station and Configuration	Vacuum Gain Parameters				Vacuum System Noise Temperature Parameters			Figures
	G_0† Transmit	G_0† Receive	G_1	γ	T_1	T_2	a	
DSS 24 (Goldstone)								
X-Only, Non-Diplexed (MASER)	—	68.11	0.000027	51.5	23.18	0.0	0.0	
S/X, Non-Diplexed (MASER)	—	68.06	0.000027	51.5	24.58	0.0	0.0	
DSS 25 (Goldstone)								
X/Ka, Non-Diplexed (MASER)	—	68.37	0.000028	47.5	22.13	14.0	0.15	10, 16
X/Ka, Non-Diplexed (HEMT)	—	68.37	0.000028	47.5	35.93	14.0	0.15	
X/Ka, Diplexed (MASER)	67.1	68.37	0.000028	47.5	29.63	14.0	0.15	
X/Ka, Diplexed (HEMT)	67.1	68.37	0.000028	47.5	43.43	14.0	0.15	
DSS 26 (Goldstone)								
X-Only, Diplexed (HEMT-1)	67.1	68.29	0.000028	45.0	25.8	4.5	0.08	
X-Only, Diplexed (HEMT-2)	67.1	68.29	0.000028	45.0	26.5	4.5	0.08	

Notes:

† G_0 values are nominal at the frequency specified in Tables 4, 6, and 7. Other parameters apply to all frequencies within the same band.

Table A-2. X-Band Vacuum Gain and System Noise Temperature Parameters (Continued)

Station and Configuration	Vacuum Gain Parameters				Vacuum System Noise Temperature Parameters			Figures
	G_0† Transmit	G_0† Receive	G_1	γ	T_1	T_2	a	
DSS 34 (Canberra)								
X-Only, Non-Diplexed (HEMT)	—	68.29	0.000023	47.5	28.00	0.0	0.0	
X-Only, Diplexed (HEMT)	67.1	68.29	0.000023	47.5	35.50	0.0	0.0	
S/X, Non-Diplexed (HEMT)	—	68.24	0.000023	47.5	29.70	0.0	0.0	
S/X, Diplexed (HEMT)	67.1	68.24	0.000023	47.5	37.20	0.0	0.0	8, 14
DSS 54 (Madrid)								
X-Only, Non-Diplexed (MASER)	—	68.29	0.000023	47.5	21.07	4.0	0.1	9, 15
X-Only, Diplexed (MASER)	67.1	68.29	0.000023	47.5	28.62	4.0	0.1	
S/X, Non-Diplexed (MASER)	—	68.24	0.000023	47.5	22.82	4.0	0.1	
S/X, Diplexed (MASER)	67.1	68.24	0.000023	47.5	30.22	4.0	0.1	

Notes:

† G_0 values are nominal at the frequency specified in Tables 4, 6, and 7. Other parameters apply to all frequencies within the same band.

Table A-3. Ka-Band Vacuum Gain and System Noise Temperature Parameters

Station and Configuration	Vacuum Gain Parameters				Vacuum System Noise Temperature Parameters			Figures
	G_0† Transmit	G_0† Receive	G_1	γ	T_1	T_2	a	
DSS 25 (Goldstone)								
Ka-Only, Diplex (HEMT)	79.5	78.98	0.00052	45.0	28.41	2.9	0.013	
X/Ka, Diplex (HEMT)	79.5	78.83	0.00052	45.0	31.91	2.9	0.013	11, 17

Notes:

   † G_0 values are nominal at the frequency specified in Tables 5 and 7. Other parameters apply to all frequencies within the same band.

Table A-4. S-, X-, and Ka-Band Zenith Atmospheric Attenuation (A_{ZEN})

Station	A_{ZEN}, dB*		
	CD† = 0.00	CD† = 0.50	CD† = 0.90
S-Band			
Goldstone	0.033	0.032	0.031
Canberra	0.036	0.035	0.034
Madrid	0.034	0.033	0.033
X-Band			
Goldstone	0.037	0.040	0.047
Canberra	0.040	0.048	0.059
Madrid	0.038	0.045	0.053
Ka-Band			
Goldstone	0.116	0.177	0.274

Notes:

   *   From Table 2 in module 105,
   †   CD = cumulative distribution.

105, Rev. A
Atmospheric and Environmental Effects

December 15, 2002

Prepared by:

S.D. Slobin 12-9-02
_____
S. D. Slobin,   Date
Antenna System Engineer

Approved by:

A. J. Freiley 12-9-02
_____
A. J. Freiley   Date
Antenna Product Domain Service
System Development Engineer

Released by:

$\begin{bmatrix} \text{Signature on File} \\ \text{at DSMS Library} \end{bmatrix}$ 2/10/03
_____
DSMS Document Release   Date

Change Log

Rev	Issue Date	Affected Paragraphs	Change Summary
Initial	11/30/2000	All	All
A	12/15/2002	All	Provides monthly weather statistics for all stations and frequency bands

Note to Readers

There are two sets of document histories in the 810-005 document that are reflected in the header at the top of the page. First, the overall document is periodically released as a revision when major changes affect a majority of the modules. For example, this document is part of Revision E. Second, the individual modules also change, starting as the initial issue that has no revision letter. When a module is changed, a change letter is appended to the module number on the second line of the header and a summary of the changes is entered in the module's change log.

Contents

Illustrations

Tables

1 Introduction

1.1 Purpose

This module provides sufficient information concerning atmospheric, environmental, and extraterrestrial effects to enable a flight project to design a telecommunications link at the L-, S-, X, and Ka-band frequencies used by the DSN.

1.2 Scope

Statistics of atmospheric attenuation and noise temperature at each tracking antenna site are presented for those microwave frequencies used by the DSN. In this module, the values of attenuation and noise temperature increase are given relative to a no-atmosphere (vacuum) condition thus, this presentation is compatible for use with the vacuum gain and noise temperature presentations of antenna performance given in modules 101 for 70-m antennas, 102 for 26-m antennas, 103 for 34-m high-efficiency (HEF) antennas, and 104 for 34-m beam-waveguide (BWG) antennas.

Statistics of wind speed at Goldstone are given. These are used both to determine the statistics of antenna gain reduction due to wind loading and also to ascertain the percentage of time an antenna will be unusable due to excessive wind speed.

Extraterrestrial effects are primarily the increased system noise temperature due to hot body noise from the Sun, Moon, planets, and galactic radio sources. These effects are significant only when the antenna beam is in the vicinity of these noise sources during tracking of spacecraft.

Charged-particle effects are given in module 106, Solar Corona and Solar Wind Effects.

2 General Information

2.1 Atmospheric Attenuation and Noise Temperature

The principal sources of atmospheric attenuation and noise temperature weather effects are oxygen, water vapor, clouds, and rain. These two effects are related, and higher atmospheric attenuation produces a higher noise contribution. Also, atmospheric effects generally increase with increasing frequency. Ka-band effects are larger than X-band effects, which are larger than S-band and L-band effects.

In the 810-005 antenna performance modules (modules 101, 102, 103, and 104), *effective antenna gain* (vacuum gain minus atmospheric attenuation) is presented in the figures for various atmospheric attenuation values. Strictly speaking, the gain of an antenna is not a function of atmospheric attenuation; however for stand-alone use, the effective gain, including atmospheric loss, is a useful concept, and the expressions for gain in the appendices of those modules include a term for atmospheric attenuation. Similarly, system operating noise temperature as presented in the appendices of those modules also includes a term for atmospheric noise contribution, although the *antenna temperature* (due to spillover, LNA contribution, waveguide loss, etc.) is also not a function of atmosphere contribution. The vacuum system noise temperature as given in those modules includes the nearly constant contribution from the cosmic background, which adds to the basic antenna temperature value.

Design control tables used for telecommunications link design typically carry separate entries for atmospheric attenuation of the received or transmitted signal and atmospheric noise contribution as a function of elevation angle and weather condition. It is important in those DCTs that the antenna gain and system operating noise temperature values reflect the vacuum performance of the antenna, so as to prevent double-bookkeeping of the atmospheric attenuation and noise temperature contributions.

The atmospheric models presented here give L-band (1.7 GHz), S-band (2.3 GHz), X-band (8.4 GHz), and Ka-band (32.0 GHz) atmospheric noise temperature and attenuation statistics in the form of cumulative distributions (CDs) for each effect. A cumulative distribution of 0.90 (90% weather) means that 90% of the time a particular weather effect (noise temperature or attenuation) is less than or equal to a given value. Conversely, that particular effect is exceeded only 10% of the time. Qualitatively, the weather conditions associated with selected cumulative distributions are described as follows:

CD	=	0.00	clear dry, lowest weather effect
CD	=	0.25	average clear weather
CD	=	0.50	clear humid, or very light clouds
CD	=	0.90	very cloudy, no rain
CD	>	0.95	very cloudy, rain

By their very natures, clouds and rain are poorly modeled, and the water vapor radiometer data used here are sparse for the larger weather effects, which are exceeded only 5% of the time.

The Ka-band model presented here is based on actual water vapor radiometer noise temperature measurements made at 31.4 GHz at all three DSN sites (Goldstone, Canberra, and Madrid). Used in the modeling were 66 months of Goldstone data covering the period October 1993 through August 2002, 35 months of Canberra data covering the period June 1999 through August 2002, and 112 months of Madrid data covering the period September 1990 through August 2002. There were missing months of data from each station. Note also that different numbers of months of data went into the model for each of the separate months (e.g., there may have been 6 Februaries, but only 4 Marches). It is felt that because of the large amount of Madrid data (more than 9 years), the results will fairly accurately represent true long-term statistics. The 5-1/2 years of Goldstone data will give a moderately accurate long-term model. The three years of Canberra data will probably not give a very accurate long-term model, and future updates of the Canberra model are likely to show relatively large changes in the distributions. Cumulative distributions at 31.4 GHz for each of the 12 months were calculated, then increased by 0.3 K (the oxygen-only difference due to frequency) to create a model for 32 GHz. A year-average model was developed by calculating the average noise temperature of all the 12 months, at each CD level.

L-/S-band and X-band statistics were created from the Ka-band (32 GHz) statistics by subtracting out the 0% CD baseline (calculated for nominal temperatures and pressures, with 0% relative humidity), frequency squaring to the appropriate frequency (for example, $[8.42/32.0]^2$) and then adding in the 0% CD baseline at the new frequency. Note that the 0% CD baselines for the DSN sites differ because of different heights above sea level.

Atmospheric attenuation statistics were created from the noise temperature statistics by methods given in Sections 2.1.1 and 2.1.3 below. The year-average attenuation statistics were calculated from the year-average noise temperature values rather than by calculating the average of all the monthly attenuations. These two methods give very slightly different results.

It should be noted that although the noise temperature statistics are the best qualitative measures for comparison of different locations and different frequencies, especially when dealing with low-noise systems (where the atmospheric noise is a large part of the total system noise temperature), the basic data base of atmospheric effects is actually the attenuation statistics. Given a station location, frequency, and CD of interest, the attenuation data base value is extracted, modeled to the elevation angle of interest (Section 2.1.2), and then the appropriate atmospheric noise temperature is calculated (Section 2.1.3). In this way, the original zenith noise temperature statistics (Tables 1 through 9) can be re-calculated from the zenith attenuation values (Tables 10 through 18) using the method given in Section 2.1.3.

The atmospheric models thus generated for a particular complex (for example, Goldstone) should be used for all antennas at that complex (for example, DSS 14, DSS 15, DSS 24, etc.), regardless of the small altitude differences among the antennas.

Zenith atmospheric noise temperature statistics for the three DSN sites at S-band are provided in Tables 1 through 3. Tables 4 through 6 provide similar statistics for X-band and Tables 7 through 9 cover Ka-band. The tables include the maximum and minimum value for each CD level, the year average for that CD level and the average value for each month. These noise temperature statistics should be used only in a qualitative sense to describe the relative levels of atmospheric noise contributions at different locations and cumulative distributions. They should not be used for elevation modeling as this is properly performed using the calculated attenuation at a given elevation angle as a starting point and following the process that is described below.

The use of these statistics depends on the context in which the antenna temperature is stated. When a nominal antenna zenith T_{op} (operating system noise temperature) is stated, it is considered to include the CD = 25% (average clear sky) value for the appropriate frequency and location. However, "vacuum" antenna temperatures are sometimes used to describe the performance of an antenna independent of location. In this case the operating system noise temperature should be referred to as $T_{op, vac}$.

Tables 10 through 18 provide similar presentations for zenith atmospheric attenuation. It can be noted that the L-/S-band attenuations do not monotonically increase as a function of CD, whereas the corresponding noise temperatures do. This is an artifact of the relationship between the modeled mean physical temperature of the atmosphere and the noise temperature used to calculate the corresponding attenuation. This relationship is seen below. In any case, the atmospheric effect at L-/S-band is nearly constant (to within 0.1 K and 0.003 dB over the CD range from 0% to 90%), and this small anomaly does not contribute to significant errors in modeling telecommunications performance.

The tolerances of atmospheric noise temperature and attenuation, as given in Tables 1 through 18, should be considered to be 5% of the stated values at zenith, or 5% of the values calculated for elevation angles other than zenith. (see Section 2.1.5, below).

Figures 1, 2, and 3 show the L-/S-band noise temperature statistics for Goldstone, Canberra, and Madrid respectively. Figures 4, 5, and 6 show X-band statistics for the three complexes. Figures 7, 8, and 9 provide the Ka-band statistics. On each figure, the year-average cumulative distribution, the minimum envelope value, and the maximum envelope values are given for all the individual months at each CD value stated in Tables 1–9. The year-average model from the previous revision of module 105 (dated November 30, 2000) is also given to aid the user in assessing the changes from one model to the next. Curves of zenith attenuation are not given, although using a rule-of thumb that a medium with 1 dB attenuation radiates a noise temperature of approximately 60 K, the Ka-band curves can be used to make rough estimates of the zenith attenuation at the various frequencies. This relationship is nearly linear over the range from 0 to 1 dB.

For Ka-band, using 90% CD as a reference point, it is seen qualitatively that the Goldstone year-average model shows better weather than the previous module 105 presented; Canberra shows identical weather, although better at higher CDs; and Madrid slightly worse at 90% and slightly better above 96%.

For other nearby frequencies within the L-, S-, X-, and Ka-bands, the weather-effects models presented here should be used without modification.

2.1.1 *Calculation of Mean Atmospheric Physical Temperature*

The mean physical temperature of the atmosphere is modeled to be a function of weather condition, or cumulative distribution. This reflects the assumption that those effects that are of larger value (for example, high noise temperature) occur closer to the surface and hence are at a higher average physical temperature than those that have a lesser effect. The mean atmospheric physical temperature is modeled as

$$T_p = 255 + 25 \times CD \text{ , K} \tag{1}$$

where

CD = cumulative distribution of weather effect ($0.0 \le \text{CD} \le 0.99$).

Note that the maximum value of T_p thus becomes nearly 280 K.

2.1.2 *Elevation Angle Modeling*

Only the attenuation should be modeled as a function of elevation angle. The atmospheric noise temperature contribution at any elevation angle can be calculated from the modeled attenuation at that elevation angle. Elevation angle modeling can be performed using either a flat-Earth or a round-Earth model. A flat-Earth model is used here, wherein the attenuation increases with decreasing elevation angle:

$$A(\theta) = A_{zen} \times AM = \frac{A_{zen}}{\sin(\theta)} \text{ , dB} \tag{2}$$

where

θ = elevation angle of antenna beam

A_{zen} = zenith atmospheric attenuation (dB), as given in Tables 10 through 18

AM = number of air masses (1.0 at zenith)

The flat-Earth approximation produces a slightly higher attenuation then would be obtained with a round-Earth model for low elevation angles but is valid to within 1% to 3% at a 6-deg elevation angle, depending on the frequency and the amount of water vapor in the atmosphere.

2.1.3 *Calculation of Noise Temperature From Attenuation*

An attenuating atmosphere creates a noise temperature contribution to ground antenna system temperature. The atmospheric noise temperature at any elevation angle (θ) is calculated from the attenuation by

$$T_{atm}(\theta) = T_p \left[1 - \frac{1}{L(\theta)} \right], \text{K} \tag{3}$$

where

T_p =   mean physical temperature of atmosphere (K), calculated above

$L(\theta)$ =   loss factor of atmosphere   = $10^{\left[\frac{A(\theta)}{10} \right]}$

$A(\theta)$ =   atmospheric attenuation at any elevation angle (dB), calculated above

Note that typical values of L range from about 1.01 to 2.0

2.1.4   *Cosmic Background Adjustment*

The noise temperature contribution of the cosmic background is reduced by atmospheric attenuation. For the bands of interest, the effective cosmic background noise before atmospheric attenuation is

T_c = 2.7   (L-band and S-band)

      = 2.5   (X-band)

      = 2.0   (Ka-band)

With atmosphere, the effective cosmic background effect is

$$T_c'(\theta) = \frac{T_c}{L(\theta)}, \text{K} \tag{4}$$

where

T_c =   effective cosmic background noise (K) without atmosphere

$L(\theta)$ =   loss factor of atmosphere at the elevation angle of interest, as calculated from Section 2.1.3.

The expressions for $T_{op, \, vac}$ in the telecommunications interface modules (for example, module 101) include the effective cosmic background contribution reduced by the effects of average clear weather. These values are within a few tenths of a Kelvin of the values given above, and variations in T'_c as a function of weather condition and elevation angle are typically neglected, as being at the sub-1K level.

2.1.5   *Example of Use of Attenuation Statistics to Calculate Atmospheric Noise Temperature, $T_{atm}(\theta, CD)$, and $T_{op}(\theta, CD)$*

The following example will show a typical calculation of atmospheric noise temperature and attenuation for a particular situation. The parameters for the example are

DSS 43, Canberra

Ka-band (32 GHz)

90% year average weather (CD = 0.90)

20-deg elevation angle (2.924 air masses)

From Table 17, the year average zenith attenuation is given as

$$A_{zen} = 0.404 \text{ dB}.$$

The attenuation at 20-deg elevation is

$$A\left(20^\circ, 90\%\right) = \frac{0.404}{\sin(20)} = 1.181 \text{ dB}$$

The loss factor L at 20-deg elevation is

$$L\left(20^\circ, 90\%\right) = 10^{0.1181} = 1.312$$

The atmospheric mean physical temperature is

$$T_p = 255 + 25 \times 0.90 = 277.5 \text{ K}$$

The atmospheric noise temperature at 20-deg elevation is

$$T_{atm}\left(20^\circ, 90\%\right) = 277.5\left(1 - \frac{1}{1.312}\right) = 65.991 \text{ K}$$

The operating system noise temperature at any elevation angle and for any weather condition is given by

$$T_{op}\left(\theta, CD\right) = T_{op,vac}\left(\theta\right) + T_{atm}\left(\theta, CD\right), \text{ K} \tag{5}$$

where

$T_{op,vac}(\theta)$ =   vacuum system temperature at elevation angle θ from the appropriate antenna performance module (101, 102, 103 or 104).

2.1.6   *Best/Worst Month Ranges of Atmospheric Noise Temperature and Attenuation*

Although the absolute accuracy of the 31.4-GHz water vapor radiometer measurements used to create the noise temperature statistics is thought to be on the order of the values stated in paragraph 2.1, the month-to-month variation of average noise temperature at any

CD varies much more than this at all values of cumulative distribution greater than about 10%. A particular month might be the "worst" at the 90% CD level, but merely "moderate" at lower CD levels. An example is a winter month that has a large amount of rain but when not raining has low humidity and low noise temperature contribution. At this time, there are insufficient data to characterize "best" and "worst" months individually; however, tolerances on the mean statistics as given in Tables 1 through 18 can give the user a feeling of what yearly variations in atmospheric effects may be expected.

Inspection of Tables 1 through 18 and Figures 1 through 9 will show that fictitious "best month" and "worst month" statistics can be generated from the values giving the minimum and maximum envelope values of noise temperature and attenuation, without regard to the variability among the months as a function of CD. At high values of CD, the adverse (maximum envelope) yearly tolerances can be as high as 40% of the year-average value of an effect. It should be noted that adverse tolerances for both noise temperature and attenuation give INCREASES from the values in Tables 1 through 18. An adverse VALUE is a mean PLUS the adverse tolerance. For mission planning purposes, with no need to create a model for a specific month, it may be sufficient to use the year-average value at a particular CD, and use the maximum/minimum envelope values to define very conservative adverse/favorable tolerances, with triangular distribution. For specific-month planning purposes, it may be sufficient to use the values given in Tables 1 through 18, with ±5% tolerances (triangular distribution) as stated above. A very conservative approach (acknowledging that any individual month in the future can be well outside the historical range of available data) would be to use the "maximum" envelope as the model for a possible "bad" month. Note also, that for particular months, characterized by "bad weather", year-to-year variation of noise temperature and attenuation statistics can be quite large.

2.2 Rainfall Statistics

To assist the user in determining which months may have large rainfall-related atmospheric noise temperature and attenuation increases, rainfall data are presented for the three DSN antenna locations. Months with large average rainfall amounts may not necessarily correspond to months with large noise temperature and attenuation values. Comparison with Tables 1 through 18 should be made.

Table 19 presents the monthly and year-average rainfall amounts for the three DSN antenna locations. The Goldstone data (1973–2000) were taken at the administration center, located near the middle of the Goldstone antenna complex. Some antennas may be located as much as 10 miles from this location. The Canberra data (1966–2002) were taken at the Tidbinbilla Nature Reserve, located about 3 miles southwest of the antenna site. The Madrid data (1961–1990) are the averages of the rainfall at two locations: Avila, about 20 miles northwest of the antenna site, and Madrid (Quatro Vientos) about 20 miles east of the antenna site. Although these averages may not exactly reflect the rainfall at the antenna site, the relative monthly amounts are undoubtedly correct.

2.3　　　　*Wind Loading*

The effect of wind loading must be modeled probabilistically, since wind velocity varies randomly over time and space. Figure 10 shows the probability distribution of wind speed for Goldstone. Similar data for the Madrid and Canberra complexes will be supplied when available. The wind load on a particular antenna is dependent on the design of that antenna. Consequently, information about wind-load effect on antenna gain is listed in the appropriate antenna module.

Statistics show that Goldstone is the windiest of the three Deep Space Network antenna complexes. The DSS 14 70-m antenna is *stowed* (pointed vertically) when wind gusts exceed 55 mph (88 km/hr). The frequency of occurrence of this event can be deduced from a relationship between wind gusts and average wind speed. This relationship is found to be: maximum hourly wind speed = 0.62 × strongest gust. Thus, for 55-mph (88 km/hr) gusts, the maximum hourly wind speed is found to be 34 mph (55 km/hr). From Figure 10, it is seen that this speed is exceeded approximately 2 % (175 hours) of the year and 4 % (29 hours) of the worst month. Actual practice has shown that no antenna has been stowed more than about 10 hours per year due to excessive wind-gust occurrences.

2.4　　　　*Hot Body Noise*

2.4.1　　　*Solar Noise*

The increase in system noise when tracking near the Sun depends on the intensity of solar radiation at the received frequency and on the position of the Sun relative to the antenna gain pattern. The subreflector support structure (typically a quadripod, but a tripod at the DSS 13 BWG antenna) introduces nonuniformities in the sidelobe structure. Increases in noise temperature are typically greater in directions at right angles to the planes established by the subreflector support legs and the center of the reflector surface. Thus, a quadripod-type antenna will have four enhanced regions of noise temperature, and a tripod-type antenna will have six. With an azimuth-elevation (AZ–EL) or X–Y mounted antenna, the plane containing the Sun–Earth–probe (SEP) angle will rotate through the sidelobes during a tracking pass. This causes the solar noise to fluctuate during a track even if the SEP angle is constant.

A large number of measurements were made at Goldstone from 1987 to 1996 to determine the system noise temperature effects of tracking near the Sun (within about five deg from the center of the solar disk). These measurements were made at S-, X-, and Ka-bands on both 26- and 34-meter antennas.

Figure 11 shows the 10.7-cm (2800-MHz) solar radio flux during solar cycle 23 (1996-2007, the expected "maximum" should have occurred in late 2000 or early 2001). The flux is measured in solar flux units (SFU) where one SFU = 1×10^{-22} W/m^2/Hz. Updated solar flux predictions can be found at the National Oceanic and Atmospheric Administration (NOAA) Space Environment Center web site <http://www.sec.noaa.gov/weekly.html> (Solar Cycle Progression and Prediction Plots). Solar flux predictions can be used to model S- and X-band

solar noise temperature contributions using the ratio of predicted solar flux to the solar flux that existed at the time the antenna noise temperatures were measured.

The general characteristic of the 11-year cycle of 2800-MHz solar flux is a rapid rise to a peak approximately 4–5 years after the minimum, followed by a 7–6 year gradual decrease. From cycle to cycle, the peak flux can vary by as much as a factor of two. The 10.7-cm flux is varied during solar cycle 23 from a minimum of about 70 SFU during 1996 to a maximum of about 190 ± 20 SFU during 2000–2001 and returning to an expected minimum of about 70 SFU during 2006.

Figure 12 shows X-band system noise temperature increases as measured at the Goldstone DSS 15 HEF antenna. These measurements show the increased effect for the Sun located (offset) at right angles to the quadripod legs. The quadripod legs are arranged in an "X" configuration, with 90-deg spacing. The measurements were made in November 1987 (near the beginning of the solar cycle) with a measured 2800-MHz flux value of 101 SFU and an 8800-MHz flux value of 259 SFU. The following expression may be used as an upper limit of X-band solar noise contribution at DSS 15 as shown in Figure 12.

$$T_{sun} = 800e^{-2.0\theta}, \text{ K} \tag{6}$$

where

θ = offset angle between center of beam and center of solar disk, deg

Figure 13 shows S-band (2295 MHz) total system noise temperature measurements made on the Goldstone DSS 16, 26-m antenna on December 20, 1989. This antenna has no quadripod, and it can be assumed that the noise temperature values shown are independent of solar "clock angle" around the center of the antenna beam. The reported 2800-MHz solar flux at the time of the experiment was 194 SFU; at 8800 MHz it was 290 SFU. Note that compared to the November 1987 flux (Figure 12), the 2800-MHz flux has nearly doubled, but the 8800-MHz flux has only increased about 12 percent. The S-band solar contribution shown in Figure 13 can be modeled as

$$T_{sun} = 1400e^{-1.4\theta}, \text{ K} \tag{7}$$

where

θ = offset angle between center of beam and center of solar disk, deg

Figures 14 and 15 are contour plots of the DSS 12, 34-m HA–DEC total system noise temperature versus declination and cross-declination antenna pointing offsets. DSS 12 has been decommissioned since the measurements were made, but the figures are included because they are representative of the effects of the quadripod on solar noise at other antennas. The quadripod legs are arranged in a "+" configuration with 90-deg spacing, hence the peaks at right angles to the legs.

Figure 14 is a contour plot of total S-band system noise temperature versus declination and cross-declination antenna pointing offsets at DSS 12.The contour interval is 50 K. These measurements were made on January 12, 1990. On this day the reported 2800-MHz solar flux was 173 SFU.

Figure 15 is a contour plot of total X-band system noise temperature versus declination and cross-declination antenna pointing offsets at DSS 12. The contour interval, measurement date, and flux values are identical with those in Figure 14. The reported 8800-MHz solar flux was 272 SFU.

Figures 16 and 17 show the X-band (8.4-GHz) and Ka-band (32-GHz) solar noise contributions at the DSS 13, 34-m research and development beam waveguide antenna as a function of offset angle from the center of the sun. These data were taken during mid-March, 1996, when the 10.7-cm solar flux was about 70 SFU (the minimum at the end of solar cycle 22 and at the beginning of solar cycle 23) and should be considered as representative of what is expected at the operational DSN beam waveguide antennas.

The following expressions give an approximate upper envelope for the noise contributions shown in Figures 16 and 17 as a function of offset angle

$$T_{sun} = \begin{vmatrix} 1400e^{-5.1\theta}, & 0.35 < \theta \le 0.75\deg \\ 86e^{-1.4\theta}, & \theta > 0.75\deg \end{vmatrix}, \text{ at X-band} \tag{8}$$

$$T_{sun} = \begin{vmatrix} 5000e^{-6.6\theta}, & 0.35 < \theta \le 0.75\deg \\ 100e^{-1.4\theta}, & \theta > 0.75\deg \end{vmatrix}, \text{ at Ka-band.} \tag{9}$$

At offset angles less than 0.35 deg (0.08 deg from the edge of the solar disk), solar noise contributions are likely to be in excess of 300 K at both frequencies. At offsets greater than 4.0 degrees, the solar contribution is negligible.

All noise contribution expressions given above should be compared with values shown in the corresponding figures to assess their validity. Note that these expressions should be considered valid only for the flux values given at the time of measurement. For predictive purposes, Figure 11 may be used to obtain future predicted 2800-MHz solar flux, and the noise contributions at S- and X-band can be modeled as described below.

During the 11-year solar cycle, the S-band flux varies by a factor of 3 (reference Figure 11) while the corresponding X-band flux varies by a factor of 2. For cycle 23, when the S-band range is expected to be from 70 SFU to as much as 210 SFU, the X-band range is predicted to be from about 200 SFU to about 400 SFU. The predicted X-band flux can be derived from the predicted S-band flux by the following expression.

$$FLUX, X = 200 + \frac{200(FLUX, S - 70)}{140} \tag{10}$$

For example, in January 2003 the mean S-band flux is predicted to be 125 SFU (from Figure 11). The mean predicted X-band flux would be 264 SFU.

The predicted solar noise contribution can be calculated based on measured noise contributions described above. For example, using the equation provided for Figure 12 (Equation 6) and the predicted X-band solar flux in January of 2002 (264 SFU), the predicted X-band solar noise contribution for a 2-degree offset angle using the 34-m HEF antenna would be

$$T_{sun} = \frac{264}{259} 800 e^{-2.0 \times 2.0} = 14.6 \text{ K} \tag{11}$$

At Ka-band, the solar flux varies little over the solar cycle and the relationship between noise temperature increase and offset angle depicted in Figure 17 can be used at all times.

Figure 18 shows examples of measured S-band system noise temperature made with a 64-m antenna tracking Pioneer 8 (November 1968, near the solar maximum) and Helios (April 1975, near the solar minimum). For all practical purposes, these curves may be used to predict S-band performance for the DSN 70-m antennas. The "maximum" and "minimum" curves for each month show the solar "clock angle" effect due to sidelobes at right angles to the quadripod legs.

Figure 19 shows a theoretical curve of X-band 70-m antenna noise temperature as a function of SEP angle. This curve is generated based on an assumed X-band blackbody disk temperature of 23,000 K, representing an "average" value during the solar cycle. An expression giving quiet Sun brightness temperature, T_b (K), as a function of wavelength (mm) has been found to be

$$T_b = 5672 \lambda^{0.24517}, \quad \text{K} \tag{12}$$

For S-band (2.3 GHz), T_b = 18700 K. For X-band (8.5 GHz) T_b = 13600 K. For Ka-band (32 GHz) T_b = 9750 K. The active Sun may be expected to have an X-band brightness temperature of as much as two to four times as high as the 13600 K calculated above.

2.4.2   *Lunar Noise*

For an antenna pointed near the Moon, a noise temperature determination similar to that made for the Sun should be carried out. The blackbody disk temperature of the Moon is about 240 K, and its apparent diameter is almost exactly that of the Sun's (approximately 0.5 deg). Figures 12 through 19 may be used for lunar calculations, with the noise temperature values scaled by 240/23000. Figures 13, 14, 15, and 18 include clear-sky system noise temperatures, which must be subtracted out before scaling in order to determine the lunar noise temperature increase. Nevertheless, at offset angles greater than 2 deg, the lunar noise contribution is negligible.

2.4.3   *Planetary Noise*

The increase in system noise temperature when tracking near a planet can be calculated by the formula

$$T_{pl} = \left(\frac{T_k G d^2}{16 R^2} \right) e^{-2.77 \left(\theta / \theta_0 \right)^2} , \text{ K} \tag{13}$$

where

T_k = blackbody disk temperature of the planet, K

d = planet diameter, km

R = distance to planet, km

θ = angular distance from planet center to antenna beam center

θ_0 = antenna half-power beamwidth (full beamwidth at half power)

G = antenna gain, ratio $\left[10^{\left(G(\text{dBi})/10 \right)} \right]$, including atmospheric attenuation.

Table 20 presents all the parameters needed for calculation of planetary noise contributions. Also given are the maximum values of expected X-band noise contributions for the mean minimum distance from Earth, with the antenna beam pointed at the center of the planet ($\theta = 0$). Corresponding S-band noise temperature increases will be approximately 1/13 as large as the X-band increases because of the lower antenna gain (wider beamwidth) at the lower frequency.

In the case of Jupiter, there is a significant and variable non-thermal component of the noise temperature. Thus the effective blackbody disk temperature at S-band appears to be much higher than at X-band. The S-band noise temperature increase will be approximately 1/6 the X-band values for average Jupiter emission; it will be about 1/3 the X-band values for maximum Jupiter emission. Except for Venus and Jupiter at inferior conjunction (minimum distance), the noise contribution from the planets at S-band is negligible.

The expression for T_{pl} assumes that the angular extent of the radiating source is small compared to the antenna beamwidth. This approximation is adequate at X-band except for Venus near inferior conjunction (apparent diameter = 0.018 deg) using a 70-m antenna at X-band (beamwidth = 0.032 deg). At Ka-band with a 34-m antenna (beamwidth = 0.0174 deg), the approximation is not adequate for Venus near inferior conjunction and may not be adequate for Mars near inferior conjunction (apparent diameter = 0.005 deg). The expression also aassumes that the antenna main beam has a Gaussian shape, with circular symmetry. Antenna gains and half-power beamwidths are given in modules 101, 102, 103, and 104.

2.4.4 *Galactic Noise*

The center of the Milky Way galaxy is located near –30 degrees declination, 17 h 40 min right ascension. It is possible for a spacecraft with a declination of –30 deg to be in the vicinity of the galactic center, and an increase of system noise temperature would then be observed. A declination of –30 degrees is not typically achieved by spacecraft moving in the plane of the ecliptic, but there are some circumstances (for example, a flight out of the ecliptic) where this location may be observed. Galactic noise temperature contributions at frequencies above 10 GHz are typically insignificant. At S-band, looking directly at the galactic center, a noise temperature increase of about 10 K would be observed. A map of the galactic noise distribution can be seen in chapter 8 of the classic reference J. D. Kraus, *Radio Astronomy*, Cygnus-Quasar Books, Powell, Ohio, 1986.
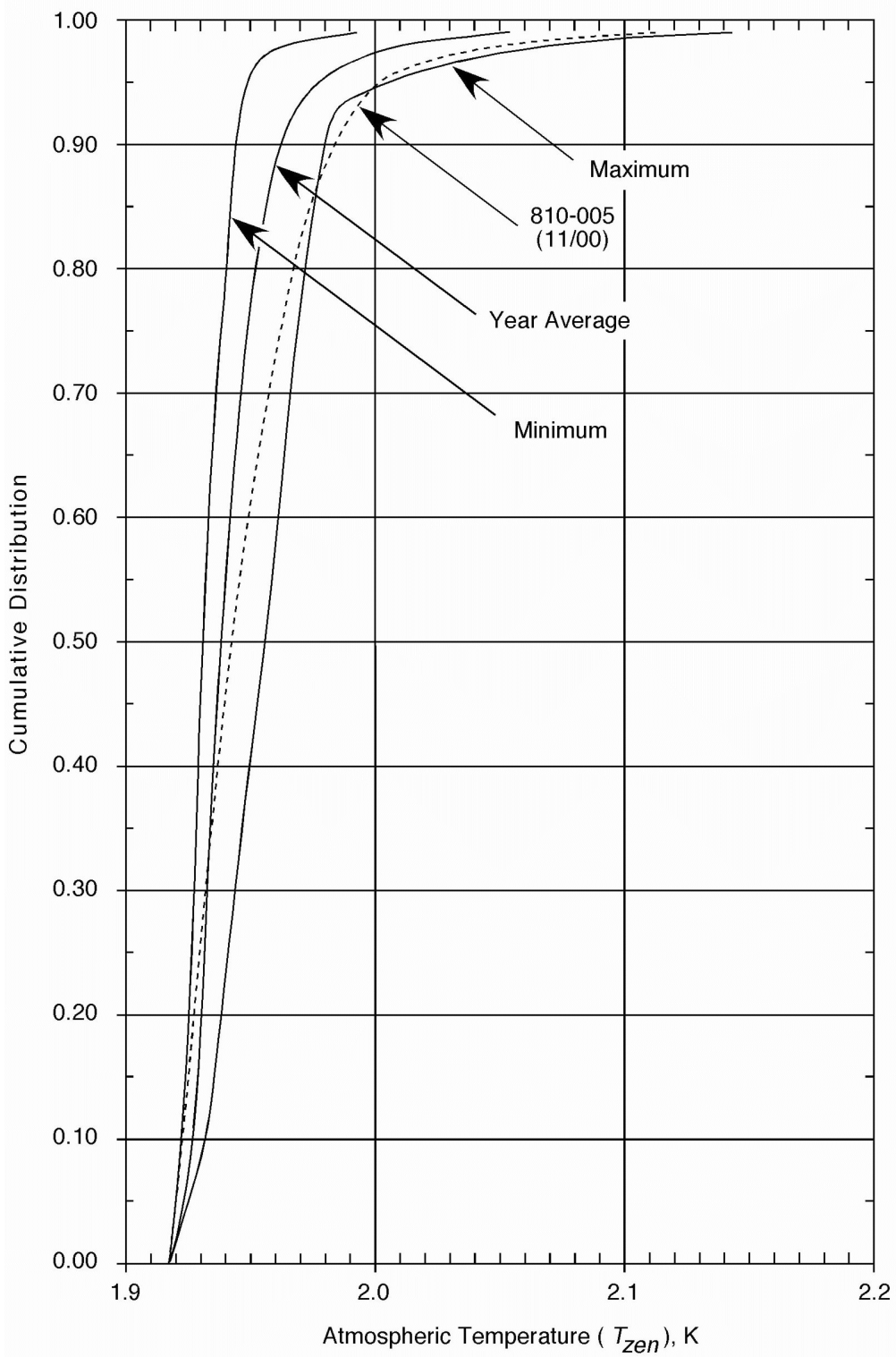
Figure 1. Cumulative Distributions of Zenith Atmospheric Noise Temperature
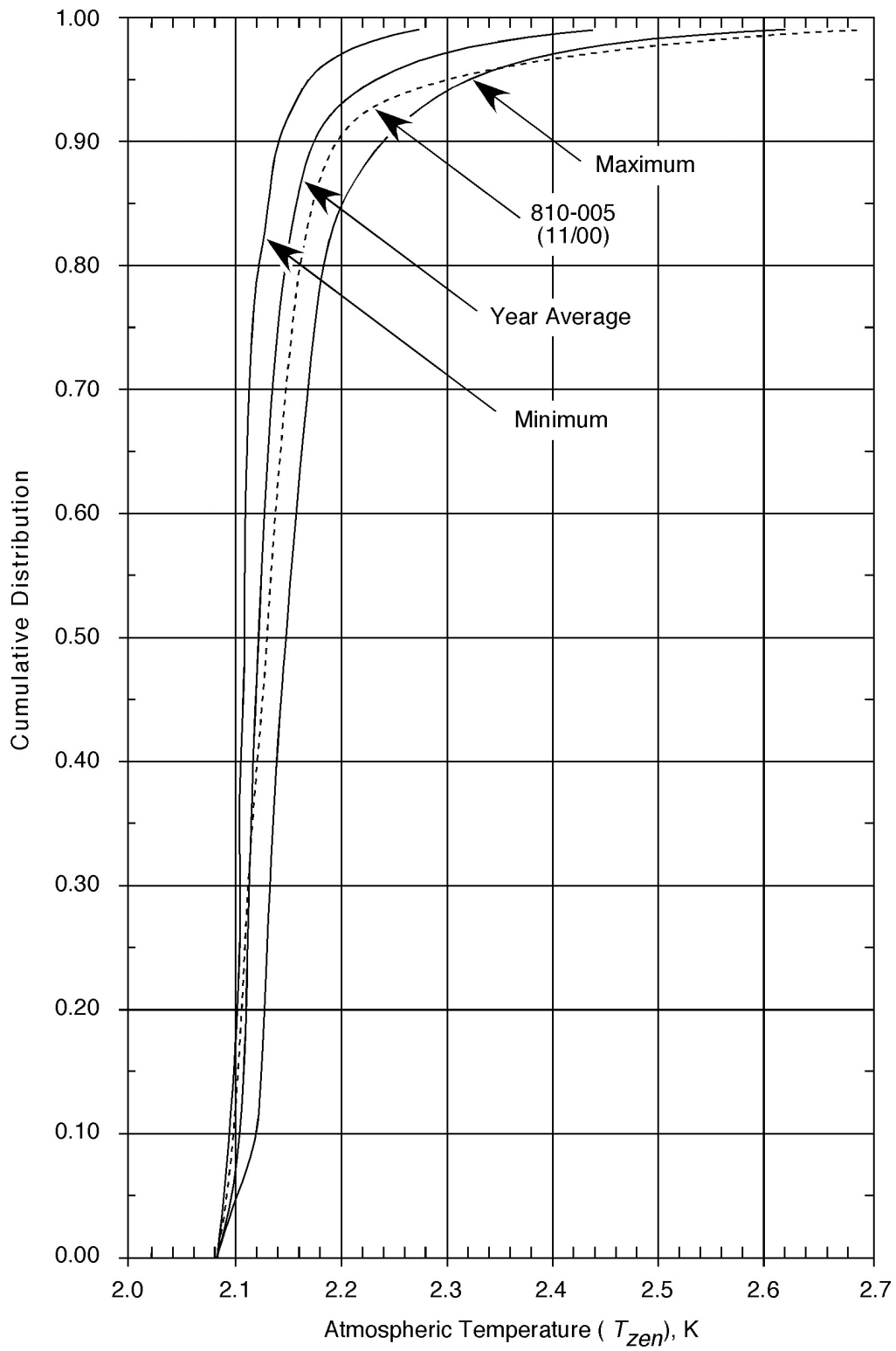at L-Band and S-Band, Goldstone DSCC

Figure 2. Cumulative Distributions of Zenith Atmospheric Noise Temperature at L-Band and S-Band, Canberra DSCC

Figure 3. Cumulative Distributions of Zenith Atmospheric Noise Temperature
at L-Band and S-Band, Madrid DSCC

Figure 4.   Cumulative Distributions of Zenith Atmospheric Noise Temperature
at X-Band, Goldstone DSCC
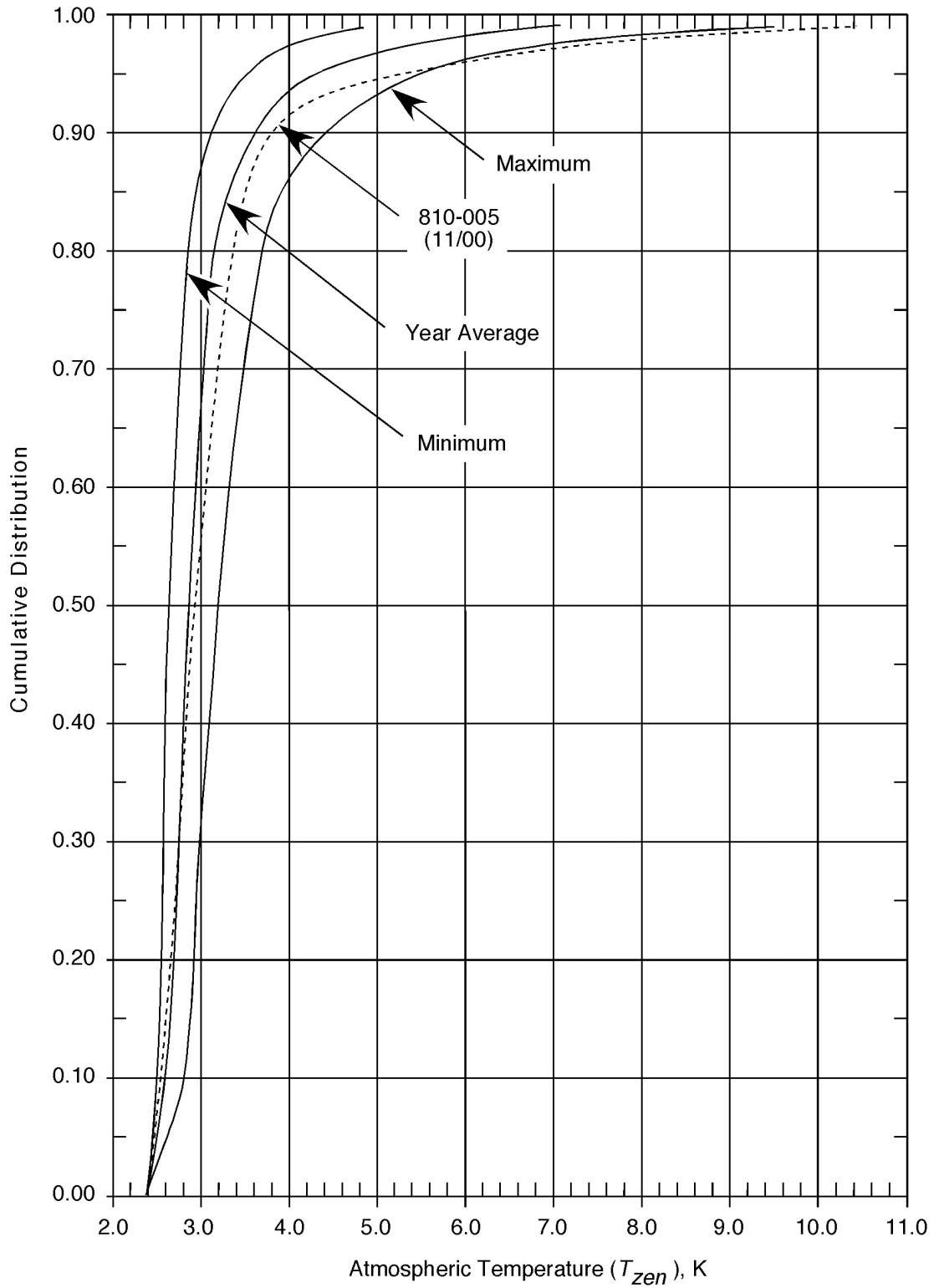
Figure 5.   Cumulative Distributions of Zenith Atmospheric Noise Temperature
at X-Band, Canberra DSCC
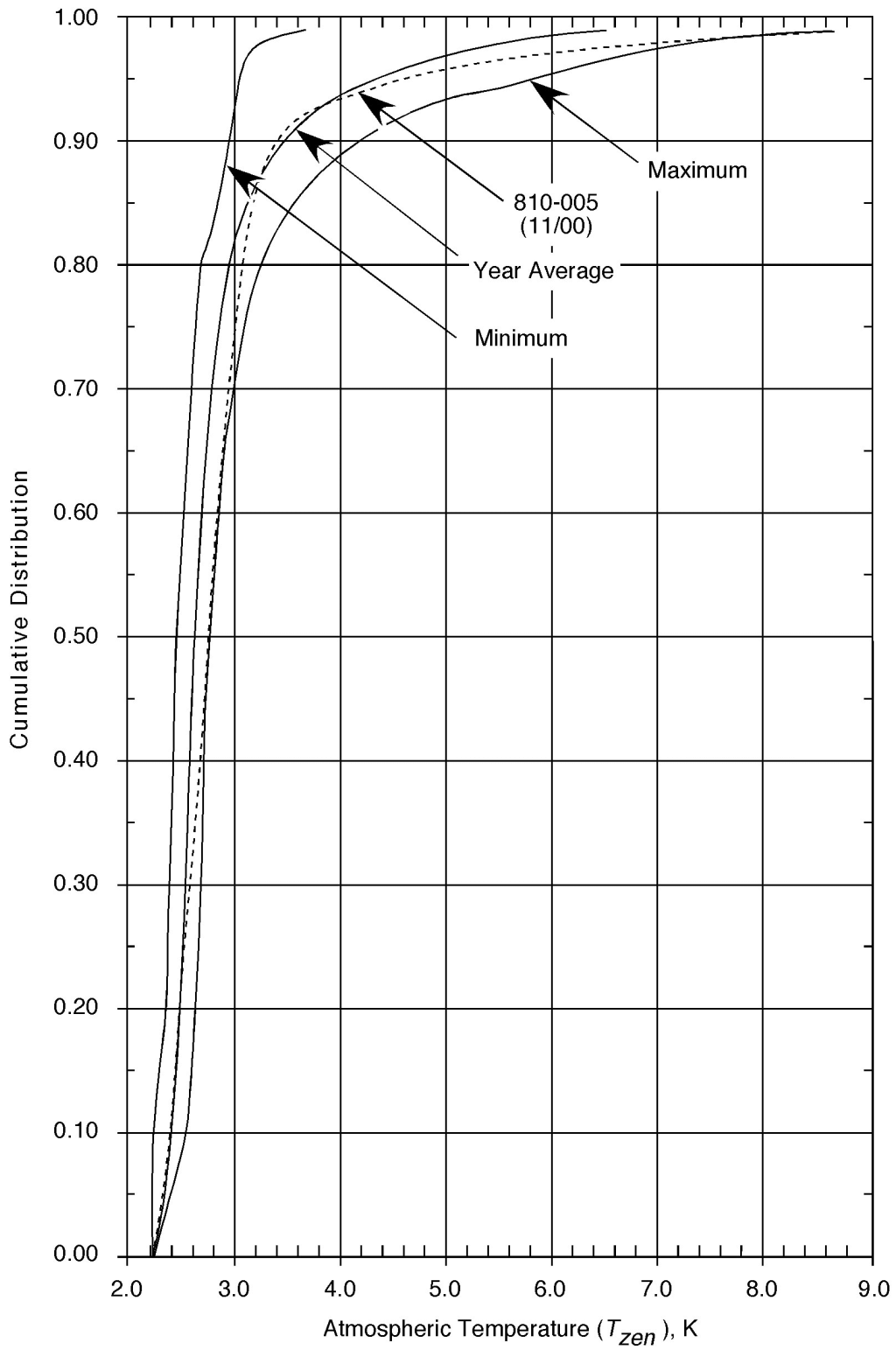
Figure 6. Cumulative Distributions of Zenith Atmospheric Noise Temperature at X-Band, Madrid DSCC
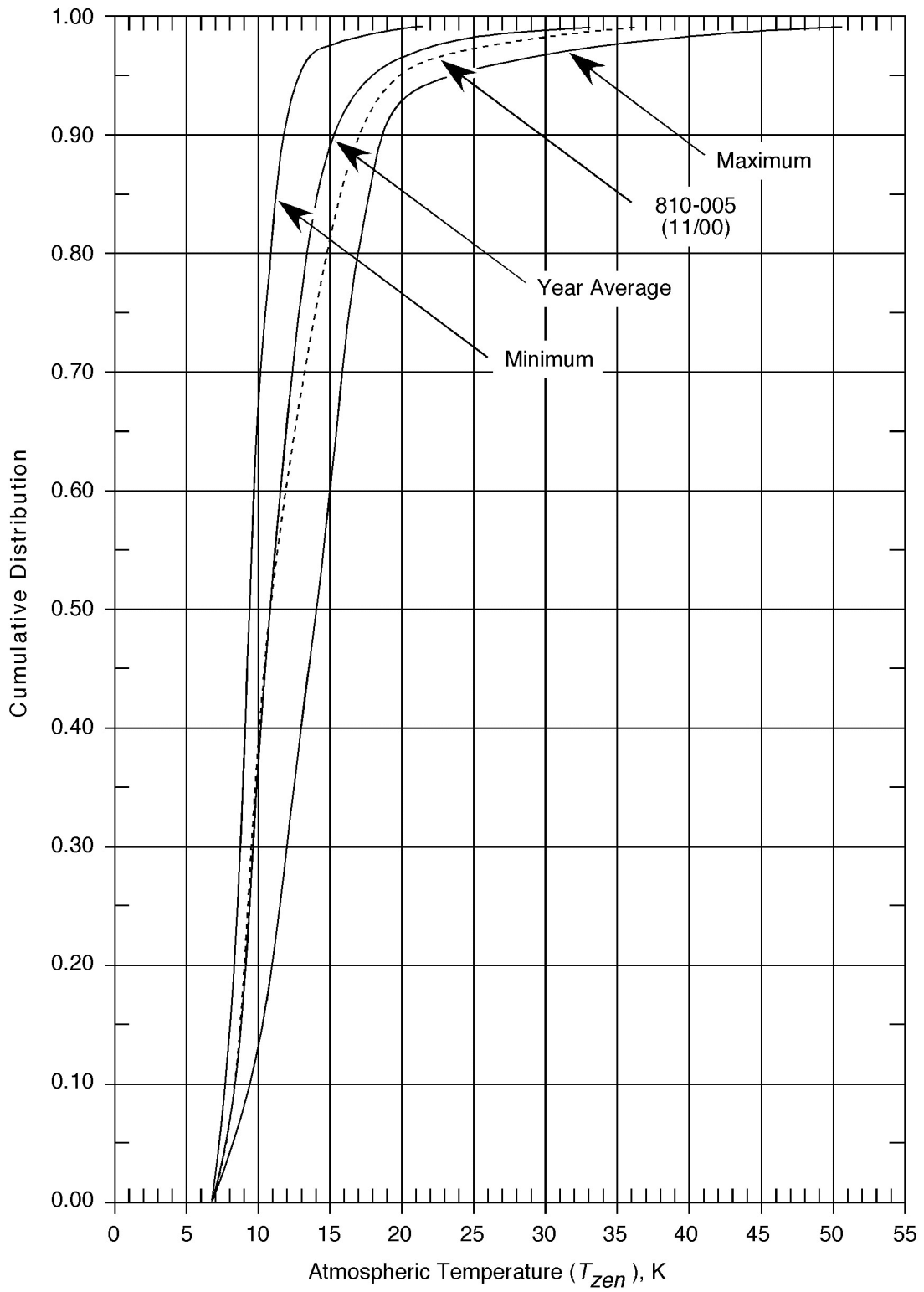
Figure 7.   Cumulative Distributions of Zenith Atmospheric Noise Temperature
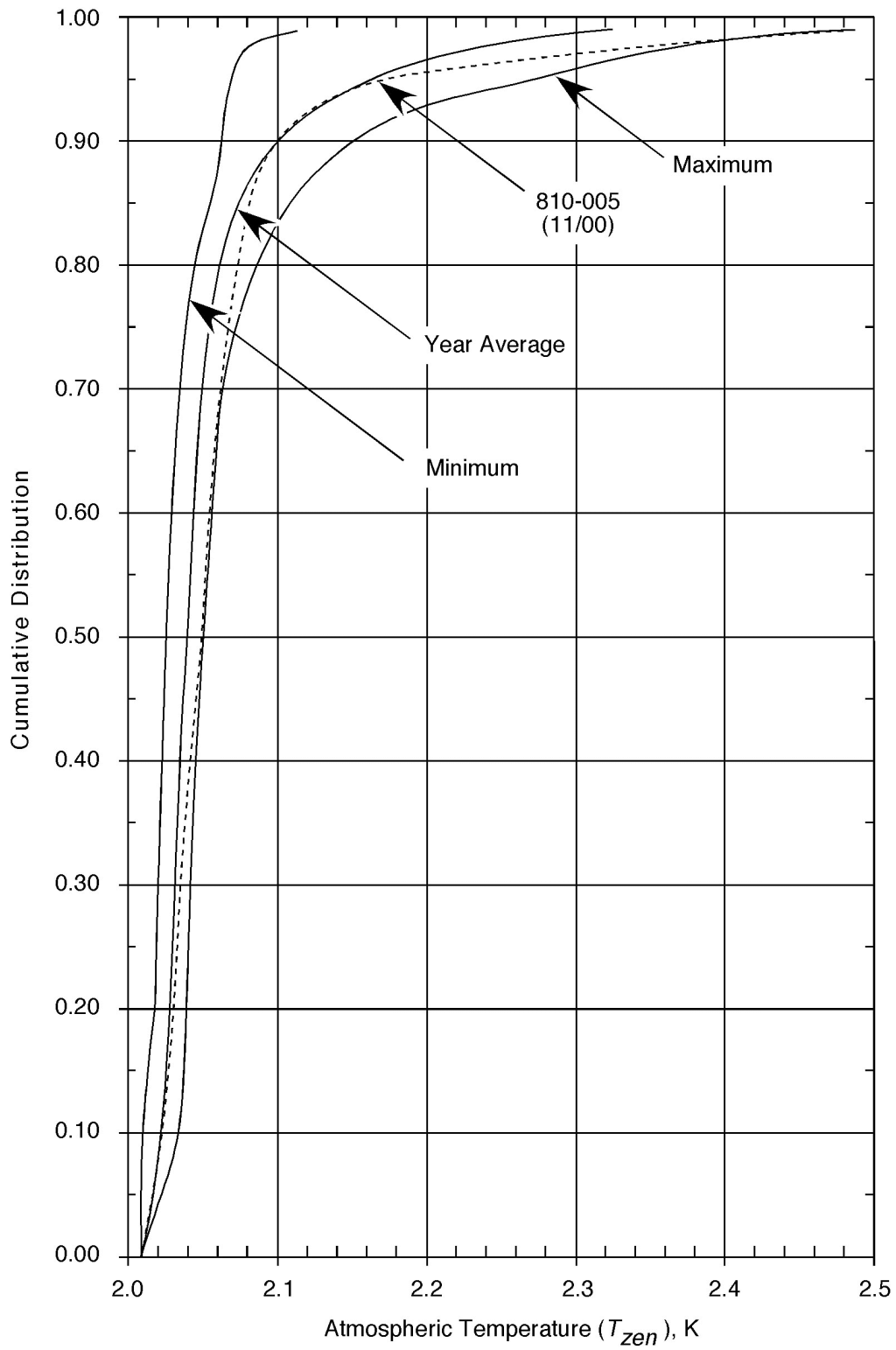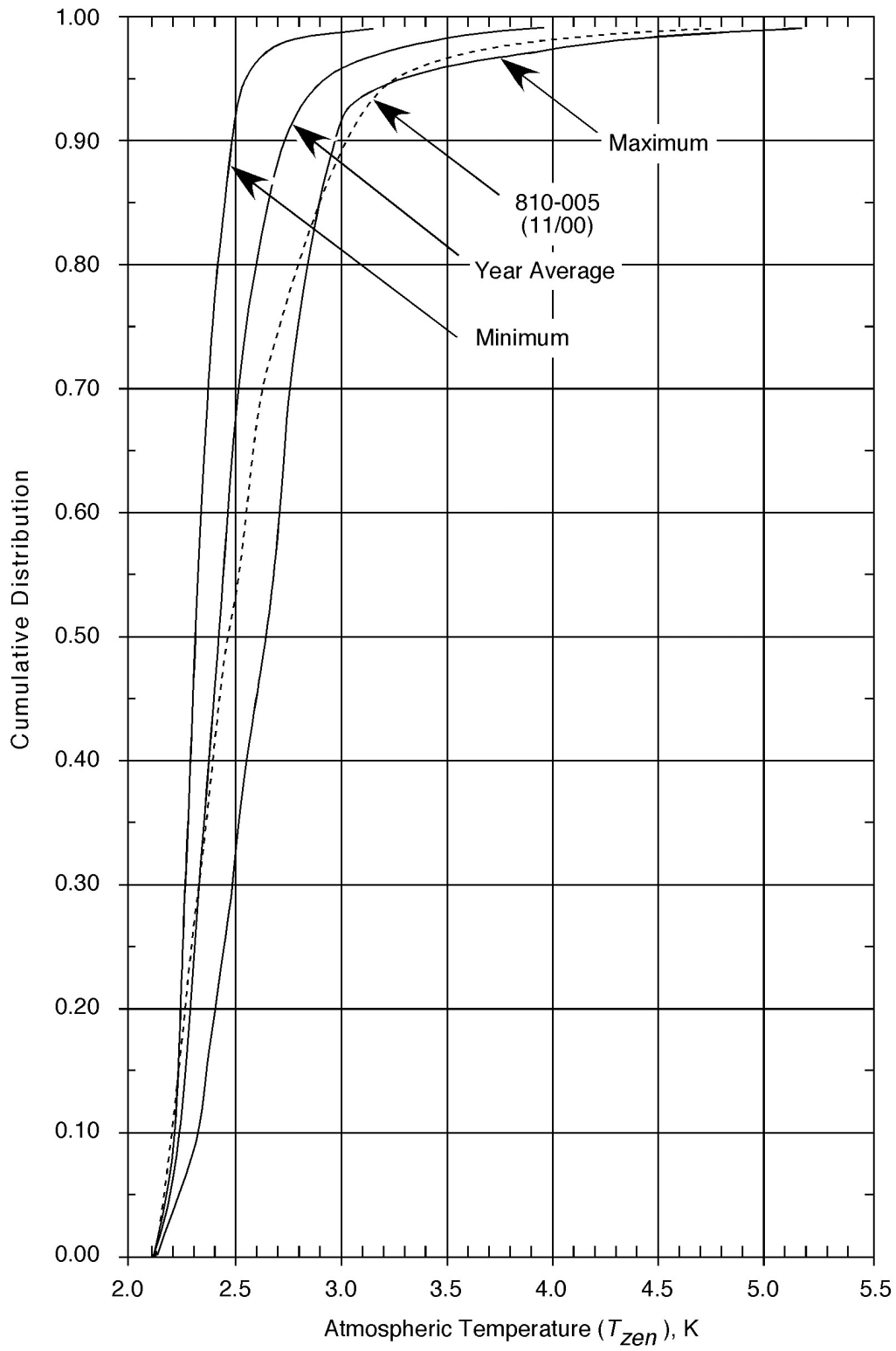at Ka-Band, Goldstone DSCC
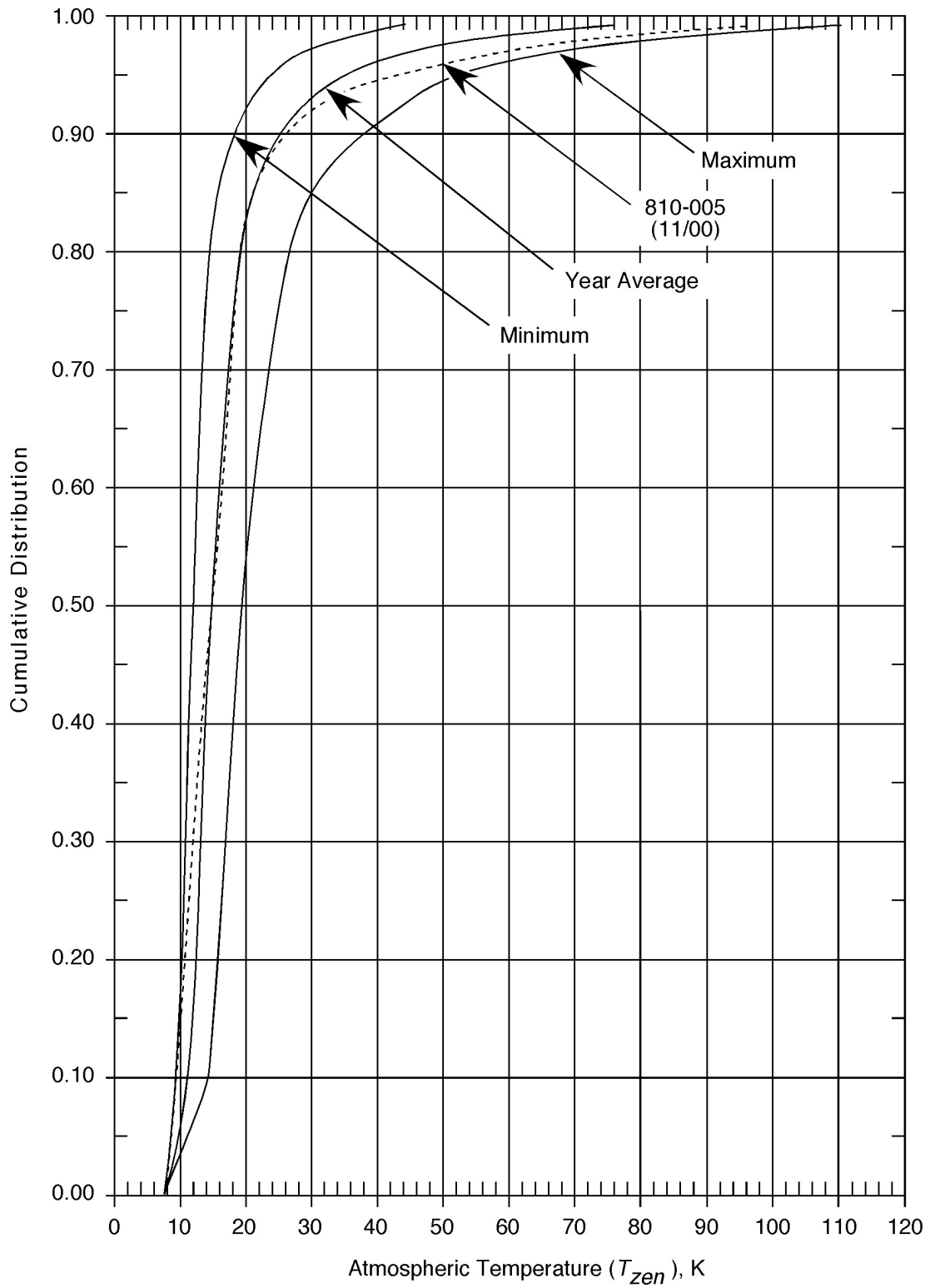
Figure 8.   Cumulative Distributions of Zenith Atmospheric Noise Temperature
at Ka-Band, Canberra DSCC
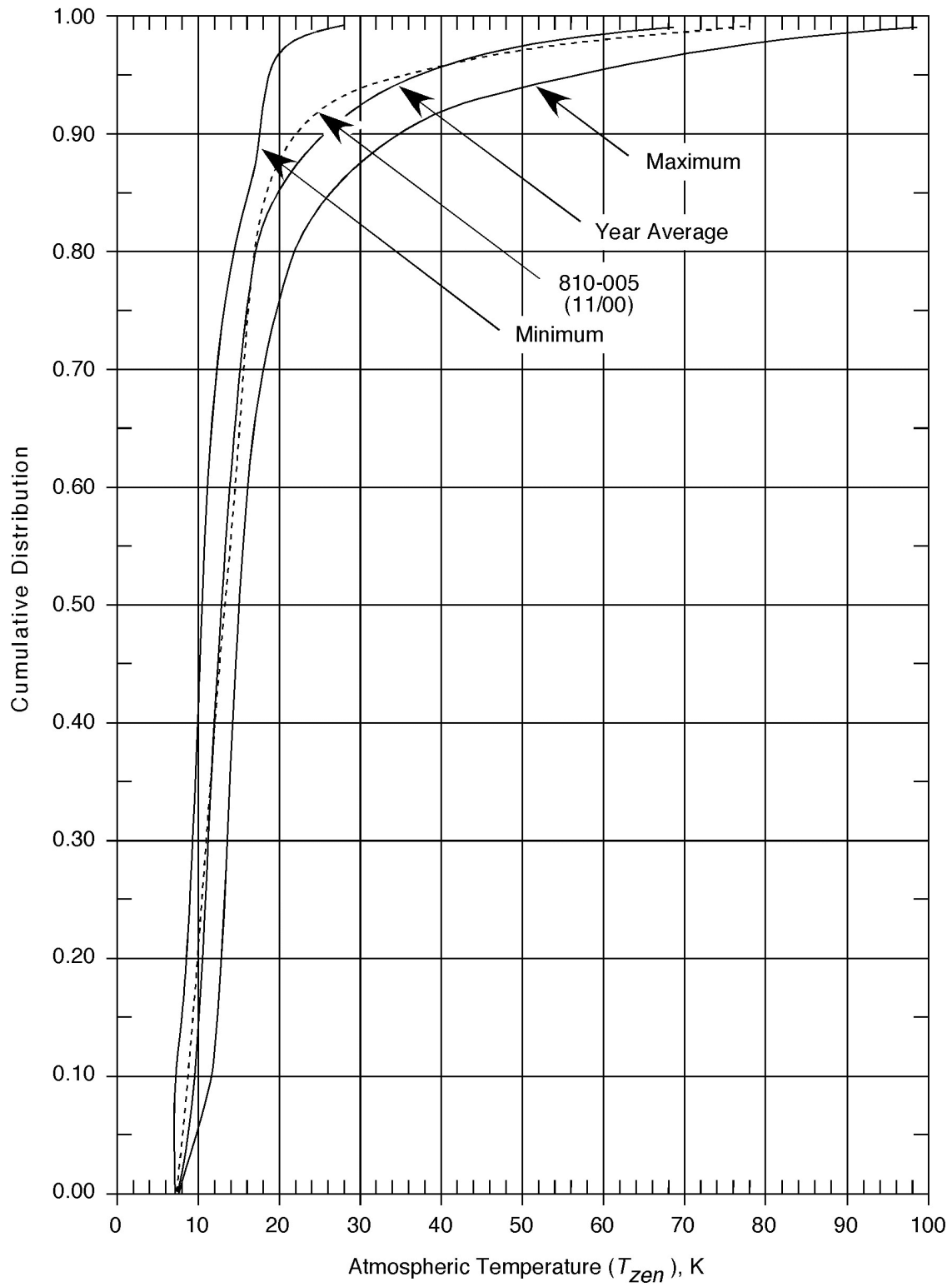
Figure 9. Cumulative Distributions of Zenith Atmospheric Noise Temperature
at Ka-Band, Madrid DSCC
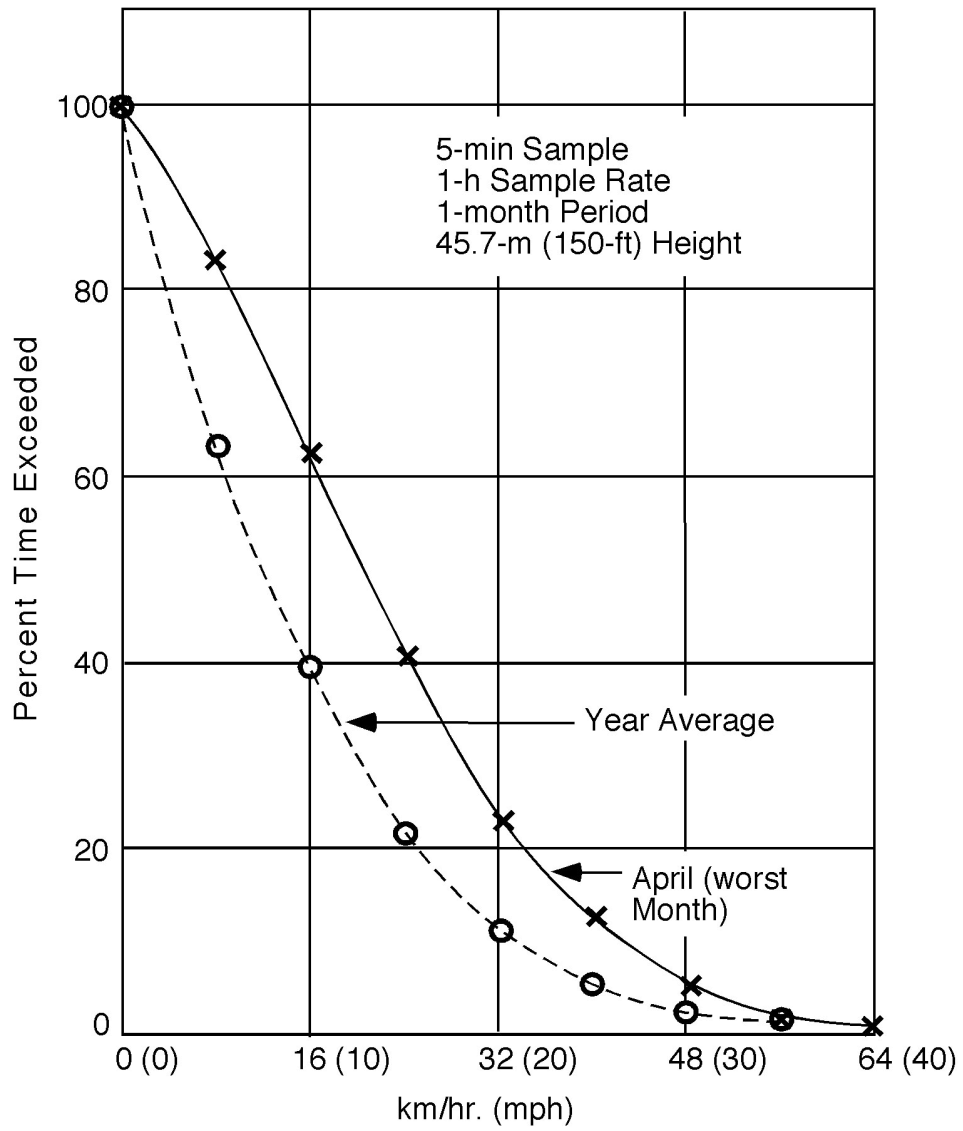
Figure 10. Probability Distribution of Wind Conditions at Goldstone
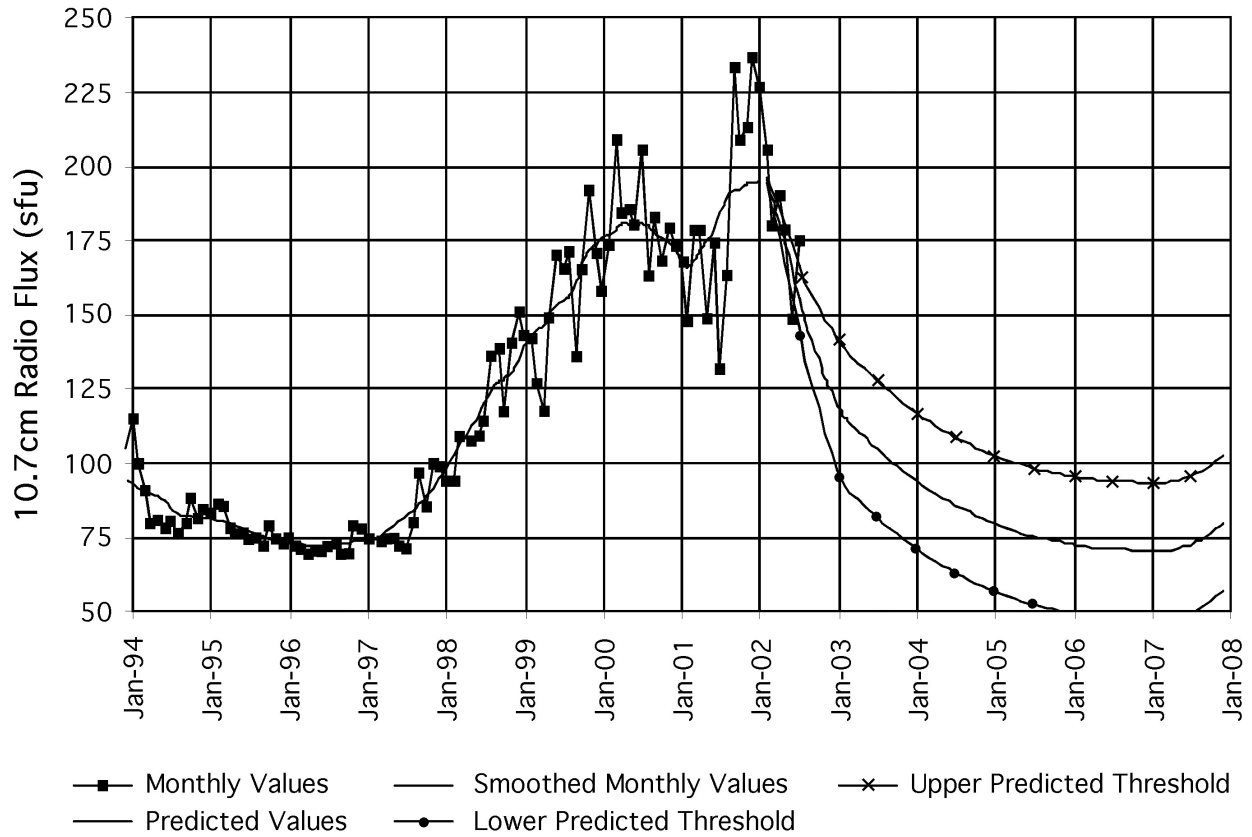
Figure 11.   Solar Radio Flux at 2800 MHz (10.7 cm wavelength) During Solar Cycle 23
(1996–2007)
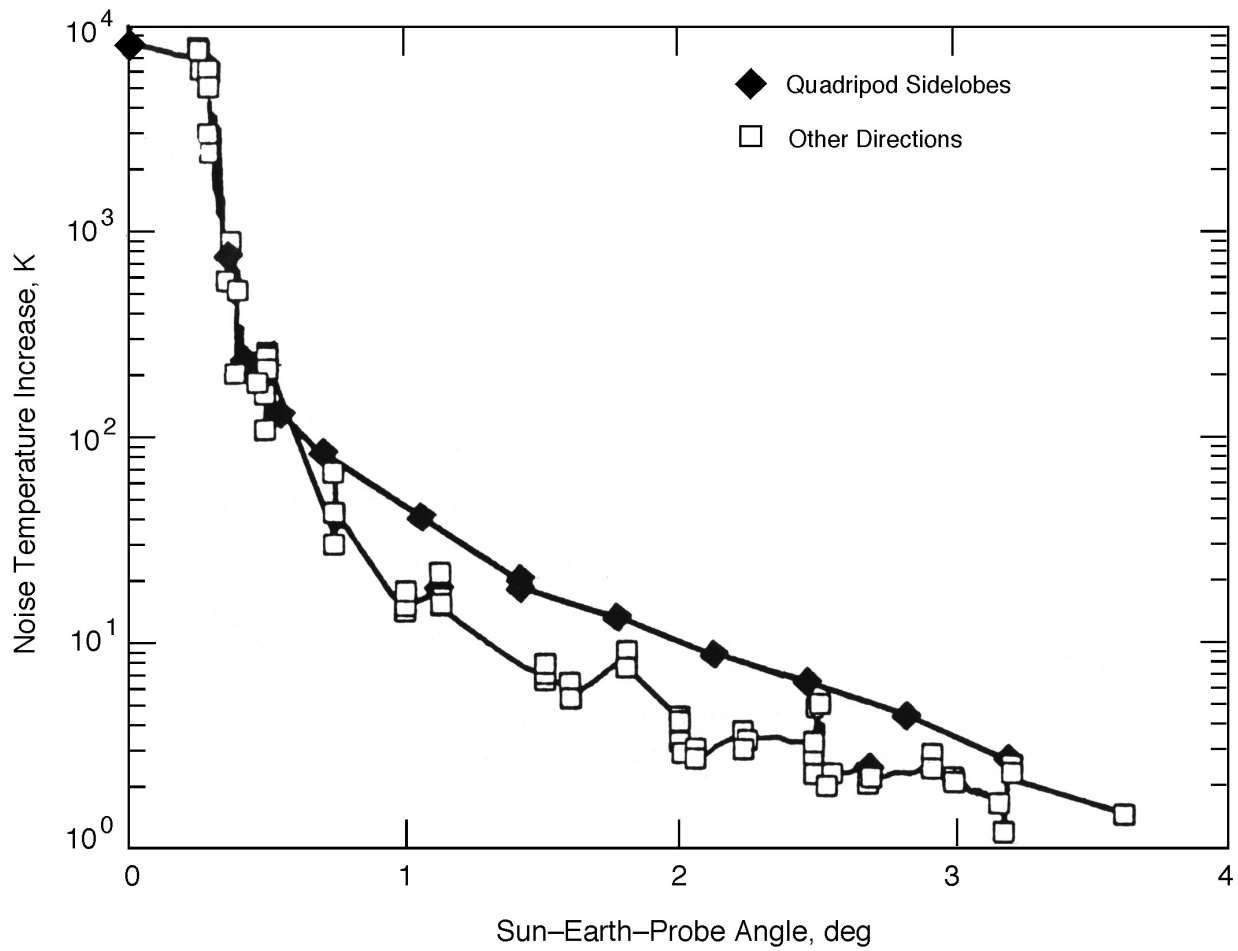
Figure 12. DSS 15 HEF Antenna X-Band System Noise Temperature Increases Due to the Sun at Various Offset Angles, Showing Larger Increases Perpendicular to Quadripod Directions
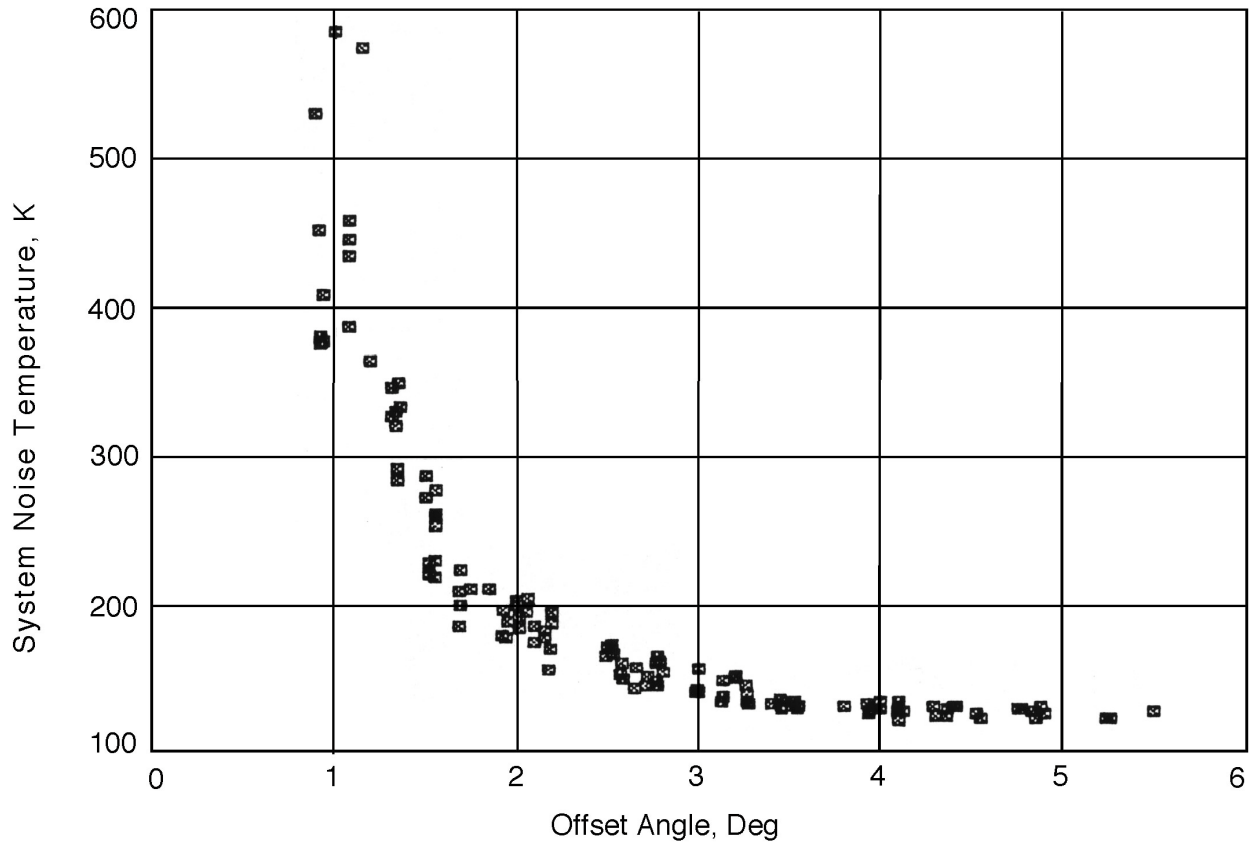
Figure 13. DSS 16 S-Band Total System Noise Temperature at Various Offset Angles from the Sun
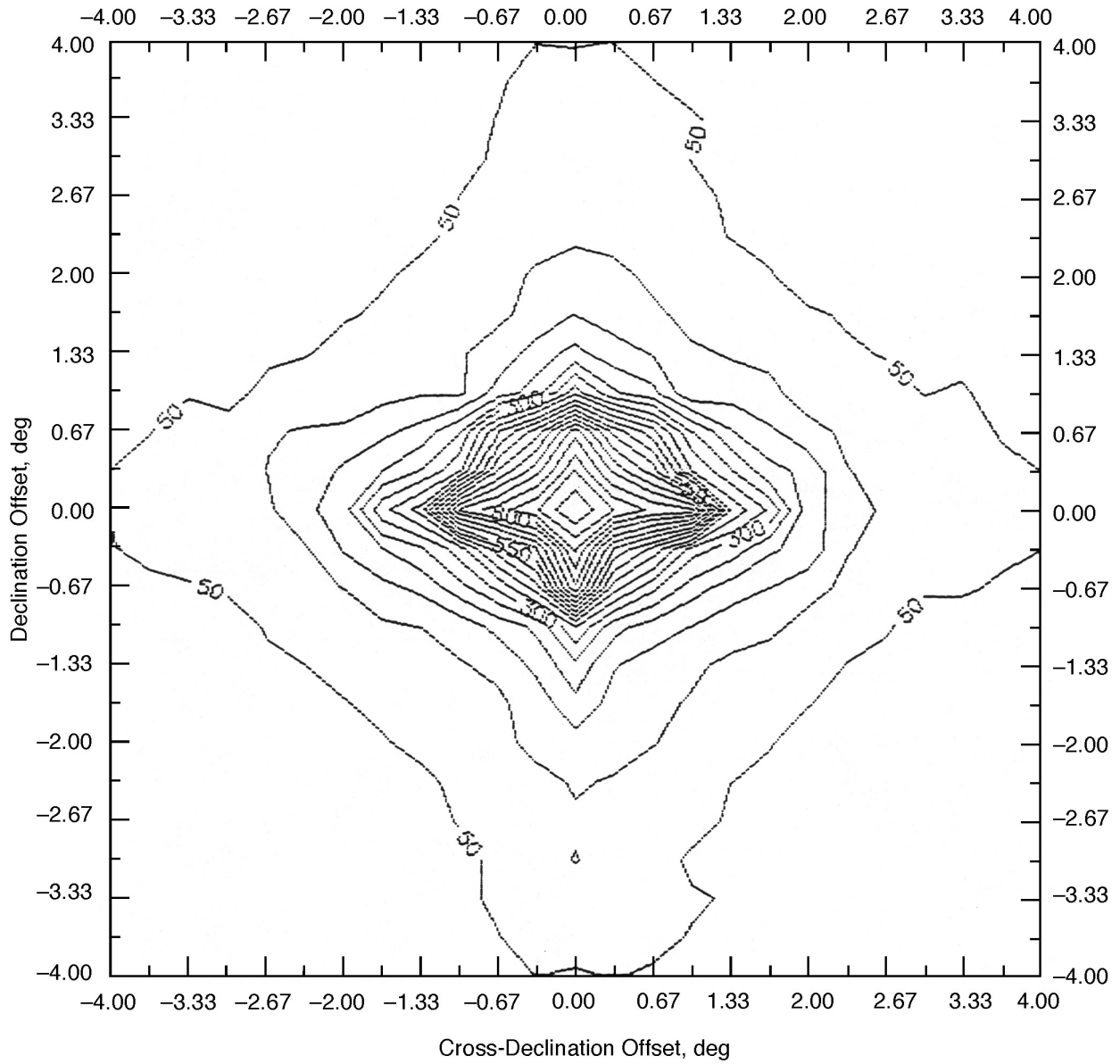
Figure 14. DSS 12 S-Band Total System Noise Temperature at Various Declination and Cross-Declination Offsets from the Sun
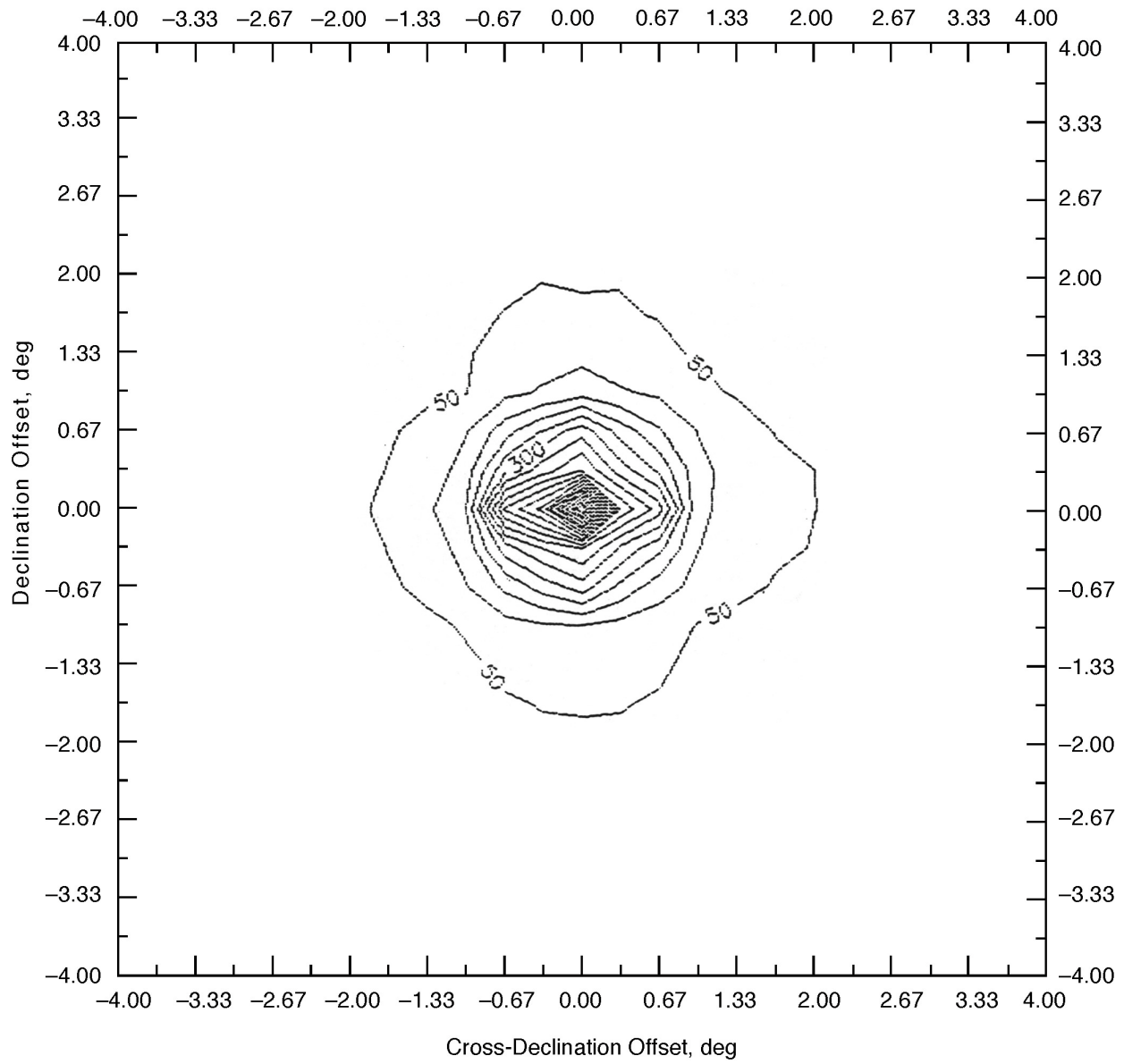
Figure 15. DSS 12 X-Band Total System Noise Temperature at Various Declination and Cross-Declination Offsets from the Sun
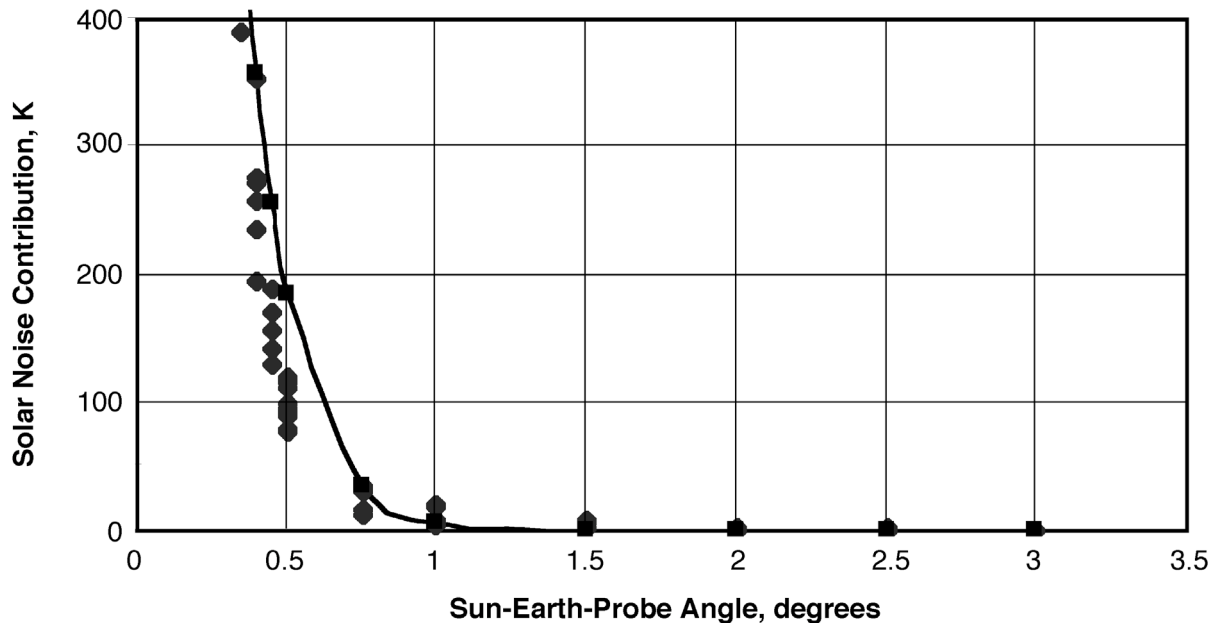
Figure 16. DSS 13 Beam-Waveguide Antenna X-Band Noise Temperature Increase Versus Offset Angle, March 1996
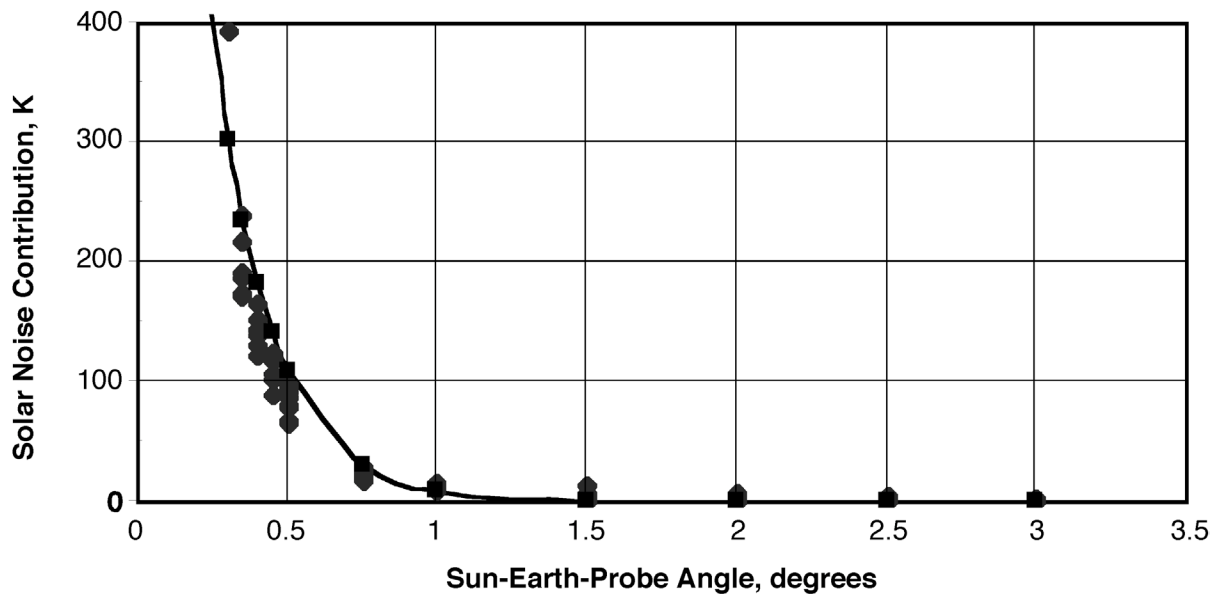
Figure 17. DSS 13 Beam-Waveguide Antenna Ka-Band Noise Temperature Increase Versus Offset Angle, March 1996
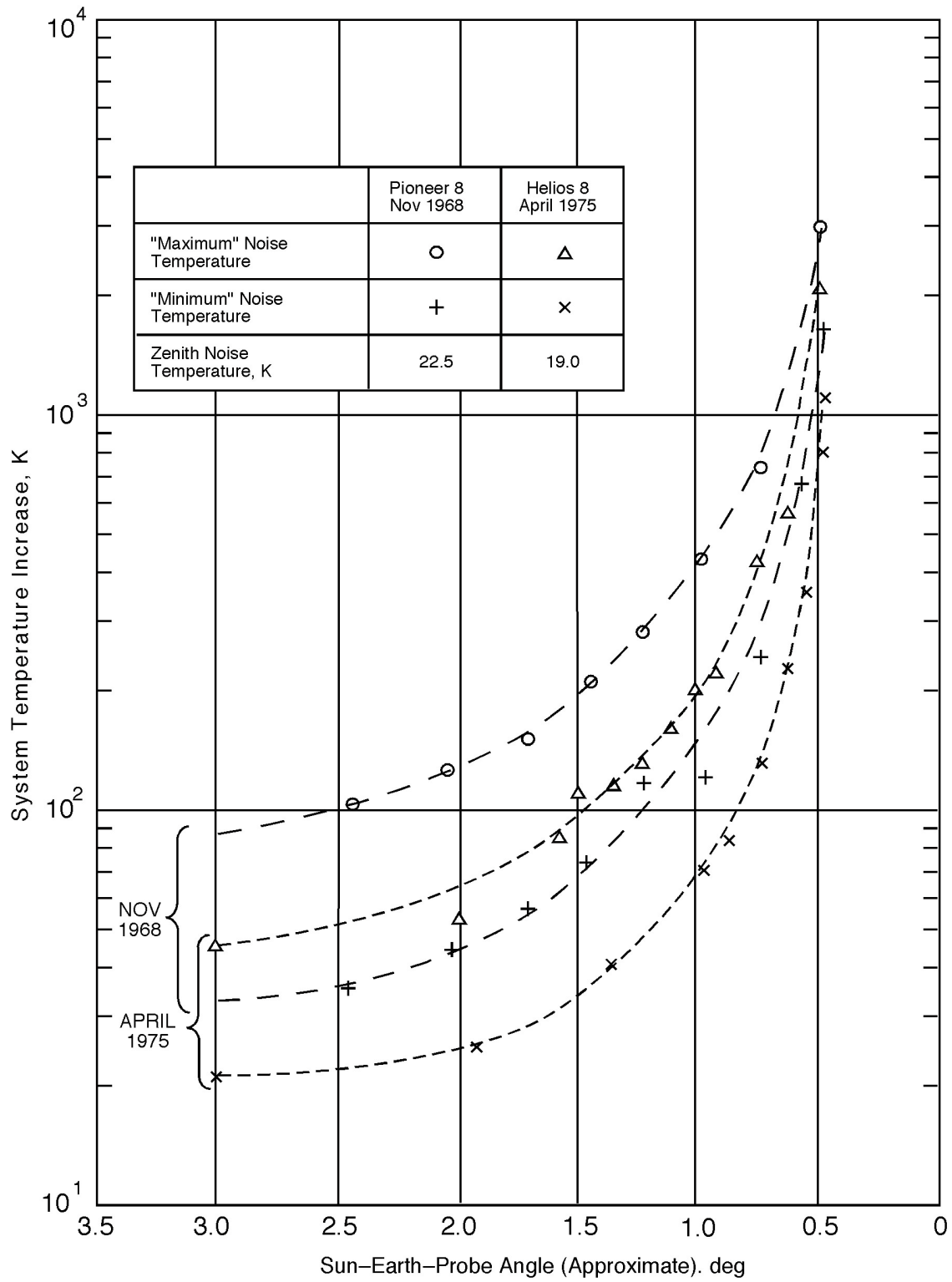
Figure 18. Total S-Band System Noise Temperature for 70-m Antennas Tracking Spacecraft Near the Sun (Derived from 64-m Measurements)
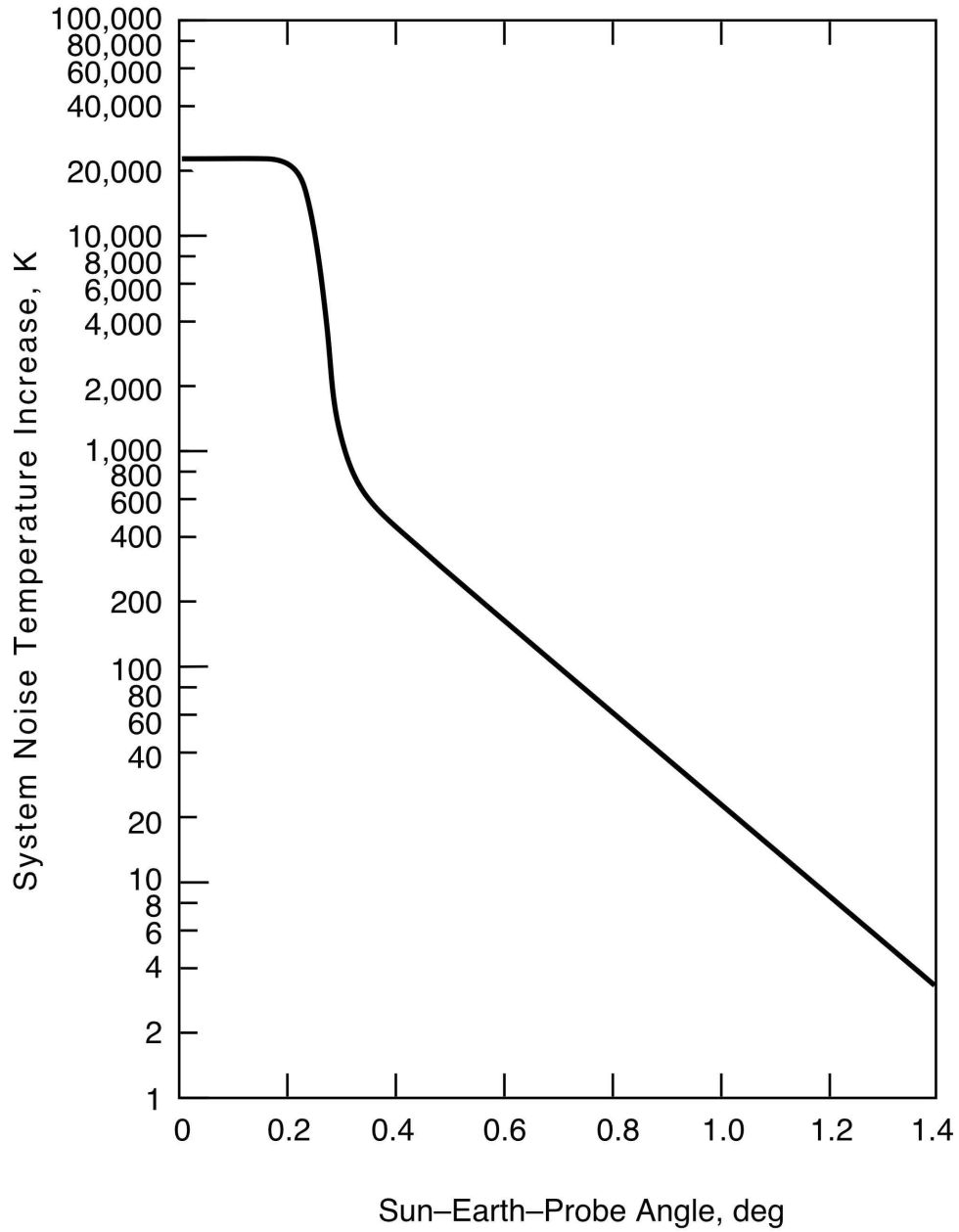
Figure 19. X-Band Noise Temperature Increase for 70-m Antennas as a Function
of Sun-Earth-Probe Angle, Nominal Sun, 23,000 K Disk Temperature

Table 1. Cumulative Distributions of Zenith Atmospheric Noise Temperature at L- and S-Bands for Goldstone DSCC, K

CD	January	February	March	April	May	June
0.000	1.917	1.917	1.917	1.917	1.917	1.917
0.100	1.923	1.923	1.923	1.924	1.926	1.925
0.200	1.925	1.925	1.925	1.927	1.929	1.928
0.250	1.926	1.925	1.926	1.927	1.930	1.929
0.300	1.927	1.927	1.927	1.929	1.932	1.930
0.400	1.928	1.928	1.929	1.930	1.935	1.933
0.500	1.930	1.930	1.931	1.932	1.938	1.936
0.600	1.933	1.932	1.932	1.934	1.941	1.941
0.700	1.938	1.935	1.935	1.936	1.945	1.947
0.800	1.945	1.940	1.938	1.939	1.950	1.952
0.850	1.951	1.945	1.941	1.940	1.954	1.955
0.900	1.963	1.954	1.945	1.943	1.961	1.961
0.925	1.978	1.961	1.947	1.945	1.967	1.967
0.930	1.981	1.963	1.948	1.945	1.968	1.968
0.950	2.002	1.975	1.952	1.948	1.983	1.975
0.960	2.017	1.984	1.957	1.950	1.990	1.981
0.975	2.059	2.005	1.973	1.956	2.010	2.001
0.980	2.075	2.015	1.982	1.963	2.016	2.011
0.990	2.142	2.051	2.022	1.992	2.042	2.051

Table 1 (Cont'd). Cumulative Distributions of Zenith Atmospheric Noise Temperature at L- and S-Bands for Goldstone DSCC, K

| CD	July	August	September	October	November	December	Minimum	Year Average	Maximum
0.000	1.917	1.917	1.917	1.917	1.917	1.917	1.917	1.917	1.917
0.100	1.929	1.930	1.932	1.927	1.924	1.922	1.922	1.926	1.932
0.200	1.934	1.935	1.935	1.930	1.926	1.925	1.925	1.929	1.935
0.250	1.936	1.937	1.936	1.930	1.927	1.925	1.925	1.930	1.937
0.300	1.938	1.940	1.939	1.932	1.929	1.927	1.927	1.931	1.940
0.400	1.942	1.945	1.943	1.935	1.931	1.928	1.928	1.934	1.945
0.500	1.947	1.951	1.948	1.937	1.934	1.930	1.930	1.937	1.951
0.600	1.954	1.955	1.952	1.940	1.939	1.932	1.932	1.941	1.955
0.700	1.962	1.959	1.958	1.943	1.943	1.935	1.935	1.945	1.962
0.800	1.969	1.963	1.964	1.948	1.948	1.941	1.938	1.950	1.969
0.850	1.972	1.967	1.967	1.952	1.952	1.947	1.940	1.954	1.972
0.900	1.977	1.972	1.975	1.958	1.958	1.957	1.943	1.960	1.977
0.925	1.981	1.976	1.980	1.961	1.961	1.964	1.945	1.966	1.981
0.930	1.982	1.976	1.980	1.961	1.961	1.967	1.945	1.967	1.982
0.950	1.987	1.983	1.986	1.966	1.965	1.985	1.948	1.975	2.002
0.960	1.991	1.987	1.992	1.970	1.968	1.997	1.950	1.982	2.017
0.975	2.003	2.000	2.008	1.983	1.978	2.028	1.956	2.000	2.059
0.980	2.011	2.001	2.024	1.990	1.989	2.042	1.963	2.010	2.075
0.990	2.049	2.009	2.098	2.025	2.031	2.098	1.992	2.051	2.142

Table 2. Cumulative Distributions of Zenith Atmospheric Noise Temperature at
L- and S-Bands for Canberra DSCC, K

CD	January	February	March	April	May	June
0.000	2.085	2.085	2.085	2.085	2.085	2.085
0.100	2.108	2.116	2.121	2.106	2.100	2.099
0.200	2.115	2.123	2.127	2.111	2.103	2.105
0.250	2.117	2.127	2.129	2.113	2.104	2.106
0.300	2.120	2.131	2.131	2.115	2.106	2.107
0.400	2.124	2.139	2.137	2.119	2.108	2.109
0.500	2.132	2.147	2.141	2.123	2.111	2.112
0.600	2.139	2.156	2.149	2.128	2.114	2.115
0.700	2.148	2.168	2.158	2.133	2.119	2.118
0.800	2.159	2.183	2.167	2.143	2.133	2.124
0.850	2.166	2.198	2.174	2.150	2.143	2.129
0.900	2.180	2.239	2.187	2.164	2.164	2.140
0.925	2.193	2.271	2.202	2.186	2.190	2.157
0.930	2.196	2.278	2.207	2.191	2.198	2.165
0.950	2.220	2.319	2.231	2.217	2.239	2.204
0.960	2.236	2.346	2.244	2.236	2.269	2.221
0.975	2.286	2.428	2.281	2.288	2.339	2.261
0.980	2.316	2.475	2.310	2.314	2.358	2.281
0.990	2.476	2.616	2.394	2.387	2.439	2.330

Table 2 (Cont'd). Cumulative Distributions of Zenith Atmospheric Noise Temperature at
L- and S-Bands for Canberra DSCC, K

CD	July	August	September	October	November	December	Minimum	Year Average	Maximum
0.000	2.085	2.085	2.085	2.085	2.085	2.085	2.085	2.085	2.085
0.100	2.097	2.097	2.101	2.102	2.109	2.102	2.097	2.105	2.121
0.200	2.100	2.101	2.105	2.107	2.114	2.109	2.100	2.110	2.127
0.250	2.102	2.102	2.107	2.108	2.117	2.112	2.102	2.112	2.129
0.300	2.103	2.103	2.108	2.110	2.119	2.115	2.103	2.114	2.131
0.400	2.105	2.105	2.112	2.113	2.124	2.120	2.105	2.118	2.139
0.500	2.108	2.107	2.115	2.117	2.129	2.125	2.107	2.122	2.147
0.600	2.111	2.110	2.119	2.123	2.135	2.132	2.110	2.128	2.156
0.700	2.115	2.114	2.125	2.131	2.144	2.141	2.114	2.134	2.168
0.800	2.122	2.121	2.133	2.146	2.162	2.157	2.121	2.146	2.183
0.850	2.128	2.128	2.140	2.158	2.179	2.172	2.128	2.155	2.198
0.900	2.138	2.144	2.152	2.181	2.206	2.197	2.138	2.174	2.239
0.925	2.151	2.161	2.164	2.208	2.232	2.219	2.151	2.195	2.271
0.930	2.155	2.166	2.169	2.215	2.239	2.227	2.155	2.200	2.278
0.950	2.171	2.190	2.198	2.262	2.279	2.261	2.171	2.233	2.319
0.960	2.183	2.212	2.220	2.288	2.303	2.278	2.183	2.253	2.346
0.975	2.209	2.285	2.266	2.365	2.392	2.322	2.209	2.310	2.428
0.980	2.223	2.309	2.296	2.414	2.432	2.343	2.223	2.339	2.475
0.990	2.274	2.394	2.423	2.532	2.547	2.412	2.274	2.435	2.616

Table 3. Cumulative Distributions of Zenith Atmospheric Noise Temperature at
L- and S-Bands for Madrid DSCC, K

CD	January	February	March	April	May	June
0.000	2.008	2.008	2.008	2.008	2.008	2.008
0.100	2.014	2.013	2.018	2.019	2.026	2.029
0.200	2.017	2.017	2.022	2.023	2.031	2.034
0.250	2.018	2.018	2.023	2.024	2.032	2.035
0.300	2.020	2.019	2.025	2.026	2.034	2.037
0.400	2.023	2.022	2.028	2.028	2.038	2.041
0.500	2.027	2.025	2.031	2.032	2.041	2.044
0.600	2.032	2.029	2.035	2.036	2.044	2.047
0.700	2.042	2.034	2.041	2.042	2.048	2.051
0.800	2.066	2.042	2.052	2.054	2.057	2.055
0.850	2.092	2.054	2.063	2.066	2.075	2.059
0.900	2.139	2.077	2.088	2.084	2.114	2.065
0.925	2.192	2.102	2.116	2.102	2.155	2.070
0.930	2.201	2.107	2.122	2.106	2.163	2.072
0.950	2.272	2.145	2.157	2.142	2.211	2.085
0.960	2.299	2.167	2.179	2.163	2.237	2.098
0.975	2.361	2.227	2.237	2.211	2.298	2.140
0.980	2.380	2.247	2.259	2.225	2.320	2.169
0.990	2.450	2.324	2.335	2.276	2.394	2.282

Table 3 (Cont'd). Cumulative Distributions of Zenith Atmospheric Noise Temperature at
L- and S-Bands for Madrid DSCC, K

CD	July	August	September	October	November	December	Minimum	Year Average	Maximum
0.000	2.008	2.008	2.008	2.008	2.008	2.008	2.008	2.008	2.008
0.100	2.032	2.032	2.029	2.023	2.008	2.013	2.008	2.021	2.032
0.200	2.036	2.037	2.034	2.031	2.018	2.018	2.017	2.026	2.037
0.250	2.037	2.038	2.036	2.033	2.020	2.020	2.018	2.028	2.038
0.300	2.039	2.040	2.038	2.036	2.023	2.023	2.019	2.030	2.040
0.400	2.043	2.043	2.042	2.041	2.026	2.027	2.022	2.033	2.043
0.500	2.045	2.047	2.046	2.047	2.030	2.032	2.025	2.037	2.047
0.600	2.048	2.050	2.051	2.054	2.036	2.038	2.029	2.042	2.054
0.700	2.052	2.053	2.055	2.062	2.044	2.049	2.034	2.048	2.062
0.800	2.055	2.058	2.061	2.082	2.058	2.073	2.042	2.059	2.082
0.850	2.057	2.060	2.065	2.105	2.079	2.099	2.054	2.073	2.105
0.900	2.061	2.064	2.072	2.147	2.121	2.142	2.061	2.098	2.147
0.925	2.063	2.067	2.079	2.189	2.164	2.181	2.063	2.123	2.192
0.930	2.064	2.067	2.081	2.197	2.171	2.187	2.064	2.128	2.201
0.950	2.067	2.071	2.095	2.256	2.229	2.235	2.067	2.164	2.272
0.960	2.069	2.074	2.110	2.283	2.253	2.257	2.069	2.182	2.299
0.975	2.077	2.083	2.159	2.350	2.316	2.316	2.077	2.231	2.361
0.980	2.084	2.090	2.196	2.377	2.333	2.334	2.084	2.251	2.380
0.990	2.117	2.119	2.333	2.481	2.400	2.397	2.117	2.326	2.481

Table 4. Cumulative Distributions of Zenith Atmospheric Noise Temperature at X-Band
for Goldstone DSCC, K

CD	January	February	March	April	May	June
0.000	2.135	2.135	2.135	2.135	2.135	2.135
0.100	2.218	2.210	2.220	2.233	2.257	2.246
0.200	2.241	2.238	2.247	2.266	2.297	2.284
0.250	2.249	2.249	2.256	2.276	2.310	2.296
0.300	2.264	2.264	2.268	2.291	2.331	2.315
0.400	2.288	2.286	2.292	2.311	2.372	2.346
0.500	2.317	2.309	2.318	2.333	2.421	2.395
0.600	2.355	2.334	2.342	2.361	2.463	2.464
0.700	2.416	2.376	2.373	2.390	2.510	2.536
0.800	2.506	2.450	2.424	2.426	2.578	2.603
0.850	2.599	2.510	2.455	2.448	2.634	2.647
0.900	2.758	2.634	2.509	2.483	2.728	2.725
0.925	2.956	2.732	2.543	2.507	2.805	2.807
0.930	2.991	2.758	2.549	2.511	2.825	2.817
0.950	3.277	2.911	2.607	2.547	3.020	2.912
0.960	3.475	3.039	2.678	2.576	3.113	3.002
0.975	4.041	3.324	2.885	2.666	3.381	3.262
0.980	4.265	3.452	3.010	2.755	3.462	3.395
0.990	5.160	3.944	3.553	3.147	3.824	3.943

Table 4 (Cont'd). Cumulative Distributions of Zenith Atmospheric Noise Temperature at
X-Band for Goldstone DSCC, K

CD	July	August	September	October	November	December	Minimum	Year Average	Maximum
0.000	2.135	2.135	2.135	2.135	2.135	2.135	2.135	2.135	2.135
0.100	2.294	2.306	2.332	2.268	2.227	2.207	2.207	2.251	2.332
0.200	2.365	2.375	2.374	2.303	2.262	2.239	2.238	2.291	2.375
0.250	2.387	2.402	2.393	2.315	2.274	2.248	2.248	2.305	2.402
0.300	2.422	2.447	2.425	2.336	2.292	2.263	2.263	2.327	2.447
0.400	2.474	2.512	2.481	2.375	2.325	2.284	2.284	2.362	2.512
0.500	2.545	2.592	2.553	2.408	2.366	2.307	2.307	2.405	2.592
0.600	2.630	2.652	2.612	2.444	2.426	2.335	2.334	2.451	2.652
0.700	2.739	2.695	2.690	2.488	2.487	2.382	2.373	2.507	2.739
0.800	2.830	2.760	2.766	2.552	2.556	2.460	2.424	2.576	2.830
0.850	2.878	2.805	2.813	2.600	2.603	2.541	2.448	2.628	2.878
0.900	2.946	2.876	2.915	2.681	2.680	2.676	2.483	2.718	2.946
0.925	2.996	2.924	2.981	2.725	2.726	2.773	2.507	2.790	2.996
0.930	3.009	2.934	2.989	2.732	2.731	2.801	2.511	2.804	3.009
0.950	3.074	3.019	3.066	2.793	2.777	3.048	2.547	2.921	3.277
0.960	3.126	3.078	3.141	2.850	2.824	3.208	2.576	3.009	3.475
0.975	3.295	3.246	3.356	3.022	2.963	3.631	2.666	3.256	4.041
0.980	3.404	3.272	3.577	3.120	3.098	3.819	2.755	3.386	4.265
0.990	3.912	3.377	4.578	3.585	3.663	4.570	3.147	3.938	5.160

Table 5. Cumulative Distributions of Zenith Atmospheric Noise Temperature at X-Band
for Canberra DSCC, K

CD	January	February	March	April	May	June
0.000	2.327	2.327	2.327	2.327	2.327	2.327
0.100	2.631	2.741	2.815	2.607	2.531	2.513
0.200	2.725	2.841	2.895	2.679	2.568	2.594
0.250	2.763	2.892	2.924	2.705	2.587	2.612
0.300	2.792	2.948	2.953	2.732	2.607	2.626
0.400	2.853	3.057	3.021	2.783	2.641	2.656
0.500	2.955	3.162	3.087	2.843	2.678	2.691
0.600	3.057	3.287	3.187	2.902	2.714	2.730
0.700	3.177	3.439	3.303	2.978	2.782	2.777
0.800	3.321	3.641	3.433	3.101	2.974	2.849
0.850	3.419	3.848	3.527	3.198	3.112	2.918
0.900	3.604	4.396	3.704	3.385	3.387	3.063
0.925	3.780	4.829	3.898	3.687	3.738	3.299
0.930	3.821	4.921	3.963	3.757	3.848	3.401
0.950	4.138	5.483	4.287	4.109	4.399	3.929
0.960	4.361	5.843	4.465	4.366	4.802	4.164
0.975	5.027	6.950	4.966	5.062	5.740	4.695
0.980	5.435	7.580	5.350	5.412	5.997	4.965
0.990	7.589	9.469	6.492	6.392	7.091	5.622

Table 5 (Cont'd). Cumulative Distributions of Zenith Atmospheric Noise Temperature at
X-Band for Canberra DSCC, K

CD	July	August	September	October	November	December	Minimum	Year Average	Maximum
0.000	2.327	2.327	2.327	2.327	2.327	2.327	2.327	2.327	2.327
0.100	2.485	2.491	2.548	2.550	2.649	2.562	2.485	2.594	2.815
0.200	2.532	2.539	2.600	2.617	2.723	2.648	2.532	2.663	2.895
0.250	2.551	2.556	2.621	2.640	2.755	2.693	2.551	2.692	2.924
0.300	2.567	2.570	2.643	2.662	2.790	2.731	2.567	2.718	2.953
0.400	2.598	2.598	2.688	2.705	2.858	2.801	2.598	2.772	3.057
0.500	2.636	2.628	2.732	2.760	2.924	2.871	2.628	2.831	3.162
0.600	2.676	2.669	2.785	2.837	3.002	2.958	2.669	2.900	3.287
0.700	2.725	2.723	2.863	2.942	3.117	3.079	2.723	2.992	3.439
0.800	2.823	2.807	2.966	3.153	3.362	3.298	2.807	3.144	3.641
0.850	2.907	2.900	3.062	3.310	3.594	3.501	2.900	3.275	3.848
0.900	3.045	3.125	3.232	3.625	3.955	3.834	3.045	3.530	4.396
0.925	3.222	3.351	3.396	3.982	4.312	4.131	3.222	3.802	4.829
0.930	3.265	3.413	3.464	4.077	4.403	4.234	3.265	3.881	4.921
0.950	3.484	3.741	3.852	4.704	4.938	4.690	3.484	4.313	5.483
0.960	3.649	4.037	4.146	5.064	5.266	4.920	3.649	4.590	5.843
0.975	3.999	5.018	4.766	6.097	6.453	5.522	3.999	5.358	6.950
0.980	4.187	5.340	5.165	6.757	7.003	5.794	4.187	5.749	7.580
0.990	4.874	6.481	6.882	8.346	8.552	6.732	4.874	7.043	9.469

Table 6. Cumulative Distributions of Zenith Atmospheric Noise Temperature at X-Band
for Madrid DSCC, K

CD	January	February	March	April	May	June
0.000	2.239	2.239	2.239	2.239	2.239	2.239
0.100	2.314	2.310	2.378	2.386	2.483	2.522
0.200	2.364	2.358	2.425	2.442	2.545	2.585
0.250	2.379	2.372	2.442	2.456	2.564	2.604
0.300	2.401	2.392	2.466	2.475	2.592	2.634
0.400	2.439	2.423	2.502	2.512	2.639	2.677
0.500	2.492	2.470	2.551	2.561	2.679	2.722
0.600	2.565	2.524	2.605	2.620	2.723	2.767
0.700	2.695	2.588	2.684	2.700	2.775	2.816
0.800	3.013	2.697	2.829	2.859	2.897	2.877
0.850	3.365	2.855	2.984	3.019	3.137	2.922
0.900	4.006	3.167	3.322	3.264	3.662	3.004
0.925	4.714	3.499	3.697	3.506	4.213	3.074
0.930	4.835	3.567	3.773	3.562	4.320	3.095
0.950	5.796	4.089	4.239	4.047	4.971	3.280
0.960	6.151	4.379	4.536	4.328	5.324	3.452
0.975	6.990	5.186	5.323	4.965	6.142	4.021
0.980	7.242	5.454	5.623	5.155	6.438	4.411
0.990	8.190	6.491	6.646	5.847	7.435	5.921

Table 6 (Cont'd). Cumulative Distributions of Zenith Atmospheric Noise Temperature at
X-Band for Madrid DSCC, K

CD	July	August	September	October	November	December	Minimum	Year Average	Maximum
0.000	2.239	2.239	2.239	2.239	2.239	2.239	2.239	2.239	2.239
0.100	2.560	2.563	2.519	2.442	2.235	2.312	2.235	2.419	2.563
0.200	2.618	2.626	2.588	2.542	2.373	2.375	2.358	2.487	2.626
0.250	2.636	2.645	2.611	2.571	2.397	2.398	2.372	2.506	2.645
0.300	2.662	2.674	2.646	2.616	2.436	2.436	2.392	2.536	2.674
0.400	2.704	2.717	2.699	2.688	2.483	2.500	2.423	2.582	2.717
0.500	2.744	2.760	2.754	2.765	2.538	2.565	2.470	2.633	2.765
0.600	2.784	2.806	2.814	2.855	2.615	2.649	2.524	2.694	2.855
0.700	2.825	2.851	2.874	2.972	2.717	2.794	2.588	2.774	2.972
0.800	2.873	2.910	2.951	3.241	2.910	3.114	2.697	2.931	3.241
0.850	2.902	2.943	3.002	3.544	3.196	3.461	2.855	3.111	3.544
0.900	2.948	2.997	3.095	4.108	3.757	4.037	2.948	3.447	4.108
0.925	2.981	3.029	3.196	4.674	4.342	4.572	2.981	3.791	4.714
0.930	2.987	3.036	3.218	4.779	4.438	4.650	2.987	3.855	4.835
0.950	3.034	3.086	3.414	5.576	5.212	5.289	3.034	4.336	5.796
0.960	3.064	3.125	3.614	5.940	5.540	5.592	3.064	4.587	6.151
0.975	3.168	3.253	4.272	6.842	6.389	6.380	3.168	5.244	6.990
0.980	3.257	3.344	4.769	7.208	6.619	6.624	3.257	5.512	7.242
0.990	3.702	3.734	6.609	8.606	7.512	7.475	3.702	6.514	8.606

Table 7. Cumulative Distributions of Zenith Atmospheric Noise Temperature at Ka-Band
for Goldstone DSCC, K

CD	January	February	March	April	May	June
0.000	6.700	6.700	6.700	6.700	6.700	6.700
0.100	7.904	7.785	7.925	8.119	8.463	8.302
0.200	8.227	8.181	8.321	8.594	9.041	8.856
0.250	8.354	8.342	8.441	8.731	9.233	9.031
0.300	8.564	8.563	8.626	8.948	9.531	9.304
0.400	8.915	8.888	8.967	9.237	10.127	9.748
0.500	9.325	9.218	9.346	9.563	10.837	10.450
0.600	9.870	9.575	9.688	9.962	11.441	11.447
0.700	10.764	10.181	10.134	10.383	12.115	12.488
0.800	12.058	11.252	10.868	10.909	13.100	13.459
0.850	13.395	12.119	11.316	11.226	13.912	14.098
0.900	15.703	13.903	12.100	11.726	15.260	15.217
0.925	18.556	15.328	12.600	12.070	16.383	16.399
0.930	19.068	15.702	12.683	12.133	16.670	16.548
0.950	23.198	17.912	13.523	12.651	19.479	17.919
0.960	26.054	19.756	14.550	13.068	20.820	19.226
0.975	34.229	23.875	17.527	14.366	24.702	22.976
0.980	37.463	25.724	19.338	15.656	25.866	24.904
0.990	50.394	32.834	27.182	21.314	31.090	32.814

Table 7 (Cont'd). Cumulative Distributions of Zenith Atmospheric Noise Temperature at
Ka-Band for Goldstone DSCC, K

CD	July	August	September	October	November	December	Minimum	Year Average	Maximum
0.000	6.700	6.700	6.700	6.700	6.700	6.700	6.700	6.700	6.700
0.100	8.999	9.167	9.539	8.617	8.028	7.746	7.746	8.383	9.539
0.200	10.021	10.163	10.153	9.130	8.529	8.197	8.181	8.951	10.163
0.250	10.341	10.559	10.424	9.301	8.701	8.337	8.337	9.150	10.559
0.300	10.848	11.213	10.890	9.606	8.969	8.549	8.549	9.468	11.213
0.400	11.592	12.143	11.701	10.170	9.444	8.854	8.854	9.982	12.143
0.500	12.618	13.303	12.736	10.649	10.037	9.186	9.186	10.606	13.303
0.600	13.848	14.174	13.595	11.156	10.899	9.585	9.575	11.270	14.174
0.700	15.424	14.787	14.714	11.805	11.782	10.264	10.134	12.070	15.424
0.800	16.742	15.727	15.812	12.722	12.786	11.389	10.868	13.069	16.742
0.850	17.426	16.371	16.487	13.410	13.465	12.566	11.226	13.816	17.426
0.900	18.419	17.398	17.964	14.581	14.576	14.521	11.726	15.114	18.419
0.925	19.131	18.090	18.919	15.220	15.229	15.921	12.070	16.154	19.131
0.930	19.323	18.247	19.040	15.317	15.304	16.325	12.133	16.363	19.323
0.950	20.260	19.474	20.152	16.204	15.976	19.884	12.651	18.053	23.198
0.960	21.008	20.321	21.234	17.020	16.651	22.199	13.068	19.326	26.054
0.975	23.451	22.752	24.331	19.512	18.657	28.306	14.366	22.890	34.229
0.980	25.032	23.123	27.535	20.927	20.607	31.025	15.656	24.767	37.463
0.990	32.362	24.643	41.986	27.647	28.774	41.871	21.314	32.743	50.394

Table 8. Cumulative Distributions of Zenith Atmospheric Noise Temperature at Ka-Band
for Canberra DSCC, K

CD	January	February	March	April	May	June
0.000	7.274	7.274	7.274	7.274	7.274	7.274
0.100	11.671	13.259	14.320	11.313	10.215	9.957
0.200	13.019	14.694	15.485	12.360	10.760	11.133
0.250	13.570	15.432	15.895	12.740	11.030	11.390
0.300	13.996	16.240	16.314	13.120	11.320	11.594
0.400	14.873	17.813	17.305	13.865	11.810	12.023
0.500	16.347	19.333	18.255	14.730	12.340	12.530
0.600	17.820	21.135	19.690	15.580	12.870	13.093
0.700	19.554	23.330	21.375	16.675	13.844	13.780
0.800	21.631	26.251	23.250	18.455	16.624	14.809
0.850	23.048	29.237	24.613	19.853	18.614	15.805
0.900	25.721	37.155	27.169	22.553	22.586	17.897
0.925	28.258	43.415	29.972	26.919	27.655	21.311
0.930	28.846	44.748	30.911	27.935	29.242	22.786
0.950	33.438	52.852	35.590	33.007	37.206	30.415
0.960	36.657	58.057	38.148	36.725	43.020	33.801
0.975	46.274	74.052	45.395	46.781	56.575	41.481
0.980	52.169	83.148	50.943	51.827	60.285	45.372
0.990	83.280	110.437	67.432	65.986	76.082	54.859

Table 8 (Cont'd). Cumulative Distributions of Zenith Atmospheric Noise Temperature at
Ka-Band for Canberra DSCC, K

CD	July	August	September	October	November	December	Minimum	Year Average	Maximum
0.000	7.274	7.274	7.274	7.274	7.274	7.274	7.274	7.274	7.274
0.100	9.563	9.638	10.470	10.500	11.923	10.670	9.563	11.125	14.320
0.200	10.235	10.333	11.213	11.467	12.993	11.917	10.235	12.134	15.485
0.250	10.505	10.580	11.523	11.800	13.452	12.553	10.505	12.539	15.895
0.300	10.743	10.789	11.840	12.113	13.957	13.103	10.743	12.927	16.314
0.400	11.188	11.190	12.493	12.737	14.940	14.117	11.188	13.696	17.813
0.500	11.730	11.619	13.128	13.533	15.893	15.133	11.619	14.548	19.333
0.600	12.313	12.215	13.887	14.633	17.030	16.381	12.215	15.554	21.135
0.700	13.028	12.988	15.017	16.155	18.682	18.143	12.988	16.881	23.330
0.800	14.442	14.200	16.511	19.203	22.224	21.303	14.200	19.075	26.251
0.850	15.655	15.547	17.889	21.470	25.576	24.236	15.547	20.962	29.237
0.900	17.645	18.804	20.349	26.021	30.782	29.038	17.645	24.643	37.155
0.925	20.202	22.063	22.720	31.181	35.946	33.327	20.202	28.581	43.415
0.930	20.824	22.967	23.690	32.545	37.255	34.818	20.824	29.714	44.748
0.950	23.988	27.691	29.298	41.607	44.979	41.402	23.988	35.956	52.852
0.960	26.372	31.975	33.550	46.812	49.729	44.727	26.372	39.964	58.057
0.975	31.422	46.147	42.500	61.731	66.869	53.428	31.422	51.054	74.052
0.980	34.134	50.786	48.262	71.255	74.809	57.345	34.134	56.695	83.148
0.990	44.061	67.266	73.060	94.217	97.186	70.896	44.061	75.397	110.437

Table 9. Cumulative Distributions of Zenith Atmospheric Noise Temperature at Ka-Band
for Madrid DSCC, K

CD	January	February	March	April	May	June
0.000	7.000	7.000	7.000	7.000	7.000	7.000
0.100	8.081	8.027	9.008	9.129	10.527	11.095
0.200	8.807	8.715	9.680	9.934	11.424	12.001
0.250	9.020	8.918	9.928	10.128	11.700	12.279
0.300	9.345	9.209	10.275	10.413	12.094	12.701
0.400	9.893	9.661	10.801	10.941	12.778	13.321
0.500	10.660	10.343	11.505	11.649	13.349	13.978
0.600	11.705	11.122	12.284	12.505	13.985	14.626
0.700	13.588	12.034	13.426	13.658	14.740	15.331
0.800	18.184	13.617	15.527	15.956	16.508	16.218
0.850	23.264	15.894	17.764	18.261	19.967	16.865
0.900	32.518	20.404	22.635	21.803	27.555	18.056
0.925	42.747	25.199	28.054	25.304	35.506	19.059
0.930	44.501	26.176	29.154	26.115	37.057	19.361
0.950	58.380	33.714	35.887	33.118	46.457	22.041
0.960	63.503	37.904	40.178	37.171	51.554	24.514
0.975	75.622	49.567	51.540	46.376	63.371	32.733
0.980	79.259	53.436	55.884	49.123	67.655	38.373
0.990	92.957	68.414	70.648	59.108	82.045	60.183

Table 9 (Cont'd). Cumulative Distributions of Zenith Atmospheric Noise Temperature at
Ka-Band for Madrid DSCC, K

CD	July	August	September	October	November	December	Minimum	Year Average	Maximum
0.000	7.000	7.000	7.000	7.000	7.000	7.000	7.000	7.000	7.000
0.100	11.629	11.685	11.048	9.928	6.945	8.053	6.945	9.596	11.685
0.200	12.472	12.584	12.045	11.382	8.940	8.957	8.715	10.578	12.584
0.250	12.729	12.868	12.368	11.802	9.280	9.297	8.918	10.860	12.868
0.300	13.108	13.287	12.877	12.451	9.852	9.845	9.209	11.288	13.287
0.400	13.719	13.901	13.650	13.489	10.522	10.775	9.661	11.954	13.901
0.500	14.290	14.523	14.437	14.599	11.318	11.708	10.343	12.697	14.599
0.600	14.866	15.183	15.311	15.893	12.425	12.920	11.122	13.569	15.893
0.700	15.470	15.844	16.170	17.581	13.910	15.023	12.034	14.731	17.581
0.800	16.164	16.691	17.282	21.475	16.699	19.634	13.617	16.996	21.475
0.850	16.577	17.169	18.017	25.853	20.829	24.646	15.894	19.592	25.853
0.900	17.245	17.946	19.369	33.998	28.929	32.965	17.245	24.452	33.998
0.925	17.715	18.413	20.820	42.171	37.379	40.700	17.715	29.422	42.747
0.930	17.803	18.505	21.142	43.694	38.756	41.828	17.803	30.341	44.501
0.950	18.487	19.229	23.978	55.198	49.934	51.055	18.487	37.290	58.380
0.960	18.918	19.803	26.856	60.459	54.681	55.436	18.918	40.915	63.503
0.975	20.416	21.652	36.364	73.478	66.936	66.807	20.416	50.405	75.622
0.980	21.709	22.960	43.548	78.764	70.263	70.341	21.709	54.276	79.259
0.990	28.129	28.596	70.125	98.968	83.164	82.632	28.129	68.747	98.968

Table 10. Cumulative Distributions of Zenith Atmospheric Attenuation at
L- and S-Bands for Goldstone DSCC, dB

CD	January	February	March	April	May	June
0.000	0.033	0.033	0.033	0.033	0.033	0.033
0.100	0.033	0.033	0.033	0.033	0.033	0.033
0.200	0.032	0.032	0.032	0.032	0.032	0.032
0.250	0.032	0.032	0.032	0.032	0.032	0.032
0.300	0.032	0.032	0.032	0.032	0.032	0.032
0.400	0.032	0.032	0.032	0.032	0.032	0.032
0.500	0.031	0.031	0.031	0.031	0.032	0.032
0.600	0.031	0.031	0.031	0.031	0.031	0.031
0.700	0.031	0.031	0.031	0.031	0.031	0.031
0.800	0.031	0.031	0.031	0.031	0.031	0.031
0.850	0.031	0.031	0.031	0.031	0.031	0.031
0.900	0.031	0.031	0.031	0.031	0.031	0.031
0.925	0.031	0.031	0.031	0.030	0.031	0.031
0.930	0.031	0.031	0.031	0.030	0.031	0.031
0.950	0.031	0.031	0.031	0.030	0.031	0.031
0.960	0.032	0.031	0.031	0.030	0.031	0.031
0.975	0.032	0.031	0.031	0.031	0.031	0.031
0.980	0.032	0.031	0.031	0.031	0.031	0.031
0.990	0.033	0.032	0.032	0.031	0.032	0.032

Table 10 (Cont'd). Cumulative Distributions of Zenith Atmospheric Attenuation at
L- and S-Bands for Goldstone DSCC, dB

CD	July	August	September	October	November	December	Minimum	Year Average	Maximum
0.000	0.033	0.033	0.033	0.033	0.033	0.033	0.033	0.033	0.033
0.100	0.033	0.033	0.033	0.033	0.033	0.033	0.033	0.033	0.033
0.200	0.032	0.032	0.032	0.032	0.032	0.032	0.032	0.032	0.032
0.250	0.032	0.032	0.032	0.032	0.032	0.032	0.032	0.032	0.032
0.300	0.032	0.032	0.032	0.032	0.032	0.032	0.032	0.032	0.032
0.400	0.032	0.032	0.032	0.032	0.032	0.032	0.032	0.032	0.032
0.500	0.032	0.032	0.032	0.032	0.032	0.031	0.031	0.032	0.032
0.600	0.032	0.032	0.032	0.031	0.031	0.031	0.031	0.031	0.032
0.700	0.031	0.031	0.031	0.031	0.031	0.031	0.031	0.031	0.031
0.800	0.031	0.031	0.031	0.031	0.031	0.031	0.031	0.031	0.031
0.850	0.031	0.031	0.031	0.031	0.031	0.031	0.031	0.031	0.031
0.900	0.031	0.031	0.031	0.031	0.031	0.031	0.031	0.031	0.031
0.925	0.031	0.031	0.031	0.031	0.031	0.031	0.030	0.031	0.031
0.930	0.031	0.031	0.031	0.031	0.031	0.031	0.030	0.031	0.031
0.950	0.031	0.031	0.031	0.031	0.031	0.031	0.030	0.031	0.031
0.960	0.031	0.031	0.031	0.031	0.031	0.031	0.030	0.031	0.032
0.975	0.031	0.031	0.031	0.031	0.031	0.032	0.031	0.031	0.032
0.980	0.031	0.031	0.032	0.031	0.031	0.032	0.031	0.031	0.032
0.990	0.032	0.031	0.033	0.032	0.032	0.033	0.031	0.032	0.033

Table 11. Cumulative Distributions of Zenith Atmospheric Attenuation at
L- and S-Bands for Canberra DSCC, dB

CD	January	February	March	April	May	June
0.000	0.036	0.036	0.036	0.036	0.036	0.036
0.100	0.036	0.036	0.036	0.036	0.036	0.036
0.200	0.035	0.036	0.036	0.035	0.035	0.035
0.250	0.035	0.036	0.036	0.035	0.035	0.035
0.300	0.035	0.035	0.035	0.035	0.035	0.035
0.400	0.035	0.035	0.035	0.035	0.035	0.035
0.500	0.035	0.035	0.035	0.035	0.034	0.034
0.600	0.035	0.035	0.035	0.034	0.034	0.034
0.700	0.034	0.035	0.035	0.034	0.034	0.034
0.800	0.034	0.035	0.034	0.034	0.034	0.034
0.850	0.034	0.035	0.034	0.034	0.034	0.034
0.900	0.034	0.035	0.034	0.034	0.034	0.034
0.925	0.034	0.036	0.035	0.034	0.034	0.034
0.930	0.034	0.036	0.035	0.034	0.034	0.034
0.950	0.035	0.036	0.035	0.035	0.035	0.034
0.960	0.035	0.037	0.035	0.035	0.035	0.035
0.975	0.036	0.038	0.036	0.036	0.037	0.035
0.980	0.036	0.039	0.036	0.036	0.037	0.036
0.990	0.039	0.041	0.037	0.037	0.038	0.036

Table 11 (Cont'd). Cumulative Distributions of Zenith Atmospheric Attenuation at
L- and S-Bands for Canberra DSCC, dB

CD	July	August	September	October	November	December	Minimum	Year Average	Maximum
0.000	0.036	0.036	0.036	0.036	0.036	0.036	0.036	0.036	0.036
0.100	0.036	0.036	0.036	0.036	0.036	0.036	0.036	0.036	0.036
0.200	0.035	0.035	0.035	0.035	0.035	0.035	0.035	0.035	0.036
0.250	0.035	0.035	0.035	0.035	0.035	0.035	0.035	0.035	0.036
0.300	0.035	0.035	0.035	0.035	0.035	0.035	0.035	0.035	0.035
0.400	0.035	0.035	0.035	0.035	0.035	0.035	0.035	0.035	0.035
0.500	0.034	0.034	0.034	0.035	0.035	0.035	0.034	0.035	0.035
0.600	0.034	0.034	0.034	0.034	0.034	0.034	0.034	0.034	0.035
0.700	0.034	0.034	0.034	0.034	0.034	0.034	0.034	0.034	0.035
0.800	0.034	0.034	0.034	0.034	0.034	0.034	0.034	0.034	0.035
0.850	0.034	0.034	0.034	0.034	0.034	0.034	0.034	0.034	0.035
0.900	0.034	0.034	0.034	0.034	0.035	0.035	0.034	0.034	0.035
0.925	0.034	0.034	0.034	0.035	0.035	0.035	0.034	0.034	0.036
0.930	0.034	0.034	0.034	0.035	0.035	0.035	0.034	0.034	0.036
0.950	0.034	0.034	0.034	0.035	0.036	0.035	0.034	0.035	0.036
0.960	0.034	0.035	0.035	0.036	0.036	0.036	0.034	0.035	0.037
0.975	0.034	0.036	0.035	0.037	0.037	0.036	0.034	0.036	0.038
0.980	0.035	0.036	0.036	0.038	0.038	0.037	0.035	0.037	0.039
0.990	0.035	0.037	0.038	0.039	0.040	0.038	0.035	0.038	0.041

Table 12. Cumulative Distributions of Zenith Atmospheric Attenuation at
L- and S-Bands for Madrid DSCC, dB

CD	January	February	March	April	May	June
0.000	0.034	0.034	0.034	0.034	0.034	0.034
0.100	0.034	0.034	0.034	0.034	0.034	0.034
0.200	0.034	0.034	0.034	0.034	0.034	0.034
0.250	0.034	0.034	0.034	0.034	0.034	0.034
0.300	0.034	0.034	0.034	0.034	0.034	0.034
0.400	0.033	0.033	0.033	0.033	0.034	0.034
0.500	0.033	0.033	0.033	0.033	0.033	0.033
0.600	0.033	0.033	0.033	0.033	0.033	0.033
0.700	0.033	0.033	0.033	0.033	0.033	0.033
0.800	0.033	0.032	0.033	0.033	0.033	0.033
0.850	0.033	0.032	0.033	0.033	0.033	0.032
0.900	0.034	0.033	0.033	0.033	0.033	0.032
0.925	0.034	0.033	0.033	0.033	0.034	0.032
0.930	0.034	0.033	0.033	0.033	0.034	0.032
0.950	0.036	0.034	0.034	0.034	0.035	0.033
0.960	0.036	0.034	0.034	0.034	0.035	0.033
0.975	0.037	0.035	0.035	0.034	0.036	0.033
0.980	0.037	0.035	0.035	0.035	0.036	0.034
0.990	0.038	0.036	0.036	0.035	0.037	0.036

Table 12 (Cont'd). Cumulative Distributions of Zenith Atmospheric Attenuation at
L- and S-Bands for Madrid DSCC, dB

CD	July	August	September	October	November	December	Minimum	Maximum	Year Average
0.000	0.034	0.034	0.034	0.034	0.034	0.034	0.034	0.034	0.034
0.100	0.034	0.034	0.034	0.034	0.034	0.034	0.034	0.034	0.034
0.200	0.034	0.034	0.034	0.034	0.034	0.034	0.034	0.034	0.034
0.250	0.034	0.034	0.034	0.034	0.034	0.034	0.034	0.034	0.034
0.300	0.034	0.034	0.034	0.034	0.034	0.034	0.034	0.034	0.034
0.400	0.034	0.034	0.034	0.034	0.033	0.033	0.033	0.033	0.034
0.500	0.033	0.033	0.033	0.033	0.033	0.033	0.033	0.033	0.033
0.600	0.033	0.033	0.033	0.033	0.033	0.033	0.033	0.033	0.033
0.700	0.033	0.033	0.033	0.033	0.033	0.033	0.033	0.033	0.033
0.800	0.033	0.033	0.033	0.033	0.033	0.033	0.032	0.033	0.033
0.850	0.032	0.033	0.033	0.033	0.033	0.033	0.032	0.033	0.033
0.900	0.032	0.032	0.033	0.034	0.033	0.034	0.032	0.033	0.034
0.925	0.032	0.032	0.033	0.034	0.034	0.034	0.032	0.033	0.034
0.930	0.032	0.032	0.033	0.034	0.034	0.034	0.032	0.033	0.034
0.950	0.032	0.032	0.033	0.035	0.035	0.035	0.032	0.034	0.036
0.960	0.032	0.032	0.033	0.036	0.035	0.035	0.032	0.034	0.036
0.975	0.032	0.033	0.034	0.037	0.036	0.036	0.032	0.035	0.037
0.980	0.032	0.033	0.034	0.037	0.036	0.036	0.032	0.035	0.037
0.990	0.033	0.033	0.036	0.039	0.037	0.037	0.033	0.036	0.039

Table 13. Cumulative Distributions of Zenith Atmospheric Attenuation at X-Band
for Goldstone DSCC, dB

CD	January	February	March	April	May	June
0.000	0.037	0.037	0.037	0.037	0.037	0.037
0.100	0.038	0.037	0.038	0.038	0.038	0.038
0.200	0.038	0.038	0.038	0.038	0.039	0.038
0.250	0.038	0.038	0.038	0.038	0.039	0.038
0.300	0.038	0.038	0.038	0.038	0.039	0.038
0.400	0.038	0.038	0.038	0.038	0.039	0.039
0.500	0.038	0.038	0.038	0.038	0.039	0.039
0.600	0.038	0.038	0.038	0.038	0.040	0.040
0.700	0.039	0.038	0.038	0.038	0.040	0.041
0.800	0.040	0.039	0.038	0.038	0.041	0.041
0.850	0.041	0.040	0.039	0.039	0.042	0.042
0.900	0.043	0.041	0.039	0.039	0.043	0.043
0.925	0.046	0.043	0.040	0.039	0.044	0.044
0.930	0.047	0.043	0.040	0.039	0.044	0.044
0.950	0.051	0.046	0.041	0.040	0.047	0.046
0.960	0.054	0.048	0.042	0.040	0.049	0.047
0.975	0.063	0.052	0.045	0.042	0.053	0.051
0.980	0.067	0.054	0.047	0.043	0.054	0.053
0.990	0.081	0.062	0.056	0.049	0.060	0.062

Table 13 (Cont'd). Cumulative Distributions of Zenith Atmospheric Attenuation at X-Band
for Goldstone DSCC, dB

CD	July	August	September	October	November	December	Minimum	Year Average	Maximum
0.000	0.037	0.037	0.037	0.037	0.037	0.037	0.037	0.037	0.037
0.100	0.039	0.039	0.040	0.038	0.038	0.037	0.037	0.038	0.040
0.200	0.040	0.040	0.040	0.039	0.038	0.038	0.038	0.038	0.040
0.250	0.040	0.040	0.040	0.039	0.038	0.038	0.038	0.038	0.040
0.300	0.040	0.041	0.040	0.039	0.038	0.038	0.038	0.039	0.041
0.400	0.041	0.041	0.041	0.039	0.038	0.038	0.038	0.039	0.041
0.500	0.042	0.042	0.042	0.039	0.039	0.038	0.038	0.039	0.042
0.600	0.043	0.043	0.042	0.039	0.039	0.038	0.038	0.040	0.043
0.700	0.044	0.043	0.043	0.040	0.040	0.038	0.038	0.040	0.044
0.800	0.045	0.044	0.044	0.040	0.041	0.039	0.038	0.041	0.045
0.850	0.045	0.044	0.044	0.041	0.041	0.040	0.039	0.042	0.045
0.900	0.046	0.045	0.046	0.042	0.042	0.042	0.039	0.043	0.046
0.925	0.047	0.046	0.047	0.043	0.043	0.044	0.039	0.044	0.047
0.930	0.047	0.046	0.047	0.043	0.043	0.044	0.039	0.044	0.047
0.950	0.048	0.047	0.048	0.044	0.043	0.048	0.040	0.046	0.051
0.960	0.049	0.048	0.049	0.045	0.044	0.050	0.040	0.047	0.054
0.975	0.052	0.051	0.052	0.047	0.046	0.057	0.042	0.051	0.063
0.980	0.053	0.051	0.056	0.049	0.048	0.060	0.043	0.053	0.067
0.990	0.061	0.053	0.072	0.056	0.057	0.072	0.049	0.062	0.081

Table 14. Cumulative Distributions of Zenith Atmospheric Attenuation at X-Band
for Canberra DSCC, dB

CD	January	February	March	April	May	June
0.000	0.040	0.040	0.040	0.040	0.040	0.040
0.100	0.045	0.046	0.048	0.044	0.043	0.043
0.200	0.046	0.048	0.049	0.045	0.043	0.044
0.250	0.046	0.048	0.049	0.045	0.043	0.044
0.300	0.046	0.049	0.049	0.045	0.043	0.044
0.400	0.047	0.050	0.050	0.046	0.043	0.044
0.500	0.048	0.052	0.050	0.046	0.044	0.044
0.600	0.049	0.053	0.052	0.047	0.044	0.044
0.700	0.051	0.055	0.053	0.048	0.045	0.044
0.800	0.053	0.058	0.055	0.049	0.047	0.045
0.850	0.054	0.061	0.056	0.051	0.049	0.046
0.900	0.057	0.069	0.058	0.053	0.053	0.048
0.925	0.059	0.076	0.061	0.058	0.059	0.052
0.930	0.060	0.078	0.062	0.059	0.060	0.053
0.950	0.065	0.086	0.067	0.064	0.069	0.062
0.960	0.068	0.092	0.070	0.068	0.075	0.065
0.975	0.079	0.109	0.078	0.079	0.090	0.074
0.980	0.085	0.119	0.084	0.085	0.094	0.078
0.990	0.119	0.150	0.102	0.100	0.112	0.088

Table 14 (Cont'd). Cumulative Distributions of Zenith Atmospheric Attenuation at X-Band
for Canberra DSCC, dB

CD	July	August	September	October	November	December	Minimum	Year Average	Maximum
0.000	0.040	0.040	0.040	0.040	0.040	0.040	0.040	0.040	0.040
0.100	0.042	0.042	0.043	0.043	0.045	0.043	0.042	0.044	0.048
0.200	0.043	0.043	0.044	0.044	0.046	0.044	0.043	0.045	0.049
0.250	0.043	0.043	0.044	0.044	0.046	0.045	0.043	0.045	0.049
0.300	0.043	0.043	0.044	0.044	0.046	0.045	0.043	0.045	0.049
0.400	0.043	0.043	0.044	0.045	0.047	0.046	0.043	0.046	0.050
0.500	0.043	0.043	0.045	0.045	0.048	0.047	0.043	0.046	0.052
0.600	0.043	0.043	0.045	0.046	0.049	0.048	0.043	0.047	0.053
0.700	0.044	0.044	0.046	0.047	0.050	0.049	0.044	0.048	0.055
0.800	0.045	0.045	0.047	0.050	0.053	0.052	0.045	0.050	0.058
0.850	0.046	0.046	0.048	0.052	0.057	0.055	0.046	0.052	0.061
0.900	0.048	0.049	0.051	0.057	0.062	0.060	0.048	0.056	0.069
0.925	0.051	0.053	0.053	0.063	0.068	0.065	0.051	0.060	0.076
0.930	0.051	0.054	0.054	0.064	0.069	0.067	0.051	0.061	0.078
0.950	0.055	0.059	0.060	0.074	0.078	0.074	0.055	0.068	0.086
0.960	0.057	0.063	0.065	0.080	0.083	0.077	0.057	0.072	0.092
0.975	0.063	0.079	0.075	0.096	0.101	0.087	0.063	0.084	0.109
0.980	0.066	0.084	0.081	0.106	0.110	0.091	0.066	0.090	0.119
0.990	0.076	0.102	0.108	0.132	0.135	0.106	0.076	0.111	0.150

Table 15. Cumulative Distributions of Zenith Atmospheric Attenuation at X-Band
for Madrid DSCC, dB

CD	January	February	March	April	May	June
0.000	0.038	0.038	0.038	0.038	0.038	0.038
0.100	0.039	0.039	0.040	0.040	0.042	0.043
0.200	0.040	0.040	0.041	0.041	0.043	0.043
0.250	0.040	0.040	0.041	0.041	0.043	0.044
0.300	0.040	0.040	0.041	0.041	0.043	0.044
0.400	0.040	0.040	0.041	0.041	0.043	0.044
0.500	0.041	0.040	0.042	0.042	0.044	0.044
0.600	0.041	0.041	0.042	0.042	0.044	0.045
0.700	0.043	0.041	0.043	0.043	0.044	0.045
0.800	0.048	0.043	0.045	0.045	0.046	0.046
0.850	0.053	0.045	0.047	0.048	0.050	0.046
0.900	0.063	0.050	0.052	0.051	0.058	0.047
0.925	0.074	0.055	0.058	0.055	0.066	0.048
0.930	0.076	0.056	0.059	0.056	0.068	0.049
0.950	0.091	0.064	0.067	0.064	0.078	0.051
0.960	0.097	0.069	0.071	0.068	0.084	0.054
0.975	0.110	0.081	0.084	0.078	0.097	0.063
0.980	0.114	0.086	0.088	0.081	0.101	0.069
0.990	0.129	0.102	0.104	0.092	0.117	0.093

Table 15 (Cont'd). Cumulative Distributions of Zenith Atmospheric Attenuation at X-Band
for Madrid DSCC, dB

CD	July	August	September	October	November	December	Minimum	Year Average	Maximum
0.000	0.038	0.038	0.038	0.038	0.038	0.038	0.038	0.038	0.038
0.100	0.043	0.043	0.043	0.041	0.038	0.039	0.038	0.041	0.043
0.200	0.044	0.044	0.043	0.043	0.040	0.040	0.040	0.042	0.044
0.250	0.044	0.044	0.044	0.043	0.040	0.040	0.040	0.042	0.044
0.300	0.044	0.044	0.044	0.044	0.040	0.040	0.040	0.042	0.044
0.400	0.045	0.045	0.044	0.044	0.041	0.041	0.040	0.043	0.045
0.500	0.045	0.045	0.045	0.045	0.041	0.042	0.040	0.043	0.045
0.600	0.045	0.045	0.046	0.046	0.042	0.043	0.041	0.044	0.046
0.700	0.045	0.046	0.046	0.048	0.044	0.045	0.041	0.044	0.048
0.800	0.046	0.046	0.047	0.051	0.046	0.049	0.043	0.047	0.051
0.850	0.046	0.047	0.047	0.056	0.051	0.055	0.045	0.049	0.056
0.900	0.046	0.047	0.049	0.065	0.059	0.064	0.046	0.054	0.065
0.925	0.047	0.048	0.050	0.074	0.068	0.072	0.047	0.060	0.074
0.930	0.047	0.048	0.051	0.075	0.070	0.073	0.047	0.061	0.076
0.950	0.048	0.048	0.054	0.088	0.082	0.083	0.048	0.068	0.091
0.960	0.048	0.049	0.057	0.093	0.087	0.088	0.048	0.072	0.097
0.975	0.050	0.051	0.067	0.108	0.100	0.100	0.050	0.082	0.110
0.980	0.051	0.052	0.075	0.113	0.104	0.104	0.051	0.087	0.114
0.990	0.058	0.058	0.104	0.136	0.118	0.118	0.058	0.102	0.136

Table 16. Cumulative Distributions of Zenith Atmospheric Attenuation at Ka-Band
for Goldstone DSCC, dB

CD	January	February	March	April	May	June
0.000	0.116	0.116	0.116	0.116	0.116	0.116
0.100	0.135	0.133	0.136	0.139	0.145	0.142
0.200	0.140	0.139	0.141	0.146	0.154	0.150
0.250	0.141	0.141	0.143	0.148	0.156	0.153
0.300	0.144	0.144	0.145	0.151	0.161	0.157
0.400	0.149	0.148	0.150	0.154	0.169	0.163
0.500	0.154	0.152	0.154	0.158	0.180	0.173
0.600	0.162	0.157	0.159	0.163	0.188	0.188
0.700	0.175	0.165	0.165	0.169	0.198	0.204
0.800	0.195	0.181	0.175	0.176	0.212	0.218
0.850	0.216	0.195	0.182	0.180	0.224	0.227
0.900	0.253	0.223	0.194	0.188	0.246	0.245
0.925	0.300	0.246	0.201	0.193	0.264	0.264
0.930	0.308	0.252	0.203	0.194	0.268	0.266
0.950	0.377	0.288	0.216	0.202	0.315	0.289
0.960	0.426	0.319	0.233	0.208	0.337	0.310
0.975	0.568	0.388	0.281	0.229	0.402	0.373
0.980	0.625	0.419	0.311	0.250	0.422	0.405
0.990	0.863	0.542	0.444	0.344	0.512	0.542

Table 16 (Cont'd). Cumulative Distributions of Zenith Atmospheric Attenuation at Ka-Band
for Goldstone DSCC, dB

CD	July	August	September	October	November	December	Minimum	Year Average	Maximum
0.000	0.116	0.116	0.116	0.116	0.116	0.116	0.116	0.116	0.116
0.100	0.154	0.157	0.164	0.148	0.138	0.133	0.133	0.144	0.164
0.200	0.171	0.173	0.173	0.155	0.145	0.139	0.139	0.152	0.173
0.250	0.175	0.179	0.177	0.157	0.147	0.141	0.141	0.155	0.179
0.300	0.183	0.190	0.184	0.162	0.151	0.144	0.144	0.160	0.190
0.400	0.194	0.204	0.196	0.170	0.158	0.148	0.148	0.167	0.204
0.500	0.210	0.222	0.212	0.176	0.166	0.152	0.152	0.176	0.222
0.600	0.229	0.234	0.224	0.183	0.179	0.157	0.157	0.185	0.234
0.700	0.253	0.242	0.241	0.192	0.192	0.167	0.165	0.197	0.253
0.800	0.273	0.256	0.257	0.206	0.207	0.184	0.175	0.211	0.273
0.850	0.283	0.265	0.267	0.216	0.217	0.202	0.180	0.223	0.283
0.900	0.298	0.281	0.291	0.234	0.234	0.233	0.188	0.243	0.298
0.925	0.309	0.292	0.306	0.244	0.245	0.256	0.193	0.260	0.309
0.930	0.313	0.295	0.308	0.246	0.246	0.263	0.194	0.263	0.313
0.950	0.328	0.315	0.326	0.260	0.256	0.321	0.202	0.291	0.377
0.960	0.340	0.328	0.344	0.273	0.267	0.360	0.208	0.312	0.426
0.975	0.381	0.369	0.396	0.314	0.300	0.464	0.229	0.371	0.568
0.980	0.407	0.375	0.450	0.338	0.333	0.511	0.250	0.403	0.625
0.990	0.534	0.400	0.706	0.452	0.471	0.704	0.344	0.541	0.863

Table 17. Cumulative Distributions of Zenith Atmospheric Attenuation at Ka-Band
for Canberra DSCC, dB

CD	January	February	March	April	May	June
0.000	0.126	0.126	0.126	0.126	0.126	0.126
0.100	0.201	0.230	0.248	0.195	0.176	0.171
0.200	0.223	0.253	0.267	0.212	0.184	0.190
0.250	0.232	0.264	0.273	0.217	0.187	0.194
0.300	0.238	0.277	0.279	0.223	0.191	0.196
0.400	0.251	0.302	0.293	0.233	0.198	0.202
0.500	0.274	0.326	0.307	0.246	0.205	0.208
0.600	0.297	0.354	0.329	0.258	0.212	0.216
0.700	0.323	0.389	0.355	0.274	0.226	0.225
0.800	0.356	0.436	0.384	0.302	0.271	0.240
0.850	0.378	0.486	0.405	0.324	0.303	0.256
0.900	0.422	0.624	0.447	0.368	0.369	0.290
0.925	0.465	0.737	0.495	0.442	0.455	0.346
0.930	0.475	0.761	0.511	0.459	0.482	0.371
0.950	0.555	0.913	0.593	0.547	0.622	0.502
0.960	0.612	1.013	0.639	0.613	0.727	0.561
0.975	0.786	1.337	0.770	0.796	0.983	0.698
0.980	0.897	1.533	0.874	0.891	1.055	0.769
0.990	1.535	2.181	1.198	1.168	1.378	0.948

Table 17 (Cont'd). Cumulative Distributions of Zenith Atmospheric Attenuation at Ka-Band
for Canberra DSCC, dB

CD	July	August	September	October	November	December	Minimum	Year Average	Maximum
0.000	0.126	0.126	0.126	0.126	0.126	0.126	0.126	0.126	0.126
0.100	0.164	0.166	0.180	0.181	0.206	0.184	0.164	0.192	0.248
0.200	0.174	0.176	0.191	0.196	0.223	0.204	0.174	0.208	0.267
0.250	0.178	0.180	0.196	0.201	0.230	0.214	0.178	0.214	0.273
0.300	0.181	0.182	0.200	0.205	0.237	0.222	0.181	0.219	0.279
0.400	0.187	0.187	0.210	0.214	0.252	0.238	0.187	0.230	0.302
0.500	0.195	0.193	0.219	0.225	0.266	0.253	0.193	0.243	0.326
0.600	0.203	0.201	0.229	0.242	0.283	0.272	0.201	0.258	0.354
0.700	0.213	0.212	0.246	0.265	0.308	0.299	0.212	0.278	0.389
0.800	0.234	0.230	0.269	0.314	0.366	0.350	0.230	0.312	0.436
0.850	0.253	0.252	0.291	0.351	0.422	0.399	0.252	0.343	0.486
0.900	0.285	0.305	0.331	0.428	0.511	0.480	0.285	0.404	0.624
0.925	0.327	0.359	0.370	0.516	0.601	0.554	0.327	0.471	0.737
0.930	0.338	0.374	0.386	0.540	0.624	0.581	0.338	0.490	0.761
0.950	0.391	0.454	0.482	0.702	0.764	0.698	0.391	0.600	0.913
0.960	0.431	0.529	0.556	0.798	0.853	0.759	0.431	0.671	1.013
0.975	0.518	0.784	0.717	1.084	1.188	0.922	0.518	0.876	1.337
0.980	0.566	0.871	0.823	1.278	1.353	0.997	0.566	0.985	1.533
0.990	0.744	1.194	1.315	1.783	1.854	1.269	0.744	1.364	2.181

Table 18. Cumulative Distributions of Zenith Atmospheric Attenuation at Ka-Band
for Madrid DSCC, dB

CD	January	February	March	April	May	June
0.000	0.121	0.121	0.121	0.121	0.121	0.121
0.100	0.138	0.138	0.155	0.157	0.181	0.191
0.200	0.150	0.148	0.165	0.169	0.195	0.205
0.250	0.153	0.151	0.168	0.172	0.199	0.209
0.300	0.157	0.155	0.173	0.176	0.205	0.215
0.400	0.165	0.161	0.181	0.183	0.215	0.224
0.500	0.177	0.171	0.191	0.193	0.222	0.233
0.600	0.192	0.183	0.202	0.206	0.231	0.242
0.700	0.222	0.196	0.219	0.223	0.242	0.251
0.800	0.297	0.221	0.252	0.260	0.269	0.264
0.850	0.382	0.257	0.289	0.297	0.326	0.274
0.900	0.541	0.332	0.370	0.355	0.454	0.292
0.925	0.725	0.412	0.462	0.414	0.593	0.308
0.930	0.757	0.429	0.481	0.428	0.621	0.313
0.950	1.021	0.560	0.599	0.549	0.792	0.358
0.960	1.122	0.634	0.675	0.621	0.887	0.399
0.975	1.371	0.848	0.886	0.788	1.117	0.541
0.980	1.448	0.922	0.969	0.839	1.204	0.641
0.990	1.754	1.218	1.264	1.031	1.508	1.052

Table 18 (Cont'd). Cumulative Distributions of Zenith Atmospheric Attenuation at Ka-Band
for Madrid DSCC, dB

CD	July	August	September	October	November	December	Minimum	Year Average	Maximum
0.000	0.121	0.121	0.121	0.121	0.121	0.121	0.121	0.121	0.121
0.100	0.201	0.202	0.190	0.171	0.119	0.138	0.119	0.165	0.202
0.200	0.213	0.215	0.206	0.194	0.152	0.152	0.148	0.180	0.215
0.250	0.217	0.219	0.211	0.201	0.157	0.157	0.151	0.184	0.219
0.300	0.222	0.226	0.218	0.211	0.166	0.166	0.155	0.191	0.226
0.400	0.231	0.234	0.230	0.227	0.176	0.180	0.161	0.200	0.234
0.500	0.238	0.242	0.241	0.244	0.188	0.194	0.171	0.211	0.244
0.600	0.246	0.251	0.254	0.263	0.205	0.213	0.183	0.224	0.263
0.700	0.254	0.260	0.266	0.290	0.228	0.246	0.196	0.241	0.290
0.800	0.263	0.272	0.282	0.353	0.272	0.322	0.221	0.277	0.353
0.850	0.269	0.279	0.293	0.427	0.340	0.406	0.257	0.319	0.427
0.900	0.279	0.290	0.314	0.568	0.478	0.549	0.279	0.401	0.568
0.925	0.286	0.297	0.338	0.714	0.627	0.687	0.286	0.486	0.725
0.930	0.287	0.299	0.343	0.742	0.651	0.707	0.287	0.501	0.757
0.950	0.298	0.310	0.391	0.958	0.857	0.879	0.298	0.624	1.021
0.960	0.305	0.320	0.440	1.061	0.947	0.962	0.305	0.689	1.122
0.975	0.330	0.350	0.606	1.325	1.190	1.187	0.330	0.864	1.371
0.980	0.351	0.372	0.736	1.438	1.257	1.259	0.351	0.938	1.448
0.990	0.460	0.468	1.253	1.896	1.532	1.520	0.460	1.225	1.896

Table 19. Monthly and Year-Average Rainfall Amounts at the DSN Antenna Locations

Month	Goldstone		Canberra		Madrid	
	inches	mm	inches	mm	inches	mm
January	1.02	25.9	3.61	91.7	1.48	37.5
February	1.18	30.0	2.74	69.7	1.38	35.0
March	0.90	22.9	2.90	73.6	1.10	28.0
April	0.20	5.1	2.85	72.4	1.87	47.5
May	0.19	4.8	2.94	74.8	1.56	39.5
June	0.04	1.0	2.70	68.7	1.26	32.0
July	0.35	8.9	3.36	85.3	0.57	14.5
August	0.59	15.0	3.90	99.0	0.59	15.0
September	0.39	9.9	3.73	94.7	1.16	29.5
October	0.15	3.8	3.70	94.0	1.54	39.0
November	0.23	5.8	3.50	88.8	2.01	51.0
December	0.57	14.5	2.42	61.4	1.75	44.5
Year Average	5.81	147.6	38.67	982.1	16.26	413.0

Table 20. Parameters for X-Band Planetary Noise Calculation, plus X-Band and Ka-Band Noise
Temperatures at Mean Minimum Distance from Earth

Planet	Diameter (km)		Mean Distance from Earth (10^6 km)		Mean Distance from Sun		Blackbody Disk Temp (K)	T_{Planet} at Mean Minimum Distance (K)		
								X-Band		Ka-Band
	polar	equatorial	min.	max.	(10^6 km)	AU		70-m (74.4 dBi gain)	34-m (68.3 dBi gain)	34-m (78.8 dBi gain)
Mercury		4880	91.7	207.5	57.9	0.387	625	3.05	0.75	8.39
Venus		12104	41.4	257.8	108.2	0.723	490	72.10	17.70	198.58
Earth		12757	–	–	149.6	1.000	250–300 [1]	–	–	–
Mars		6794	78.3	377.5	227.9	1.523	180	2.33	0.57	6.43
Jupiter	134102	142984	628.7	927.9	778.3	5.203	152	13.53	3.32	37.27
Saturn	108728	120536	1279.8	1579.0	1429.4	9.555	155	2.37	0.58	6.52
Uranus		51118	2721.4	3020.6	2871.0	19.191	160	0.10	0.02	0.27
Neptune		49532	4354.4	4653.6	4504.0	30.107	160	0.04	0.01	0.10
Pluto		2274	5763.9	6063.1	5913.5	39.529	160	0.00	0.00	0.00

Note:
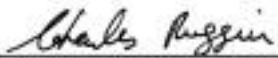
1. Ocean (250) and Land (300)

201
Frequency and Channel Assignments

Effective November 30, 2000
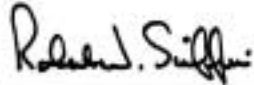
Document Owner:

Approved by:

C. J. Ruggier   Date
Tracking System Engineer

12/12/00

A. Kwok   Date
Tracking and Navigation Services
System Development Engineer

12/13/00

Prepared by:

Released by:

R. W. Sniffin   Date

12/11/00

[Signature on file at TMOD Library]

TMOD Document Release   Date

Change Log

Rev	Issue Date	Affected Paragraphs	Change Summary
Initial	1/15/2001	All	All

Note to Readers

There are two sets of document histories in the 810-005 document, and these histories are reflected in the header at the top of the page. First, the entire document is periodically released as a revision when major changes affect a majority of the modules. For example, this module is part of 810-005, Revision E. Second, the individual modules also change, starting as an initial issue that has no revision letter. When a module is changed, a change letter is appended to the module number on the second line of the header and a summary of the changes is entered in the module's change log.

This is a new module in Revision E of 810-005.

Contents

Tables

1 Introduction

1.1 Purpose and Scope

This module provides basic information about the frequencies that are available in the Deep Space Network (DSN) and presents the way certain of the DSN frequency allocations have been divided into channels. It does not specify which stations can or will support assigned frequencies. That information is contained in the appropriate Telecommunications Interfaces modules (101, 70-m Antenna Subnet Telecommunications Interfaces; 102, 26-m Antenna Subnet Telecommunications Interfaces; 103, 34-m HEF Antenna Subnet Telecommunications Interfaces; or 104, 34-m BWG Stations Telecommunications Interfaces) of this handbook. It also does not include propagation characteristics of the frequencies. This information is provided in module 105 (Atmospheric and Environmental Effects) and module 106 (Solar Corona and Solar Wind Effects) of this handbook.

2 General Information

The DSN has developed channel plans to provide for orderly selection and assignment of frequencies for deep-space missions (Category B, greater than 2 million km from Earth). (The DSN has not developed channel plans for near-Earth missions [Category A, less than 2 million km from Earth].) The deep space channel plans are based on bandwidth, hardware implementation, and transponder turnaround-ratio considerations. The plans must allow phase coherent uplink (Earth-to-space) and downlink (space-to-Earth) transmissions.

Through international agreements, the International Telecommunications Union (ITU) allocates and regulates portions of the frequency spectrum for both commercial and government use. The primary objective of the ITU is to establish regulatory procedures for the coordinated use of frequencies by those agencies permitted to operate in the allocated bands. The ITU has allocated certain bands to deep space (Category B) research. In some cases, the deep space missions may be required to conditionally share a frequency band between multiple users in the same band.

The Consultative Committee for Space Data Systems (CCSDS) is an international organization for space agencies interested in mutually developing standard transmission and data handling techniques to support space research, including space science and applications. As a member of the CCSDS, NASA has submitted recommendations for various space systems applications. As an example, the standard NASA K_a-band spacecraft transponder turnaround ratio was first presented for review and approval to the CCSDS prior to its implementation.

The National Telecommunications and Information Administration (NTIA), an agency of the U.S. Department of Commerce, is the Executive Branch's principal authority on domestic and international telecommunications and information technology issues. During the planning phase of all missions using the DSN, the proposed operating frequencies and other

operating parameters are reviewed by the NTIA for approval through the System Review process. The NTIA evaluations are based upon the technical and regulatory criteria for the efficient and coordinated use of the frequency spectrum by NASA missions.

2.1 *Tracking Modes of Operation*

The following paragraphs describe the various ways in which the telecommunications link can be configured for radio tracking. The source of the uplink signal and the choice of references for measuring the received frequency determine the mode of operation.

2.1.1 *One-way*

The spacecraft generates the downlink signal(s) from an onboard oscillator. The DSN compares the received frequency against a locally generated frequency.

2.1.2 *Two-way*

The DSN transmits a signal to the spacecraft. The spacecraft tracks the phase of the uplink signal and generates a phase coherent downlink signal. The DSN compares the received frequency with the same reference frequency from which the uplink was generated.

2.1.3 *Three-way*

The spacecraft is tracked by two stations—one with the two-way mode while the other receives and compares the signal to a locally generated frequency. The most common application of this mode is during the handover between stations at two different Deep Space Communication Complexes (DSCCs).

2.1.4 *Coherent Three-way*

Coherent three-way tracking is three-way tracking when the transmitting and receiving stations share a common reference frequency.

2.2 *Spacecraft Transponder Turnaround Ratios*

To measure two-way or three-way Doppler shift, the spacecraft must transmit a downlink signal that is phase coherent with the uplink signal. Table 1 provides the recommended spacecraft transponder turnaround ratios for various uplink and downlink frequency bands. The tracking equipment at the DSN 34-m and 70-m stations can accommodate other turnaround ratios but this support must be negotiated through the JPL Frequency Manager, who is resident in the Plans and Commitments Program Office <http://deepspace.jpl.nasa.gov/advmiss/>.

Table 1. Spacecraft Transponder Turnaround Ratios

Uplink	Downlink	Ratio (downlink/uplink)
S	S	240/221
S	X	880/221
S	K_a	3344/221
X	S	240/749
X	X	880/749
X	K_a	3344/749
K_a	S	240/3599*
K_a	X	880/3599*
K_a	K_a	3344/3599*

* While these are the recommended ratios, all existing K_a-band spacecraft have used turnaround ratios negotiated through the JPL Frequency Manager.

2.3   Frequency Bands Allocated by the International Telecommunication Union (ITU)

Frequency ranges have been allocated by the ITU for use in deep space and near-Earth research. These ranges are listed in Table 2.

Table 2. Allocated Frequency Bands

Band Designation	Deep Space Bands (for spacecraft greater than 2 million km from Earth)		Near Earth Bands (for spacecraft less than 2 million km from Earth)	
	Uplink (Earth to space)	Downlink (space to Earth)	Uplink (Earth to space)	Downlink (space to Earth)
S-band	2110–2120	2290–2300	2025–2110	2200–2290
X-band	7145–7190	8400–8450	7190–7235	8450–8500
Ka-band	34200–34700	31800–32300		

2.4   *Deep Space Coherent Frequency Channels*

The DSN has divided the frequency ranges allocated for deep space use into channels for tracking support associated with a given transponder ratio. The frequency ranges allocated for near-Earth uses do not have a formal channelization plan. Tables 3, 4, and 5 list the 42-channel assignments by frequency bands. Note that frequencies out of the allocated ranges for deep space research are not shown in the tables.

The S-band downlink center frequency ($F_{ch}(14) = 2295$ MHz) is used to derive all entries in the tables using the expressions

$$F_{ch}(n{-}1) = F_{ch}(n) - (10/27), \text{ rounded to the nearest hertz for } n = 2 \text{ to } 14$$

$$F_{ch}(n{+}1) = F_{ch}(n) + (10/27), \text{ rounded to the nearest hertz for } n = 14 \text{ to } 41$$

where $F_{ch}(n)$ is the center frequency (in MHz) of channel n rounded to the nearest Hz, and the ratio 10/27 is the spacing (in MHz) between the centers of two adjacent channels.

Frequencies for other columns are derived by the procedure described below. The calculated downlink frequencies may differ by 1 or 2 hertz between the tables because each table assumes an integer uplink frequency and precise turnaround ratios.

    (1)   The uplink frequency specified in the table is calculated from the expression

$$f_{ch}(n) = F_{ch}(n) \times TM/240, \text{ rounded to the nearest hertz,}$$

where

$f_{ch}(n)$ is the frequency of uplink channel n being calculated;

$F_{ch}(n)$ is the frequency of channel n calculated for the S-band downlink column (including values for out-of-band channels);

TM is the transmit multiplier of a frequency band, that is, $TM = 221$, 749, and 3599 for S uplink, X uplink, and K$_a$ uplink.

    (2)   The downlink frequencies specified in the table are calculated from the expression

$$F_{ch}(n) = f_{ch}(n) \times TR, \text{ rounded to the nearest hertz,}$$

where

$F_{ch}(n)$ is the frequency of channel n for the downlink columns;

$f_{ch}(n)$ is the frequency of channel n in the uplink column;

TR is the turnaround ratio for the downlink frequency band as provided in Table 1.

The DSN only supports two-way or three-way tracking with uplink and downlink frequencies having the same channel number. Therefore, only channels 5 through 27 fully support coherent uplink and downlink for all frequency bands. Channel 28, for example, supports S- or X-band uplink with coherent X- or K_a-band downlink, but not with coherent S-band downlink.

Before selecting operating frequencies or channels for a project, the telecommunication designer should consult the JPL Frequency Manager, who is resident in the Plans and Commitments Program Office <http://deepspace.jpl.nasa.gov/advmiss/>, to avoid frequency interference with other spacecraft, present or planned.

Table 3. Frequency and Channel Assignments for S-band Uplink

Channel	S-band U/L (MHz)	S-band D/L (MHz)	X-band D/L (MHz)	K_a-band D/L (MHz)
5	2110.243056	2291.666667	8402.777780	31930.555562
6	2110.584105	2292.037037	8404.135803	31935.716050
7	2110.925154	2292.407407	8405.493826	31940.876538
8	2111.266204	2292.777778	8406.851853	31946.037042
9	2111.607253	2293.148148	8408.209876	31951.197530
10	2111.948303	2293.518519	8409.567903	31956.358033
11	2112.289352	2293.888889	8410.925927	31961.518521
12	2112.630401	2294.259259	8412.283950	31966.679009
13	2112.971451	2294.629630	8413.641977	31971.839512
14	2113.312500	2295.000000	8415.000000	31977.000000
15	2113.653549	2295.370370	8416.358023	31982.160488
16	2113.994599	2295.740741	8417.716050	31987.320991
17	2114.335648	2296.111111	8419.074073	31992.481479
18	2114.676697	2296.481481	8420.432097	31997.641967
19	2115.017747	2296.851852	8421.790124	32002.802470
20	2115.358796	2297.222222	8423.148147	32007.962958
21	2115.699846	2297.592593	8424.506174	32013.123462
22	2116.040895	2297.962963	8425.864197	32018.283950
23	2116.381944	2298.333333	8427.222220	32023.444438
24	2116.722994	2298.703704	8428.580248	32028.604941
25	2117.064043	2299.074074	8429.938271	32033.765429
26	2117.405092	2299.444444	8431.296294	32038.925917
27	2117.746142	2299.814815	8432.654321	32044.086420
28	2118.087191		8434.012344	32049.246908
29	2118.428241		8435.370371	32054.407411
30	2118.769290		8436.728395	32059.567899
31	2119.110339		8438.086418	32064.728387
32	2119.451389		8439.444445	32069.888891
33	2119.792438		8440.802468	32075.049379

Table 4. Frequency and Channel Assignments for X-band Uplink

Channel	X-band U/L (MHz)	S-band D/L (MHz)	X-band D/L (MHz)	Ka-band D/L (MHz)
1	7147.286265	2290.185185		31909.913580
2	7148.442131	2290.555556		31915.074083
3	7149.597994	2290.925926	8400.061729	31920.234571
4	7150.753857	2291.296296	8401.419752	31925.395059
5	7151.909723	2291.666667	8402.777779	31930.555562
6	7153.065586	2292.037037	8404.135802	31935.716050
7	7154.221449	2292.407407	8405.493825	31940.876538
8	7155.377316	2292.777778	8406.851853	31946.037042
9	7156.533179	2293.148148	8408.209877	31951.197530
10	7157.689045	2293.518519	8409.567903	31956.358033
11	7158.844908	2293.888889	8410.925927	31961.518521
12	7160.000771	2294.259259	8412.283950	31966.679009
13	7161.156637	2294.629630	8413.641977	31971.839512
14	7162.312500	2295.000000	8415.000000	31977.000000
15	7163.468363	2295.370370	8416.358023	31982.160488
16	7164.624229	2295.740741	8417.716050	31987.320991
17	7165.780092	2296.111111	8419.074073	31992.481479
18	7166.935955	2296.481481	8420.432097	31997.641967
19	7168.091821	2296.851852	8421.790123	32002.802470
20	7169.247684	2297.222222	8423.148147	32007.962958
21	7170.403551	2297.592593	8424.506175	32013.123462
22	7171.559414	2297.962963	8425.864198	32018.283950
23	7172.715277	2298.333333	8427.222221	32023.444438
24	7173.871143	2298.703704	8428.580248	32028.604941
25	7175.027006	2299.074074	8429.938271	32033.765429
26	7176.182869	2299.444444	8431.296295	32038.925917
27	7177.338735	2299.814815	8432.654321	32044.086420
28	7178.494598		8434.012345	32049.246908
29	7179.650464		8435.370372	32054.407411
30	7180.806327		8436.728395	32059.567899
31	7181.962190		8438.086418	32064.728387
32	7183.118057		8439.444446	32069.888891
33	7184.273920		8440.802469	32075.049379
34	7185.429783		8442.160493	32080.209867
35	7186.585649		8443.518520	32085.370370
36	7187.741512		8444.876543	32090.530858
37	7188.897378		8446.234570	32095.691361

Table 5. Frequency and Channel Assignments for K_a-band Uplink

Channel	K_a-band U/L (MHz)	S-band D/L (MHz)	X-band D/L (MHz)	K_a-band D/L (MHz)
1	34343.235337	2290.185185		31909.913578
2	34348.789359	2290.555556		31915.074080
3	34354.343365	2290.925926	8400.061729	31920.234569
4	34359.897372	2291.296296	8401.419752	31925.395058
5	34365.451394	2291.666667	8402.777779	31930.555560
6	34371.005401	2292.037037	8404.135802	31935.716049
7	34376.559407	2292.407407	8405.493826	31940.876538
8	34382.113429	2292.777778	8406.851853	31946.037040
9	34387.667436	2293.148148	8408.209876	31951.197529
10	34393.221458	2293.518519	8409.567903	31956.358031
11	34398.775465	2293.888889	8410.925926	31961.518520
12	34404.329471	2294.259259	8412.283950	31966.679009
13	34409.883493	2294.629630	8413.641977	31971.839511
14	34415.437500	2295.000000	8415.000000	31977.000000
15	34420.991507	2295.370370	8416.358023	31982.160489
16	34426.545529	2295.740741	8417.716050	31987.320991
17	34432.099535	2296.111111	8419.074074	31992.481480
18	34437.653542	2296.481481	8420.432097	31997.641969
19	34443.207564	2296.851852	8421.790124	32002.802471
20	34448.761571	2297.222222	8423.148147	32007.962960
21	34454.315593	2297.592593	8424.506174	32013.123462
22	34459.869599	2297.962963	8425.864198	32018.283951
23	34465.423606	2298.333333	8427.222221	32023.444440
24	34470.977628	2298.703704	8428.580248	32028.604942
25	34476.531635	2299.074074	8429.938271	32033.765431
26	34482.085641	2299.444444	8431.296295	32038.925920
27	34487.639663	2299.814815	8432.654322	32044.086422
28	34493.193670		8434.012345	32049.246911
29	34498.747692		8435.370372	32054.407414
30	34504.301699		8436.728395	32059.567902
31	34509.855705		8438.086419	32064.728391
32	34515.409727		8439.444446	32069.888894
33	34520.963734		8440.802469	32075.049382
34	34526.517741		8442.160492	32080.209871
35	34532.071763		8443.518519	32085.370373
36	34537.625769		8444.876543	32090.530862
37	34543.179791		8446.234570	32095.691365
38	34548.733798		8447.592593	32100.851853
39	34554.287805		8448.950616	32106.012342
40	34559.841827			32111.172845
41	34565.395833			32116.333333
42	34570.949840			32121.493822

202, Rev. A
34-m and 70-m Doppler

December 15, 2002

Document Owner:

Charles Ruggier   12/17/02

C. J. Ruggier   Date

Tracking System Engineer

Approved by:

Jeff B Berner   1/6/03

J. B. Berner   Date

Telecommunication Service System
Development Engineer

Author

Peter W. Kinman   8/30/02

P. W. Kinman   Date

Released by:

$\begin{bmatrix} \text{Signature on File} \\ \text{at DSMS Library} \end{bmatrix}$ 2/10/03

DSMS Document Release   Date

Change Log

Rev	Issue Date	Affected Paragraphs	Change Summary
Initial	11/30/2000	All	All
A	12/15/2002	Many	Added discussion of one-way Doppler error and X-Up/S-Down Solar Phase Scintillation errors. Renumbered all equations

Note to Readers

There are two sets of document histories in the 810-005 document that are reflected in the header at the top of the page. First, the overall document is periodically released as a revision when major changes affect a majority of the modules. For example, the original release of this document was part of Revision E. Second, the individual modules also change, starting as the initial issue that has no revision letter. When a module is changed, a change letter is appended to the module number on the second line of the header and a summary of the changes is entered in the module's change log.

Contents

Illustrations

Table

1. Introduction

1.1 Purpose

This module provides sufficient information for the telecommunications engineer to understand the capabilities and limitations of the equipment used for Doppler measurement at the Deep Space Network (DSN) 34-m and 70-m stations.

1.2 Scope

The scope of this module is limited to those features of the Downlink Channel at the 34-m High-efficiency (34-m HEF), 34-m Beam Waveguide (34-m BWG), and 70-m stations that relate to the measurement of and reporting of the Doppler effect. This module does not discuss the capabilities of the equipment used for Doppler measurement at the DSN 34-m High-speed Beam Waveguide (HSB) station.

2. General Information

The relative motion of a transmitter and receiver causes the received frequency to differ from that of the transmitter. This is the Doppler effect. In deep space communications it is usual to define Doppler as the transmitted frequency (the uplink) minus the received frequency (the downlink) divided by the ratio that was used onboard the spacecraft (the transponding ratio) to generate the downlink frequency. For the receding spacecraft that are typical of deep space exploration, the Doppler so defined is a positive quantity. Since the frequency of a carrier equals the rate-of-change of carrier phase, the Downlink Channel supports Doppler measurement by extracting the phase of the downlink carrier (Reference 1).

There are three types of Doppler measurement: one-way, two-way, and three-way. In all of these cases, the accumulating downlink carrier phase is measured and recorded. When the measurement is one-way, the frequency of the spacecraft transmitter must typically be inferred. A much more accurate Doppler measurement is possible when the spacecraft coherently transponds a carrier arriving on the uplink. In such a case, the downlink carrier frequency is related to the uplink carrier frequency by a multiplicative constant, the transponding ratio. Also, the downlink carrier phase equals the uplink carrier phase multiplied by this transponding ratio. Thus, when an uplink signal is transmitted by the DSN and the spacecraft coherently transponds this uplinked signal, a comparison of the uplink transmitter phase record with the downlink receiver phase record gives all the information necessary for an accurate computation of the combined Doppler on uplink and downlink. When one Deep Space Station (DSS) both provides the uplink and receives the downlink, so that there are two "nodes" (the DSS and the spacecraft) present, then it is a two-way measurement. When one DSS provides the uplink and another receives the downlink, so that there are three nodes present, then it is a three-way measurement.

Figure 1 illustrates one-way Doppler measurement. The measurement is referenced to the signal originating on the spacecraft. The frequency stability of the spacecraft

oscillator used to generate the downlink carrier will, in general, limit the performance of this Doppler measurement. Usually, only Ultra-Stable Oscillators (USOs) are used for one-way Doppler measurement.

Figure 2, Two/Three-Way Doppler Measurement, illustrates the more usual means of measuring Doppler. The measurement originates at a DSS. The uplink carrier frequency is synthesized within the exciter from a highly stable frequency reference provided by the Frequency and Timing Subsystem (FTS). Since this reference is much more stable than anything that a spacecraft-borne oscillator could provide, a two-way or three-way Doppler measurement is more accurate than a one-way measurement. The uplink carrier may be either constant or varied in accord with a tuning plan. In either case, the phase of the uplink carrier is recorded for use in the computation of a Doppler effect.

For all Doppler measurements (one-, two-, and three-way), the downlink signal is routed from the Antenna Feed/Low Noise Amplifier (LNA) to the Downlink Channel. This is reflected in Figures 1 and 2. Within the Radio-frequency to Intermediate-frequency Downconverter (RID), which is located at the antenna, a local oscillator is generated by frequency multiplication of a highly stable frequency reference from the FTS and the incoming downlink signal is heterodyned with this local oscillator. The Intermediate-Frequency (IF) signal that results is sent to the Signal Processing Center (SPC).

In the SPC, the IF to Digital Converter (IDC) alters the frequency of the IF signal by a combination of up-conversion and down-conversion to a final analog frequency of approximately 200 MHz and then performs analog-to-digital conversion. The final analog stage of down-conversion uses a local oscillator supplied by the Channel-Select Synthesizer (CSS), which is also part of the Downlink Channel. The CSS is adjusted before the beginning of a pass to a frequency appropriate for the anticipated frequency range of the incoming downlink signal. During the pass, the frequency of the CSS remains constant. The local oscillator frequencies of the CSS (and, indeed, of all local oscillators in the analog chain of down-conversion) are synthesized within the Downlink Channel from highly stable frequency references provided by the FTS. All analog stages of down-conversion are open-loop, and so the digital signal coming out of the IDC reflects the full Doppler effect on the downlink carrier.

The Receiver and Ranging Processor (RRP) accepts the signal from the IDC and extracts carrier phase with a digital phase-locked loop (Reference 2). The loop is configured to track the phase of a phase-shift keyed signal with residual carrier, a suppressed carrier, or a QPSK signal. Since every analog local oscillator is held at constant frequency during a pass, the downlink carrier phase at sky frequency (that is, the phase that arrives at the DSS antenna) is easily computed from the local oscillator frequencies and the time-varying phase extracted by the digital phase-locked loop.

Since Doppler is a difference of frequencies and a frequency is a derivative of phase, a record of phase transmitted on the uplink and of phase received on the downlink is sufficient to compute the combined uplink/downlink Doppler. It is important to note that these
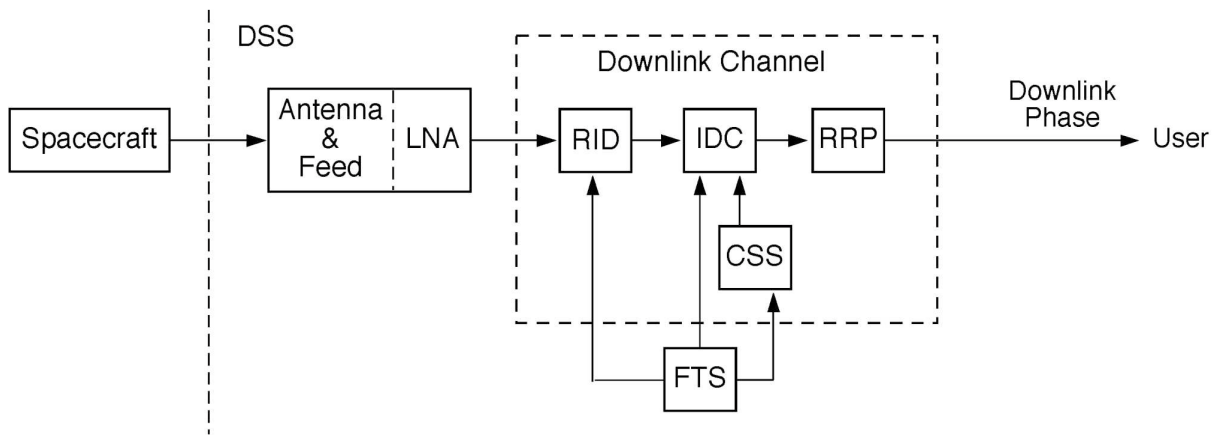
Figure 1. One-Way Doppler Measurement
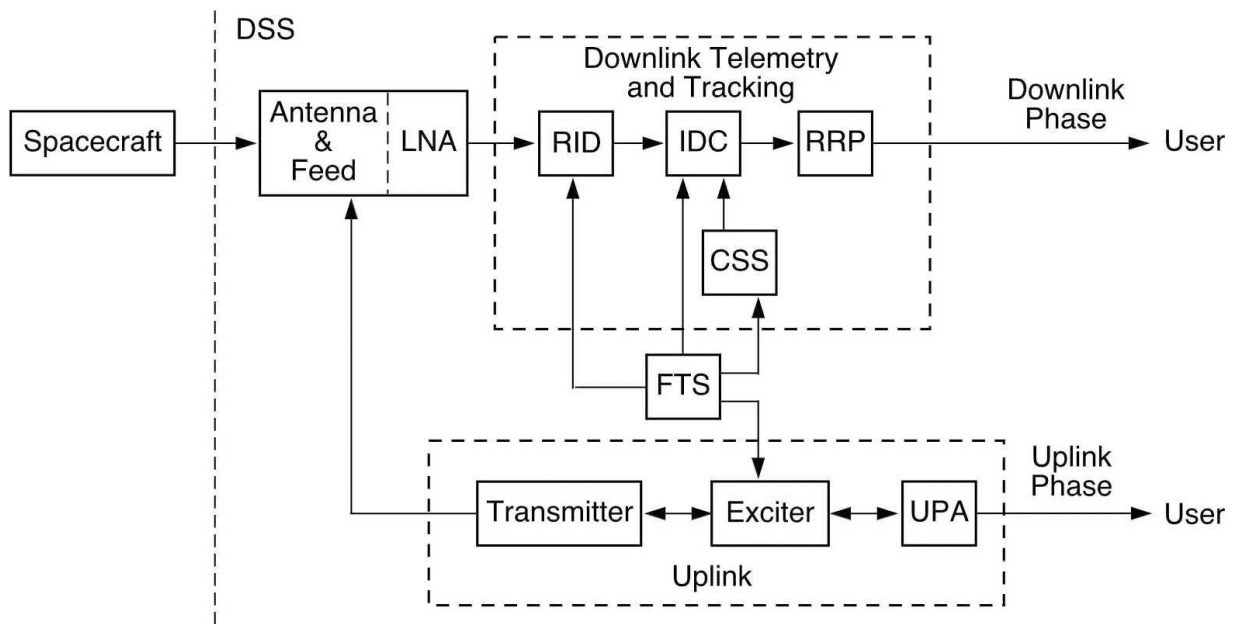
Figure 2. Two/Three-Way Doppler Measurement

phase records must account for integer as well as fractional cycles. (This is unlike many telecommunications applications where it is necessary to know the carrier phase only modulo one cycle.) The data are uplink and downlink phase counts at sky frequency (only downlink phase counts in the case of a one-way measurement). The downlink phase counts are available at 0.1-second intervals. The uplink phase counts are available from the Uplink Processor Assembly (UPA) at 1.0-second intervals.

2.1 Doppler Measurement Error

Only errors in measuring the rate-of-change of the distance between phase centers of the antennas are considered here. There are other errors that must be considered in any navigation solution, such as those introduced by propagation through the troposphere, the ionosphere, and the solar corona. Additional information on the effect of the solar corona on Doppler measurement is contained in paragraph 2.3.

Each error is characterized here as a standard deviation of range-rate σ_V and is in units of velocity. To translate any of these errors to a standard deviation of frequency σ_f, the following equation can be used.

$$\sigma_f = \frac{2 f_C}{c} \sigma_V \tag{1}$$

where

f_C = the downlink carrier frequency and

c = the speed of light in vacuum.

Equation (1) is for two-way and three-way Doppler measurement. (The factor of 2 is absent for one-way Doppler measurement.)

When tracking a residual carrier, the carrier loop signal-to-noise ratio is

$$\rho_L = \left. \frac{P_C}{N_0} \right|_{D/L} \cdot \frac{1}{B_L} \tag{2}$$

where $P_C/N_0\big|_{D/L}$ is the downlink carrier power to noise spectral density ratio, Hz.

There is an additional loss to the carrier loop signal-to-noise ratio when tracking a residual carrier with non-return-to-zero symbols in the absence of a subcarrier. This loss is due to the presence of data sidebands overlaying the residual carrier in the frequency domain and therefore increasing the effective noise level for carrier synchronization. In this case, ρ_L must be calculated as (Reference 3)

$$\rho_L = \left.\frac{P_C}{N_0}\right|_{D/L} \cdot \frac{1}{B_L} \cdot \frac{1}{1 + 2\,E_S/N_0} \tag{3}$$

where E_S/N_0 is the energy per symbol to noise spectral density ratio.

When tracking a suppressed carrier, the carrier loop signal-to-noise ratio is

$$\rho_L = \left.\frac{P_T}{N_0}\right|_{D/L} \cdot \frac{S_L}{B_L} \tag{4}$$

where

$$\left.P_T/N_0\right|_{D/L} \quad = \quad \text{downlink total signal power to noise spectral density ratio, Hz}$$

$$S_L \qquad\qquad = \quad \text{squaring loss of the Costas loop (Reference 4),}$$

$$S_L = \frac{2\dfrac{E_S}{N_0}}{1 + 2\dfrac{E_S}{N_0}} \tag{5}$$

When tracking QPSK, the carrier loop signal-to-noise ratio is

$$\rho_L = \left.\frac{P_T}{N_0}\right|_{D/L} \cdot \frac{S_{LQ}}{B_L} \tag{6}$$

where S_{LQ} is the squaring loss of the QPSK Costas loop (Reference 5),

$$S_{LQ} = \frac{1}{1 + \dfrac{9}{2\,E_{SQ}/N_0} + \dfrac{6}{\left(E_{SQ}/N_0\right)^2} + \dfrac{3}{2\left(E_{SQ}/N_0\right)^3}}, \tag{7}$$

where E_{SQ}/N_0 is the energy per quaternary channel symbol to noise spectral density ratio.

When telemetry data in a non-return to zero (NRZ) format directly modulate the carrier (that is, no subcarrier) and there is an imbalance in the data (that is, an unequal number of logical ones and zeros), a residual-carrier loop will experience an additional jitter. This jitter represents an additional error source for Doppler measurement. The size of this error contribution is strongly dependent on the statistics of the telemetry data.

2.1.1 *Measurement Error for One-Way Doppler*

Measurement error for one-way Doppler is normally dominated by the relative instability of the spacecraft oscillator and by the lack of knowledge of the exact frequency of this oscillator. Associated with one-way Doppler measurement is an unknown bias due to uncertainty in the transmitted frequency. In addition, there is a random error due to instability of the spacecraft oscillator. This latter error may be roughly modeled as

$$\sigma_V = \sqrt{2}c\sigma_y \tag{8}$$

where

σ_V = the standard deviation of range-rate in velocity units,

c = the speed of light in vacuum, and

σ_y = the Allan deviation of the spacecraft oscillator.

The Allan deviation is a function of integration time.

2.1.2 *Measurement Error for Two-Way and Three-Way Doppler*

Measurement errors for two-way coherent and three-way coherent Doppler must include the effect of jitter introduced by the spacecraft receiver. The two-way or three-way coherent Doppler measurement error due to thermal noise is approximated by

$$\sigma_V = \frac{c}{2\sqrt{2}\pi f_C T}\sqrt{\frac{1}{\rho_L} + \frac{G^2 B_L}{P_C/N_0\big|_{U/L}}} \tag{9}$$

where

T = measurement integration time, s

f_C = downlink carrier frequency, Hz

c = speed of light in vacuum, mm/s

G = transponding ratio

B_L = one-sided, noise-equivalent, loop bandwidth of downlink carrier loop, Hz

$P_C/N_0\big|_{U/L}$ = uplink carrier power to noise spectral density ratio, Hz

ρ_L = downlink carrier loop signal-to-noise ratio.

Equation (9) assumes that the transponder (uplink) carrier loop bandwidth is large compared with the DSS (downlink) carrier loop bandwidth, which is typically the case.

2.2　Carrier Tracking

The Downlink Channel can be configured to track phase-shift keyed telemetry with residual carrier or a suppressed carrier or a QPSK signal. In order to achieve good Doppler measurement performance, it is important to characterize the phase error in the carrier loop.

2.2.1　Carrier Loop Bandwidth

The one-sided, noise-equivalent, carrier loop bandwidth is denoted B_L. The user may choose to change B_L during a tracking pass, and this can be implemented without losing phase-lock, assuming the change is not too large.

There are limits on the carrier loop bandwidth. B_L can be no larger than 200 Hz. The lower limit on B_L is determined by the phase noise on the downlink. In addition, when operating in the suppressed-carrier mode, B_L is subject to the following constraint.

$$B_L \leq \frac{R_{SYM}}{20}, \text{ suppressed carrier,} \tag{10}$$

where R_{SYM} is the telemetry symbol rate.

In general, the value selected for B_L should be small in order to maximize the carrier loop signal-to-noise ratio. On the other hand, B_L must be large enough that neither of the following variables becomes too large: the static phase error due to Doppler dynamics and the contribution to carrier loop phase error variance due to phase noise on the downlink. The best B_L to select will depend on circumstances. Often, it will be possible to select a B_L of less than 1 Hz. A larger value for B_L is necessary when there is significant uncertainty in the downlink Doppler dynamics, when the downlink is one-way (or two-way non-coherent) and originates with a less stable oscillator (such as an Auxiliary Oscillator), or when the Sun-Earth-probe angle is small (so that solar phase scintillations are present on the downlink).

When tracking a spinning spacecraft, it may be necessary to set the carrier loop bandwidth to a value that is somewhat larger than would otherwise be needed. The loop bandwidth must be large enough to track out the variation due to the spin. Also, the coherent AGC in the receiver must track out the amplitude variations.

The user may select either a type 2 or type 3 carrier loop. Both loop types are perfect, meaning that the loop filter implements a true accumulation.

2.2.2　Static Phase Error in the Carrier Loop

The carrier loop, with either a type 2 or type 3 loop, has a very large tracking range; even a Doppler offset of several megahertz can be tracked. With a finite Doppler rate, however, there will be a static phase error in a type 2 loop.

Table 1, Static Phase Error (rad), shows the static phase error in the carrier loop that results from various Doppler dynamics for several different loops. These equations are based on the work reported in Reference 6. The Doppler dynamics are here defined by the parameters α and β.

α = Doppler Rate (Hz/s)

β = Doppler Acceleration (Hz/s^2)

In the presence of a persistent Doppler acceleration, a type 2 loop will periodically slip cycles.

The equations of Table 1 are valid when tracking phase-shift keyed telemetry with either residual or suppressed carrier or a QPSK signal. These equations are exactly the same as those appearing in Appendix C of module 207, 34-m and 70-m Telemetry.

2.2.3   Carrier Phase Error Variance

When the spacecraft is tracked one-way, the carrier phase error variance σ_ϕ^2 is given by

$$\sigma_\phi^2 = \frac{1}{\rho_L} + \sigma_S^2 \tag{11}$$

When the spacecraft is tracked in a two-way or three-way coherent mode, the carrier phase error variance σ_ϕ^2 is given by

$$\sigma_\phi^2 = \frac{1}{\rho_L} + \frac{G^2\left(B_{TR} - B_L\right)}{P_C/N_0\big|_{U/L}} + \sigma_S^2 \tag{12}$$

where

B_{TR} = one-sided, noise-equivalent, transponder carrier loop bandwidth, Hz

σ_S^2 = contribution to carrier loop phase error variance due to solar phase scintillations, rad^2 (see paragraph 2.3.2)

and the other parameters are as defined in paragraph 2.1.2.

It is recommended that the following constraint on carrier phase error variance be observed.

$$\sigma_\phi^2 \leq \begin{cases} 0.10 \text{ rad}^2, & \text{residual carrier} \\ 0.02 \text{ rad}^2, & \text{suppressed carrier} \end{cases} \tag{13}$$

Table 1. Static Phase Error (rad)

Loop	Constant Range-Rate $\left(\begin{array}{c}\text{Constant}\\\text{Doppler Offset}\end{array}\right)$	Constant Derivative of Range-Rate $\left(\begin{array}{c}\text{Constant}\\\text{Doppler Rate}\end{array}\right)$	Constant Second Derivative of Range-Rate $\left(\begin{array}{c}\text{Constant}\\\text{Doppler Acceleration}\end{array}\right)$
type 2, standard underdamped	0	$\dfrac{9\pi}{16B_L^2}\cdot\alpha$	$\left(\dfrac{9\pi\beta}{16B_L^2}\right)t - \dfrac{27\pi\beta}{64B_L^3}$
type 2, supercritically damped	0	$\dfrac{25\pi}{32B_L^2}\cdot\alpha$	$\left(\dfrac{25\pi\beta}{32B_L^2}\right)t - \dfrac{125\pi\beta}{128B_L^3}$
type 3, standard underdamped	0	0	$\dfrac{12167\pi}{8000B_L^3}\cdot\beta$
type 3, supercritically damped	0	0	$\dfrac{35937\pi}{16384B_L^3}\cdot\beta$

2.2.4   *Carrier Power Measurement*

When the downlink is residual-carrier, an estimate of the downlink carrier power P_C is available. When the downlink is suppressed-carrier, an estimate of the total downlink power P_T is available. This is done by first estimating $P_C/N_0\big|_{D/L}$ (with a modified version of the algorithm described in Reference 7) or $P_T/N_0\big|_{D/L}$ (with the split-symbol moments algorithm described in Reference 8). An estimate of the noise spectral density N_0 comes from continual measurements made by a noise-adding radiometer. This information is used to compute absolute power P_C or P_T. The results are reported once per second.

2.3   *Doppler Measurement With Small Sun-Earth-Probe Angles*

When the Sun-Earth-probe angle is small and the spacecraft is beyond the Sun, microwave carriers pick up phase scintillations in passing through the solar corona. There is a resulting contribution to Doppler measurement error and also an increase in the carrier loop phase error variance. The magnitudes of these effects are highly variable, depending on the activity of the Sun.

2.3.1 Doppler Measurement Error

Equations (14) and (15), below, based on the work reported in Reference 9, offer a coarse estimate of the average solar contribution to the standard deviation of Doppler measurement error. Equation (14) is valid when tracking phase-shift keyed telemetry with either residual or suppressed carrier or a QPSK signal, but only for Sun-Earth-Probe angles between 5° and 27°. In general, the standard deviation of Doppler measurement error will be the root-sum-square of the error standard deviation due to thermal noise, which is given in Equation (9), and the error standard deviation due to solar phase scintillations, which is given in Equation (14).

$$\sigma_V = \frac{0.73c\sqrt{C_{band}} \cdot \left[\sin\left(\theta_{SEP}\right)\right]^{-1.225}}{f_C T^{0.175}} \tag{14}$$

where

T = the measurement integration time in seconds,

f_C = the downlink carrier frequency in hertz,

c = the speed of light in vacuum ($\approx 3 \times 10^{11}$ mm/s), and

θ_{SEP} = the Sun-Earth-probe angle.

The result, σ_V, will have the same units as c.

The constant C_{band} depends on the uplink/downlink bands; it is given by

$$C_{band} = \begin{cases} 6.1 \times 10^{-5}, & \text{S-up/S-down} \\ 4.8 \times 10^{-4}, & \text{S-up/X-down} \\ 2.6 \times 10^{-5}, & \text{X-up/S-down} \\ 5.5 \times 10^{-6}, & \text{X-up/X-down} \\ 5.2 \times 10^{-5}, & \text{X-up/K}_a\text{-down} \\ 1.9 \times 10^{-6}, & \text{K}_a\text{-up/X-down} \\ 2.3 \times 10^{-7}, & \text{K}_a\text{-up/K}_a\text{-down} \end{cases} \tag{15}$$

Figure 3 shows σ_V as a function of Sun-Earth-probe angle for two-way or three-way Doppler measurement with an S-band uplink and an S-band downlink. The vertical axis is in units of mm/s. The three curves in that figure correspond to measurement integration times of 5, 60, and 1000 seconds. Figure 4 shows σ_V for an S-band uplink and an X-band downlink. Figure 5 shows σ_V for an X-band uplink and an X-band downlink. Figure 6 shows σ_V for an X-band uplink and an S-band downlink. Figure 7 shows σ_V for an X-band uplink and a K_a-band downlink.

2.3.2 Carrier Phase Error Variance

Equation (16), below, based on the work reported in Reference 9, offers a coarse estimate of the average solar contribution, in units of rad^2, to carrier loop phase error variance. Equation (16) is valid when tracking phase-shift keyed telemetry with either residual or suppressed carrier or a QPSK signal, but only for Sun-Earth-Probe angles between 5° and 27°.

$$\sigma_S^2 = \frac{C_{band} \cdot C_{loop}}{\left(\sin \theta_{SEP}\right)^{2.45} \cdot B_L^{1.65}}, \quad 5° \le \theta_{SEP} \le 27° \tag{16}$$

In Equation (16), θ_{SEP} is the Sun-Earth-probe angle and B_L is the carrier loop bandwidth. C_{band} is given by Equation (15) for two-way and three-way coherent operation and by

$$C_{band} = \begin{cases} 2.6 \times 10^{-5}, & \text{S - down} \\ 1.9 \times 10^{-6}, & \text{X - down} \\ 1.3 \times 10^{-7}, & \text{K}_a \text{ - down} \end{cases} \tag{17}$$

for non-coherent operation.

C_{loop} is a constant depending on the type of carrier loop selected.

$$C_{loop} = \begin{cases} 5.9, & \text{standard underdamped type 2 loop} \\ 5.0, & \text{supercritically damped type 2 loop} \\ 8.2, & \text{standard underdamped type 3 loop} \\ 6.7, & \text{supercritically damped type 3 loop} \end{cases} \tag{18}$$

Equation (16) together with Equations (15), (17), and (18) give the contribution of solar coronal phase scintillation to carrier loop phase error variance. It is used in Equation (12) to compute the total carrier loop phase error variance.
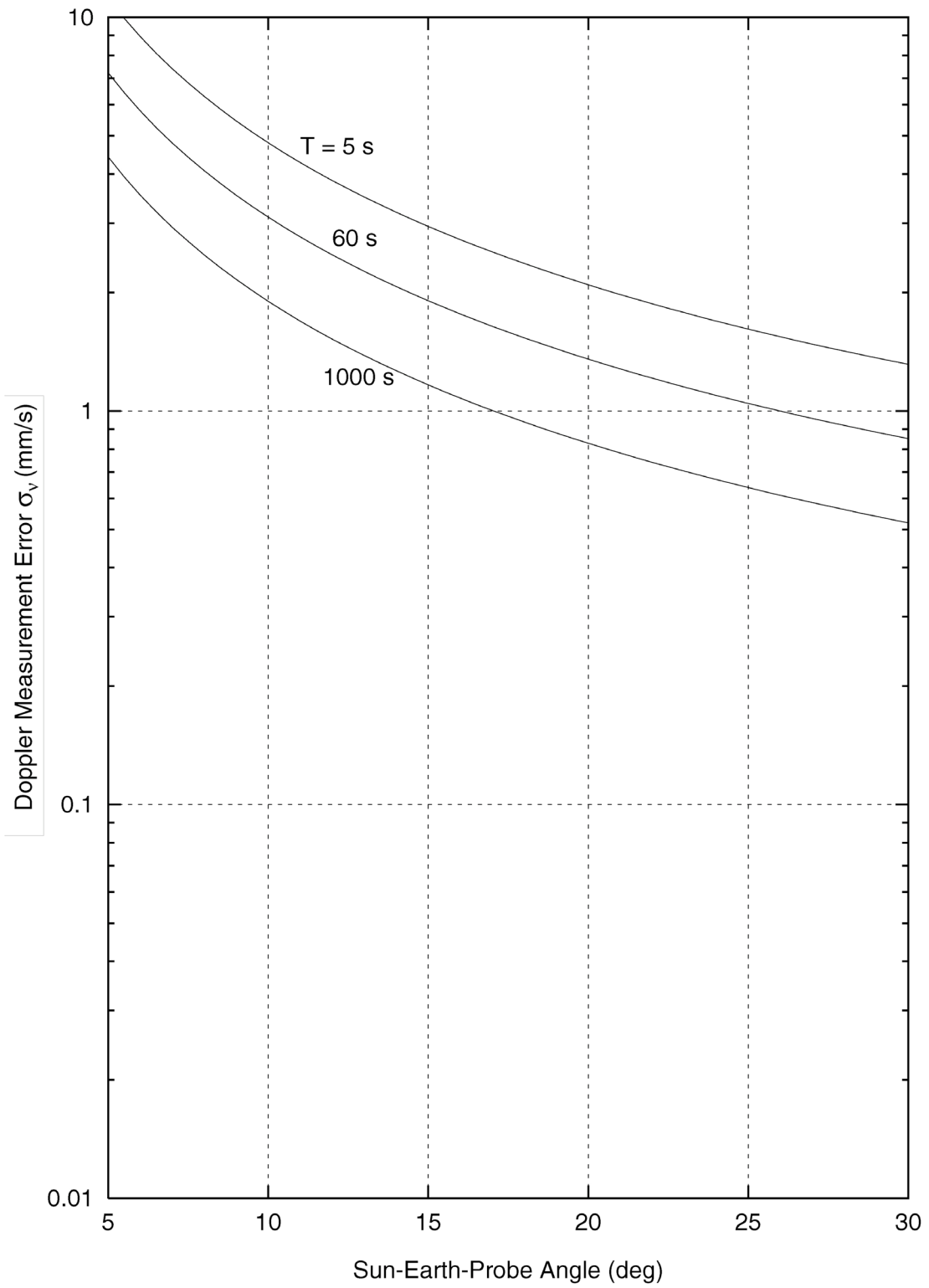
Figure 3. Doppler Measurement Error Due to Solar Phase Scintillation: S-Up/S-Down
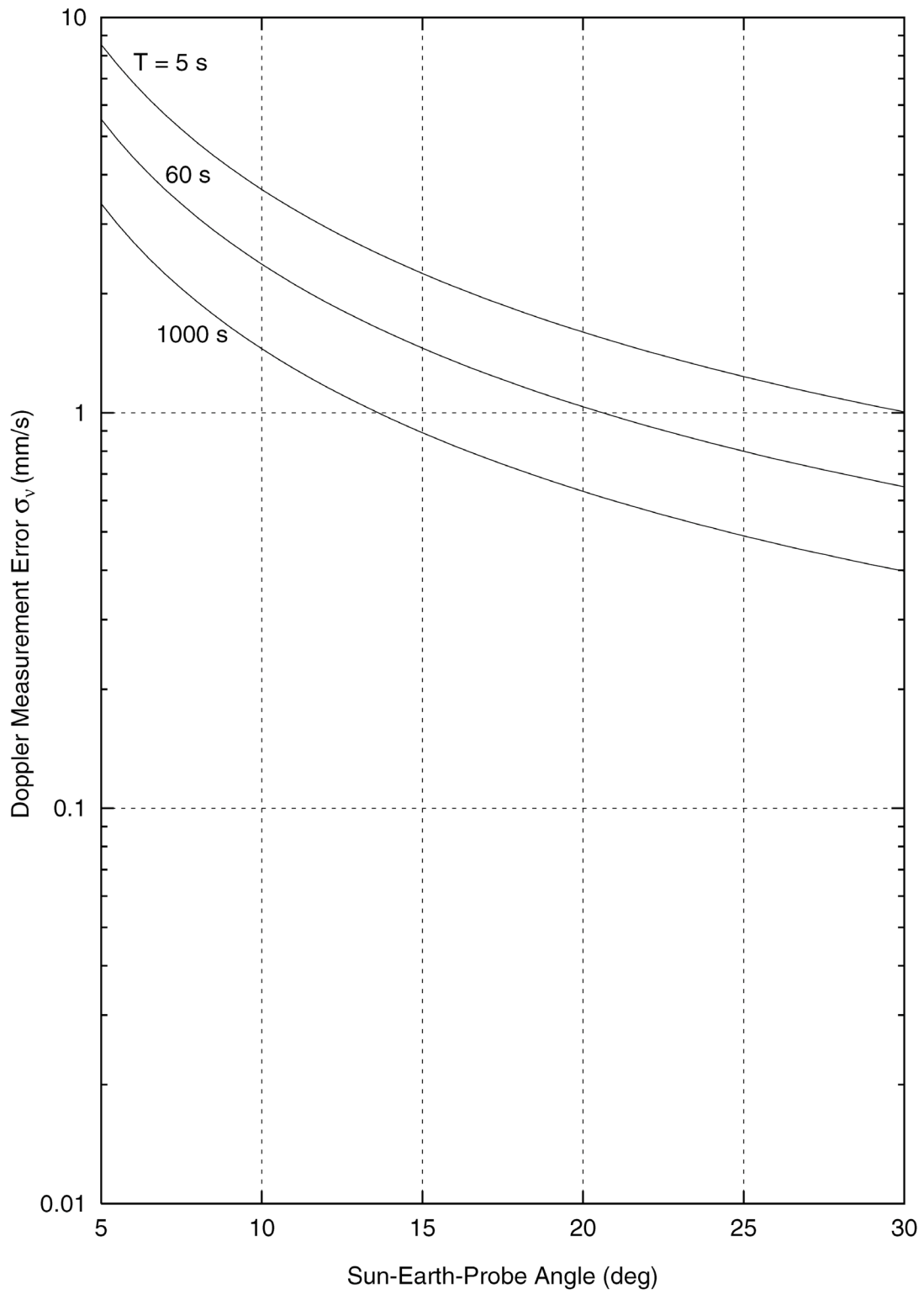
Figure 4. Doppler Measurement Error Due to Solar Phase Scintillation: S-Up/X-Down
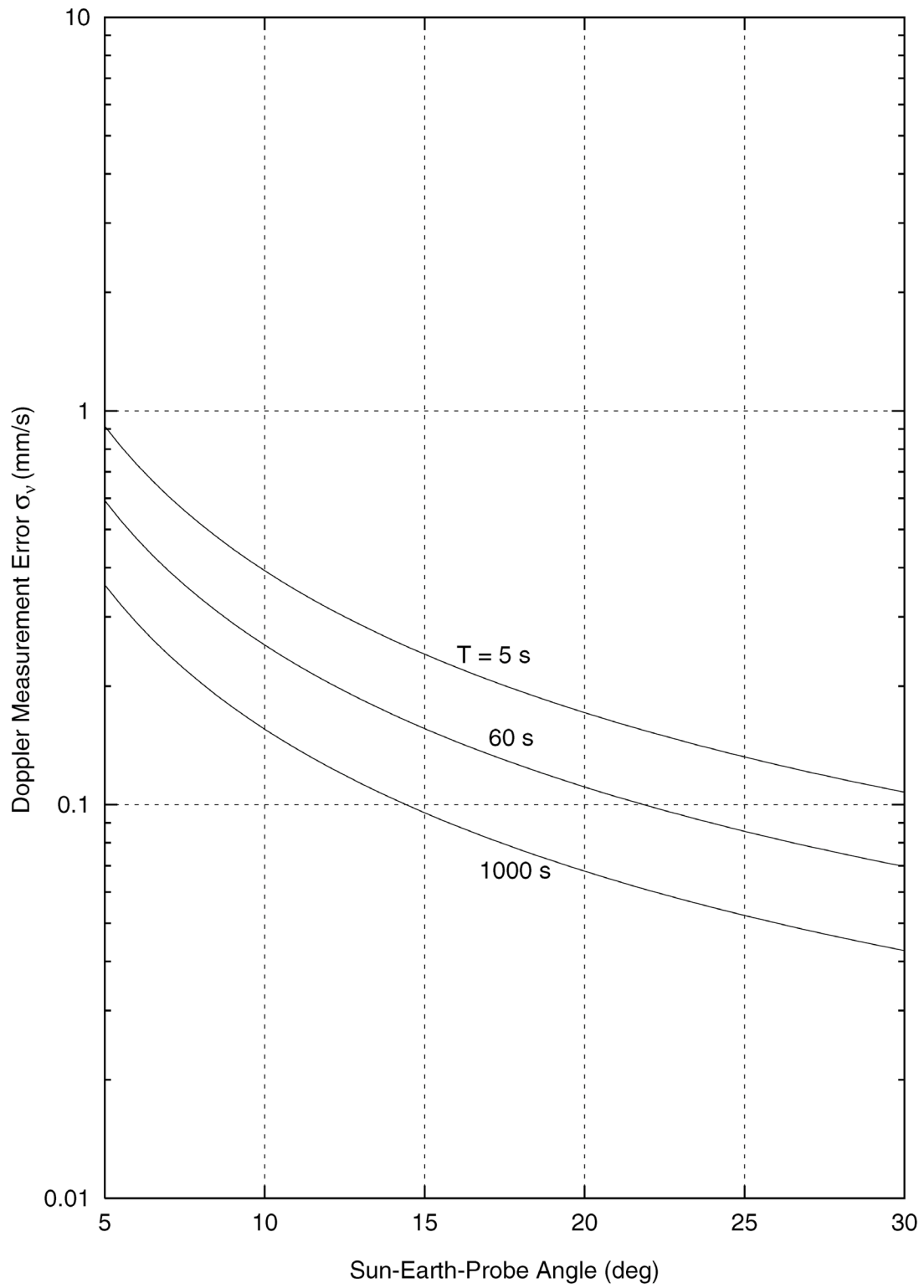
Figure 5. Doppler Measurement Error Due to Solar Phase Scintillation: X-Up/X-Down
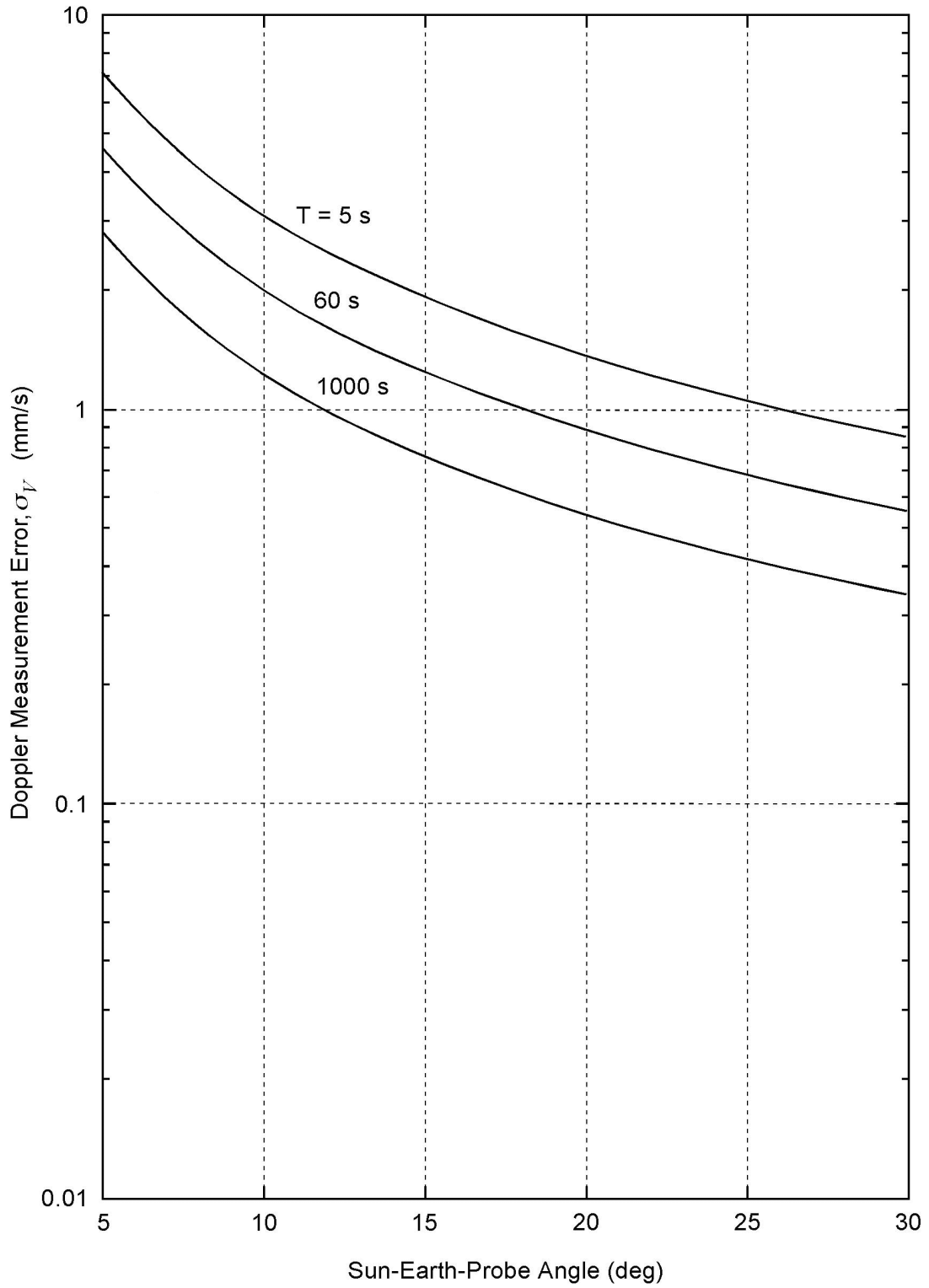
Figure 6. Doppler Measurement Error Due to Solar Phase Scintillation: X-Up/S-Down
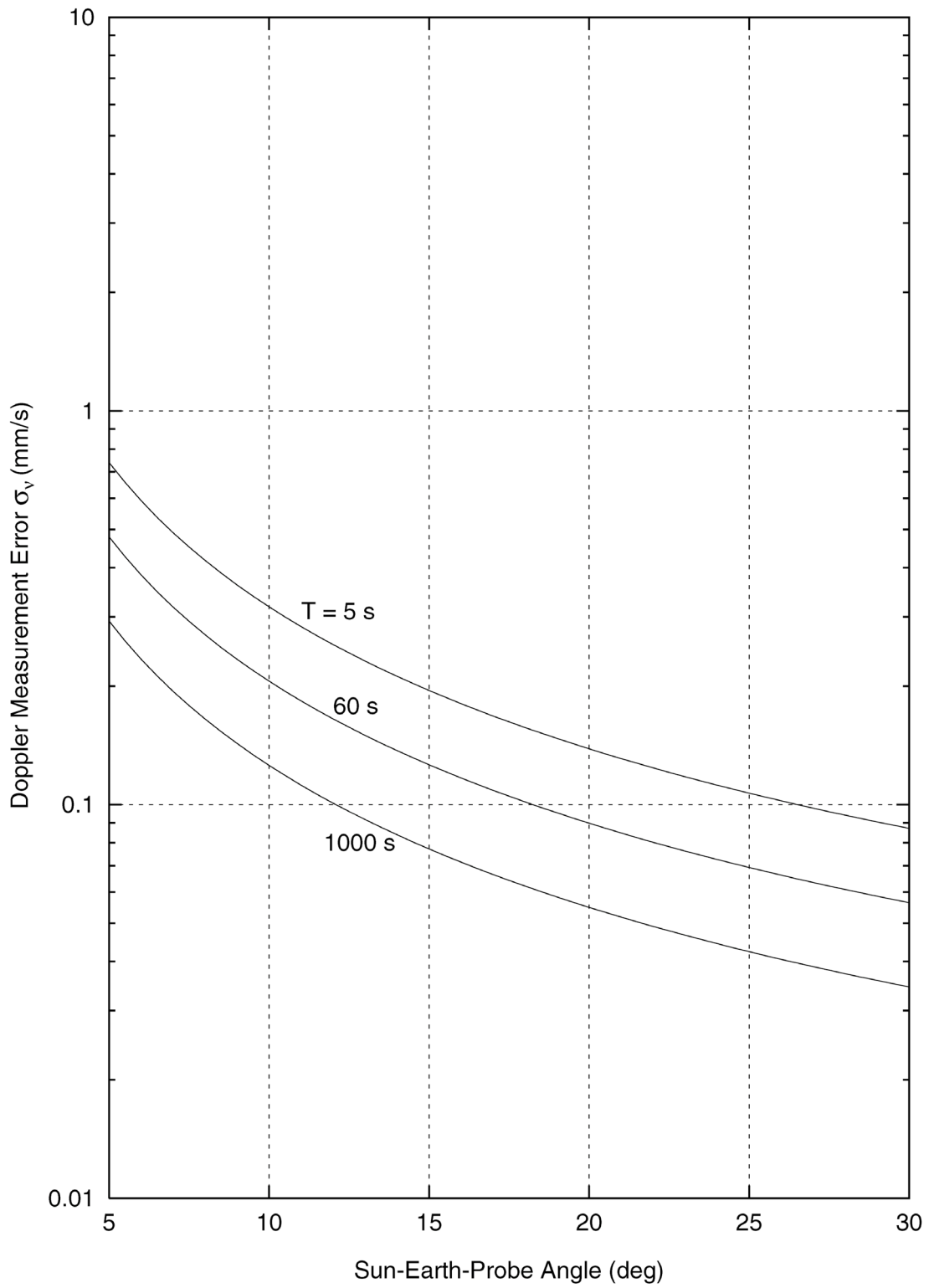
Figure 7. Doppler Measurement Error Due to Solar Phase Scintillation: X-Up/Ka-Down

Appendix A

References

1.　P. W. Kinman, "Doppler Tracking of Planetary Spacecraft," *IEEE Transactions on Microwave Theory and Techniques*, Vol. 40, No. 6, pp. 1199-1204, June 1992.

2.　J. B. Berner and K. M. Ware, "An Extremely Sensitive Digital Receiver for Deep Space Satellite Communications," *Eleventh Annual International Phoenix Conference on Computers and Communications*, pp. 577-584, Scottsdale, Arizona, April 1-3, 1992.

3.　J. Lesh, "Tracking Loop and Modulation Format Considerations for High Rate Telemetry," *DSN Progress Report 42-44*, Jet Propulsion Laboratory, Pasadena, CA, pp. 117-124, April 15, 1978.

4.　M. K. Simon and W. C. Lindsey, "Optimum Performance of Suppressed Carrier Receivers with Costas Loop Tracking," *IEEE Transactions on Communications*, Vol. COM-25, No. 2, pp. 215-227, February 1977.

5.　J. H. Yuen, editor, *Deep Space Telecommunications Systems Engineering*, Plenum Press, New York, pp. 94-97, 1983.

6.　S. A. Stephens and J. B. Thomas, "Controlled-Root Formulation for Digital Phase-Locked Loops," *IEEE Transactions on Aerospace and Electronic Systems*, Vol. 31, No. 1, pp. 78-95, January 1995.

7.　A. Monk, "Carrier-to-Noise Power Estimation for the Block-V Receiver," *TDA Progress Report 42-106*, Jet Propulsion Laboratory, Pasadena, CA, pp. 353-363, August 15, 1991.

8.　S. Dolinar, "Exact Closed-Form Expressions for the Performance of the Split-Symbol Moments Estimator of Signal-to-Noise Ratio," *TDA Progress Report 42-100*, pp. 174-179, Jet Propulsion Laboratory, Pasadena, CA, February 15, 1990.

9.　R. Woo and J. W. Armstrong, "Spacecraft Radio Scattering Observations of the Power Spectrum of Electron Density Fluctuations in the Solar Wind," *Journal of Geophysical Research*, Vol. 84, No. A12, pp. 7288-7296, December 1, 1979.

203
Sequential Ranging

Effective November 30, 2000

Document Owner: Approved by:

Charles Ruggier   12/11/00   _Kwok_   12/13/00
C.J. Ruggier   Date   A. Kwok   Date
Tracking System Engineer   Tracking and Navigation Service
                                            Systems Development Engineer

Prepared by: Released by:

R. W. Sniffin   12/11/00
R. W. Sniffin   Date   [Signature on file at TMOD Library]
                                            TMOD Document Release   Date

Change Log

Rev	Issue Date	Affected Paragraphs	Change Summary
Initial	1/15/2001	All	All

Note to Readers

There are two sets of document histories in the 810-005 document, and these histories are reflected in the header at the top of the page. First, the entire document is periodically released as a revision when major changes affect a majority of the modules. For example, this module is part of 810-005, Revision E. Second, the individual modules also change, starting as an initial issue that has no revision letter. When a module is changed, a change letter is appended to the module number on the second line of the header and a summary of the changes is entered in the module's change log.

Module 203 supersedes module TRK-30, Rev. E, dated January 15, 1998, in 810-005.

Contents

Illustrations

Tables

1 Introduction

1.1 Purpose

This module describes the Ranging capabilities of the Network Simplification Project (NSP) and provides the performance parameters of the Deep Space Network (DSN) Sequential Ranging equipment for the 70-m, the 34-m High Efficiency (HEF), and the 34-m Beam Waveguide (BWG) subnets. Appendix A gives a description of the ranging architecture and performance for the 26-m subnet and the 34-m High-speed Beam Waveguide (HSB) antenna that are not included in the NSP implementation scheme, and for the 70-m, 34-m HEF, and 34-m BWG subnets prior to the NSP implementation.

1.2 Scope

The material contained in this module covers the sequential ranging system that is utilized by both near-Earth and deep space missions. This document describes those parameters and operational considerations that are independent of the particular antenna being used to provide the telecommunications link. For antenna-dependent parameters, refer to the appropriate telecommunications interface module, modules 101, 102, 103, and 104 of this handbook. Other ranging schemes employed by the DSN include the tone ranging system, described in module 204 and the pseudo random noise (PN) and regenerative ranging, described in module 214.

2 General Information

The DSN ranging system provides a sequentially binary-coded ranging scheme to measure the round-trip light time (RTLT) between a Deep Space Station (DSS) and a spacecraft. An uplink signal is transmitted to a spacecraft where it is received by the on-board transponder, then demodulated, filtered, and remodulated onto the downlink carrier. The downlink signal received at the DSS is correlated with a Doppler-modified replica of the transmitted codes that were sent to the spacecraft approximately one RTLT earlier. Using Doppler rate-aiding, the RTLT is determined by measuring the phase difference between the received code and the transmitted code.

The three basic tracking modes are one-way, two-way, and three-way. In the one-way tracking mode, the spacecraft generates a downlink signal that is received by the Earth-based station without a transmission being made to the spacecraft. Two-way tracking consists of transmitting an uplink to a spacecraft where it is received and coherently transmitted as a downlink to the same Earth station. For the three-way tracking mode, two-way tracking is performed by an Earth station, while another station tracks the downlink signal using a different antenna and possibly a different frequency standard.

The parameters to be specified for ranging operations are explained in Paragraph 2.3. Paragraph 2.4 presents the process of range measurement that includes the evaluation of RTLT, ranging-power-to-noise ratio (P_r/N_O), figure of merit (FOM), and differenced range versus integrated Doppler (DRVID). The relationship of downlink ranging power over total power is given in Paragraph 2.5. Paragraph 2.6 provides the corrections required to determine the actual range to a spacecraft. Error contributions of the ground system are discussed in Paragraph 2.7.

2.1 Network Simplification Project Ranging

The Deep Space Network is undergoing a redesign of the uplink and downlink architecture to achieve simplified operations and increased performance. A major feature of the modification is the splitting of the ranging and Doppler uplink and downlink functions, allowing recovery from anomalies on one without affecting the other.

In contrast to the previous design that employed a separate piece of equipment called the sequential ranging assembly (SRA), the new ranging system does not require a real-time interface between the uplink and downlink elements. There is a connection between the uplink and downlink in the sense that both elements must send data to a common node. However, the digital time-tagged data can be passed to the common node in non-real time, without loss of range measurement accuracy. The lack of a hardware connection to between the uplink and downlink elements of single antenna to the ranging equipment makes it possible to perform range measurements in the three-way tracking mode.

NSP ranging replaces the SRA with separate uplink and downlink ranging processors. Local code models are generated that match the SRA sequential tone ranging. The Tracking Data Delivery Subsystem (TDDS) replaces the Metric Data Assembly (MDA) and the Radio Metric Data Conditioning (RMDC) function of preparing the data for delivery to the user.

Ranging code components cover 1 MHz to 1 Hz in steps of powers of 2 provided by software local code models. Correlation of the ranging signal to determine clock phase and range ambiguity is handled using software algorithms.

2.2 System Description

The NSP architecture for the DSN ranging system is shown in Figure 1. It consists of a front end portion, an uplink portion, and a downlink portion. The front-end portion consists of the microwave components, including a Low-noise Amplifier (LNA) and the antenna. The uplink portion includes the Uplink Ranging Assembly (URA), an exciter, the transmitter, and the controller, referred to as the Uplink Processor Assembly (UPA). The downlink portion includes the RF-to-IF Downconverter (RID), the IF-to-Digital Converter (IDC), the Receiver and Ranging Processor (RRP) and the Downlink Channel Controller (DCC). The Downlink Telemetry and Tracking Subsystem (DTT) and the Uplink Subsystem (UPL) provide the essential functional capability for NSP ranging.
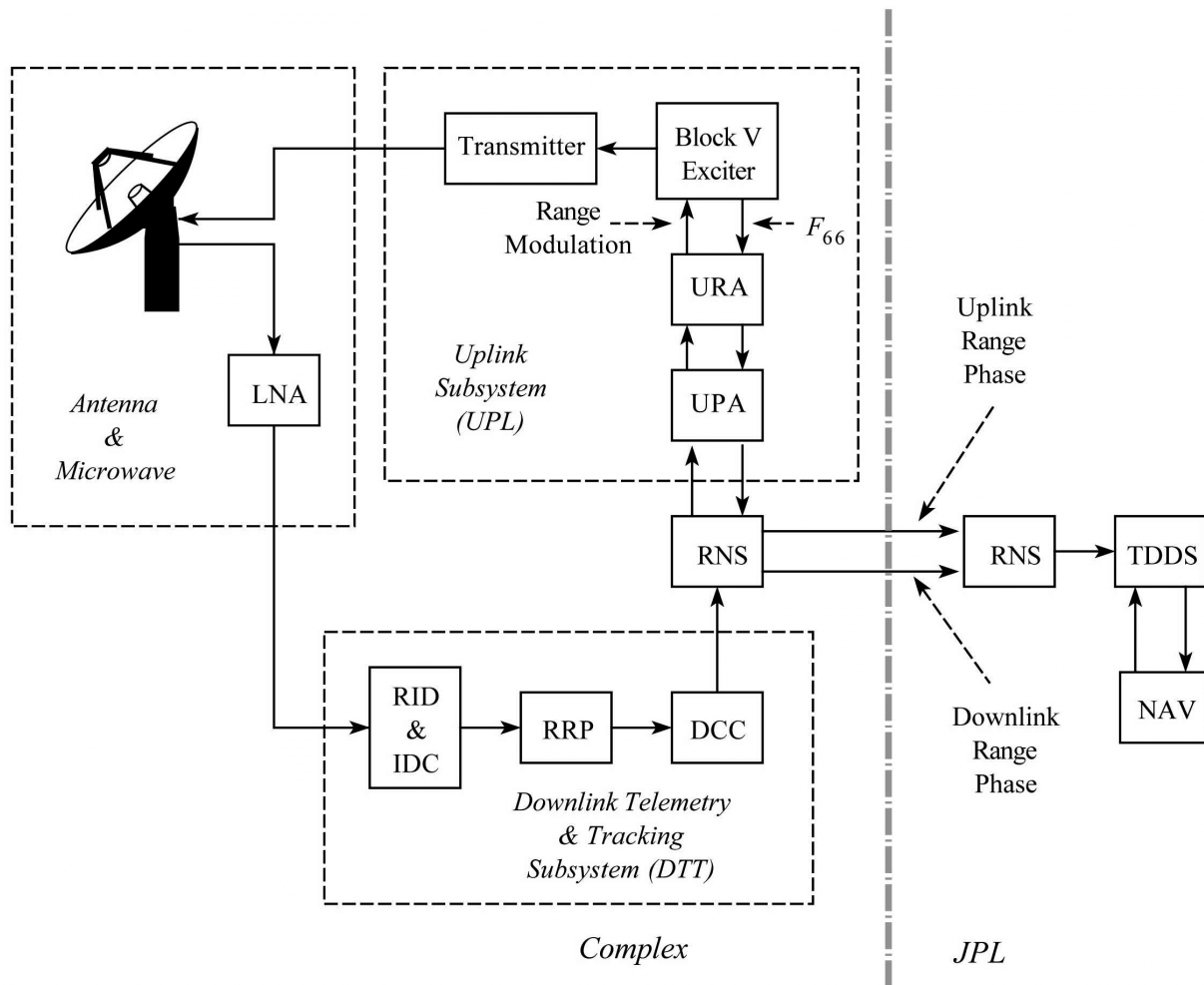
Figure 1. The NSP Era DSN Ranging System Architecture

Control of the ranging function is within the DTT. Control signals from the DTT are coupled to the URA in the UPL via the Reliable Network Service (RNS) and the UPA. The URA generates the sequential ranging codes for two-way and three-way ranging and forwards them to the exciter where they are modulated onto the uplink. It also monitors the uplink ranging phase and forwards this data to the TDDS.

The amplified downlink signal from the microwave is downconverted by the RID (located on the antenna) and fed to the IDC where it is sampled at 160 Msamples/s into an 8-bit digital signal at the RRP. After processing, the downlink range phase data are delivered to the TDDS by the Downlink Channel Controller (DCC), via the station RNS and a similar function at JPL. The TDDS formats the ranging data and passes the uplink and downlink phase information to the Navigation subsystem (NAV). Subsequently, the NAV provides the ranging data to projects.

Each DTT Controller Processing Cabinet (DCPC) is equipped with a single channel, which includes a single RRP. For spacecraft with multiple channels (for example, S-band and X-band), or for multiple spacecraft within a single antenna beamwidth, multiple DCPCs will be assigned to that antenna.

In addition to producing downlink phase information, the RRP generates a 66-MHz ranging reference analog signal with a Numerically Controlled Oscillator (NCO). The ranging reference frequency F_{RNG} (ref), is computed from the received frequency, f_r, as follows:

$$F_{RNG}(\text{ref}) = \frac{F_r}{32 \cdot K} \tag{1}$$

where:

F_r = received carrier frequency

K = normalization factor (independent of uplink frequency)

240/221 (S-down)

880/221 (X-down)

3344/221 (Ka-down).

2.3 *Parameters Specified for Ranging Operations*

The following paragraphs present the parameters that are required in ranging operations.

2.3.1 *Transmit Time and Receive Time*

The rabging system needs a transmit time (XMIT) and an a-priori estimate of the RTLT, truncated to the nearest second, in order that the code sequence sent by the UPL can be correlated for measuring the phase shift through the round-trip-time delay. When a XMIT and an approximate RTLT are specified, the DTT automatically calculates the receive time T_O by adding the two quantities, $T_O = \text{XMIT} + \text{RTLT}$. This T_O is also called the start time of the correlation process for the code sequence. The two time quantities must be specified to the nearest second.

2.3.2 *Clocks and Components*

A range measurement begins with the highest frequency code followed by subsequent codes each having a frequency exactly half of the previous one. The first code in the sequence is called the clock component and determines the resolution of the measurement. The lower frequency codes that follow are used to resolve the ambiguity (uncertainty) of the a-priori range estimate.

Table 1 shows the clocks and components used in ranging operations. A total of 21 code components are available. They are referred to as component numbers 4 through 24 as shown in the Table. The first 7 components (numbered 4 through 10) are called the clock components or simply clocks. The approximate ambiguity resolving capability of a component is listed for reference. The approximate frequencies and periods of the codes are also shown.

The exact clock frequency (F_c) to replace the approximate frequency in the second column is computed by the relationship:

$$F_C = \frac{F_{66}}{2^{2+n}} \tag{2}$$

where n is an integer from 4 to 24 that represents a code component or a component number and F_{66} is the exciter reference frequency.

The value of F_{66} used to produce Table 1 was exactly 66.000 MHz. In ranging operations, this frequency varies depending upon the transmitting (uplink) carrier frequency. F_{66} is denoted by F_{66S} or F_{66X} depending on whether it was derived from an S-band or X-band uplink frequency and can be expressed in terms of the uplink frequency as follows:

S-band uplink:

$$F_{66S} = \frac{F_{ts}}{32} \tag{3}$$

X-band Uplink

$$F_{66X} = \frac{221}{749} \times \frac{F_{tx}}{32} \tag{4}$$

where, F_{ts} and F_{tx} are the S- and X-band transmitting (uplink) frequencies.

The third column (approximate period) shows the periods of the corresponding frequencies in the second column. The fourth column (ambiguity resolving capability) lists the products of the periods and the speed of light (299,792.5 km/s), divided by a factor of 2 to determine the one-way distance.

Depending on the uncertainty of the range estimate, a flight project determines the number of components needed for ranging operations. An example in choosing the clock and components is given as follows:

Example: Suppose the spacecraft is known to be at a 10-minute RTLT from Earth to within ±100,000 km. If it is desired to resolve the ambiguity to about 40,000 km, and if the distance is desired to be resolved to within 150 m, then components 4 through 22 should be defined for ranging. That is, clock 4 (about 1 MHz) is used with the subsequent 18 components (5 through 22).

Table 1. Range Code Resolving Capability

Component Number	Approximate Frequency (Hz)	Approximate Period (s)	Approximate Ambiguity Resolving Capability (km)
4*	1,030,000.000	9.700E-07	0.1450
5*	516,000.000	1.940E-06	0.2910
6*	258,000.000	3.880E-06	0.5810
7*	129,000.000	7.760E-06	1.160
8*	64,500.000	1.550E-05	2.330
9*	32,200.000	3.100E-05	4.650
10*	16,100.000	6.210E-05	9.30
11	8,060.000	1.240E-04	18.60
12	4,030.000	2.480E-04	37.20
13	2,010.000	4.960E-04	74.40
14	1,010.000	9.930E-04	149.0
15	504.000	1.990E-03	298.0
16	252.000	3.970E-03	595.0
17	126.000	7.940E-03	1,190.0
18	62.900	1.590E-02	2,380.0
19	31.500	3.180E-02	4,760.0
20	15.700	6.360E-02	9,530.0
21	7.870	1.270E-01	19,100.0
22	3.930	2.540E-01	38,100.0
23	1.970	5.080E-01	76,200.0
24	0.983	1.020E+00	152,000.0
* available clocks			

2.3.3 Square-Wave and Sine-Wave Ranging

The DTT may process the received codes in two ranging modes. They are referred to as square-wave and sine-wave operation. For square-wave operation, the DTT processes all harmonics of the received codes. For sine-wave operation, only the fundamental (the first harmonic) is processed. Square-wave operation is the default because, with the exception of the higher frequency clock components, the codes are received as square waves. However, sine-

wave operation may be desirable if non-linearities or other processes exist that may delay the range code fundamental and its harmonics differently. The two modes can be summarized by:

Square-wave operation:	*transmit*	**square waves**
	correlate as	**square waves**
Sine-wave operation:	*transmit*	**square waves**
	correlate as	**sine waves**

Ranging with the 500-kHz and 1-MHz clocks are special cases due to the limited ranging bandwidths of most spacecraft and an intentional 1.2 MHz bandwidth limit in the DSN ranging modulators. This limit has been installed to prevent interference with services adjacent to the DSN uplink allocations . The ranging equipment presently requires the 1 MHz clock to be processed using sine-wave correlation. If square-wave correlation is specified, the 500 kHz code will be processed using the square-wave correlation algorithm although only its fundamental will have been transmitted to the spacecraft.

2.3.4 *Integration Times*

Three integration times must be specified for ranging operations. They are: T_1 for clock integration, T_2 for each lower-frequency component integration, and T_3 for DRVID measurement(s).

2.3.4.1 T_1

T_1 is the total time used to integrate the correlation samples for the clock component. It is a function of the clock frequency, the desired variance of RTLT measurements, and the ranging signal to noise spectral density and can be calculated by the following expressions:

Sine-wave operation:

$$T_1 = \frac{1}{64} \times \frac{1}{F_c^2} \times \frac{1}{\sigma^2(t)} \times \frac{1}{P_r / N_o}, \text{ s} \tag{5}$$

where

F_c = the clock frequency, Hz

$\sigma^2(t)$ = the desired variance of the RTLT measurements, s^2

P_r/N_o = the ranging signal to noise spectral density, Hz

The factor 1/64 has been derived empirically from the most probable variance of a range point when using sine-wave correlation.

Square-wave operation:

$$T_1 = \frac{1}{49} \times \frac{1}{F_c^2} \times \frac{1}{\sigma^2(t)} \times \frac{1}{P_r / N_o}, \text{ s} \tag{6}$$

where

F_c , $\sigma^2(t)$, and P_r/N_O are as above and the factor 1/49 has been derived empirically from the upper bound variance of the 1 MHz sine-wave ranging when using square-wave correlation.

The above equations can be rewritten in terms of the uncertainty $\sigma(r)$ in meters, by multiplying the uncertainty $\sigma(t)$ in seconds by the speed of light and dividing by a factor of 2. This provides:

Sine-wave operation:

$$\sigma(r) = \sqrt{\frac{352}{F_c^2(\text{MHz}) \times T_1 \times P_r / N_o}} \text{ , m} \tag{7}$$

Square-wave operation:

$$\sigma(r) = \sqrt{\frac{458}{F_c^2(\text{MHz}) \times T_1 \times P_r / N_o}} \text{ , m} \tag{8}$$

where:

F_c = the clock frequency, MHz

T_1 = the clock component integration time, s

P_r/N_O = the ranging signal to noise spectral density, Hz.

Note: The uncertainty, σ, here is only due to thermal noise. Other errors must be added to this to get the total uncertainty (see Paragraph 2.7).

Figure 2 plots integration time (T_1) as a function of P_r/N_O for sine-wave operation using a 1 MHz clock component with $\sigma(r)$ as a parameter. For a desired $\sigma(r)$, the user may find the proper integration time, T_1, for an estimated P_r/N_O (in dB-Hz). Figure 3 is a similar graph for square-wave operation using a 500-kHz clock component. This figure may also be used for lower frequency square-wave clocks by recognizing that dividing F_c by 2 will result in T_1, being multiplied by 2^2, etc.
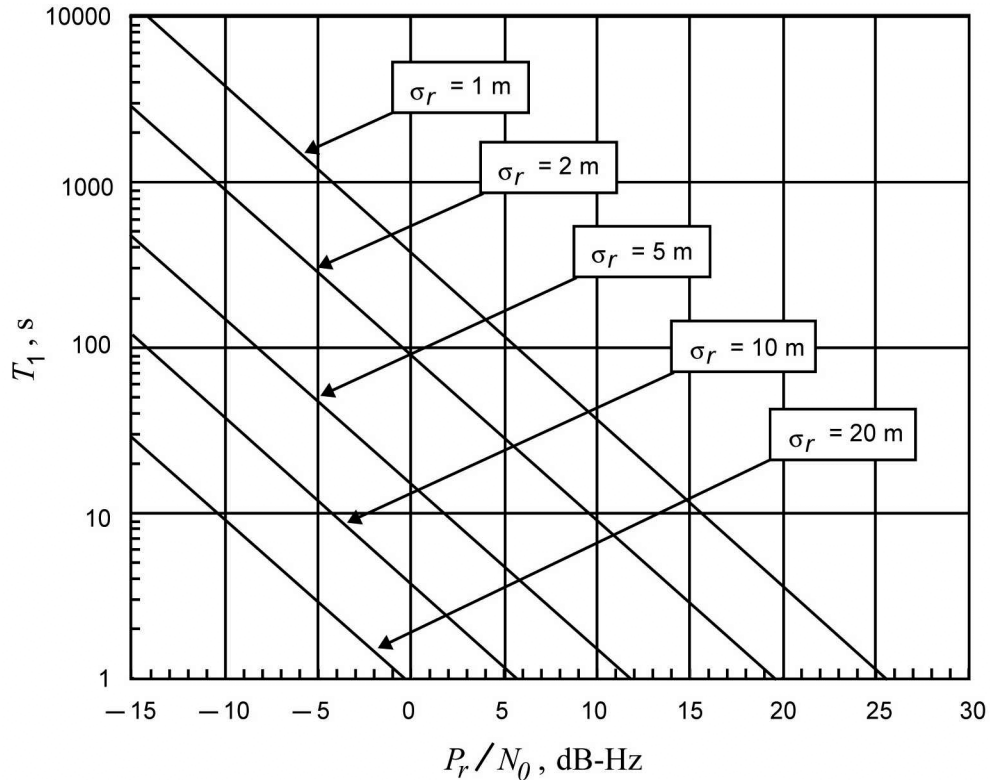
Figure 2.   Integration Time T_1 Versus P_r/N_O, Clock Frequency F_c = 1 MHz,
for Sine-Wave Ranging

Ranging is possible as long as the receiver remains in lock over the measurement time. However, there is a practical lower limit for P_r/N_O (usually about -10 dB-Hz) determined by the combination of integration times (cycle time) and the minimum number of range points needed by the project. See Cycle Time in Paragraph 2.3.4.4 for further details.

2.3.4.2 T_2

T_2 is the integration time for each of the lower-frequency components. It is a function of P_r/N_O and the probability of error in acquiring all components (excluding the clock). In general, T_2 is given by the following equation

$$T_2 = \frac{1}{P_r/N_0} \times \left\{ \text{InvErf}\left[2\left(1 - P_e\right)^{\frac{1}{n-1}} - 1\right]\right\}^2 \text{ , s} \tag{9}$$
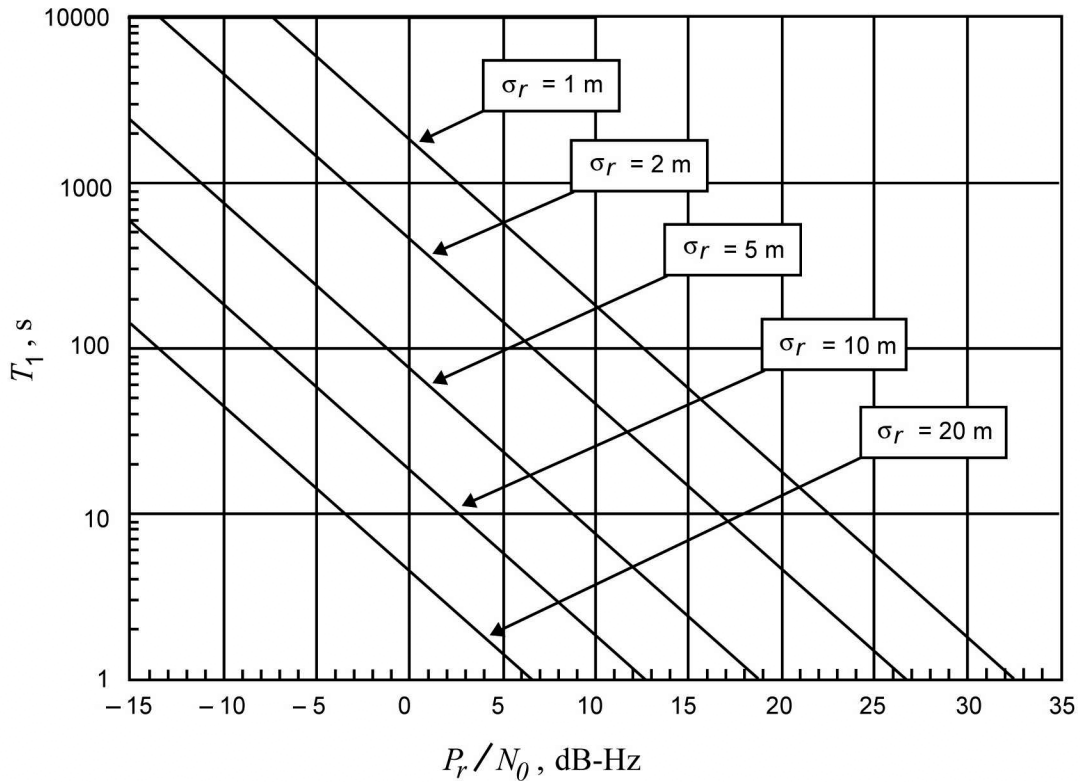
Figure 3. Integration Time T_1 Versus P_r/N_O, Clock Frequency F_c = 500 kHz, for Square-Wave Ranging

where

P_r/N_O = the ranging signal to noise spectral density, Hz

InvErf[∗] = the inverse error function of the ∗ quantity.

P_e = the probability of error in acquiring all (*n*-1) components.

n = the total number of components including the clock being acquired.

Figures 4 through 6 show T_2 versus P_r/N_O for various P_e and *n*. An appropriate T_2 for ranging operations can be determined from these curves by choosing the desired n, the desired, P_e, and the estimated P_r/N_O.
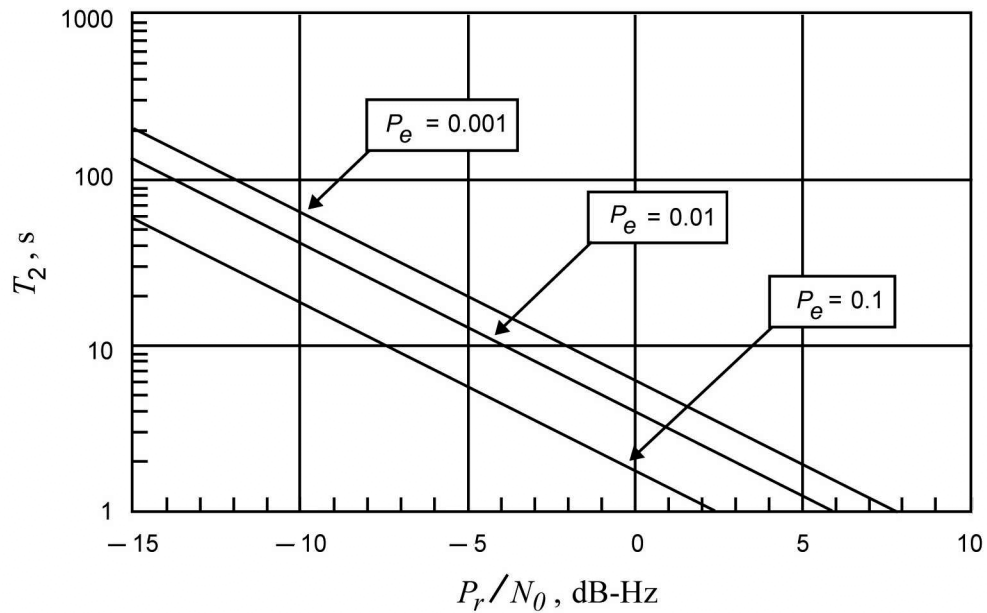
Figure 4.   Code Component Integration Time T_1 Versus P_r/N_O for Various
Probabilities of Error and $n = 5$
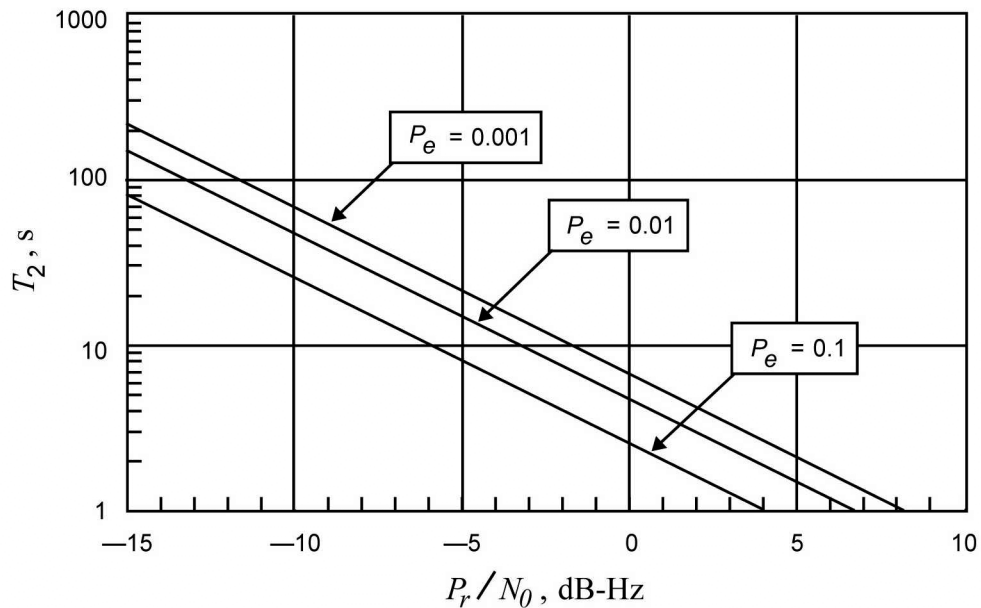
Figure 5.   Code Component Integration Time T_1 Versus P_r/N_O for Various
Probabilities of Error and $n = 10$
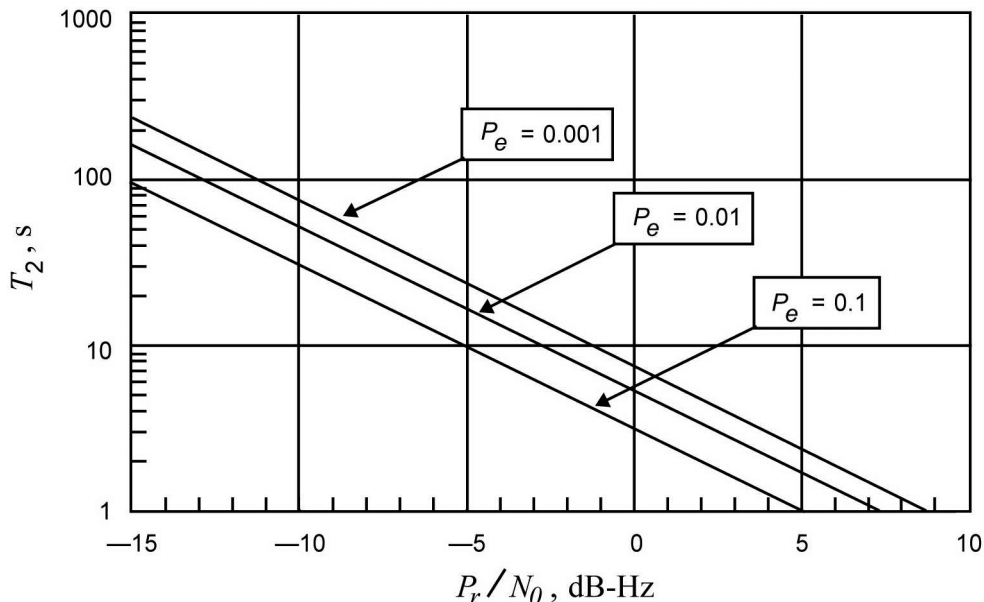
Figure 6.   Code Component Integration Time T_1 Versus P_r/N_O for Various
Probabilities of Error and $n = 20$

2.3.4.3 T_3

T_3 is the integration time for differenced range versus integrated Doppler (DRVID) measurements (see Paragraph 2.4.3 for a further discussion of DRVID). Since the phase information is already available from the clock acquisition, T_3 can be less than T_1 (typically $7/8\ T_1$).

2.3.4.3   Cycle Time

Cycle time is the total time that the DTT spends to perform measurements for the clock, the (n-1) components, and the DRVIDs. It also includes some dead time between component integrations to accomodate the 1-second inaccuracy permitted in specifying the estimated RTLT. In other words, it is the time required to complete one range acquisition. The cycle time (CYC) is automatically calculated by the DTT, and it is given by the following formula:

$$CYC = (2 + T_1) + (1 + T_2)(n - 1) + DRVN(2 + T_3) + 1,\ \text{s}$$ (10)

where:

T_1 = clock integration time

T_2 = component integration times

17

T_3 = DRVID integration time

n = the total number of components including the clock

DRVN = the number of DRVIDs specified for the acquisition.

For a typical 8-hour tracking pass, it is recommended that *CYC* be less than the following limits:

Soft limit: $CYC \leq 30$ minutes

Hard limit: $CYC \leq 55$ minutes.

The chance of getting a desired number of good range points decreases substantially as the cycle time approaches the 55-minute limit. Any glitch occurring in the system during the time of measurement will cause a range point to become invalid. It is better to stay closer to, or within the soft limit.

2.3.5 *Modulation Index*

In ranging operations, square-wave codes are modulated on the uplink carrier by the exciter phase modulator. This results in an attenuation of carrier power and a corresponding increase of power spread into the sidebands. The phase displacement of the carrier due to modulation is referred to as the modulation index and may be specified as a peak-to-peak or root mean square (RMS) value. That is, if the modulation waveform is specified as peak-to-peak value, the modulation index will define the peak-to-peak phase modulation. If, on the other hand, the modulation waveform is specified as an RMS value, the modulation index will define the RMS phase modulation The expressions for carrier power and ranging power are given in terms of the modulation index as follows:

$$P_c = P_t\left(\cos^2 \theta\right), \text{ numeric, units of power} \tag{11}$$

$$P_r = P_t\left(\sin^2 \theta\right), \text{ numeric, units of power} \tag{12}$$

where:

P_c = the carrier power

P_r = the ranging power

P_t = the total power before ranging modulation (that is, $P_t = P_c + P_r$)

θ = the modulation index in radians (or degrees).

Therefore, the carrier suppression in dB is given by:

$$\frac{P_c}{P_t} = 10\log(\cos^2 \theta) . \tag{13}$$

The modulators used in the DSN operate over the range of 0.1 to 1.5 radians, peak. It should be noted that equation 13 assumes ideal conditions, and variations between the calculated and that measured values of carrier suppression may occur depending on the amplitude, frequency, and phase responses of the modulator in use.

Example: An unmodulated signal is received by a spacecraft with $P_t = -100$ dBm. When this signal is modulated by square waves of a 30-deg modulation index, the carrier power (P_c) becomes -101.25 dBm (suppressed by 1.25 dB) and the ranging (sidebands) power (P_r) is -106.0 dBm ($P_r = -100$ dBm + $10\log(\sin(30)^2)$).

2.3.6   *Frequency Chopping*

Separation between the ranging modulation products and the carrier frequency decreases as a ranging acquisition steps through the code components of the lower frequencies. If this were allowed to continue, 1) the receiver tracking loop would follow the waveform and track out the code(s); or 2) interference occurs to the telemetry or command modulation. A frequency chopping modulation function can be enabled to prevent these problems. The function is defined by:

$$C = C_m \oplus C_c \qquad (14)$$

where:

C = modulation

C_m = the square-wave modulation of the component, *m*, being chopped

C_c = the square-wave modulation of the clock component

$\oplus$ = modulo 2 addition.

The chopping process results in a power spectrum for a sideband pair relative to the ranging power as follows:

$$\frac{P_k}{P_r} = 10\log\left\{8 \times \left[\frac{\tan\left(\frac{k\pi}{2^{m-n+1}}\right)}{k\pi}\right]^2\right\}, \text{dB} \qquad (15)$$

where:

P_k = the power of the *k*-th odd sideband pair (a perfect square wave will not have any even harmonics)

P_r = the total ranging power (all sidebands)

m = the component number being chopped

n =   the number of the clock (2 to 10)

k =   the odd sideband-pair number of the component being chopped.

The physical meaning of chopping can best be illustrated by Figure 7, which shows components C5, C6, and C7 being chopped by the 1-MHz clock, C4. The dotted lines indicate where the edges of the components would be without chopping. Note that C4 ⊕ C5 is the same as C5 shifted 1/4 cycle to the left. This occurs when a component is chopped by another component at twice its frequency.

In the chopping-disabled mode, no components are chopped until 1 kHz (C14) and the remaining lower frequency components (C15 to C24) are reached. The chopping component must be of the same or lower frequency than the clock component, and it should be no lower than 16 kHz (C10). The chopping function is handled by the ranging default software and can be overridden by directive if necessary.

2.3.7   *Other Parameters*

There are four other parameters that must also be specified for ranging operations. Their meaning and usage are briefly summarized below.

2.3.7.1   *Tolerance*

Tolerance is used to set the acceptable limit of the FOM — an estimate of the goodness of an acquisition, based on the P_r/N_0 measurement (see Paragraph 2.4.3 for additional discussion).

Tolerance may be selected over the range of 0.0% to 100.0%. As an example, if the tolerance is set to 0.0%, all range acquisitions will be declared valid. Alternately, if the tolerance is set to 100.0%, all range acquisitions will be declared invalid. A typical value set for tolerance is 99.9%. This value will flag acquisitions that have a 99.9% or better chance of being good as valid, and the rest as invalid.

An acquisition is declared valid or invalid depending upon the following criteria:

FOM ≥ Tolerance   *results in*   Acquisition declared valid

FOM < Tolerance   *results in*   Acquisition delcared invalid.

2.3.7.2   *Servo*

Servo is used to correct distortions of the data due to charged particle effect using DRVID information (See Paragraph 2.4.3 for a discussion of DRVID). When Servo is enabled, the local Doppler-corrected components will be shifted back into phase with the received components. The correction is made by setting a proper Servo value.
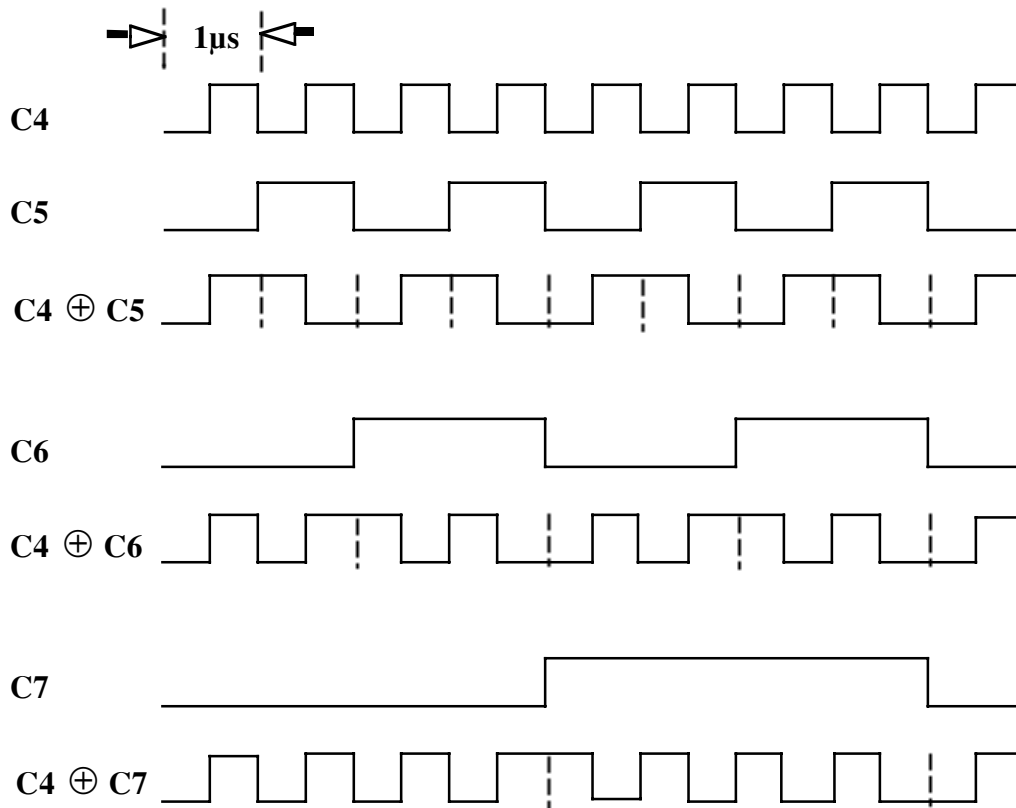
Figure 7. Chopping of C5, C6, and C7 (by C4)

Servo has a value between 0 and 1.0. It should be set to 1.0 with a noiseless signal, but if the noise level is too high, no DRVID refinement is possible and Servo should be set to 0. Note that if Servo is 1.0, the correction is made immediately; however, if Servo is set to a fractional value between 0 and 1.0, that fraction of the correction will be done on any one DRVID measurement.

2.3.7.3 Pipe

The *Pipe* parameter (for pipelining) specifies the number of range acquisitions to be made. This parameter enables multiple measurements to be initiated before the first measurement is completed. Only one acquisition is made if Pipe is disabled. If it is enabled, range measurements will be made until the total number of acquisitions reaches $(2^{15} - 1)$ or until the specified number of acquisitions. In other words, the number of range acquisitions that can be performed is between 1 and $(2^{15} - 1)$.

2.4　　　　　*Range Measurement Process*

The URA uses a reference frequency (denoted by F_{66} in this document) from the exciter to generate a sequence of square waves (or binary codes). This code sequence is phase-modulated onto the uplink carrier beginning at the transmit time. The measurement process begins at T_0 which is between 0 and 1 second before this signal is received by the RRP, one RTLT later.

The RRP contains an identical coder that is driven by a reference frequency (denoted by F_{RNG} in this document) that is derived from the received carrier frequency but scaled to the corresponding uplink frequency as discussed in paragraph 2.2. Thus, the receiver coder is able to provide a code sequence that includes compensation for the frequency shift introduced by Earth-spacecraft relative Doppler.

At T_0, the first (clock) component from the reciever coder is correlated against the received signal to produce the correlation values V_I and V_Q. The V_I s and V_Q s are used to compute the angle and amplitude of the received code; hence, the phase and signal strength are determined. The following paragraphs provide further detail.

The measurement of the phase (angle) displacement of the clock provides the resolving capability of the range measurement (See Table 1). Once the phase displacement is determined, the receiver coder is shifted by this displacement amount to produce a zero-phase shift in the in-phase channel. Since the remaining components are phase-coherent with the clock component, it is only necessary to determine if each component is in or out of phase with the previous component. This is done by integrating the V_I s and V_Q s for the time T_2 specified during initialization. If each component is in phase, no action is necessary; if one is out of phase, that component and the remaining components are shifted by half its period. This process is repeated for each component. The sum of the required shifts (plus the clock-phase shift) is the phase delay between the transmitted and received signals, and the range is determined. The process is illustrated in Figure 8.

2.4.1　　　　　*Range Measurement Technique*

The RRP measures two-way range, that is, the RTLT, by determining the phase difference between the transmitted and received modulation. This phase displacement (τ) is computed by the following expressions:

Sine-wave ranging:

$$\tau = \text{atan2}\left(\sum V_Q, \sum V_I\right), \text{radians} \tag{16}$$

Square-wave ranging:

$$\tau = \text{SGN}\left(\sum V_Q\right) \times \frac{1}{4} \times \left(1 - \frac{\sum V_I}{\left|\sum V_Q\right| + \sum V_I}\right), \text{cycles.} \tag{17}$$
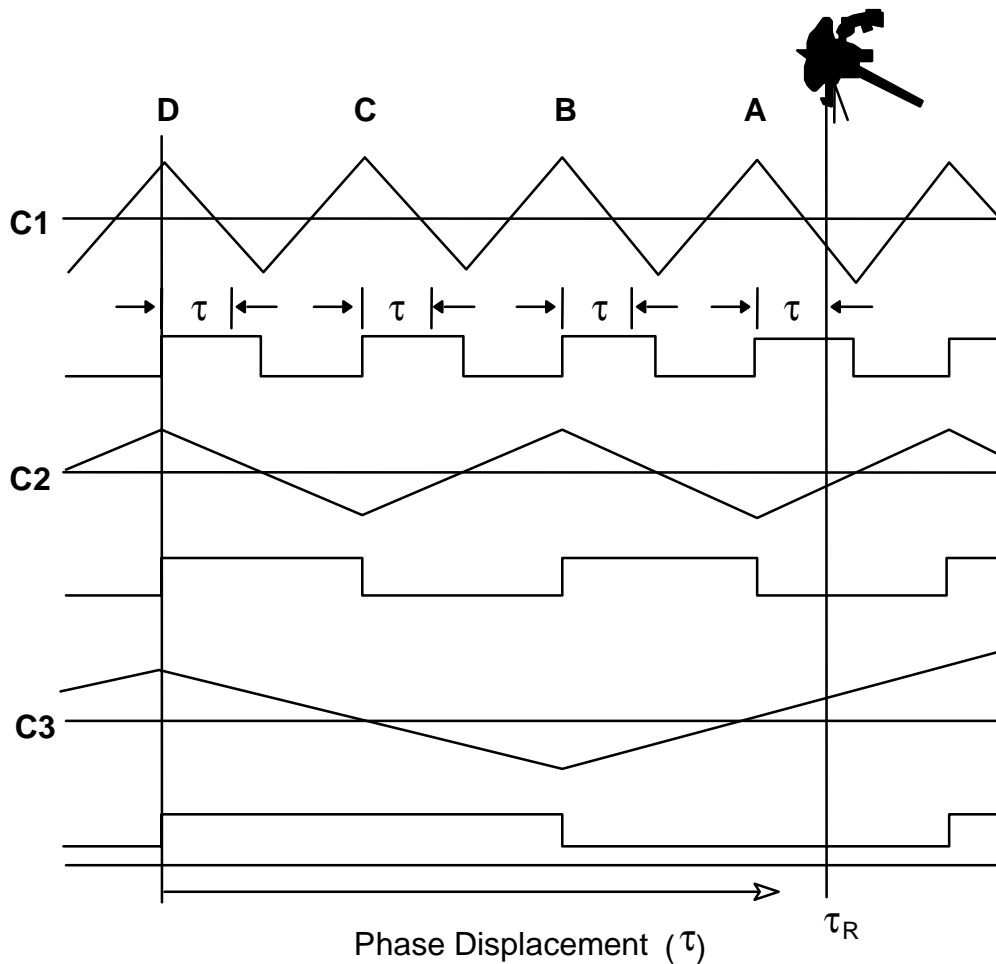
Figure 8. Component Acquisition Process

Notes:

1. Assume that the range to the spacecraft results in $\tau = \tau_R$ and that the range uncertainty is in the interval defined by C2 and C3.

2. Measurement of the phase offset of C1 indicates that the correlation amplitude is not at a peak value. The receiver coder is shifted (delayed) to bring the correlation value to a positive peak, A.

3. At A, the correlation function for C2 is at a negative peak; thus C2 is out of phase. The reference code is shifted by half the period of C2 (to bring it into phase), arriving at B.

4. At B, C3 is out of phase with C2. The reference code is shifted by half the period of C3, arriving at D.

5. The sum of the phase shifts required to bring all components into phase is τ_R, the range measurement.

where

$$V_I \text{ and } V_Q \quad = \quad \text{the in-phase and quadrature correlation values}$$

$$\text{atan2(y,x)} = \quad \text{the arctangent function that produces an angle in the proper quadrant}$$

$$\text{SGN}(*) \quad = \quad \begin{vmatrix} +1, & * \geq 0 \\ -1, & * < 0. \end{vmatrix}$$

For ranging operations, the above τ of different dimensions are converted to a measurement unit called the range units (RU). RUs have the dimension of seconds and are defined as 1/16 of the period of the reference frequency, that is

$$RU = \frac{1}{16} \times \frac{1}{F_{66}}, \text{ s} \tag{18}$$

where F_{66} is the reference frequency, F_{66S} or F_{66X} as discussed earlier.

Using the above RU equation, one may convert the measurement obtained in RUs to physical quantities such as time (nanoseconds) and distance (meters). For example, if the F_{66} used in a range measurement is 66.000 MHz and suppose the measurement obtained is 6,500,000 RU, then the equivalent RTLT delay is 6.155 ms, and the one-way distance is about 923,295 m.

2.4.2 P_r/N_0

The actual ranging power-to-noise spectral density (P_r/N_0) is evaluated at the end of the integration of all in-phase and quadrature correlation values for the clock. It combines ranging system performance with receiver noise. This ratio is given by:

$$P_r\!\big/\!N_0 = 10 \log\left(\frac{\text{Ranging Signal Power} \left(P_s\right)}{\text{Noise Power}\left(P_n\right)} \times \text{Bandwidth}\left(\text{BW}\right) \right), \text{ dB} \tag{19}$$

where, depending on a ranging operation, P_s is evaluated by two different expressions.

Sine-wave operation:

$$P_s = \frac{\left(\sum_1^N V_I\right)^2 + \left(\sum_1^N V_Q\right)^2}{N^2}, \tag{20}$$

24

Square-wave operation:

$$P_s = \frac{\left(\left| \sum_1^N V_I \right| + \left| \sum_1^N V_Q \right| \right)^2}{N^2} \tag{21}$$

where:

V_I and V_Q are the correlation values.

N is the total number of samples collected during the clock acquisition.

Noise power is estimated by adding the variances of the in-phase and quadrature correlation samples:

$$P_n = \text{Var}_I + \text{Var}_Q , \tag{22}$$

where:

Var_x is the variance function:

$$\text{Var}_x = \frac{\sum_1^N \left(x^2 \right)}{N} - \frac{\left(\sum_1^N (x) \right)^2}{N^2} \tag{23}$$

where:

x represents the correlation sample V_I s and V_Q s

N is the number of samples.

Finally, because $P_n = N_0 \times$ the process bandwith of the RRP, it is necessary to multiply P_s/P_n by the process bandwidth (1 Hz) to put it in the form of P_r/N_0.

2.4.2 *Figure of Merit*

The FOM is a probability measure which estimates the chance of successful acquisition of all lower frequency codes. The probability of making at least one error in acquiring these codes is:

$$P_e = 1 - \left[\frac{1}{2} + \frac{1}{2} \text{Erf} \left(\sqrt{\frac{P_r}{N_0} \times T_2} \right) \right]^{n-1} \tag{24}$$

where:

n = the number of components including the clock.

Erf($*$) = the error function.

P_r/N_0 = the ranging power-to-noise ratio.

T_2 = the integration time for each of the lower frequency components, s.

Therefore, the probability P_c of getting all correct measurements is:

$$P_c = 1 - P_e \tag{25}$$

$$\text{FOM} = 100 \times P_c, \text{ percent.} \tag{26}$$

The FOM is calculated following the clock phase measurement using the measured P_r/N_0, the integration time T_2, and the number of lower-frequency components. The FOM is a valid estimate only if conditions do not change. It provides a reference by which a user may judge the validity of a range measurement. Figures 9 to 11 show P_c versus P_r/N_0 for various values of T_2 and n.
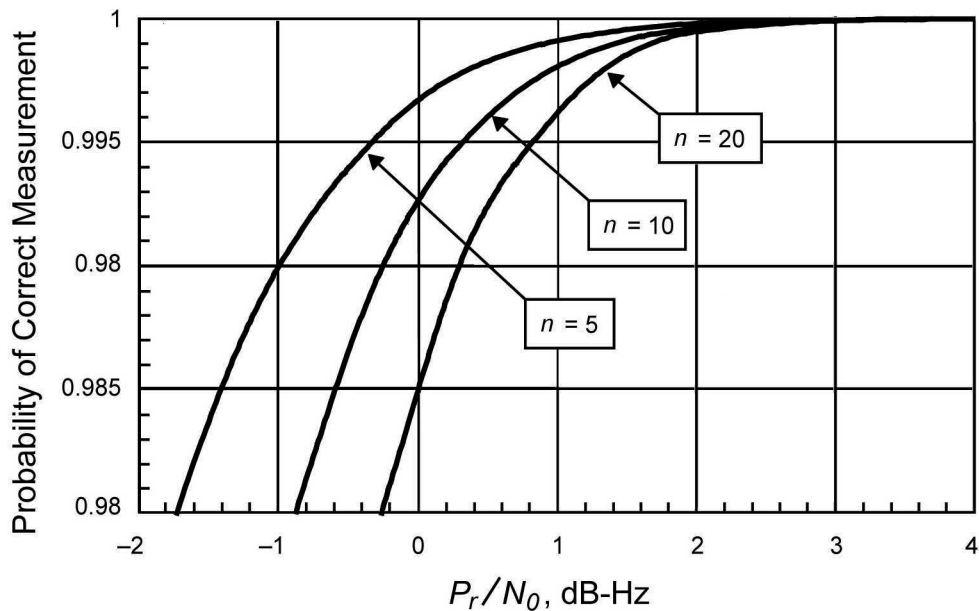
Figure 9. Figure of Merit, with $T_2 = 5$ sec for Various Frequency Components.
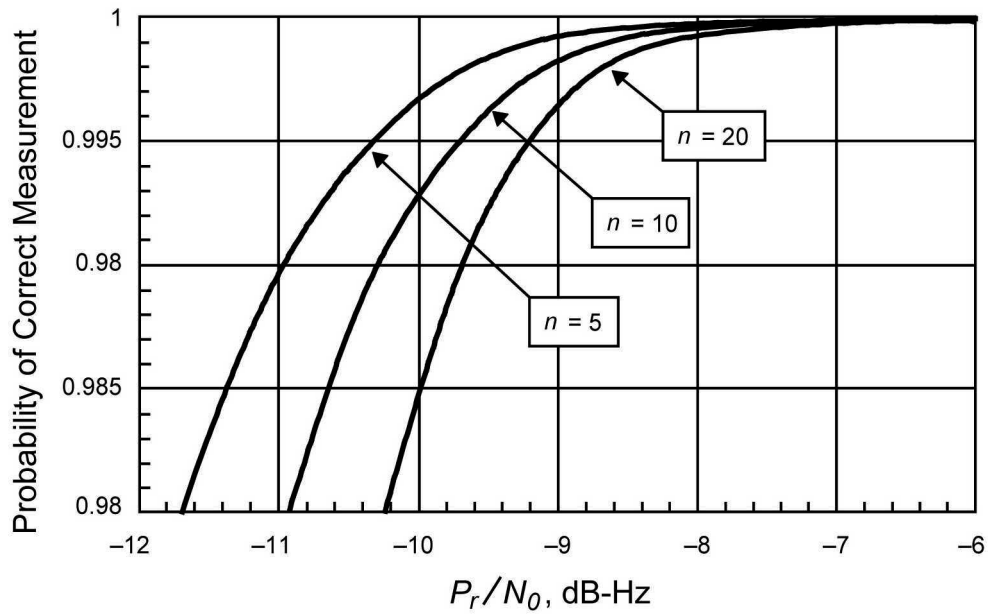
Figure 10. Figure of Merit, with $T_2 = 50$ sec for Various Frequency Components.
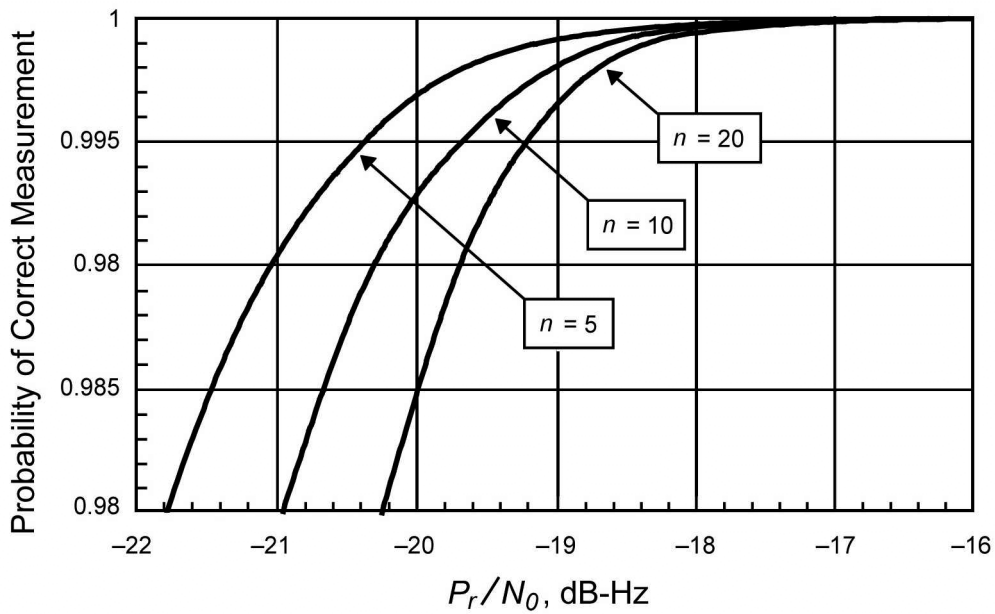
Figure 11. Figure of Merit, with $T_2 = 500$ s for Various Frequency Components.

2.4.3 *Differenced Range Versus Integrated Doppler*

Differenced range versus integrated Doppler (DRVID) may be used to calibrate the range observable and to study the electron content in the transmission medium. For a given range observable, charged particles have the effect of making the spacecraft appear further than its actual distance. As the signal propagates through the charged-particle medium, the phase velocity of the carrier increases by a certain quantity, while the group velocity of the range code decreases by exactly the same quantity.

In the NSP era, DRVID is calculated from tracking data containing the observed differences between the range measurements affected by the range-code group velocity, and the delta range measurements derived from the Doppler measurements influenced by the carrier-phase velocity. A more proper term for this quantity is pseudo-DRVID (PDRVID); however, the traditional name will be used in this article.

$$
\begin{aligned}
\mathrm{DRVID}(t) = &\{[\Phi_u(t) - \Phi_d(t)] - [\Phi_u(t - T_{cycle}) - \Phi_d(t - T_{cycle})]\} \\
&- 16 * \{r_1 * [\Theta_u(t) - \Theta_u(t - T_{cycle})] \\
&- r_2 * [\Theta_d(t) - \Theta_d(t - T_{cycle})]\} \bmod range\ ambiguity
\end{aligned}
\tag{27}
$$

where

$\Phi_u(t)$ = uplink range phase, s

$\Phi_d(t)$ = downlink range phase, s

$\Theta_u(t)$ = uplink carrier phase, RU

$\Theta_d(t)$ = downlink carrier phase, RU

T_{cycle} = anging cycle time, s

r_1 = exciter reference frequency/carrier frequency ratio
(either $1/32$ or $221/(749 \times 32)$ — see Paragraph 2.3)

r_2 = transponder turnaround ratio.

2.5 *Ratio of Downlink Ranging Power to Total Power*

For the type of currently used turn-around ranging channel, the ratio of power in the fundamental ranging sidebands to the total signal power in the downlink is a function of the uplink ranging signal-to-noise ratio. The P_r/P_t ratio for two-way ranging is given as:

$$
\left[\frac{P_r}{P_t}\right]_{DN} = 2J_1^2\left[\sqrt{2} \cdot \theta_{DN}\sqrt{\frac{\Gamma_{RNG/UP}}{1 + \Gamma_{RNG/UP}}}\right] \cdot \exp\left[-\frac{\theta_{DN}^2}{1 + \Gamma_{RNG/UP}}\right]
\tag{28}
$$

where:

$$\left[\frac{P_r}{P_t}\right]_{DN} = \text{the ratio of power in fundamental ranging sidebands to total signal power for downlink}$$

$$J_1^2[*] = \text{the Bessel function of the first kind of order one}$$

$$\theta_{DN} = \text{the downlink ranging modulation index, radians rms}$$

$$\Gamma_{RNG/UP} = \text{the uplink ranging signal-to-noise ratio at the output of the transponder's ranging channel filter, given by:}$$

$$\Gamma_{RNG/UP} = \frac{8}{\pi^2}\left[\frac{P_r}{N_0}\right]_{UP} \cdot \frac{1}{B_{RNG}} \tag{29}$$

where:

$$\left[\frac{P_r}{N_0}\right]_{UP} = \text{the ranging power to noise spectral density ratio at input to the transponder's ranging channel filter, Hz}$$

$$B_{RNG} = \text{the transponder's ranging channel filter bandwidth, Hz.}$$
A typical value for B_{RNG} is 1.5 MHz.

Figure 12 is a plot of equation 28, with $\left[\dfrac{P_r}{P_t}\right]_{DN}$ versus $\Gamma_{RNG/UP}$ for selected

values of θ_{DN}. For deep space missions, the uplink ranging signal-to-noise ratio is usually quite small, and the operating point lies on the steep curve on the left side of Figure 12. In this case, equation 28 may be approximated as follows:

$$\left[\frac{P_r}{P_t}\right]_{DN} \approx \Gamma_{RNG/UP}\,\theta_{DN}^2\,\exp(-\theta_{DN}^2),\ \Gamma_{RNG/UP} \ll 1. \tag{30}$$
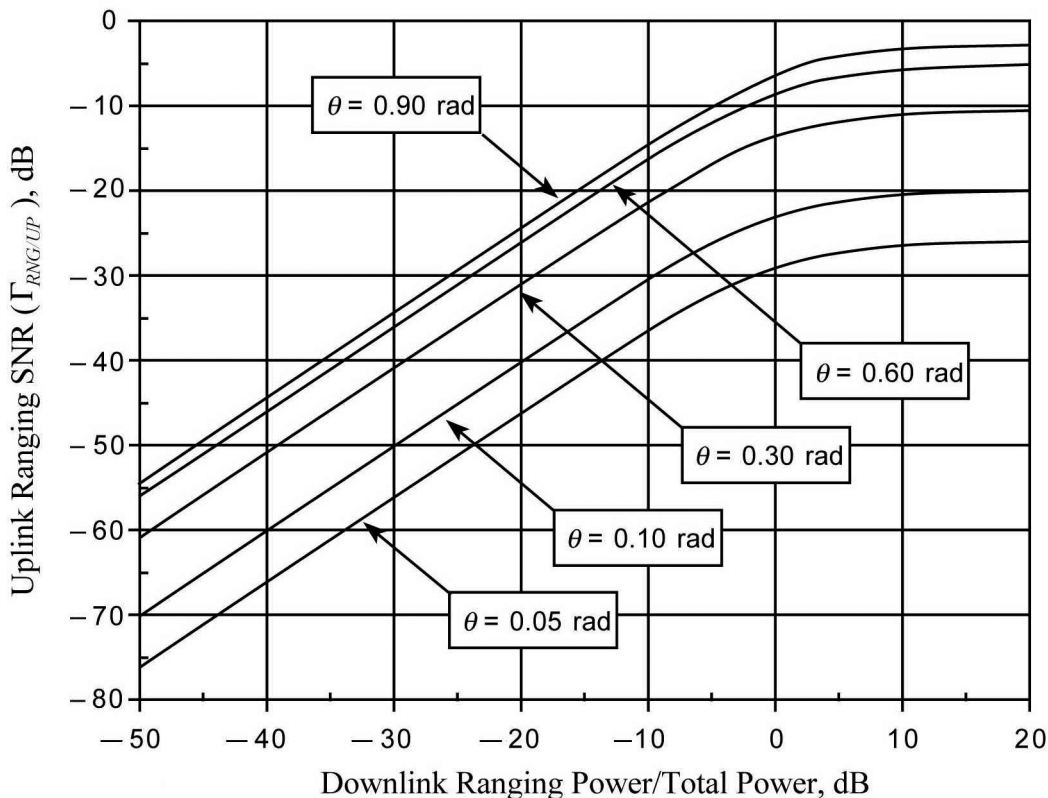
Figure 12. P_r/P_t as a Function of $\Gamma_{RNG/DN}$ for Selected Values of Modulation Index θ_{DN}

The presence of uplink noise feeding through onto the downlink has two effects on ranging performance: loss of ranging power and interference. Noise affects the ranging performance by dissipating valuable downlink power from the fundamental ranging signal sidebands. This is characterized by the above expressions for $[P_r/P_t]_{DN}$. Alternately, the potential exists for noise to interfere with the fundamental ranging sidebands, causing degradation to the ranging signal by raising its noise floor. For most deep space missions, the latter effect is not considered to cause significant degradation for two-way ranging measurements.

2.6   Range Corrections

The DTT range measurements include delays of equipment within the DSS as well as those of the spacecraft. These delays must be removed in order to determine the actual range referenced to some designated location at the antenna. Figure 13 illustrates the end-to-end range measurement and identifies the delays that must be removed before an accurate topocentric range can be established. The DSN is responsible for providing three measurements to the project. They are the DSS delay, the Z-correction, and the antenna correction.
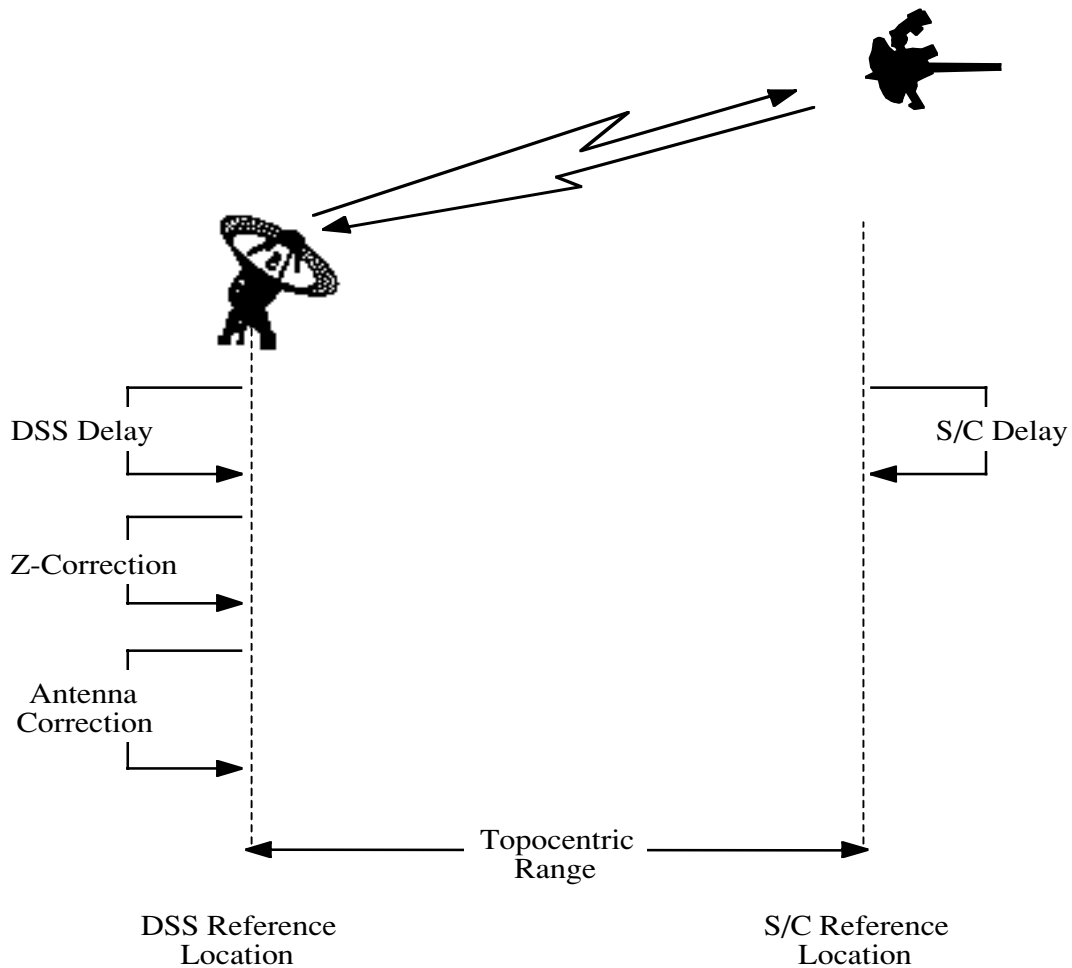
Figure 13. DSN Range Measurement

2.6.1 *DSS Delay*

The DSS delay is station and configuration dependent. It should be measured for every ranging pass. This measurement is called precal for pre-track calibration and postcal for post-track calibration. The former is done at the beginning of a ranging pass; the latter is only needed when there is a change in equipment configuration during the track or precal was not performed due to a lack of time.

The delay is measured by a test configuration, which approximates the actual ranging configuration. The signal is transmitted to the sky; however, before reaching the feedhorn, a sample is diverted to a test translator through a range calibration coupler. The test translator shifts the signal to the downlink frequency, which is fed into the coupler. The signal flows through the LNA to the DTT for calibration.

Figure 14 shows the signal path for a typical calibration of DSS delay when the uplink and downlink are in the same frequency band. The heavy lines identify the calibration path. When the uplink and downlink are in different bands, the downlink signal from the test translator is coupled into the receive path ahead of the LNA and as close to the feed as practical.

2.6.2   Z-Correction

The delay in the microwave components ahead of the coupler and the airpath (the distance from the horn aperture plane to the subreflector, to the antenna aperture plane, and finally to the antenna reference location) must be included in the calibration. Also, the translator delay must be removed. A measurement called "Z-correction" is made to obtain an adjusted DSS delay.

The Z-correction is given by the difference of two quantities: the translator delay and the microwave plus air path delay. Figure 15 relates these quantities to the physical structure of the antenna.

The test translator delay is measured by installing a zero delay device (ZDD) in place of the test translator. Since the ZDD delay is measured in the laboratory, the signal delay contributed by the test translator can be calculated to a known precision. This measurement is made approximately twice a year or when there are hardware changes in the signal path.

The microwave and air path delays are measured by physically calibrating the microwave hardware components prior to installing them on the antenna. The antenna aperture plane, the horn aperture plane, and an antenna reference location are used to determine the actual air path delay as shown in Figure 14. The antenna reference location is the perpendicular intersection of the primary antenna axis with the plane of the secondary axis. Geocentric and geodetic locations for the antenna reference location can be found in module 301.

2.6.3   Antenna Correction

An antenna correction is required when the antenna reference location is not at a fixed location with respect to the Earth. Because the NSP ranging equipment only is being installed at Azimuth-Elevation (Az-El) antennas that have a fixed reference location, no antenna correction is required. The antenna correction for the 26-m subnet antennas is described in Appendix A.
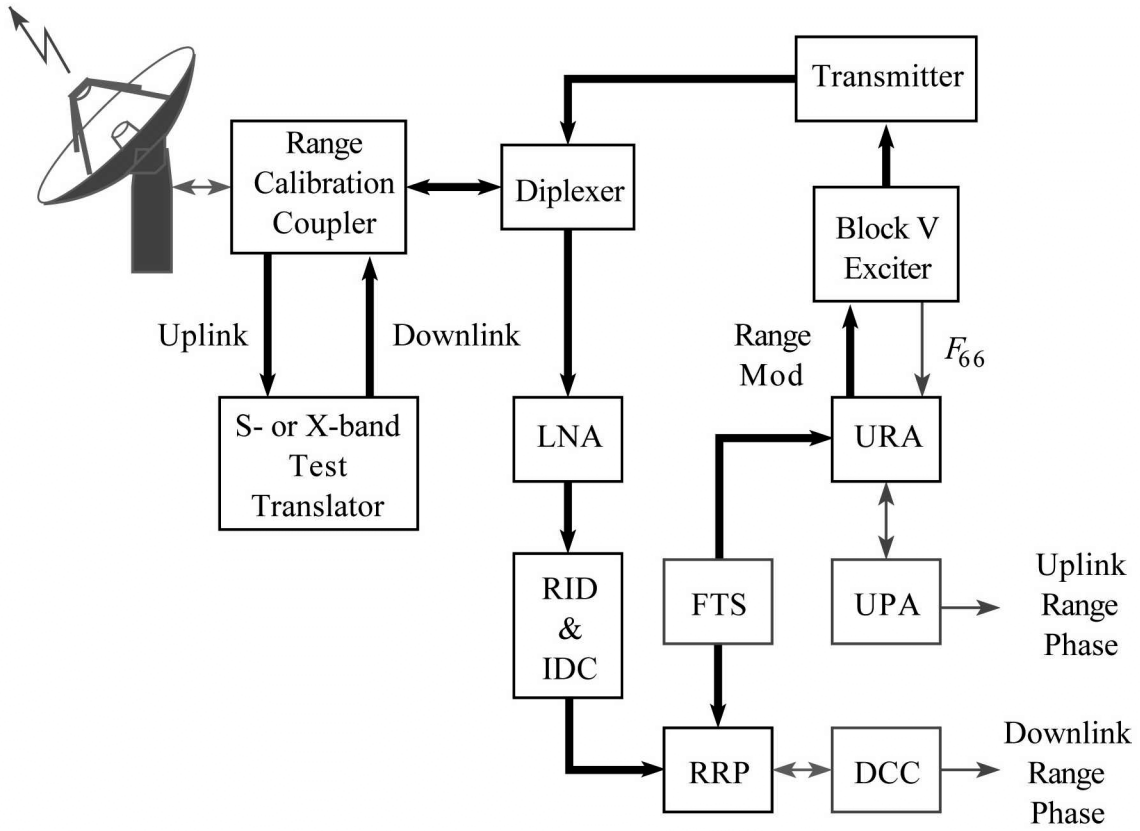
Figure 14. Typical DSS Delay Calibration

1. DSS Delay (measured pre-pass or post-pass) includes additional delay of Test Translator and cables between Test Translator and the Ranging Coupler.

2. Zero-Delay Device (ZDD) is precision test equipment used periodically to measure the delay at the Ranging Coupler and the aperture plane. However, the aperture plane is closer to a spacecraft by the delay from the reference height (T_A).

3. Z-height correction is the total round-trip delay from the Ranging Coupler to the aperture plane (heavy gray line) reduced by the calculated round-trip delay between the aperture plane and the reference height and the measured delay from the Ranging Coupler through the Test Translator.

Figure 15. Measuring the Z-Correction

2.7 *Error Contributions*

The ground system, the media, and the spacecraft contribute errors to range measurements. The error contributions of the media and spacecraft are outside the scope of this document and have not been included.

The round-trip one-sigma delay error of the DSN ranging system over a ranging pass has been estimated for the X-band system as 6.3 nanoseconds (about 0.95 meter one-way). The S-band one-sigma delay error has been estimated as 12.5 nanoseconds (about 1.9 meters one-way).

Table 2 provides a breakdown of long-term error contributions due to calibration and errors inherent within the equipment of the various subsystems that constitute the total ground system of the NSP-Era Ranging System.

Table 2. One-Sigma Range Error for NSP-Era Ranging System

Subsystem	X-band		S-band	
	Round-trip Delay (ns)	One-way Distance (m)	Round-trip Delay (ns)	One-way Distance (m)
FTS	1.00	0.15	1.00	0.15
Receiver	2.00	0.30	2.00	0.30
Exciter and Transmitter	1.33	0.20	5.33	0.80
Microwave and Antenna	2.33	0.35	2.33	0.35
Uplink Ranging Board	2.00	0.30	2.00	0.30
Downlink Ranging Board	2.00	0.30	2.00	0.30
Cables	1.33	0.20	1.33	0.20
Calibration	2.66	0.40	2.66	0.40
Reserve	3.33	0.50	10.0	1.50
Root Sum Square	6.33	0.95	12.47	1.87

Appendix A

The Current DSN Ranging System

The current DSN ranging equipment has the same functional characteristics as the equipment previously described but does not provide optimum performance with the newer digital receivers. It is therefore being replaced at the 70-m, the 34-m HEF, and all 34-m BWG stations except DSS 27. This appendix describes the architecture and performance of the current sequential ranging equipment in the 26-m subnet and at the 34-m HSB station, DSS 27. It also identifies the performance differences between the NSP ranging equipment and the existing ranging equipment when it is used at the 70-m, the 34-m HEF, and the 34-m BWG stations.

A1.0   System Description Using the Sequential Ranging Assembly

The DSS Tracking Subsystem (DTK) comprises two items of equipment, the sequential ranging assembly (SRA) and the metric data assembly (MDA). This equipment performs the range measurement, formats the radiometric data, and sends it to the NAV at JPL. The NAV processes and provides the data to projects. The Network Support Subsystem (NSS) provides radiometric predicts to the DTK. Figure A-1 shows the current DSN ranging system configuration.

The SRA generates a sequence of square-wave frequencies (ranging code components) that are modulated onto the uplink carrier by the exciter and transmitted to the spacecraft. The spacecraft on-board transponder receives the signal , demodulates and filters it, and remodulates it onto the downlink carrier. The downlink is captured and amplified at the DSS, downconverted by the RID, and received by either a multi-function receiver (MFR) or Block V receiver (BVR). The SRA correlates the demodulated downlink signal with a Doppler-modified replica of the transmitted codes using the same process as was described earlier.

The SRA has two hardware interfaces with the exciter. The first provides the reference frequency, F_{66}, from the exciter to the SRA. The second supplies the square-wave ranging modulation signal derived from this reference to the phase modulator in the exciter. The SRA also has two hardware interfaces with the receiver. The first carries the received ranging codes while the second provides a representation of the received Doppler. Each SRA has two receive channels so there are actually two pairs of interfaces between the SRA and the two receivers at each station. SRA channel 1 is normally used to process S-band (or receiver 1) data and channel 2 is used to process X-band (or receiver 2) data.
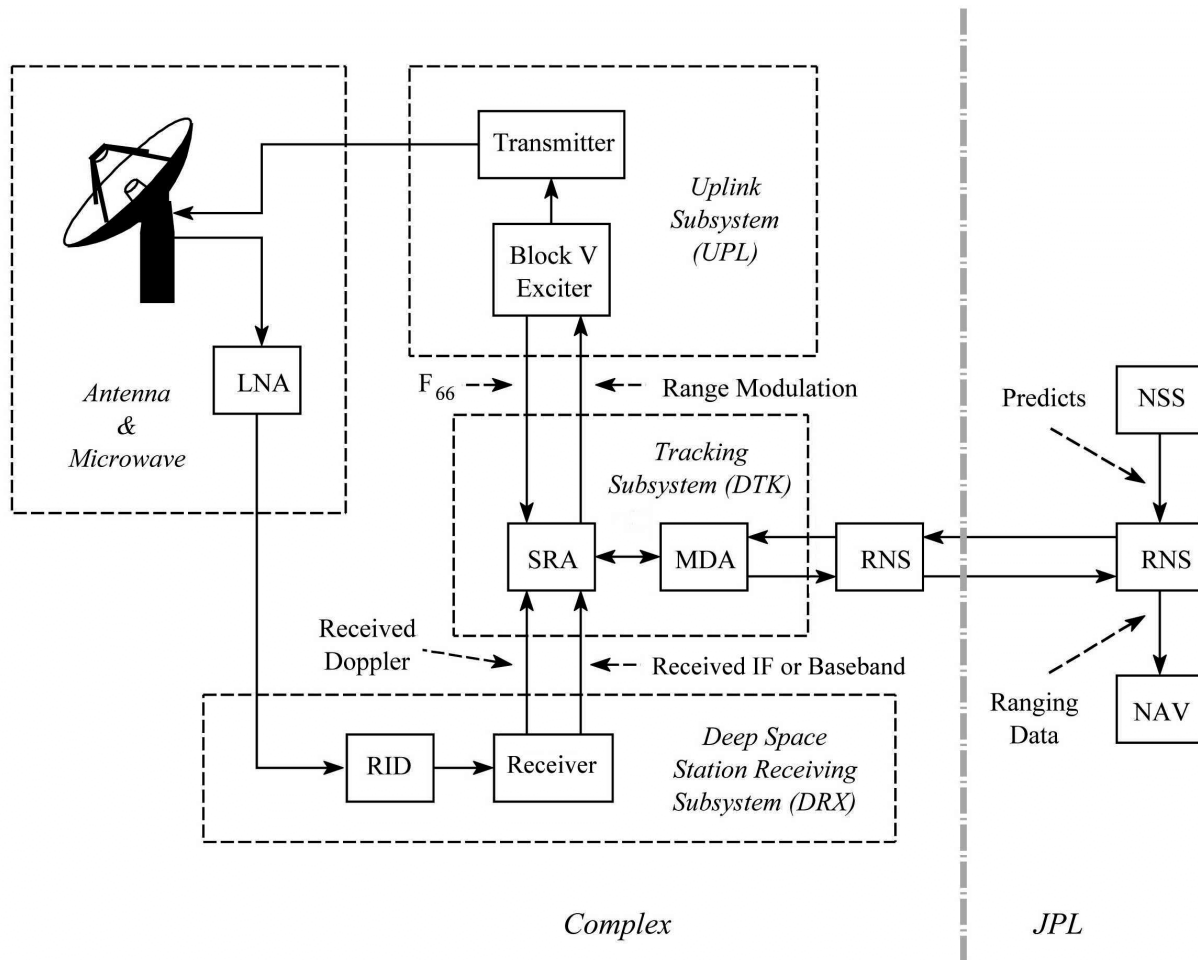
Figure A-1. Current DSN Ranging System

At the 26-m Subnet stations and the 34-m HSB antenna, the received ranging codes are provided to the SRA as a 10-MHz analog intermediate frequency (IF) from the MFR and demodulated within the SRA. At stations employing the BVR (the 70-m, the 34-m HEF, and the 34-m BWG stations), demodulation of the ranging codes are done within the receiver and the ranging baseband signal is sent to the SRA as digital data through an optical-fiber interface.

A2.0   *Range Measurement Process Using the SRA*

The SRA transmitter coder uses a reference frequency (denoted by F_{66} in this document) to generate a sequence of square waves (or binary codes). This code sequence is phase-modulated onto the uplink carrier. The measurement process begins at T_0 which is between 0 and 1 second before this signal is received by the SRA one RTLT later.

Prior to the receive time, T_0, the SRA receiver coder is referenced to the same F_{66} as the tramsnitter coder so it operates at the same frequency and phase. At T_0, a scaled Doppler reference from the tracking receiver is introduced to advance or retard the phase of the receiver coder. This has the effect of adding the frequency shift introduced by Earth-spacecraft relative Doppler to the receiver coder so the correlation can be accomplished. Having aligned the receiver coder frequency to the frequecny of the received code, the correlation to determine the phase of the received code proceeds by the same process described in paragraph 2.4.

A3.0 Performance Differences

The performance of the SRA and the NSP-era ranging are slightly different because of improvements incorporated into the new equipment and interface incompatabilitese between the SRA and digital receivers in 70-m, the 34-m HEF, and the 34-m BWG stations and the SRA. The following paragraphs summarize these differences.

A3.1 Integration Times

The SRA requires specification of the same three integration times as discussed in paragraph 2.3.4; however, their calculation and recommendations for selecting values are somewhat different.

A3.1.1 T_1

T_1, the total time used to integrate the correlation samples for the clock component, is calculated by the equations provided in paragraph 2.3.4.1 with different constants. The modified expressions are:

Sine-wave operation:

$$T_1 = \frac{1}{56} \times \frac{1}{F_c^2} \times \frac{1}{\sigma^2(t)} \times \frac{1}{P_r / N_o}, \text{ s} \qquad (A-1)$$

Square-wave operation:

$$T_1 = \frac{8}{343} \times \frac{1}{F_c^2} \times \frac{1}{\sigma^2(t)} \times \frac{1}{P_r / N_o}, \text{ s} \qquad (A-2)$$

where

F_c = the clock frequency, Hz

$\sigma^2(t)$ = the desired variance of the RTLT measurements, s^2

P_r/N_o = the ranging signal to noise spectral density, Hz.

The above equations can be rewritten in terms of the uncertainty $\sigma(r)$ in meters, by multiplying the uncertainty $\sigma(t)$ in seconds by the speed of light and dividing by a factor of 2. This provides:

Sine-wave operation:

$$\sigma(r) = \sqrt{\frac{402}{F_c^2(\text{MHz}) \times T_1 \times \dfrac{P_r}{N_o}}}\ ,\ \text{m} \tag{A-3}$$

Square-wave operation:

$$\sigma(r) = \sqrt{\frac{523}{F_c^2(\text{MHz}) \times T_1 \times \dfrac{P_r}{N_o}}}\ ,\ \text{m} \tag{A-4}$$

where:

F_c = the clock frequency, MHz

T_1 = the clock component integration time, s

P_r/N_O = the ranging signal to noise spectral density, Hz.

Note: The uncertainty σ here is only due to thermal noise. Other errors must be added to this to get the total uncertainty (see paragraph A5.0).

Figure A-2 plots integration time (T_1) as a function of P_r/N_O with $\sigma(r)$ as a parameter for the SRA usning sine-wave operation and a 1-MHz clock component. For a desired $\sigma(r)$, the user may find the proper integration time, T_1, for an estimated P_r/N_O (in dB-Hz). Figure A-3 is a similar graph for square-wave operation using a 500-kHz clock component. This figure may also be used for lower frequency square-wave clocks by recognizing that dividing F_c by 2 will result in T_1, being multiplied by 4, etc.

Ranging is possible as long as the receiver remains in lock over the measurement time. However, there is a practical lower limit for P_r/N_O (usually about -10 dB-Hz) determined by the combination of integration times (cycle time) and the minimum number of range points needed by the project. See Cycle Time in Paragraph 2.3.4.4 for further details. A P_r/N_O of -10 dB-Hz is also the recommended limit when the SRA is used with the Block V Receiver because of inefficiencies in the interface between the two pieces of equipment.

A3.1.2   *T_2*

T_2, the integration time for each of the lower frequency components, is calculated by the equation provided in paragraph 2.3.4.2 (equation 9). The figures provided there are repeated as figures A-4 through A-6 to emphasize the recommendation that the SRA should not be operated at a P_r/N_O of less than –10 dB-Hz when using the Block V Receiver.

A3.1.3   *T_3*

T_2, the integration time for DRVID measurements, is selected by the same reasoning discussed in paragraph 2.3.4.3 and is usually set at $7/8 \times T_1$, rounded to the nearest integer.

A3.2   *Other SRA Ranging Parameters*

The other SRA ranging parameters are the same as required by NSP-era ranging. This includes modulation index (paragraph 2.3.5), frequency chopping (paragraph 2.3.6), tolerance (paragraph 2.3.7.1), servo (paragraph 2.3.7.2), and pipe (paragraph 2.3.7.3).

A3.3   *SRA Calculations*

A3.3.1   *Cycle Time*

The cycle time calculated by the SRA uses the same algorithm as the NSP-era ranging discussed in paragraph 2.3.4.3.

A3.3.2   *P_r/N_o*

The actual ranging power-to-noise spectral density (P_r/N_0) is evaluated at the end of the integration of all in-phase and quadrature correlation values for the clock by the same proces that was described in paragraph 2.4.2. However, the process bandwidth of the SRA is 5 Hz as P_r/N_0 is evaluated using pairs of 0.1-second long correlation samples. Therefore, it is necessary to multiply P_n by the reciprocal of 2×0.1 s, or 5 Hz, in order to put it in the form of P_r/N_0.
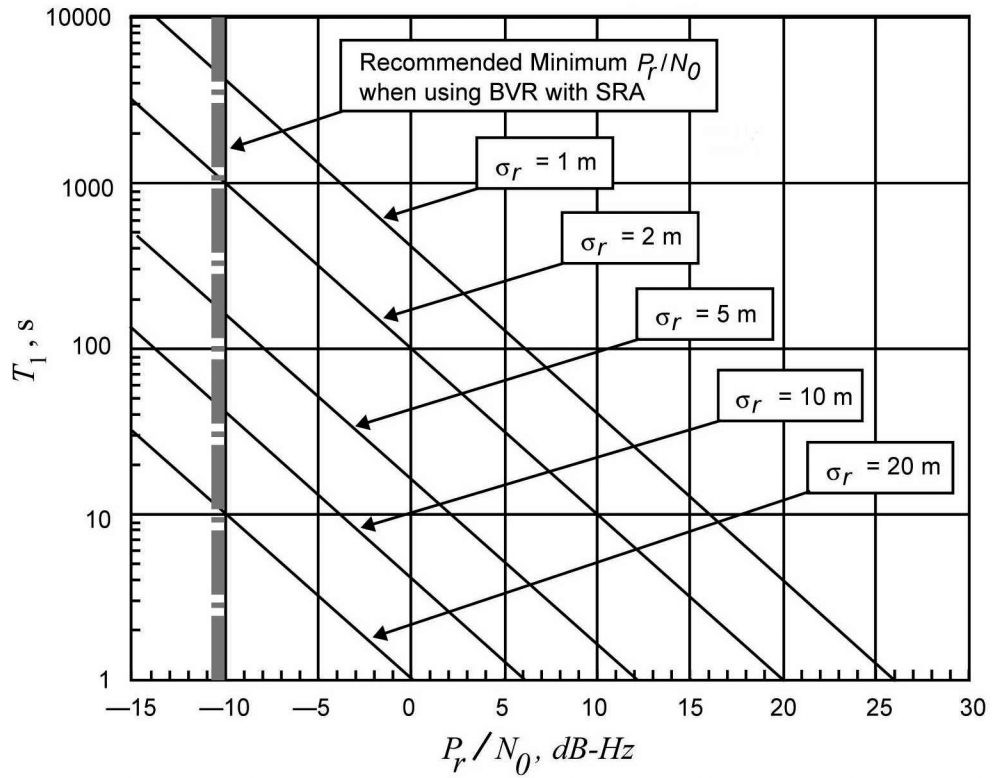
Figure A-2. Integration Time T_1 Versus P_r/N_o, Clock Frequency F_c = 1 MHz, for Sine-Wave Ranging Using the SRA
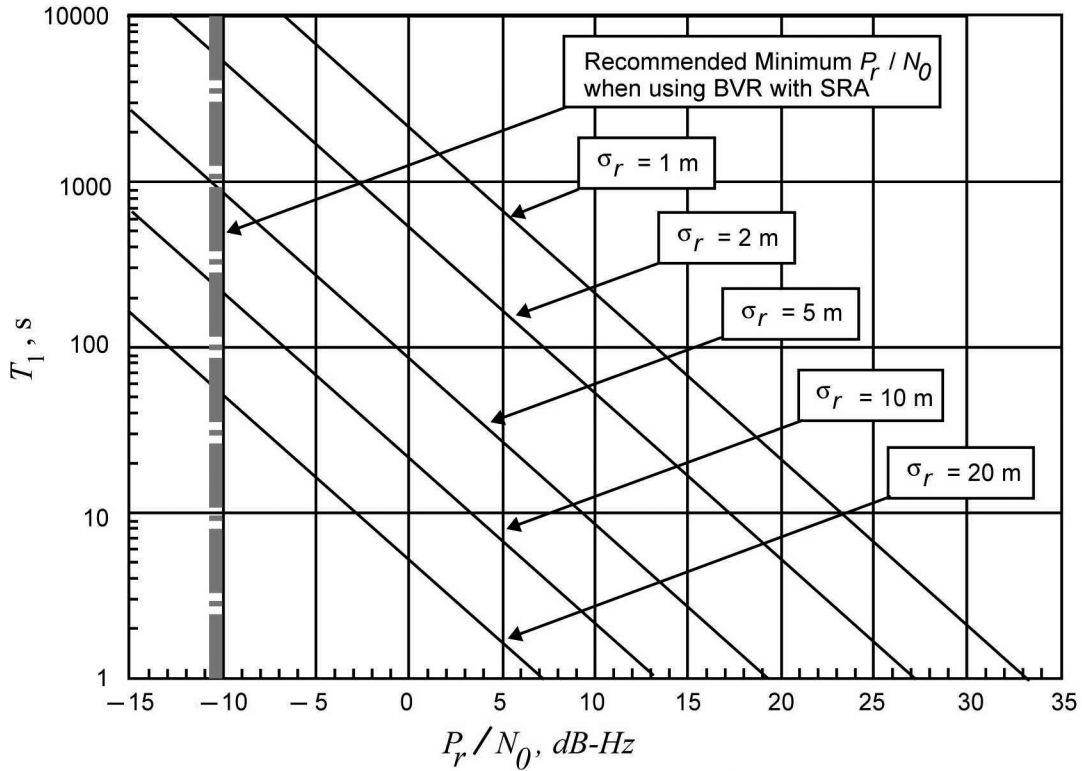
Figure A-3. Integration Time T_1 Versus P_r/N_O, Clock Frequency F_c = 500 kHz, for Square-Wave Ranging Using the SRA
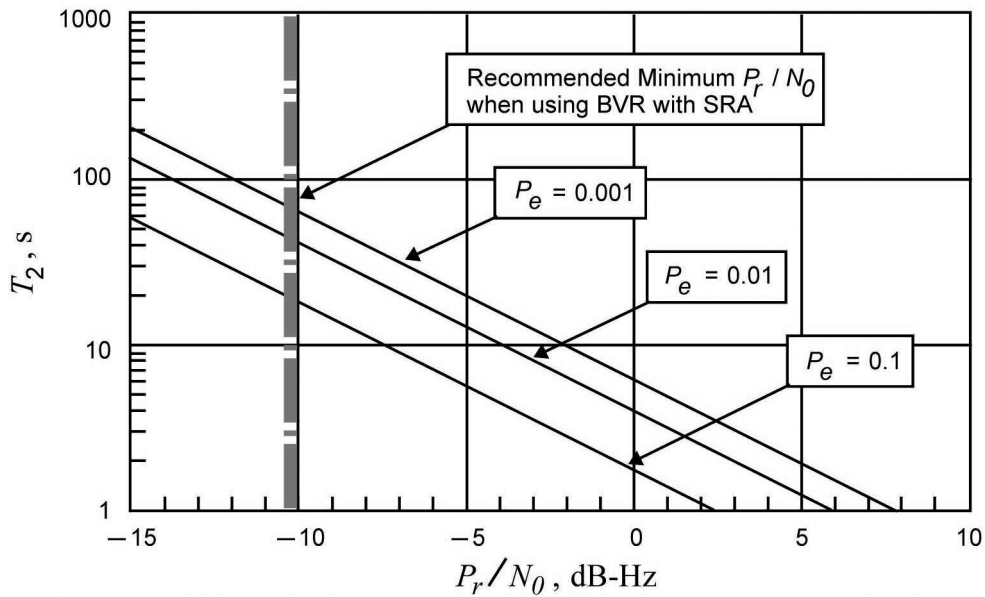
Figure A-4. Code Component Integration Time T_1 Versus P_r/N_O for Various Probabilities of Error and $n = 5$
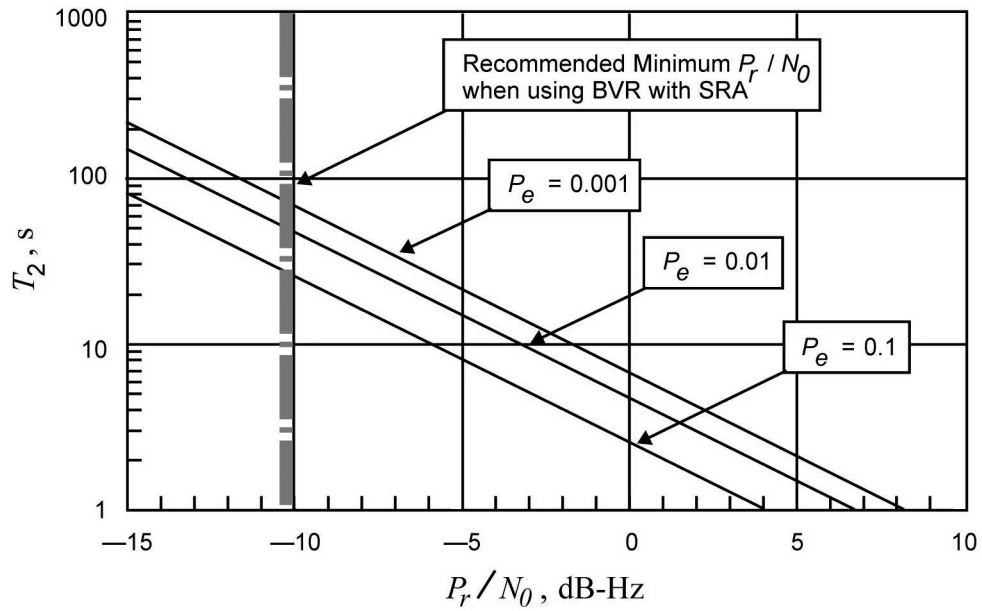
Figure A-5. Code Component Integration Time T_1 Versus P_r/N_o for Various Probabilities of Error and $n = 10$
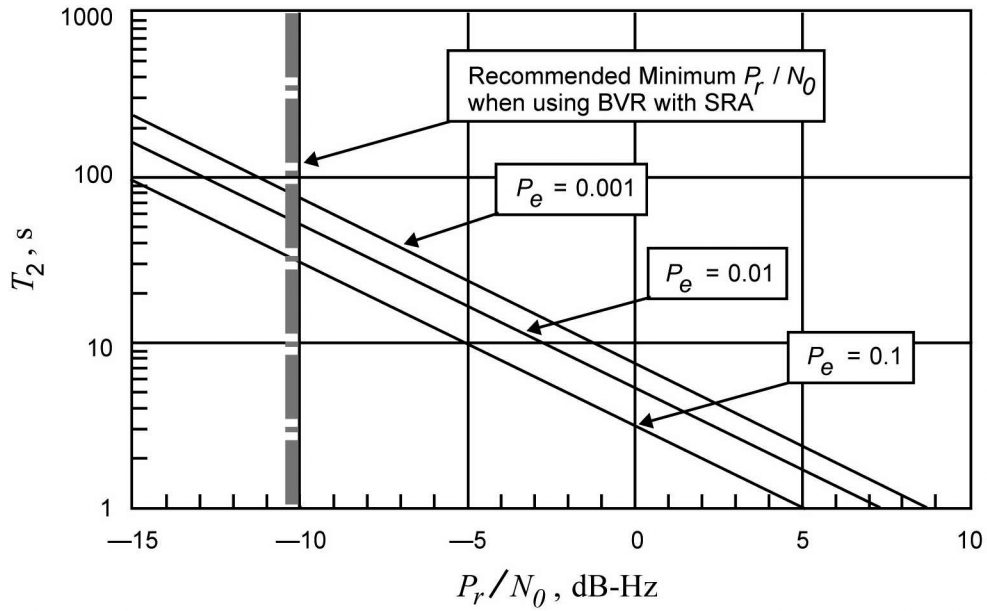
Figure A-6. Code Component Integration Time T_1 Versus P_r/N_o for Various Probabilities of Error and $n = 20$

A4.0   Range Corrections Using the SRA

The following paragraphs discuss the DSS delay and antenna calibration when using the SRA. The Z-correction (paragraph 2.6.2) is the same for both types of ranging equipment.

A4.1   DSS Delay

The DSS Delay is measured by the same technique as discussed in paragraph 2.6.1; however, calibration path is different and is illustrated in Figure A-7. This figure assumes the uplink and downlink signals are in the same frequency band. When the uplink and downlink are at different frequencies, the downlink signal from the Test Translator is coupled into the receive path ahead of the LNA and as close to the feed as practical.

A4.2   Antenna Calibration

There are two types of structurally different antennas in the DSN. They are the Azimuth-Elevation (Az-El) mount, and the X-Y mount. The first type has an azimuth axis that perpendicularly intersects the elevation axis with the result being that the antenna correction is equal to zero. The DSN 70-m, 34-m HEF, 34-m BWG, and 34-m HSB antennas are of this type.

The X-Y antennas of the 26-m subnet have a primary axis and a secondary axis that are offset from each other. This offset causes the secondary axis (the Y-axis) to move relative to the Earth as the antenna rotates and adjusts its elevation about the primary axis (the X-axis). The change of distance is calculated by the following antenna correction expression:

$$\Delta\rho_A = -6.706\cos\theta \text{, m} \tag{A-5}$$

where

θ =   the angle of the Y-axis.
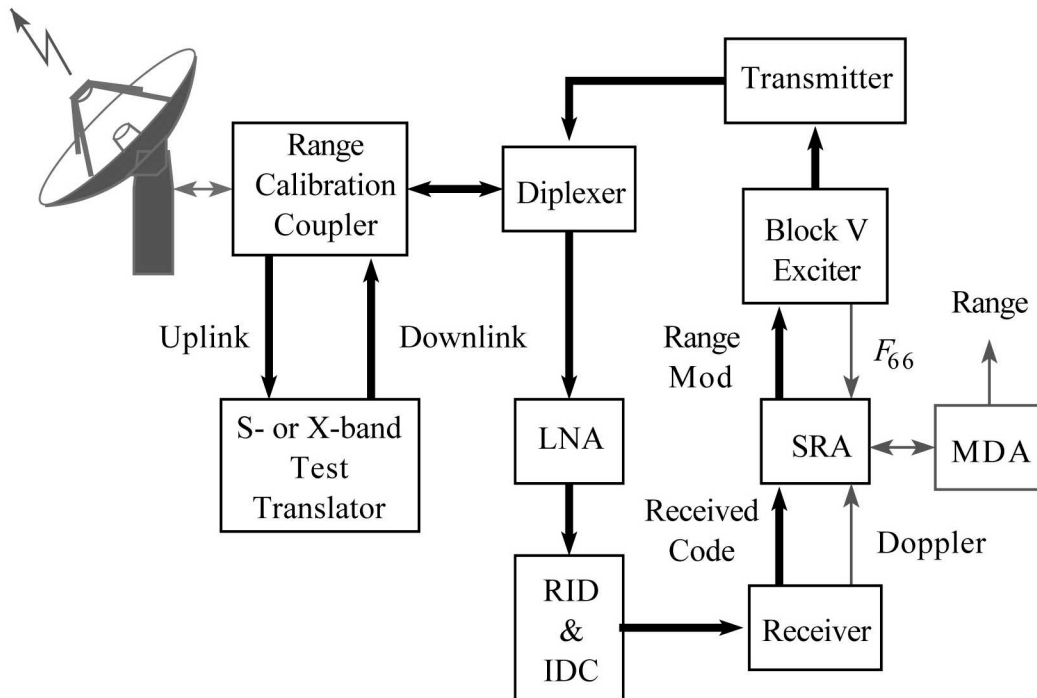
Figure A-7. Typical Range Calibration Signal Path for DSS Using SRA and MDA
Ranging Equipment

A5.0   *Error Contributions for Ranging Using the SRA*

The round-trip one-sigma-delay error of the DSN ranging system over a ranging
pass has been estimated for the X-band system as 6.3 nanoseconds (about 1.0 m one-way). The
S-band system error has been estimated as 14.5 nanoseconds (about 2.2 m one-way).

Table A1 shows a breakdown of long-term error contributions due to calibration
and errors inherent within the equipment of the various subsystems that constitute the total
ground system using the SRA and MDA ranging equipment.

Table A-1. One-Sigma Range Error for SRA/MDA-Equipped Ranging System

Subsystem	X-band		S-band	
	Round-trip Delay (ns)	One-way Distance (m)	Round-trip Delay (ns)	One-way Distance (m)
Frequency and Timing	1.00	0.15	1.00	0.15
Receiver	2.67	0.40	2.67	0.40
Exciter and Transmitter	1.33	0.20	5.33	0.80
Microwave and Antenna	2.33	0.35	2.33	0.35
Tracking	0.67	0.10	0.67	0.10
Cables	1.33	0.20	1.33	0.20
Calibration	3.33	0.50	3.33	0.50
Reserve	3.33	0.50	12.47	1.87
Root Sum Square	6.30	0.95	14.52	2.18

209
Open-Loop Radio Science

Effective November 30, 2000
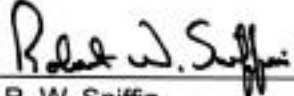
Document Owner:

Massimo Tinto   12/12/2000
Date

Approved by:

Massimo Tinto   12/13/2000
Radio Science Services   Date
System Development Engineer

Prepared by:

R. W. Sniffin   12/11/00
Date

Released by:

[Signature on file at TMOD Library]

TMOD Document Release   Date

Change Log

Rev	Issue Date	Affected Paragraphs	Change Summary
Initial	1/15/2001	All	All

Note to Readers

There are two sets of document histories in the 810-005 document, and these histories are reflected in the header at the top of the page. First, the entire document is periodically released as a revision when major changes affect a majority of the modules. For example, this module is part of 810-005, Revision E. Second, the individual modules also change, starting as an initial issue that has no revision letter. When a module is changed, a change letter is appended to the module number on the second line of the header and a summary of the changes is entered in the module's change log.

This module documents the new Radio Science Receivers that will become operational in the year 2001 and the Ka-band capability at DSS 25. The equipment that was previously documented in module RSS-10 of 810-005, Rev. D has been removed from the network.

Contents

Illustrations

Tables

1 *Introduction*

1.1 *Purpose*

This module describes the capabilities and performance of the Deep Space Network (DSN) Open-loop Radio Science equipment used for supporting radio science (RS) experiments.

1.2 *Scope*

This module discusses the open-loop radio science receiving equipment functions, architecture, operation, and performance. Although some RS experiments require uplink support and closed-loop Doppler and ranging data, this module emphasizes a description of the open-loop recording capability that is used solely during radio science experiments. Details of the closed-loop Doppler tracking system can be found in module 203, 34-m and 70-m Receiver Doppler. Details of the uplink functions can be found in the 70-m, 34-m High Efficiency (HEF), and 34-m Beam Waveguide (BWG) telecommunications interface modules 101, 103, and 104.

2 *General Information*

Radio science experiments involve measurements of small changes in the phase, frequency, amplitude, and polarization of the radio signal propagating from an interplanetary spacecraft to an Earth receiving station. By properly analyzing these data, investigators can infer characteristic properties of the atmosphere, ionosphere, and planetary rings of planets and satellites, measure gravitational fields and ephemeredes of planets, monitor the solar plasma and magnetic fields activities, and test aspects of the theory of general relativity. Details of the Radio Science System applications may be found in the JPL Publication 80-93, Rev. 1, written by S.W. Asmar and N.A. Renzetti, titled: *The Deep Space Network as an Instrument for Radio Science Research*.

2.1 *Functions*

The functions of the DSN with respect to conducting radio science experiments can be summarized as follows:

- Providing an uplink carrier signal to the spacecraft with a pure spectrum, including low phase noise and stable frequency.

- Acquisition, down conversion, digitization, and recording of the downlink carrier with minimal degradation to its frequency, phase, and amplitude stability.

- Providing assurance that the expected signals are being acquired and recorded.

2.2 *Hardware Configuration*

All radio science experiments require use of the antenna, microwave, antenna-mounted receiving, and frequency and timing equipment at the stations. They also require the Ground Communications Facility (GCF) to deliver the data from the stations to users and the Advanced Multi-mission Operations System (AMMOS) at JPL, where experiments are monitored. DSN stations are designed to meet radio science requirements for stability. However, one of the beam waveguide stations at the Goldstone Deep Space Communications Complex (DSCC), DSS 24, is not equipped with a high-quality frequency distribution system and is not recommended for radio science applications. A block diagram of the open-loop radio science receiving capability is shown in Figure 1.

The receiving equipment on each DSN antenna produces one or more intermediate frequency (IF) signals with a nominal center frequency of 300 MHz and a bandwidth that depends on the microwave and low noise amplifier equipment on the antenna as described in modules 101, 103, and 104. These IF signals are routed to a distribution amplifier (not shown in Figure 1) that provides multiple copies of each signal for use by the Radio-science Receivers (RSRs), the telemetry and tracking receivers, and other equipment in the signal processing center (SPC). One copy of each signal is provided to the RSR IF Switch that further divides and amplifies it with the result being that any of the RSR channels can be connected to any antenna IF signal.

There are two dedicated RSRs at the Goldstone Deep Space Communications Complex (DSCC) and one at the Canberra and Madrid DSCCs. Each complex also has an online spare that is shared with other functions including very-long baseline Interferometry (VLBI). Each RSR contains two channels however the design of the system software is such that, from the user's viewpoint, each RSR channel can be considered to be an independent open-loop receiver.
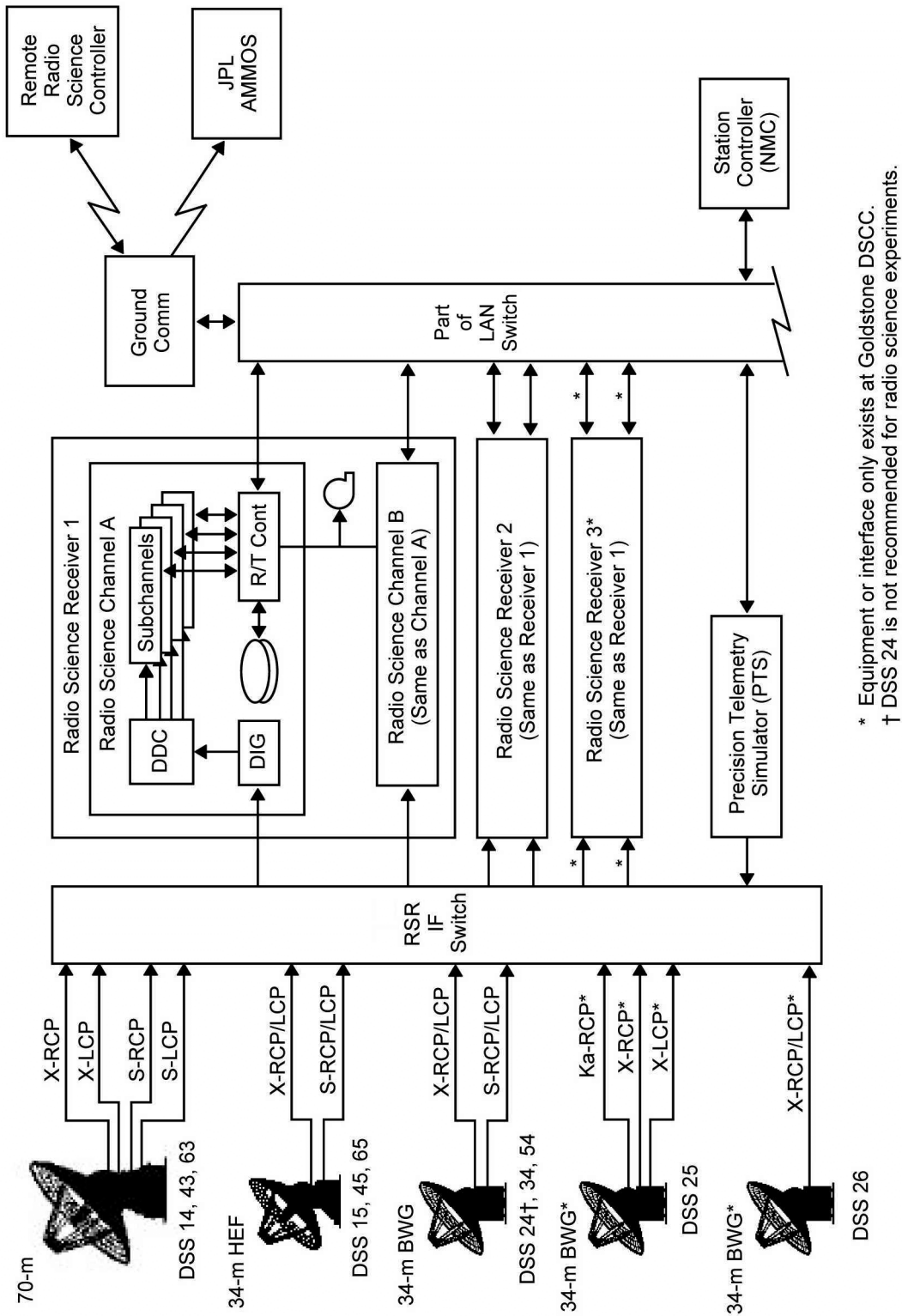
Figure 1. Radio Science Receiving Equipment Configuration

* Equipment or interface only exists at Goldstone DSCC.
† DSS 24 is not recommended for radio science experiments.

2.3 *RSR Signal Processing*

The IF signal selected by the RSR IF Switch is fed to the Digitizer (DIG) where it is filtered to limit its bandwidth to the range of 265–375 MHz centered at 320 MHz. This corresponds to a received frequency range of 2,265–2,375 MHz at S-band, 8,365–8,475 MHz at X-band, and 31,965–32,075 MHz at Ka-band. However, the actual received frequency range will depend on the characteristics of the equipment on the selected antenna. The filtered signal is downconverted to a center frequency of 64 MHz and digitized at 256 MHz with an 8-bit resolution. The resultant data are fed to the Digital Downconverter (DDC) that selects any 16-MHz bandwidth from the original bandpass with a resolution of 1 MHz and downconverts it to baseband in the form of a 16-Ms/s, 8-bit, complex data stream.

Baseband processing provides up to four subchannel filters to select frequency bands of interest for recording. The number of available filters depends on the selected bandwidths that can be broadly categorized as Narrowband, Medium Band, or Wideband. The following selection of filters is available:

- 4 Narrowband

- 2 Narrowband and 1 Medium Band

- 2 Medium Band

- 1 Wideband

The filters are specified by their bandwidths, the desired resolution (bits/sample) and an offset from the predicted sky frequency predict file. This frequency predict file is created by the DSN network support function and contains the spacecraft frequency altered by spacecraft trajectory and Earth-rotation. Table 1 lists the supported filter bandwidths and resolutions and gives the resultant data rate for each combination. Figure 2 shows the relationship between the frequency bands within the RSR

2.4 *RSR Signal Detection*

Because the RSR is an open-loop receiver, it does not have a mechanism to align its passband to (establish lock with, or track) the received signal. Instead, it relies on predicts to position its passband. This creates a risk that a predict error might result in the wrong portion of the received spectrum being processed. To assist in recognizing this, the RSR analyzes the data in each subchannel and provides a detected signal indication on the main display for that subchannel

In addition to the detected signal indication, the RSR provides a frequency-domain representation of the bandpass being recorded in each RSR subchannel using a Fast-Fourier Transform (FFT). Characteristics of the FFT such as number of points, averaging, and update rate are under user control.

Table 1. Supported Bandwiths and Resolutions with Resulting Data Rate

Category	Bandwidth	Resolution (b/sample)	Data Rate (b/s)
Narrowband	1 kHz	16	32,000
	2 kHz	16	64,000
	4 kHz	16	128,000
	8 kHz	16	256,000
	16 kHz	16	512,000
	25 kHz	16	800,000
	50 kHz	16	1,600,000
	100 kHz	16	3,200,000
	1 kHz	8	16,000
	2 kHz	8	32,000
	4 kHz	8	64,000
	8 kHz	8	128,000
	16 kHz	8	256,000
	25 kHz	8	400,000
	50 kHz	8	800,000
	100 kHz	8	1,600,000
Medium Band	250 kHz	16	8,000,000
	500 kHz	16	16,000,000
	250 kHz	8	4,000,000
	500 kHz	8	8,000,000
	1 MHz	8	16,000,000
	250 kHz	4	2,000,000
	500 kHz	4	4,000,000
	1 MHz	4	8,000,000
	2 MHz	4	16,000,000

Table 1. Supported Bandwiths and Resolutions with Resulting Data Rate (Continued)

Category	Bandwidth	Resolution (b/sample)	Data Rate (b/s)
Medium Band (Continued)	250 kHz	2	1,000,000
	500 kHz	2	2,000,000
	1 MHz	2	4,000,000
	2 MHz	2	8,000,000
	4 MHz	2	16,000,000
	250 kHz	1	500,000
	500 kHz	1	1,000,000
	1 MHz	1	2,000,000
	2 MHz	1	4,000,000
	4 MHz	1	8,000,000
Wideband	8 MHz	2	32,000,000
	8 MHz	1	16,000,000
	16 MHz	1	32,000,000

2.5 *RSR Operation*

The radio science equipment operates in both a link-assigned and a stand-alone mode. In the link-assigned mode, the Network Monitor and Control (NMC) function receives monitor data from the RSR for incorporation into the data set for tracking support and provides a workstation from which the RSR can be operated. RSRs that are not assigned to a link may be operated in a stand-alone mode without interference to any activities in process at the complex. Monitor data is not forwarded to the NMC by RSRs operating in the stand-alone mode.

The RSR employs a client-server architecture where each RSR channel acts as a server capable of accepting connections from up to five users operating the radio science client software at any time. In the link-assigned mode, one of these five clients is the NMC workstation. The RSR does not recognize any client as being superior to the others so it is up to the user to assign responsibility for control to one client with the other clients operating in a passive mode. One RSR client is required for each RSR channel being controlled or observed. Thus, a complex radio science experiment involving four RSR channels would require four RSR clients at the control point.

ANALOG IF

DIGITIZED BAND

128-MHz (nominal), samples at 256 Ms/s, 8-bit samples

Variable, 1-MHz steps

BASEBAND CHANNEL

16-MHz (nominal) samples at 16 Ms/s, I & Q, 8-bit samples

Variable, < 1-Hz steps
with Doppler Compensation

SUBCHANNELS (Up to 4)

Variable width, 1 kHz – 16 MHz
Variable Samples, I & Q, 1-bit – 16-bit
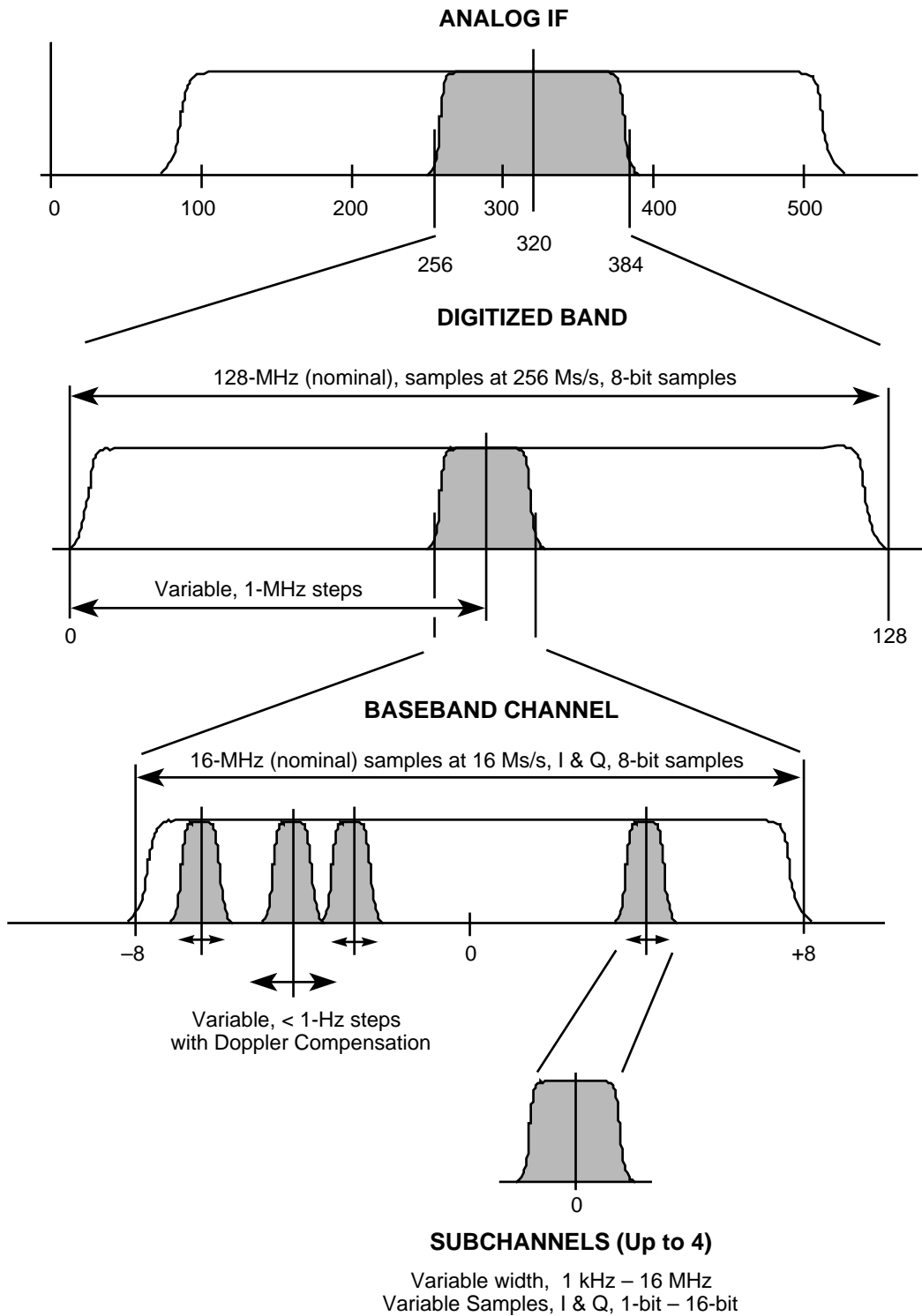
Figure 2.   Relationships Between RSR Processing Bands

All functions of the RSR may be performed from the RSR client in real time. Of special interest to the RS experimenter are the ability to adjust (slew) the predicted frequency profile, to slew the individual subchannel frequencies, to adjust FFT parameters, and to enable or disable recording for each subchannel.

2.6 *Data Delivery*

When recording is enabled, baseband samples and ancillary information, discussed below, are formatted into a file of data blocks and stored on disk drives for delivery to JPL or other users. A separate data file is created for each subchannel. Data delivery is normally via the Reliable Network System (RNS). Data also may be obtained via File Transfer Protocol (FTP) or Digital Linear Tape (DLT) cartridges. The format is the same independent of the method of delivery.

2.6.1 *Ancillary Data*

The following ancillary data are included as a header for each data block. A detailed description of the data blocks is contained in TMOD Document 820-013, module 0159.

- Data record version

- Subchannel identification

- Time tag for first sample in block

- Station and pass identification

- Spacecraft identification

- Receiver configuration

2.7 *Performance*

The principal characteristics of the RSRs are summarized in Table 2. In addition, radio science experiments are influenced by the overall stability of equipment at the stations. The following sections provide information on the techniques used to validate RS equipment stability.

2.7.1 *Frequency Stability*

Long-term frequency stability tests are conducted with the exciter/ transmitter equipment and the Radio Science open-loop receiving equipment. An uplink signal generated by the exciter is translated at the antenna to a downlink frequency. The downlink signal is passed through the RF-IF downconverter at the antenna and into the RSR. In doing this test, however, instability in the frequency and timing equipment and the mechanical vibrations of the antenna are not included. This is because frequency and timing instability is cancelled out, while the mechanical vibrations of the antenna are not present in these data. Measurements of these items can however be obtained via other means, making it possible to provide an estimate of the

Table 2. Radio Science Receiver Characteristics

Parameter	Value	Remarks
Number of Channels		Note: Any channel may be connected to any received spectrum
Goldstone	4	2 additional channels are available shared with other applications
Canberra and Madrid	2	2 additional channels are available shared with other applications
Frequency Ranges Covered		
At RSR Input (MHz)	265 – 375	
Referenced to L-band (MHz)	1,645 –1,755	L-band receive capability at 70-m subnet is 1,628–1,708 MHz
Referenced to S-band (MHz)	2,265 – 2,375	S-band downlink allocation is 2,200–2,290 MHz for Earth orbiter application and 2,290–2,300 MHz for deep space applications
Referenced to X-band (MHz)	8,365 – 8,475	X-band downlink allocation is 8,400–8,450 MHz for deep space application and 8,450–8,500 MHz for Earth orbiter applications
IF Attenuation		
Range (dB)	0 – 31.5	
Resolution (dB)	0.5	
Doppler Compensation		
Maximum Doppler Shift (km/s)	30	At all downlink frequencies
Maximum Doppler Rate (m/s^2)	17	At all downlink frequencies
Maximum Doppler Acceleration (m/s^3)	0.3	At all downlink frequencies
Maximum Tuning Error (Hz)	0.5	At all downlink frequencies
Manual Offset (MHz)	–8.0 to +8.0	
Baseband Bandwidth (MHz)	16	

Table 2. Radio Science Receiver Characteristics (Continued)

Parameter	Value	Remarks
Baseband Resolution (MHz)	1	Positioning of baseband within IF or RF bandwidth
Number of Subchannels Available for each RSR	1 – 4	Configuration depends on data volume.
Subchannel Tuning		
Tuning (MHz)	±8	From center of baseband
Resolution (Hz)	<1	
Recording Bandwidths		See Table 2 for exact values.
Narrowband (NB), kHz	1 – 100	1 – 4-subchannels
Medium Band (MB), kHz	250 – 4,000	2 or 1 with 2 NB subchannels
Wideband (WB), MHz	8 or 16	NB and MB subchannels are not available
Resolutions (bits/sample)	16 – 1	Depends on selected bandwidth. See Table 2 for available resolutions.
Time Tagging		
Resolution (μs)	1	
Accuracy ((μs)	1	With respect to station clock
Signal Detection Display		1 for each subchannel being recorded
Number of points in FFT	100 – 4096	Default is 1000
Spectra Averaging	1 – 100	Default is 10
FFT Interval (s)	1 – 10,000	Default is 10

overall frequency stability of the stations. The long-term frequency stability is presented in terms of the Allan deviation over a specified integration time. Table 3 shows uplink and downlink Allan deviation requirements for the 34-m HEF, 34-m BWG, and 70-m antennas. Repeated testing has always produced estimates better than these requirements.

2.7.2   *Phase Noise*

Phase stability (Spectral Purity) testing characterizes stability over very short integration times. The region of the frequency band where phase noise measurements are performed can be as far as 10 kHz off the carrier frequency. Such measurements are reported in dB relative to the carrier (dBc), in a 1-Hz band at a specified distance from the carrier. Table 4

contains the required phase noise levels, at specified offsets, for the 34-m HEF, 34-m BWG, and 70-m subnets. As is the case with frequency stability measurements, repeated testing ensures these requirements are not exceeded.

2.7.3   *Amplitude Stability*

Amplitude stability tests measure the amplitude fluctuations produced by the open-loop receiving system relative to a constant (mean) amplitude input signal. The amplitude stability performance is specified in terms of a threshold on the amplitude fluctuations relative to the mean amplitude, and the corresponding probability that such fluctuations will not exceed such a threshold. An analysis indicates that 99.7% of the time, the amplitude stability at the 70-m, 34-m HEF, and 34-m BWG stations at S- and X-bands is less than 0.2 dB including the gain variation due to antenna pointing errors.

2.8   *Precision Telemetry Simulator*

The Precision Telemetry Simulator (PTS) is an external device that provides IF test signals for performance verification of the radio science equipment. Its signals are generated in the digital domain and subsequently converted to analog, with signal conditions driven from predicts. At least two simulated signals can be generated, each having its own characteristics in terms of Doppler and signal level, etc. The PTS signals are injected into the RSR via the RSR IF Switch.

3   *Proposed Capabilities*

The following paragraphs discuss capabilities that have not yet been implemented by the DSN but have adequate maturity to be considered for spacecraft mission and equipment design. Telecommunications engineers are advised that any capabilities discussed in this section cannot be committed to except by negotiation with the Telecommunications and Mission Operations Directorate (TMOD) Plans and Commitments Program Office.

3.1   *70-m X-band Uplink Implementation*

The 70-m X-band uplink implementation that has been completed at DSS 14 and DSS 43 will be extended to DSS 63. As a result, all 70-m stations will have the same capabilities and performance as described for DSS 14 and 43 in Tables 2, 3, and 4.

Table 3. Uplink and Downlink Allan Deviation Requirements

Averaging Time, s	Allan Deviation			
	1	10	100	1000
Station and Band				
34-m HEF				
X-band U/L	1.0×10^{-12}	1.1×10^{-13}	4.5×10^{-15}	4.3×10^{-15}
S-band D/L	4.1×10^{-13}	7.2×10^{-14}	9.1×10^{-15}	5.3×10^{-15}
X-band D/L	4.0×10^{-13}	4.9×10^{-14}	5.3×10^{-15}	4.7×10^{-15}
34-m BWG				
S-band U/L (DSS 24, 34, 54)	1.0×10^{-12}	1.1×10^{-13}	4.5×10^{-15}	4.3×10^{-15}
X-band U/L (DSS 25, 26, 34, 54)	1.0×10^{-12}	1.1×10^{-13}	4.5×10^{-15}	4.3×10^{-15}
S-band D/L (DSS 34, 54)	4.1×10^{-13}	7.2×10^{-14}	9.1×10^{-15}	5.3×10^{-15}
X-band D/L (DSS 25, 26, 34, 54)	4.0×10^{-13}	4.9×10^{-14}	5.3×10^{-15}	4.7×10^{-15}
Ka-band U/L (DSS 25)	No Rqmt.	No Rqmt.	1.1×10^{-14}	2.1×10^{-15}
Ka-band D/L (DSS 25)	1.3×10^{-13}	7.5×10^{-14}	6.8×10^{-15}	2.2×10^{-15}
70-m				
S-band U/L	1.5×10^{-12}	2.3×10^{-13}	1.1×10^{-14}	1.1×10^{-14}
X-band U/L (DSS 14, 43)	1.5×10^{-12}	2.3×10^{-13}	1.1×10^{-14}	1.1×10^{-14}
S-band D/L	4.1×10^{-13}	7.2×10^{-14}	9.1×10^{-15}	5.3×10^{-15}
X-band D/L	4.0×10^{-13}	4.9×10^{-14}	5.3×10^{-15}	4.7×10^{-15}

Table 4. Uplink and Downlink Phase Noise Requirements

Offset from Carrier, Hz	Phase Noise, dBc			
	1	10	100	10 k
Station and Band				
34-m HEF				
X-band U/L	–52.3	–61.8	–65.9	–65.9
S-band D/L	–62.8	–72.2	–76.7	–76.7
X-band D/L	–51.5	–60.9	–65.5	–65.5
34-m BWG				
S-band U/L (DSS 24, 34, 54)	–63.5	–72.5	–77.1	–77.1
X-band U/L (DSS 25, 26, 34, 54)	–52.3	–61.8	–65.9	–65.9
S-band D/L (DSS 34, 54)	–62.8	–72.2	–76.8	–76.8
X-band D/L (DSS 25, 26, 34, 54)	–51.6	–61.0	–65.5	–65.5
X-band D/L (DSS 25)	–59.7	–65.6	–66.0	–66.0
Ka-band D/L (DSS 25)	–55.2	–63.7	–64.0	–64.0
70-m				
S-band U/L	–63.5	–72.5	–77.1	–77.1
X-band U/L (DSS 14, 43)	–52.3	–61.8	–65.9	–65.9
S-band D/L	–62.8	–72.2	–76.7	–76.7
X-band D/L	–51.5	–60.9	–65.5	–65.5
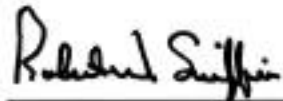
301
Coverage and Geometry

Effective November 30, 2000

Document Owner:

R. W. Sniffin   12/11/00

R. W. Sniffin   Date

Approved by:

A. Kwok   12/13/00

A. Kwok   Date
Tracking and Navigation Service
Systems Development Engineer

Released by:

[Signature on file at TMOD Library]

TMOD Document Release   Date

Change Log

Rev	Issue Date	Affected Paragraphs	Change Summary
Initial	1/15/2001	All	All

Note to Readers

There are two sets of document histories in the 810-005 document, and these histories are reflected in the header at the top of the page. First, the entire document is periodically released as a revision when major changes affect a majority of the modules. For example, this module is part of 810-005, Revision E. Second, the individual modules also change, starting as an initial issue that has no revision letter. When a module is changed, a change letter is appended to the module number on the second line of the header and a summary of the changes is entered in the module's change log.

This module is essentially the same as 810-005, Rev. D, module GEO-10, Rev. E. Information relating to decommissioned antennas has been removed, coverage charts have been revised to reflect new capabilities, and a significant uplink coverage restriction at the DSS 54 station is documented.

Contents

Illustrations

Figure   **Page**

Tables

Table   **Page**

1   Introduction

1.1   Purpose

This module describes the geometry and surveillance visibility provided by the DSN for support of spacecraft telecommunications.

1.2   Scope

This module provides the Deep Space Network (DSN) station coordinates that are required for spacecraft navigation and to locate the stations with respect to other points on the Earth's surface. Coverage charts are provided to illustrate areas of coverage and non-coverage from selected combinations of stations for spacecraft at selected altitudes. Horizon masks are included so the effects of terrain masking can be anticipated.

2   General Information

2.1   Station Locations

The following paragraphs discuss the important concepts relating to establishing the location of the DSN antennas.

2.1.1   Antenna Reference Point

The coordinates provided by this module refer to a specific point on each antenna. For antennas where the axes intersect, the reference point is the intersection of the axes. For antennas for which the axes do not intersect, the reference point is the intersection of the primary (lower) axis with a plane, perpendicular to the primary axis, and containing the secondary (upper) axis. Table 1 lists the DSN antennas by type and provides the axis offset where appropriate. The effect of this offset on the range observable is discussed in module 203 of this handbook.

The 11-m antennas are unique in that the azimuth axis is tilted from the local vertical by a 7-degree wedge that is rotated to a position with respect to north called the "train angle" before the start of each track. This causes the station location to be displaced away from the train angle along a circular path having a radius equal to the axis offset. The vector ($\Delta \mathbf{r}_b$), which must be added to the station coordinates to compensate for this effect, can be derived from the train angle that is supplied to the user as part of the tracking data (see module 302) and the north and east station vectors ($\mathbf{N}$ and $\mathbf{E}$) which are functions of the station geodetic coordinates.

Table 1. DSN Antenna Types

Antenna Type	Station Identifiers	Primary and Secondary Axes	Axis Offset
70-m	14, 43, 63	Az/El	0
34-m High Efficiency (HEF)	15, 45, 65	Az/El	0
34-m Beam Waveguide (BWG)	24, 25, 26, 34, 54	Az/El	0
34-m High-speed Beam Waveguide (HSB)	27, 28†	Az/El	1.83 m
26-m	16, 46, 66	X/Y	6.706 m
11-m OVLBI	23, 33, 53	Tilt/Az/El	0.391 m

Az/El Antenna's azimuth plane is tangent to the Earth's surface, and antenna at 90-degrees elevation is pointing at zenith.

X/Y   Primary axis (X) is aligned horizontally in an east-west (26-m antennas) or north-south (9-m antenna) direction. Secondary axis is aligned vertically in a north-south (26-m antennas) or east-west (9-m antenna) plane.

Tilt/Az/El   The azimuth axis of the Az/El mount is tilted to avoid an overhead keyhole. The direction of tilt is fixed for each pass and results in an apparent shift in the actual station location from the specified station location.

† DSS 28 is not presently in service.

$$\Delta \mathbf{r}_b \quad = \quad -0.391\cos\sigma\, \mathbf{N} - 0.391\sin\sigma\, \mathbf{E} \tag{1}$$

where:

σ =   the train angle

$$\mathbf{N} = \begin{bmatrix} -\sin\phi_g \cos\lambda \\ -\sin\phi_g \sin\lambda \\ \cos\phi_g \end{bmatrix} \tag{2}$$

$$\mathbf{E} = \begin{bmatrix} -\sin\lambda \\ -\cos\lambda \\ 0 \end{bmatrix} \tag{3}$$

$$\phi_g \quad = \quad \text{Station Geodetic Latitude (Table 5)}$$

$$\lambda \quad = \quad \text{Station Longitude.}$$

2.1.2 IERS Terrestrial Reference Frame

To use station locations with sub-meter accuracy, it is necessary to clearly define a coordinate system that is global in scope as opposed to the regional coordinate systems referenced in previous editions of this document. The International Earth Rotation Service (IERS) has been correlating station locations from many different services and has established a coordinate frame known as the IERS Terrestrial Reference Frame (ITRF). The IERS also maintains a celestial coordinate system and coordinates delivery of Earth-orientation measurements that describe the motion of station locations in inertial space. The DSN has adopted the IERS terrestrial system to permit its users to have station locations consistent with widely available Earth-orientation information.

The IERS issues a new list of nominal station locations each year, and these locations are accurate at the few-cm level. At this level of accuracy, one must account for ongoing tectonic plate motion (continental drift), as well as other forms of crustal motion. For this reason ITRF position coordinates are considered valid for a specified epoch date, and one must apply appropriate velocities to estimate position coordinates for any other date. Relative to the ITRF, even points located on the stable part of the North American plate move continuously at a rate of about 2.5 cm/yr.

The coordinates in this module are based on the 1993 realization of the ITRF, namely ITRF93, documented in IERS Technical Note 18 [1]. ITRF93 was different from earlier realizations of the ITRF in that it was defined to be consistent with the Earth Orientation Parameters (EOP) distributed through January 1, 1997. Earlier realizations of the ITRF were known to be inconsistent (at the 1-3 cm level) with the Earth orientation distributions.

After ITRF93 was published, the IERS decided to improve the accuracy of the EOP series and make it consistent with the ITRF effective January 1, 1997. This date was chosen because it enabled a defect in the definition of universal time to be removed at a time when its contribution was zero. In anticipation of this change, ITRF94 and ITRF95 were made consistent with the pre-ITRF93 definition of the terrestrial reference frame, and all prior EOP series were recomputed in accordance with the new system.

Until this change is fully adopted by the Earth-orientation community, the DSN is delivering Earth-orientation calibrations to navigation teams that are consistent with the earlier definition and using the ITRF93 reference frame. Users interested in precise comparison with other systems should keep in mind the small systematic differences.

2.1.2.1 ITRF Coordinates

Figure 1 illustrates the ITRF coordinates and the relationship between the ITRF coordinates and geocentric coordinates discussed below. The Cartesian coordinates of the DSN station locations in the ITRF93 reference system are provided in Table 2. Table 2 also gives the characteristic position uncertainty for horizontal and vertical components.

2.1.2.2 ITRF Site Velocities

The locations given in Table 2 are for the epoch 1993.0. To transform these locations to any other epoch, the site velocities should be used. Table 3 gives the ITRF93 site velocities for the DSN stations, in both Cartesian and east-north-vertical components.

2.1.3 Geocentric Coordinates

Geocentric coordinates are used for spacecraft tracking. They relate the station location to the Earth's center of mass in terms of the geocentric radius and the angles between the station and the equatorial and hour angle planes. Geocentric coordinates for the DSN stations are provided in Table 4.

2.1.4 Geodetic Coordinates

Locations on the Earth's surface are defined with respect to the geoid. That is, the surface around or within the Earth that is normal to the direction of gravity at all points and coincides with mean sea level in the oceans. The geoid is not a regular surface because of variations in the Earth's gravitational force. To avoid having to make computations with respect to this non-mathematical surface, computations are made with respect to an ellipsoid having a semi-major (equatorial) axis and semi-minor (polar) axis that provides a best fit to the geoid in the area of interest. The ellipsoid is uniquely defined by specifying the equatorial radius and the flattening (that is, the amount that the ellipsoid deviates from a perfect sphere). The relationship between the polar and equatorial axes is given by the following expression:

$$(\text{polar axis}) = (\text{equatorial axis}) \times (1 - \text{flattening}). \tag{4}$$

Once the Cartesian coordinates (x, y, z) are known, they can be transformed to geodetic coordinates in longitude, latitude, and height with respect to an ellipsoid (λ, ϕ, h) by the following noniterative method (Reference 2):
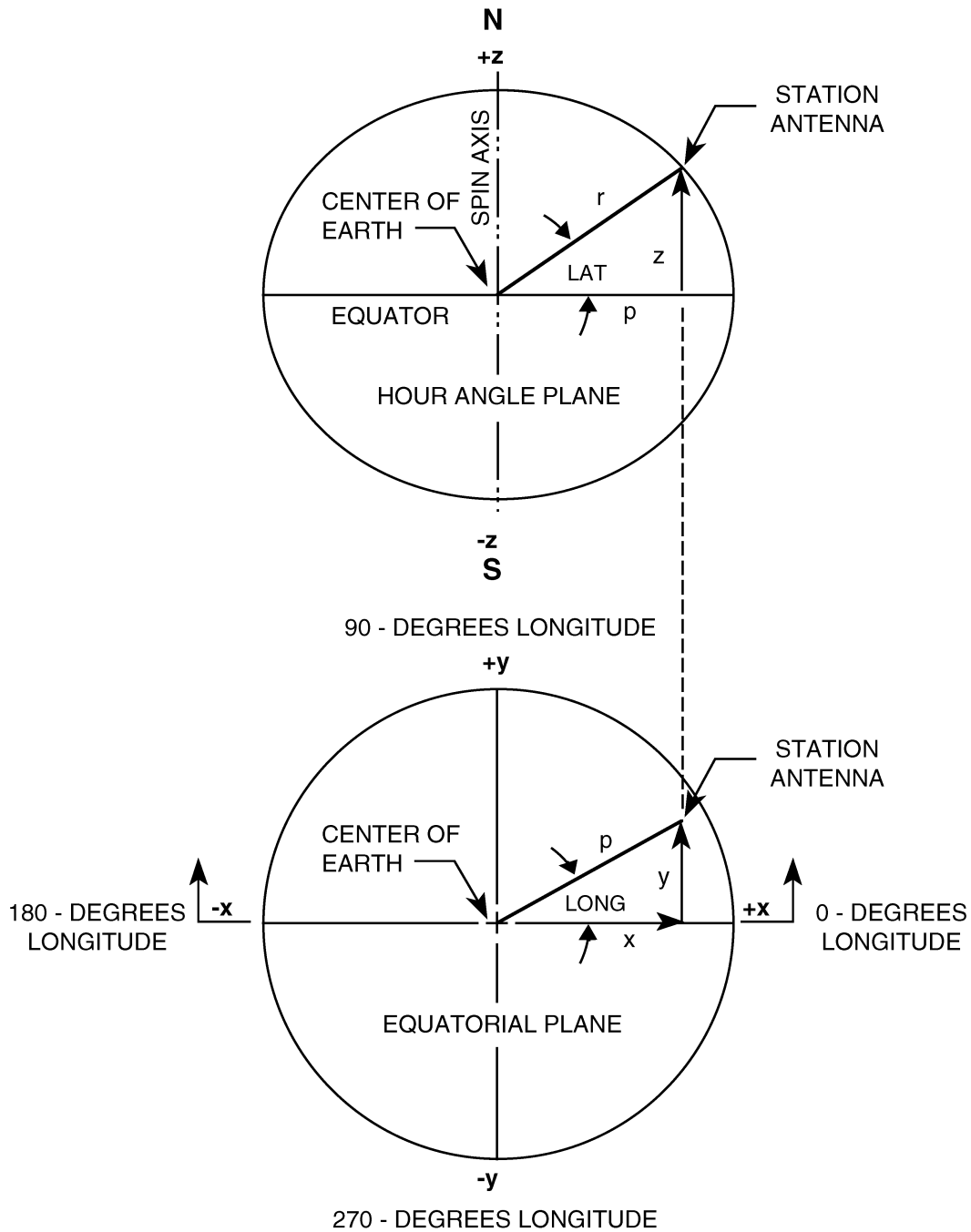
Figure 1. ITRF Cartesian and Geocentric Coordinate System Relationships

Table 2. ITRF93 Coordinates for DSN Stations

Antenna		Cartesian Coordinates			Uncertainty	
Name	Description	x(m)	y(m)	z(m)	h(m)	v(m)
DSS 13	34-m R & D	−2351112.491	−4655530.714	+3660912.787	0.04	0.05
DSS 14	70-m	−2353621.251	−4641341.542	+3677052.370	0.03	0.03
DSS 15	34-m HEF	−2353538.790	−4641649.507	+3676670.043	0.03	0.03
DSS 16	26-m X-Y	−2354763.158	−4646787.462	+3669387.069	0.05	0.10
DSS 23	11-m Tilt/Az/El	−2354757.567	−4646934.675	+3669207.824	0.05	0.10
DSS 24	34-m BWG	−2354906.495	−4646840.128	+3669242.317	0.05	0.10
DSS 25	34-m BWG	−2355022.066	−4646953.636	+3669040.895	0.05	0.10
DSS 26	34-m BWG	−2354890.967	−4647166.925	+3668872.212	0.05	0.10
DSS 27	34-m HSB	−2349915.260	−4656756.484	+3660096.529	0.05	0.10
DSS 28	Not in service	-2350101.849	−4656673.447	+3660103.577	0.05	0.10
DSS 33	11−m Tilt/Az/El	−4461083.514	+2682281.745	−3674570.392	0.03	0.10
DSS 34	34-m BWG	−4461146.756	+2682439.293	−3674393.542	0.05	0.10
DSS 43	70-m	−4460894.585	+2682361.554	−3674748.580	0.03	0.03
DSS 45	34-m HEF	−4460935.250	+2682765.710	−3674381.402	0.03	0.03
DSS 46	26-m X-Y	−4460828.619	+2682129.556	−3674975.508	0.04	0.04
DSS 53	11-m Tilt/Az/El	+4849330.129	−0360338.092	+4114758.766	0.05	0.10
DSS 54	34-m BWG	+4849434.555	−0360724.108	+4114618.643	0.05	0.10
DSS 63	70-m	+4849092.647	−0360180.569	+4115109.113	0.03	0.03
DSS 65	34-m HEF	+4849336.730	−0360488.859	+4114748.775	0.03	0.03
DSS 66	26-m X-Y	+4849148.543	−0360474.842	+4114995.021	0.05	0.10

Notes:

1. All antennas are AZ-EL type unless otherwise specified.

2. Horizontal (h) and vertical (v) uncertainties are 1-sigma.

Table 3. ITRF93 Site Velocities for DSN Stations

Complex	x(m/yr)	y(m/yr)	z(m/yr)	e(m/yr)	n(m/yr)	v(m/yr)
Goldstone (Stations 1x & 2x)	–0.0191	0.0061	–0.0047	–0.0198	–0.0057	–0.0001
Canberra (Stations 3x & 4x)	–0.0354	–0.0017	0.0412	0.0197	0.0506	0.0001
Madrid (Stations 5x & 6x)	–0.0141	0.0222	0.0201	0.0211	0.0255	0.0011

$$\lambda = \tan^{-1}\frac{y}{x} \tag{5}$$

$$\phi = \tan^{-1}\left(\frac{z(1-f)+e^2 a \sin^3\mu}{(1-f)\left(p - e^2 a \cos^3\mu\right)}\right) \tag{6}$$

$$h = p\cos\phi + z\sin - a\left(1 - e^2 \sin^2\phi\right)^{\frac{1}{2}} \tag{7}$$

where:

$$e^2 = 2f - f^2$$

$$p = \left(x^2 + y^2\right)^{\frac{1}{2}}$$

$$r = \left(p^2 + z^2\right)^{\frac{1}{2}}$$

$$\mu = \tan^{-1}\frac{z}{p}\left[(1-f)+\frac{e^2 a}{r}\right].$$

Table 5 provides geodetic coordinates derived by the preceding approach using an ellipsoid with a semi-major axis (a) of 6378136.3 m and a flattening (f) of 298.257.

Table 4. Geocentric Coordinates for DSN Stations

Antenna		Geocentric Coordinates			
Name	Description	Spin Radius (m)	Latitude (deg)	Longitude (deg)	Geocentric Radius (m)
DSS 13	34-m R & D	5215524.535	35.0660185	243.2055430	6372125.125
DSS 14	70-m	5203996.955	35.2443527	243.1104638	6371993.286
DSS 15	34-m HEF	5204234.332	35.2403133	243.1128069	6371966.540
DSS 16	26-m X-Y	5209370.715	35.1601777	243.1263523	6371965.530
DSS 23	11-m Tilt/Az/El	5209499.503	35.1581932	243.1271390	6371967.603
DSS 24	34-m BWG	5209482.486	35.1585349	243.1252079	6371973.553
DSS 25	34-m BWG	5209635.978	35.1562594	243.1246384	6371983.060
DSS 26	34-m BWG	5209766.971	35.1543411	243.1269849	6371993.032
DSS 27	34-m HSB	5216079.244	35.0571456	243.2233516	6372110.269
DSS 28	Not in service	5216089.176	35.0571462	243.2211109	6372122.448
DSS 33	11-m Tilt/Az/El	5205372.367	−35.2189880	148.9830895	6371684.945
DSS 34	34-m BWG	5205507.750	−35.2169868	148.9819620	6371693.561
DSS 43	70-m	5205251.579	−35.2209234	148.9812650	6371689.033
DSS 45	34-m HEF	5205494.708	−35.2169652	148.9776833	6371675.906
DSS 46	26-m X–Y	5205075.496	-35.2235036	148.9830794	6371676.067
DSS 53	11−m Tilt/Az/El	4862699.481	40.2375043	355.7503453	6370014.595
DSS 54	34-m BWG	4862832.239	40.2357708	355.7459008	6370025.429
DSS 63	70-m	4862450.981	40.2413537	355.7519890	6370051.221
DSS 65	34-m HEF	4862717.238	40.2373325	355.7485795	6370021.697
DSS 66	26-m X-Y	4862528.530	40.2401197	355.7485798	6370036.713

Notes:
  1. All antennas are AZ-EL type unless otherwise specified.

Table 5. Geodetic Coordinates for DSN Stations

Antenna		latitude (ϕ)			longitude (λ)			height(h)
Name	**Description**	**deg**	**min**	**sec**	**deg**	**min**	**sec**	**(m)**
DSS 13	34-m R & D	35	14	49.79342	243	12	19.95493	1071.178
DSS 14	70-m	35	25	33.24518	243	6	37.66967	1002.114
DSS 15	34-m HEF	35	25	18.67390	243	6	46.10495	0973.945
DSS 16	26-m X-Y	35	20	29.54391	243	7	34.86823	0944.711
DSS 23	11-m Tilt/Az/El	35	20	22.38335	243	7	37.70043	0946.086
DSS 24	34-m BWG	35	20	23.61555	243	7	30.74842	0952.156
DSS 25	34-m BWG	35	20	15.40450	243	7	28.69836	0960.862
DSS 26	34-m BWG	35	20	08.48213	243	7	37.14557	0970.159
DSS 27	34-m HSB	35	14	17.78052	243	13	24.06569	1053.203
DSS 28	Not in service	35	14	17.78136	243	13	15.99911	1065.382
DSS 33	11-m Tilt/Az/El	−35	24	01.76138	148	58	59.12204	0684.839
DSS 34	34-m BWG	−35	23	54.53995	148	58	55.06320	0692.750
DSS 43	70-m	−35	24	8.74388	148	58	52.55394	0689.608
DSS 45	34-m HEF	−35	23	54.46400	148	58	39.65992	0675.086
DSS 46	26-m X-Y	−35	24	18.05462	148	58	59.08571	0677.551
DSS 53	11-m Tilt/Az/El	40	25	38.48036	355	45	1.24307	0827.501
DSS 54	34-m BWG	40	25	32.23201	355	44	45.24283	0837.696
DSS 63	70-m	40	25	52.34908	355	45	7.16030	0865.544
DSS 65	34-m HEF	40	25	37.86055	355	44	54.88622	0834.539
DSS 66	26-m X-Y	40	25	47.90367	355	44	54.88739	0850.582

Notes:
1. All antennas are AZ-EL type unless otherwise specified.

14

2.2 Coverage and Mutual Visibility

The coverage and mutual visibility provided for spacecraft tracking depends on the altitude of the spacecraft, the type or types of antennas being used, the blockage of the antenna beam by the landmask and structures in the immediate vicinity of the antennas, and whether simultaneous uplink coverage is required. Receive limits are governed by the mechanical capabilities of the antennas and the terrain mask. Transmitter limits, on the other hand, are based on radiation hazard considerations to on-site personnel and the general public and are set above the terrain mask and the antenna mechanical limits.

2.2.1 Use of Transmitters Below Designated Elevation Limits

Requests for coordination to relinquish the transmitter radiation restrictions will be considered for spacecraft emergency conditions or for critical mission support requirements (conditions where low elevation or high-power transmitter radiation is critical to mission objectives). In either event, the uplink radiation power should be selected as the minimum needed for reliable spacecraft support.

2.2.1.1 Spacecraft Emergencies

The need for violation of transmitter radiation restrictions to support a spacecraft emergency will be determined by the DSN. The restrictions will be released after assuring that appropriate local authorities have been notified and precautions have been taken to ensure the safety of on-site personnel.

2.2.1.2 Critical Mission Support

If critical mission activities require the transmitter radiation restrictions to be violated, the project is responsible for notifying the DSN through their normal point of contact three months before the activity is scheduled. The request must include enough information to enable the DSN to support it before the appropriate authorities. Requests made less than three months in advance will be supported on a best-efforts basis and will have a lower probability of receiving permission to transmit. Requests will be accepted or denied a minimum of two weeks before the planned activity.

2.2.2 Mechanical Limits on Surveillance Visibility

All DSN antennas have areas of non-coverage caused by mechanical limits of the antennas. The first area is the mechanical elevation limit, which is approximately six degrees for antennas using an azimuth-elevation mount and somewhat lower for antennas with X-Y mounts. A second area of non-coverage is the area off the end or ends of the antenna's primary axis referred to as the *keyhole*.

2.2.2.1   Azimuth-Elevation Antennas

The keyhole of the DSN azimuth-elevation antennas is directly overhead and results from the fact that the antennas can only be moved over an arc of approximately 85 degrees in elevation. In order to track a spacecraft which is passing directly overhead, it is necessary to rotate the antenna 180 degrees in azimuth when the spacecraft is at zenith in order to continue the track. Thus, the size of the keyhole depends on how fast the antenna can be slewed in azimuth. Specifications on antenna motion are contained in module 302, Antenna Positioning. The location of the DSN antennas is such that overhead tracks are not required for spacecraft on normal planetary missions.

The DSN azimuth-elevation antennas have an additional restriction on antenna motion caused by the routing path of cables and hoses between the fixed and rotating portions of the antenna. This azimuth cable wrap has no effect on surveillance visibility but does place a restriction on the time between tracks due to the requirement to unwind the cables. Table 6 provides the approximate cable wrap limits for the DSN azimuth-elevation antennas.

2.2.2.2   X-Y Antennas

The DSN 26-m X-Y antennas (DSS 16, 46, and 66) have two keyholes caused by requirements for mechanical clearance in the antenna structure. The keyholes are located directly to the east and west of the 26-m antennas.

2.2.2.3   Tilt-Azimuth-Elevation Antennas

The DSN 11-m antennas (DSS 23, 33, and 53) have a keyhole above each antenna, which is offset from zenith by 7-degrees. The location of this keyhole is set before each pass to a position that will provide clearance between the keyhole and the scheduled track.

2.2.3   Coverage Charts

The following figures provide examples of coverage for various combinations of stations, spacecraft altitudes, and type of support. These figures were plotted by a program written as a collection of Microsoft Excel 97/98 macros. This program is available for download (1.7 Mbytes) from the 810-005 web site (http://eis.jpl.nasa.gov/deepspace/dsndocs/810-005/).

2.2.3.1   70-m Subnet Receive Coverage of Planetary Spacecraft

Figure 2 illustrates the receive coverage of planetary spacecraft by the DSN 70-m antenna subnet. The small ovals at each antenna location on the figure represent the 70-m antenna keyholes above each station and are approximately to scale.

Table 6. Approximate Cable Wrap Limits for Azimuth-Elevation Antennas

Antenna		Azimuth Position (Degrees)		
Name(s)	Description	Center of Wrap	CW Limit	CCW Limit
DSS 14, 63	70-m	45	310	140
DSS 43	70-m	135	40	230
DSS 15, 65	34-m HEF	135	360	270
DSS 45	34-m HEF	45	270	180
DSS 24, 25, 26, 54, 65	34-m BWG	135	360	270
DSS 34	34-m BWG	45	270	180
DSS 27	34-m HSB	135	360	270
DSS 23, 33, 53	11-m	0	380	(–) 380

2.2.3.2   *70-m Subnet Transmit Coverage of Planetary Spacecraft*

Figure 3 illustrates the transmit coverage of planetary spacecraft by the DSN 70-m antenna subnet using a 10.4-degree transmit elevation limit at DSS 14 and a 10.2-degree transmit elevation limit at DSS 43 and DSS 63. The small ovals at the antenna locations on the figure represent the 70-m antenna keyholes. The reduced coverage to the west of DSS 63 is caused by the need to have a 20.2-degree elevation limit to protect the high ground to the northwest of the station.

2.2.3.3   *34-m HEF Subnet Receive Coverage of Planetary Spacecraft*

Figure 4 illustrates the receive coverage of planetary spacecraft by the DSN 34-m HEF antenna subnet. The keyhole above each 34-m HEF antenna is very small and is somewhat exaggerated for clarity on the maps. This chart is very similar to Figure 2 but is included to show that the location of DSS 65 shifts the apparent position of the high ground to the north and west of where it is observed from DSS 63.

2.2.3.4   *34-m HEF Subnet Transmit Coverage of Planetary Spacecraft*

Figure 5 illustrates the transmit coverage of planetary spacecraft by the DSN 34-m HEF antenna subnet using a 10.6-degree transmit elevation limit at DSS 15, a 10.5-degree transmit limit at DSS 45, and a 10.3-degree limit at DSS 65. As is the case in Figure 4, the size of the circles used to indicate the keyholes on the map are larger than the actual size of the 34-m HEF antenna keyholes. Protection of the high ground at DSS 65 is provided by disabling the transmitter between 327.4 and 358.6 degrees azimuth.

2.2.3.5   34-m BWG Antennas Receive Coverage of Planetary Spacecraft

Figure 6 illustrates the receive coverage of planetary spacecraft by the DSN 34-m BWG antennas. As is the case with the other 34-m antennas, the size of the circles on the map is larger than the actual size of the antenna keyholes. This chart is very similar to Figures 2 and 4 but is included to show that the location of DSS 54 shifts the apparent position of the high ground even further to the north and west of where it is observed from DSS 63 than is the case with the DSS 65 34-m HEF antenna.

2.2.3.6   34-m BWG Antennas Transmit Coverage of Planetary Spacecraft

Figure 6 illustrates the transmit coverage of planetary spacecraft by the DSN 34-m BWG antennas. As is the case with the other 34-m antennas, the size of the circles on the map is larger than the actual size of the antenna keyholes. Protection of the high ground at DSS 54 is provided by disabling the transmitter between 267 and 3 degrees azimuth.

2.2.3.7   26-m Subnet Receive Coverage of Earth Orbiter Spacecraft

Figure 8 illustrates the receive coverage of Earth-orbiter spacecraft at altitudes of 200 km, 1000 km, and 5000 km by the DSN 26-m antenna subnet. This chart can also be used when the 34-m HSB antenna, DSS 27, is substituted for the Goldstone 26-m antenna. DSS 27 is collocated with an inactive antenna, DSS 28, approximately 14.5 km southeast of DSS 16. The inactive antenna blocks reception to the west in the same place and approximately to the same extent as the west keyhole of DSS 16.

2.2.3.8   26-m Subnet Transmit Coverage of Earth Orbiter Spacecraft

Figure 9 illustrates the transmit coverage of Earth-orbiter spacecraft at altitudes of 200 km, 1000 km, and 5000 km by the DSN 26-m antenna subnet. This chart is similar to Figure 8. However, the limits placed on transmitter operation in order to clear terrain and structures are clearly visible.

2.2.3.9   34-m BWG Antennas Receive Coverage of Earth Orbiter Spacecraft

Figure 10 illustrates the receive coverage of Earth-orbiter spacecraft by the DSN 34-m BWG antennas at altitudes of 500 km, 5000 km, and geosynchronous altitude (35789 km). As is the case with the other 34-m antennas, the size of the circles on the map is larger than the actual size of the antenna keyholes

2.2.3.10   34-m BWG Antennas Receive Coverage of Earth Orbiter Spacecraft

Figure 11 illustrates the transmit coverage of planetary spacecraft by the DSN 34-m BWG antennas. As is the case with the other 34-m antennas, the size of the circles on the map is larger than the actual size of the antenna keyholes. Protection of the high ground at DSS 54 is provided by disabling the transmitter between 267 and 3 degrees azimuth.

2.2.3.11   11-m Subnet Receive Coverage

Figure 12 illustrates the receive coverage of the 11-m Orbiting Very-long Baseline Interferometry (OVLBI) subnet at 5000 km, geosynchronous altitude (35789 km), and planetary range. The irregular coverage outlines are the result of high ground to the east of DSS 33 and northwest of DSS 54 plus blockage due to other antennas and structures at each complex.

2.2.4   Horizon Masks and Antenna Limits

Figures 13 through 30 show the horizon mask and transmitter limits for all DSN stations. The transmitter limits are identified as the L/P (low power) transmitter mask (or the H/P (high power) transmitter mask depending on the type of transmitter that is available. Only the 70-m stations have both L/P and H/P transmitters, and DSS 43 is the only station that uses different H/P and L/P transmitter limits. At DSS 43, the H/P transmitter limit is set at 10.4 degrees whereas the L/P transmitter limit is set at 10.2 degrees. DSS 14 uses a 10.4-degree limit for both transmitters, and DSS 63 uses a 10.2-degree limit except to the northwest of the station where it is set to 20.2 degrees. These masks and limits are the ones used to establish the coverage depicted in Figures 2 through 11. Each chart shows antenna coordinates in two coordinate systems. For all antennas except those with X-Y mounts, the coordinate systems are azimuth-elevation and hour angle-declination. The antennas with X-Y mounts show azimuth-elevation and X-Y coordinates.

Charts showing hour angle-declination coordinates can be used to provide an elevation profile (for estimating antenna gain and noise temperature) for spacecraft at planetary distances where the declination remains constant for an entire tracking pass. The hour angle curves on these charts have been spaced at increments of 15 degrees so that pass length may conveniently be estimated. These figures were plotted by a program written as a collection of Microsoft Excel 97/98 macros. This program is available for download (1.1 Mbytes) from the 810-5 web site (http://eis.jpl.nasa.gov/deepspace/dsndocs/810-005/). This file also contains the land mask data, which can be used to accurately calculate spacecraft rise and set times.

3   Proposed Capabilities

3.1   70-m X-band Uplink Implementation

An X-band transmit capability is being added to the 70-m antenna subnet. The X-band transmit coverage will be the same as is presently depicted in Figure 3.

3.2   34-m BWG Ka-band Implementation

A Ka-band receive capability is being added to all 34-m BWG antennas. The Ka-band receive coverage will be the same as is presently depicted in Figure 6.
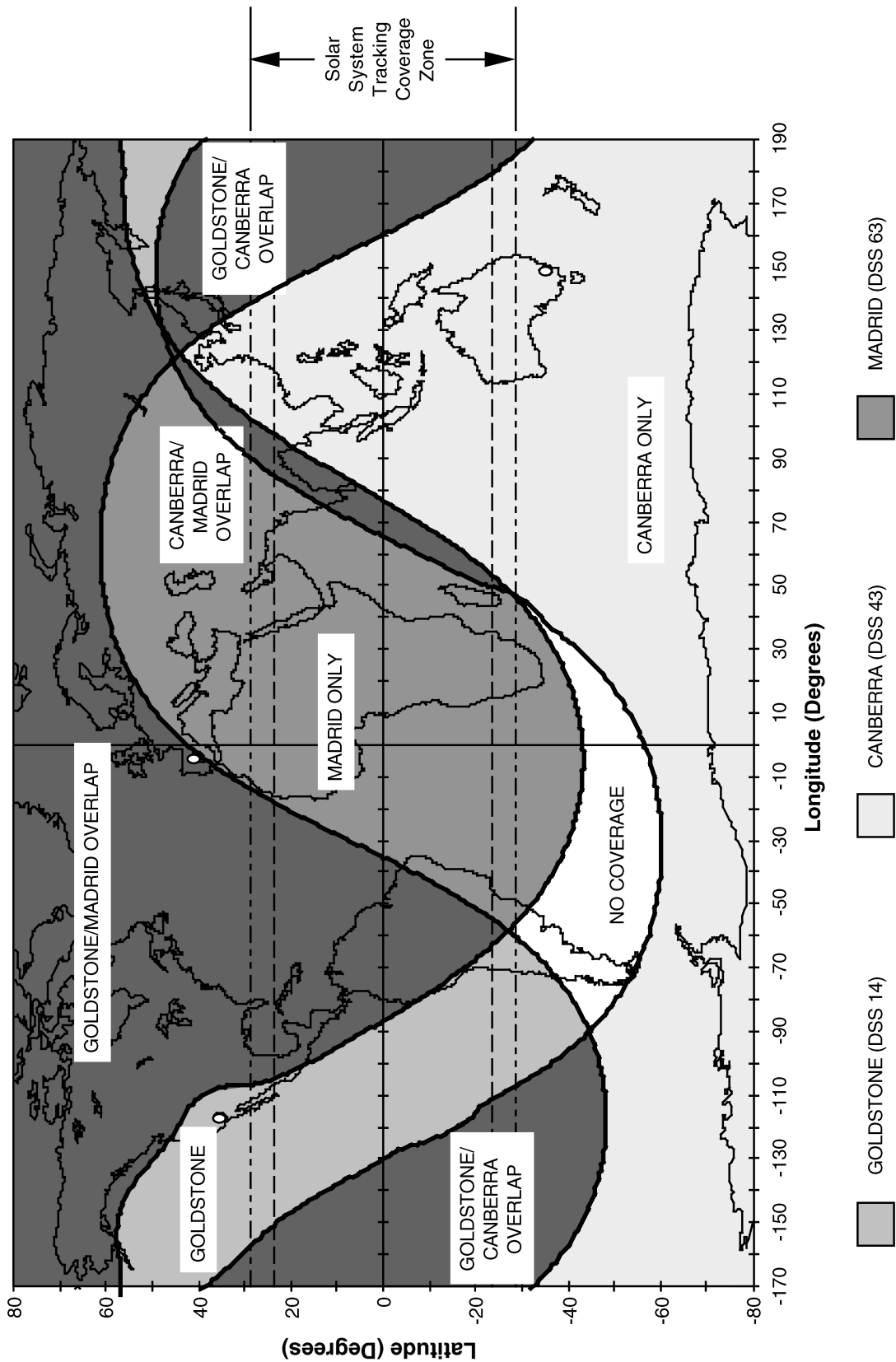
Figure 2. DSN 70-m Subnet Receive Coverage, Planetary Spacecraft
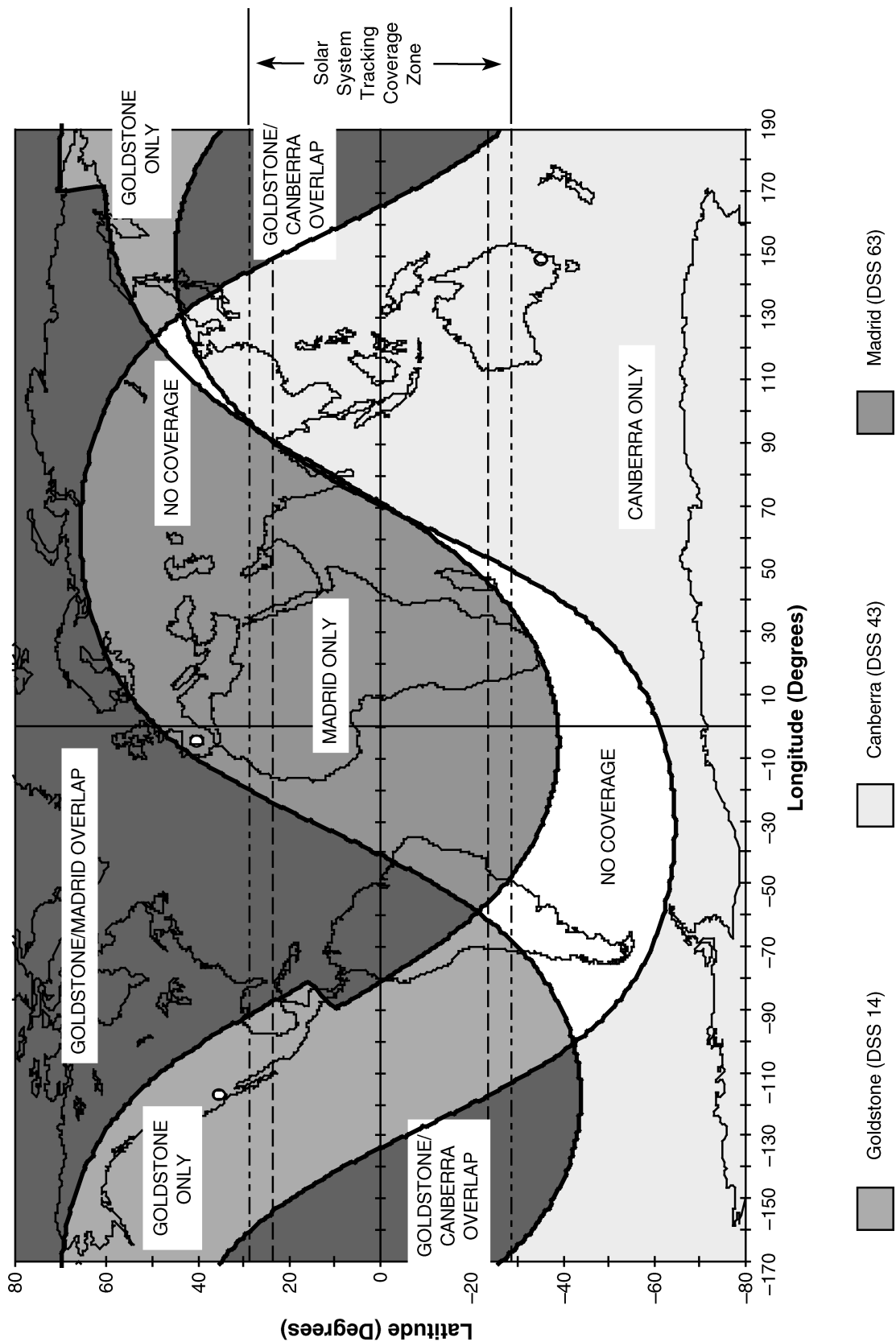
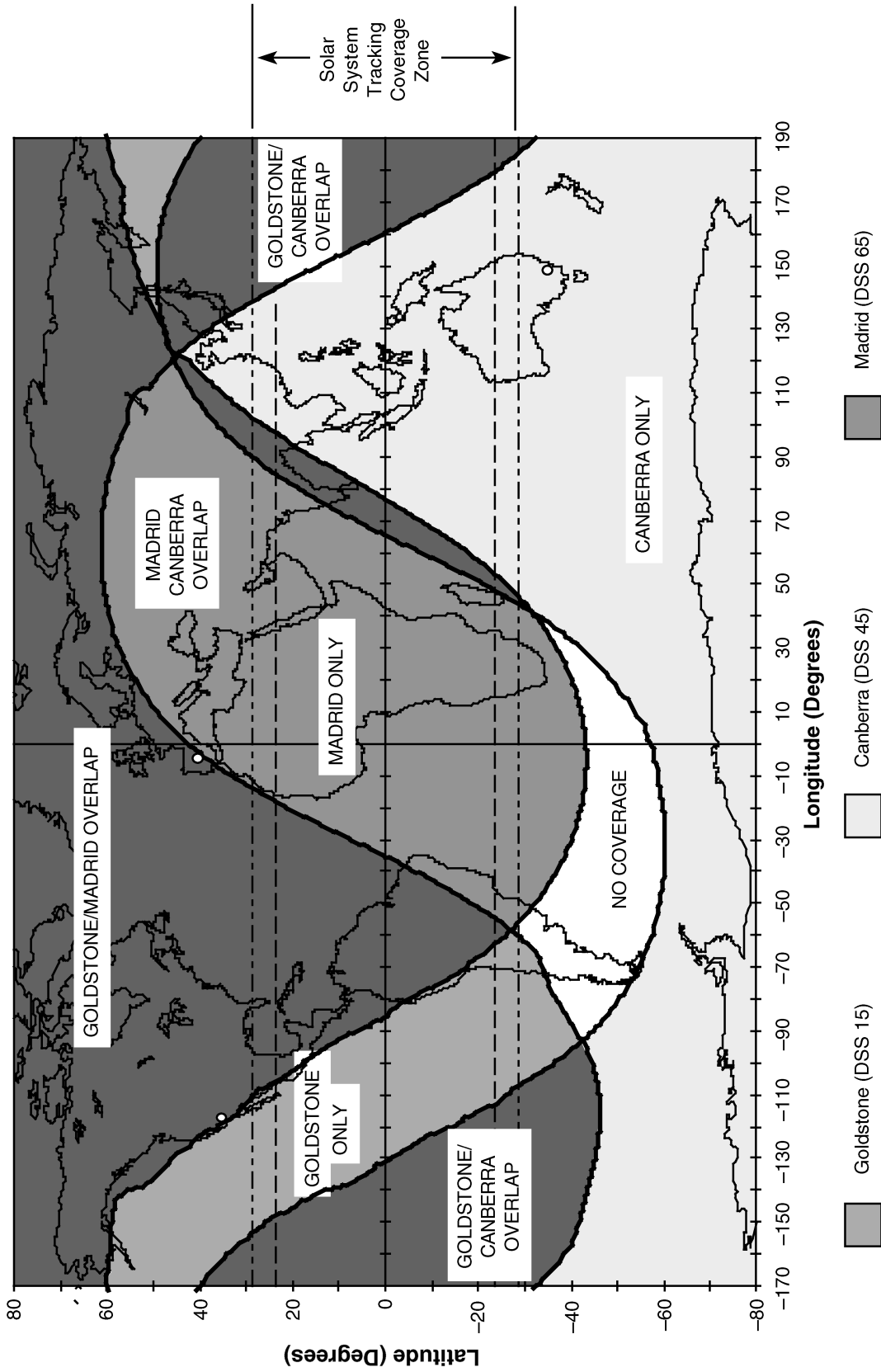Figure 3. DSN 70-m Subnet Transmit Coverage, Planetary Spacecraft

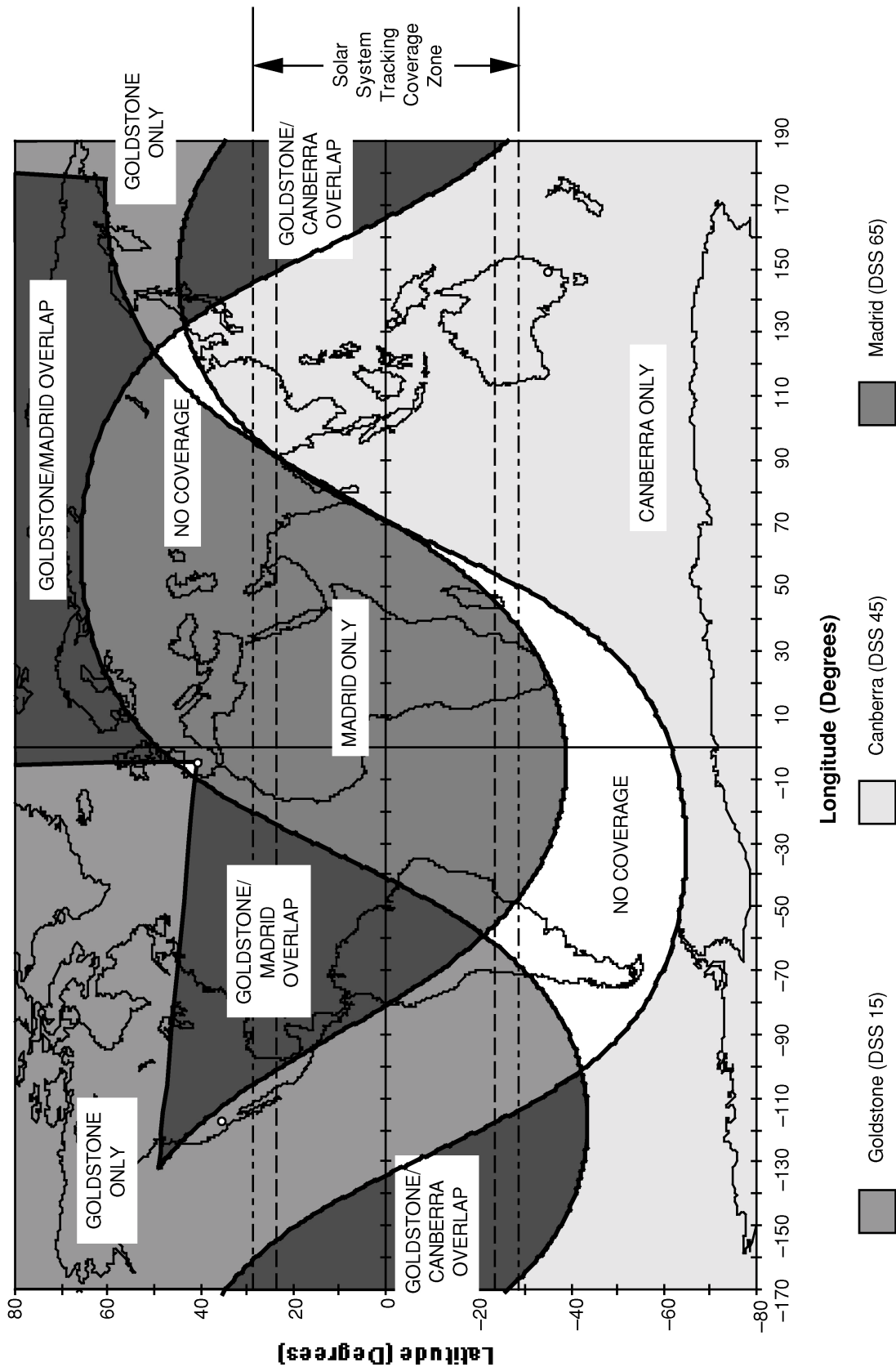Figure 4. DSN 34-m HEF Subnet Receive Coverage, Planetary Spacecraft

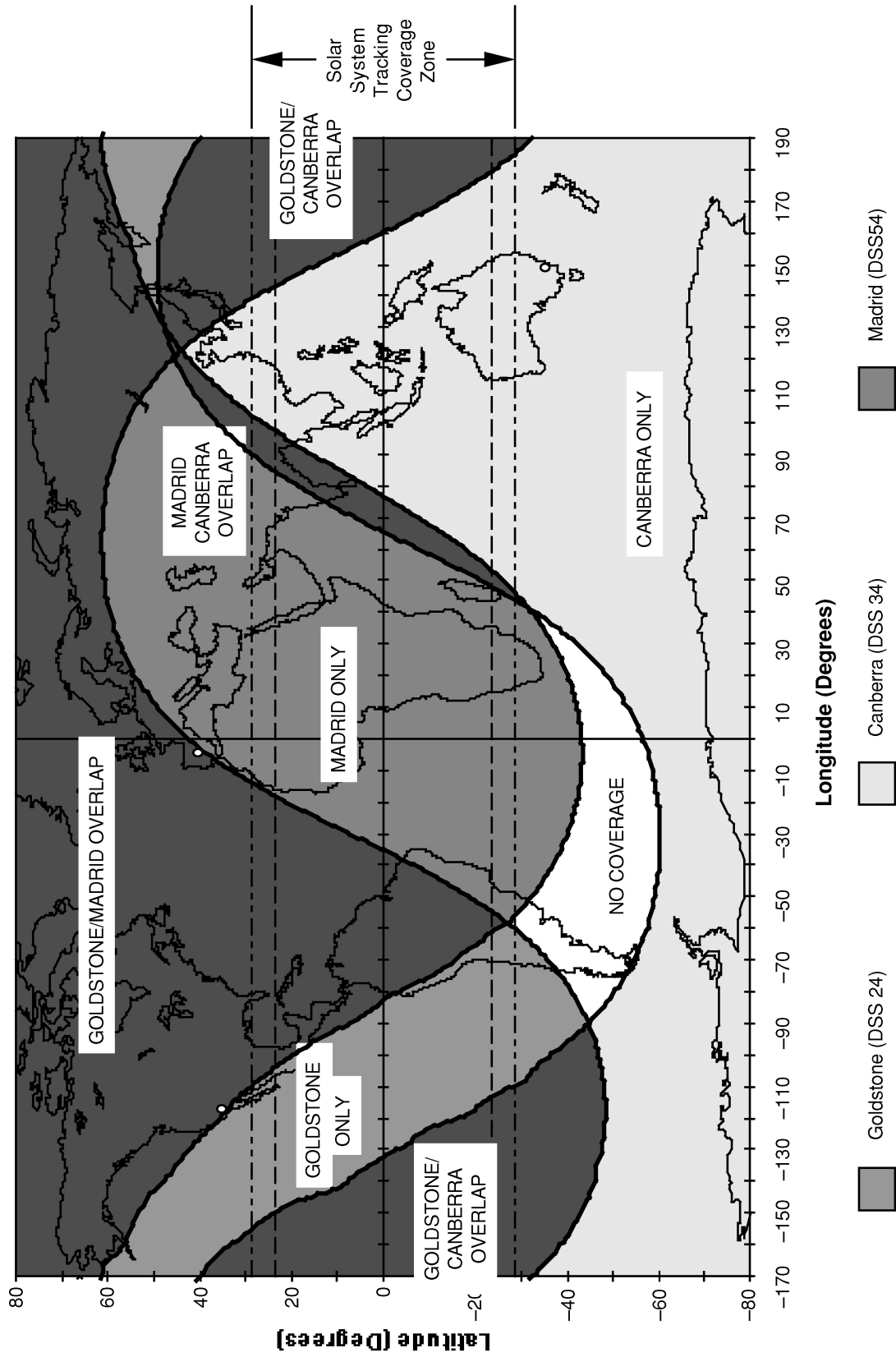Figure 5. DSN 34-m HEF Subnet Transmit Coverage, Planetary Spacecraft

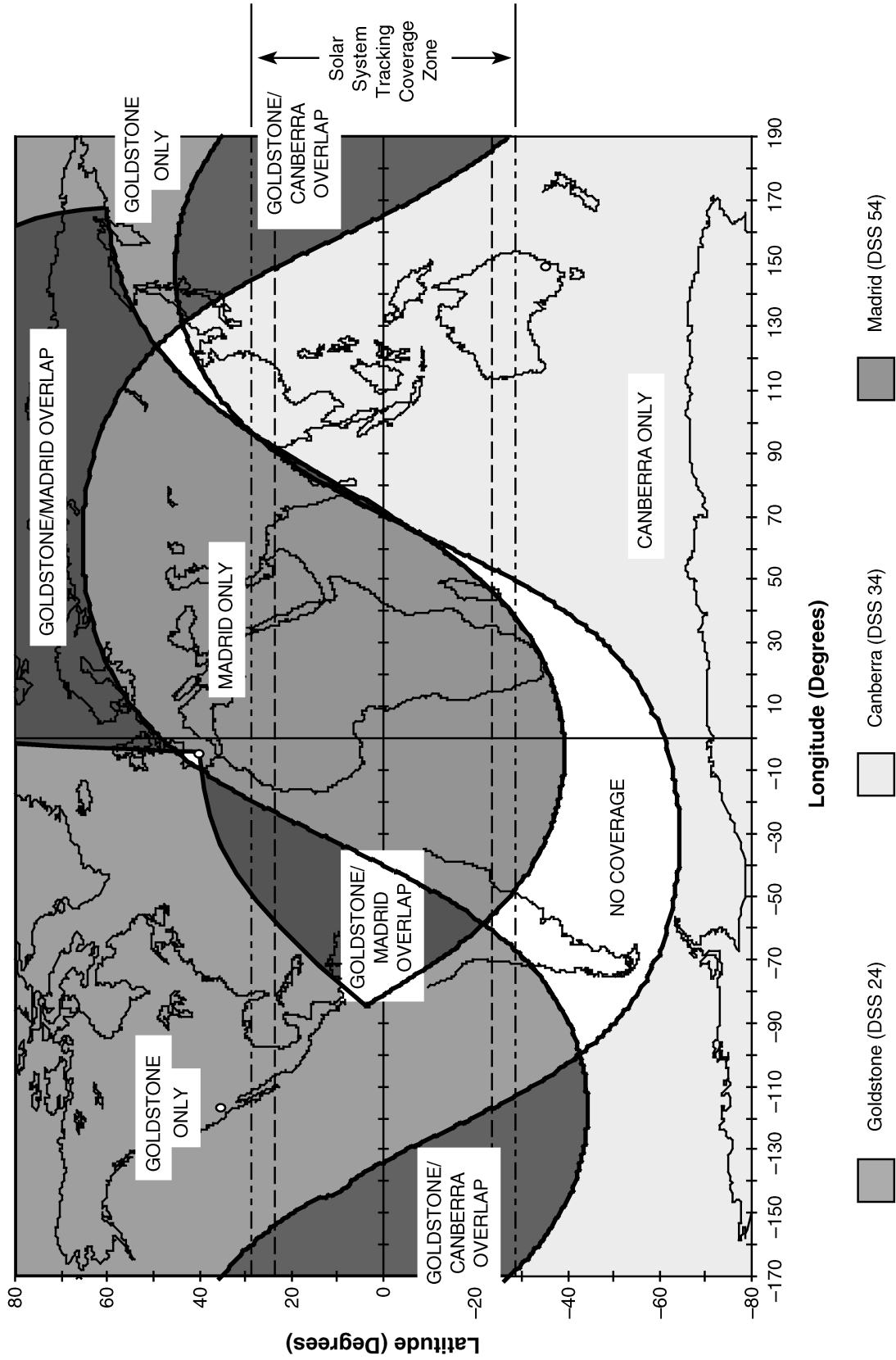Figure 6. DSN 34-m BWG Antennas Receive Coverage, Planetary Spacecraft

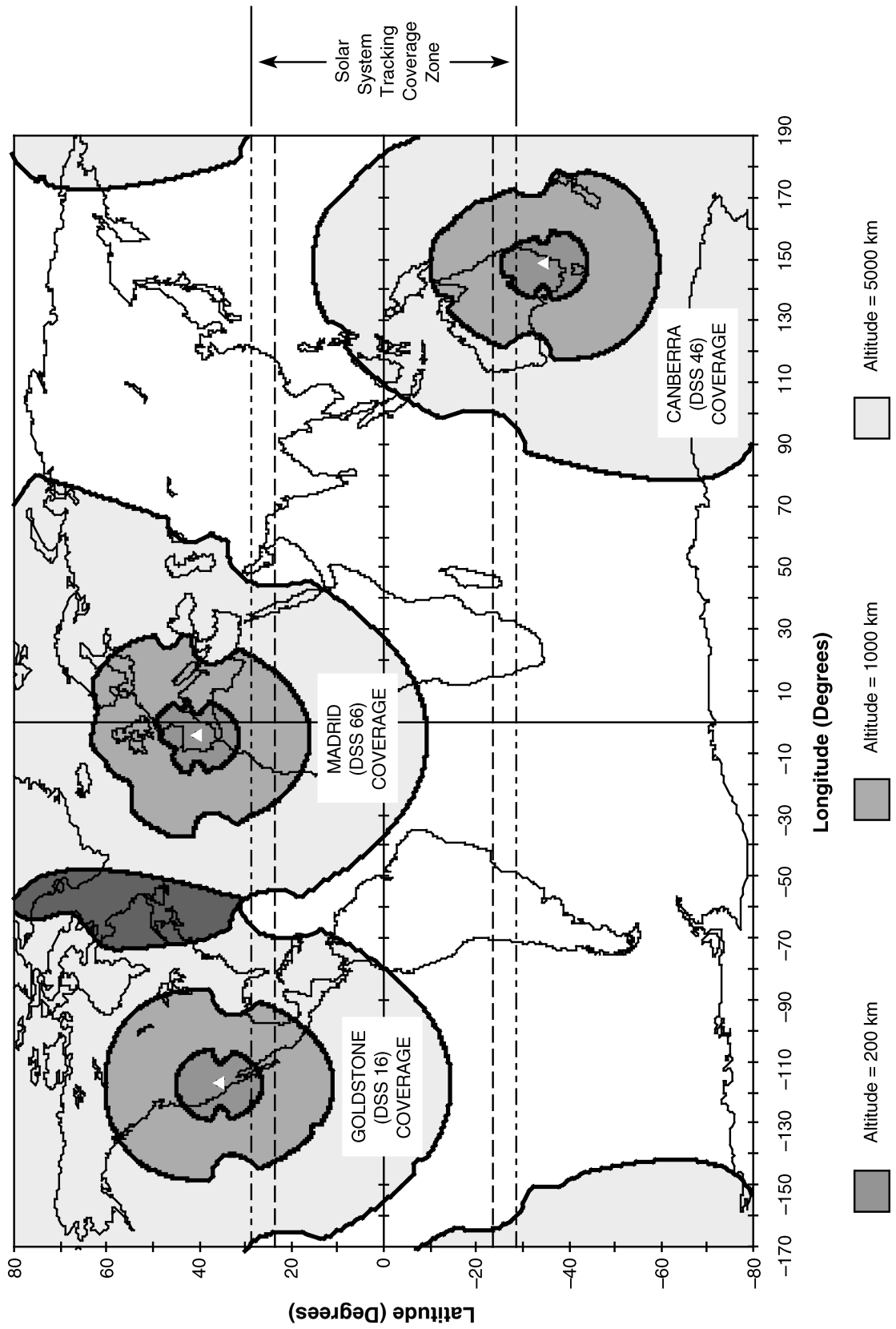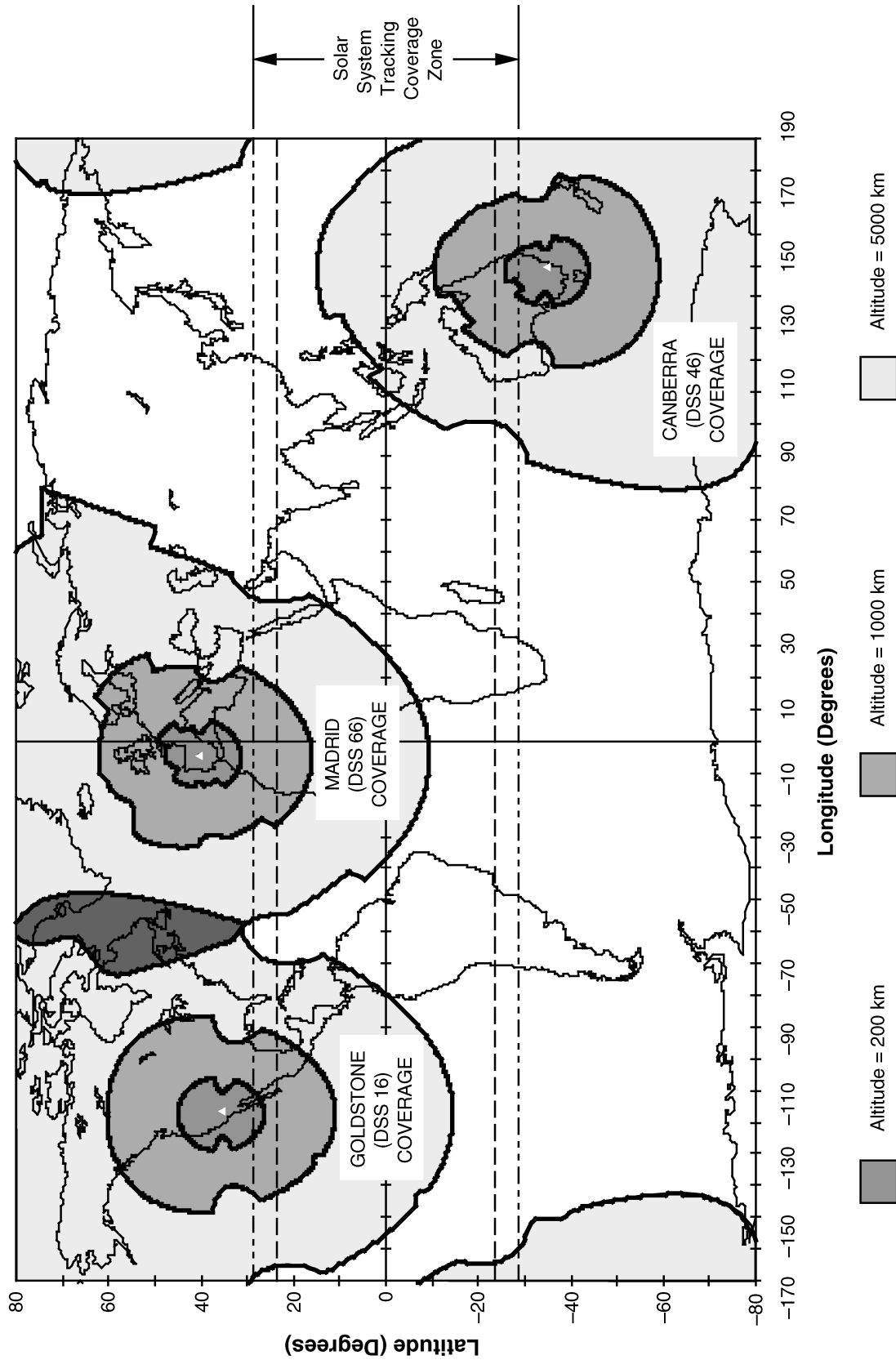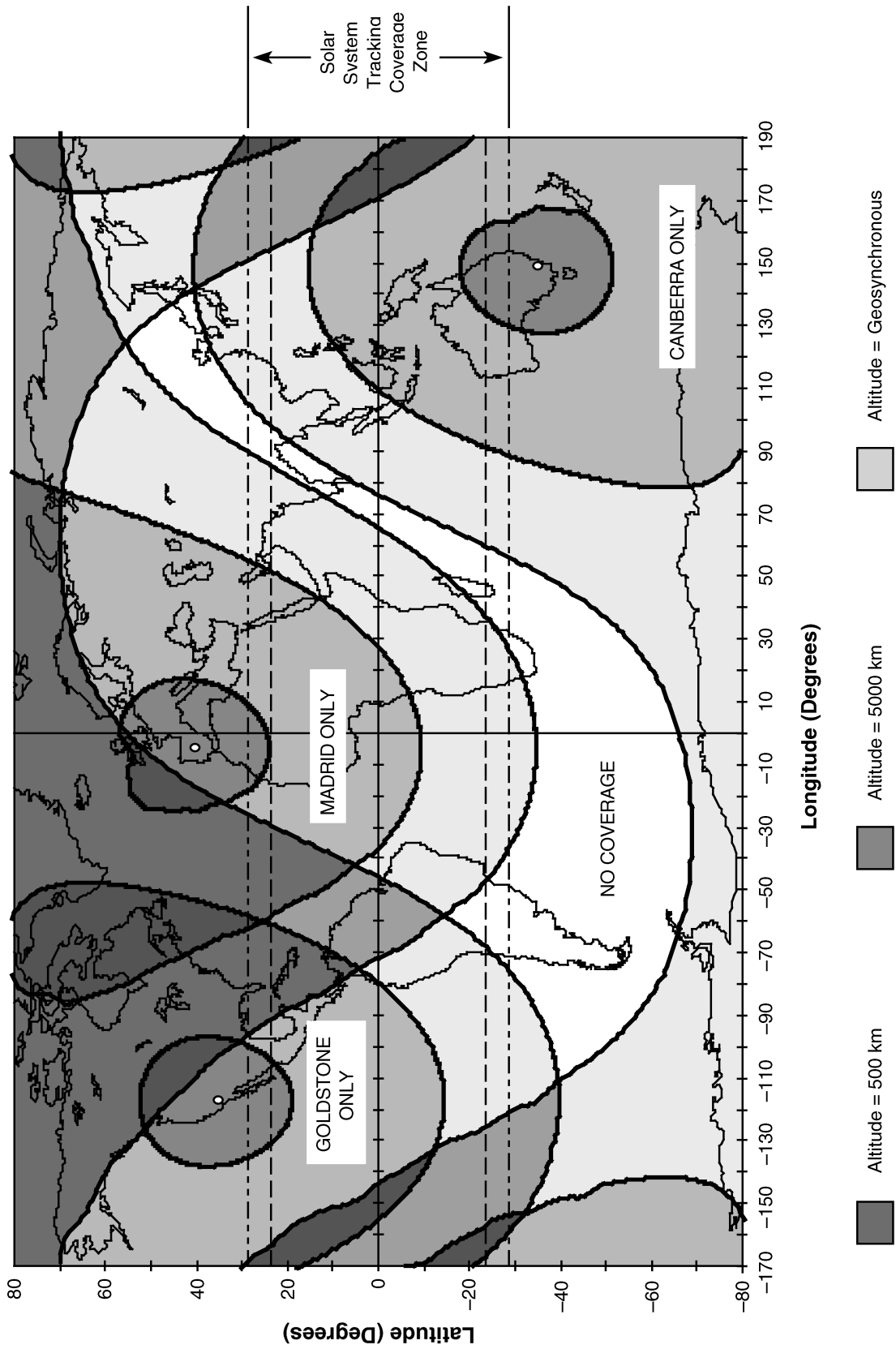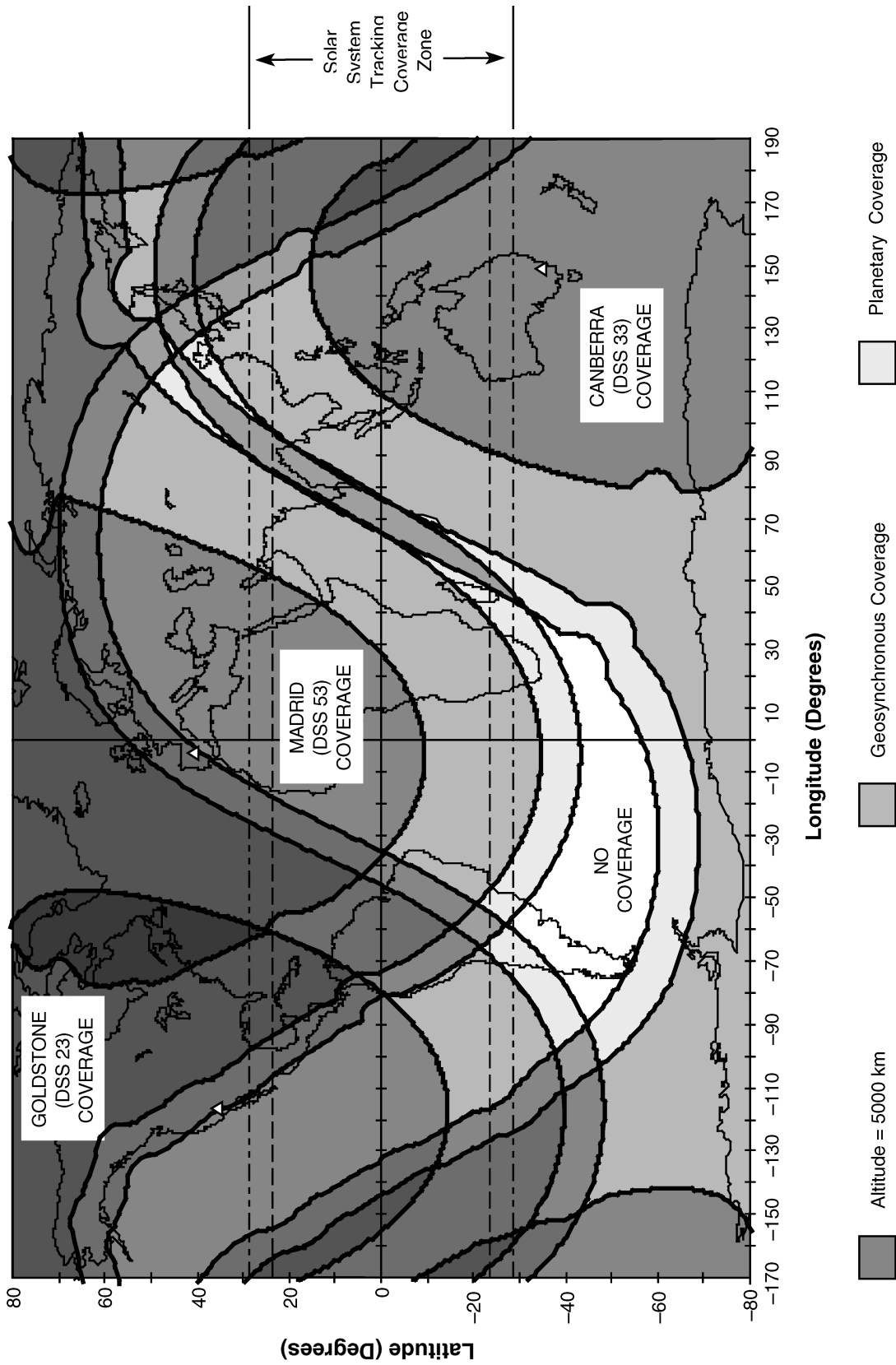Figure 7. DSN 34-m BWG Antennas Transmit Coverage, Planetary Spacecraft

Figure 8. DSN 26-m Subnet Receive Coverage, Earth Orbiter Spacecraft

Figure 9. DSN 26-m Subnet Transmit Coverage, Earth Orbiter Spacecraft

Figure 10. DSN 34-m BWG Antennas Receive Coverage, Earth Orbiter Spacecraft
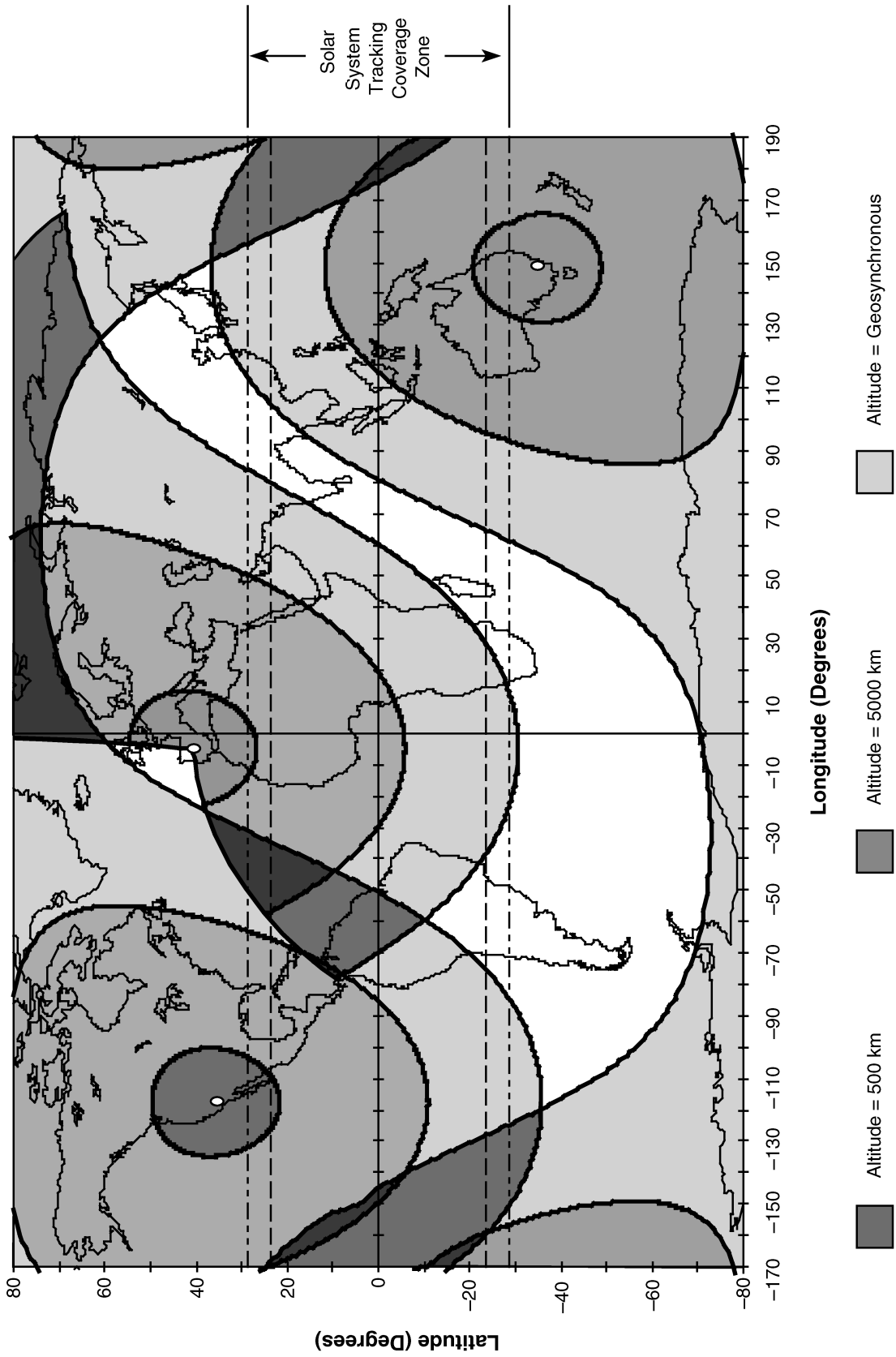
Figure 11. DSN 34-m BWG Antennas Transmit Coverage, Earth-Orbiter Spacecraft

Figure 12. DSN 11-m Subnet Earth-Orbiter and Planetary Receive Coverage
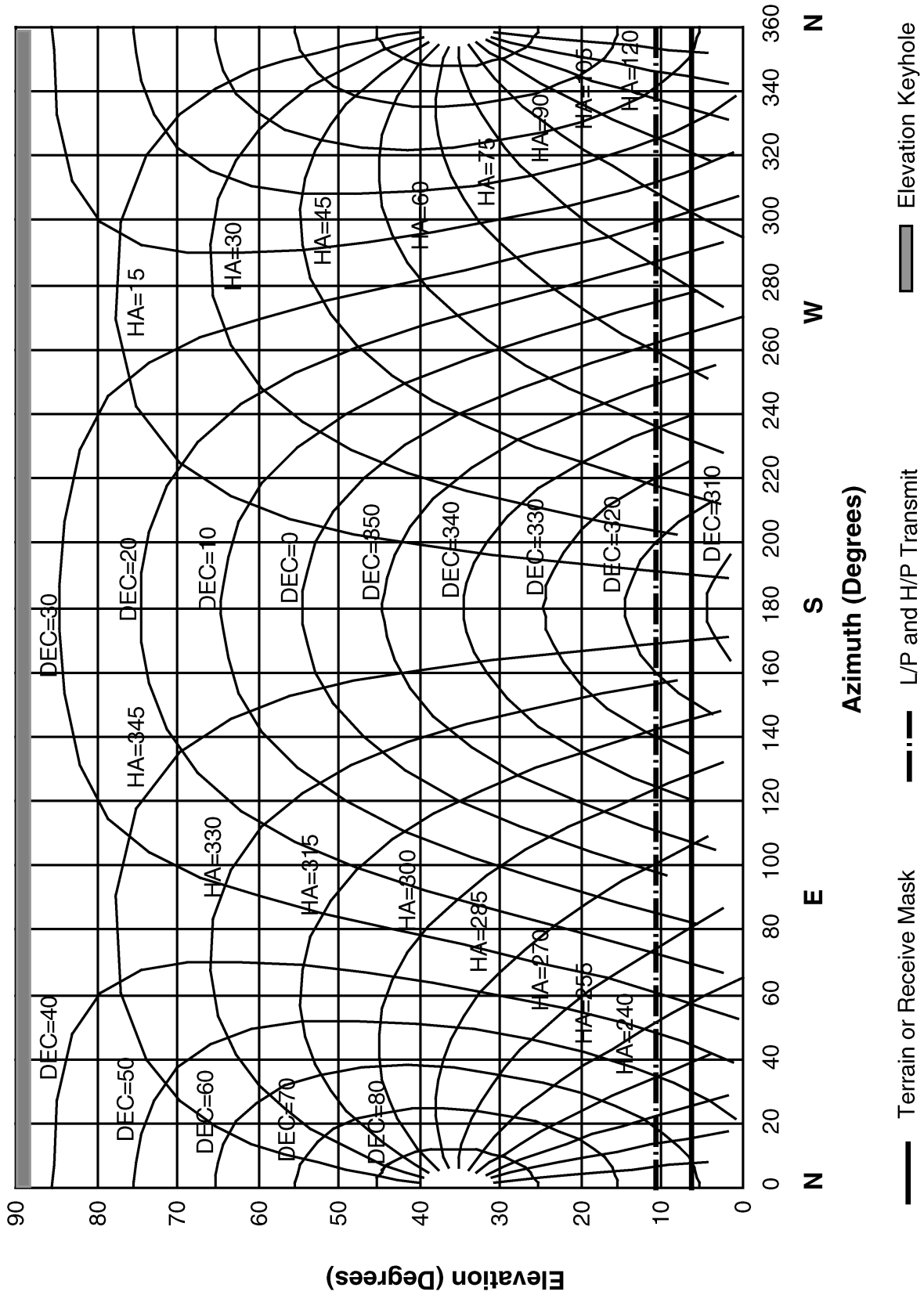
Figure 13. DSS 14 Hour-Angle and Declination Profiles and Horizon Mask
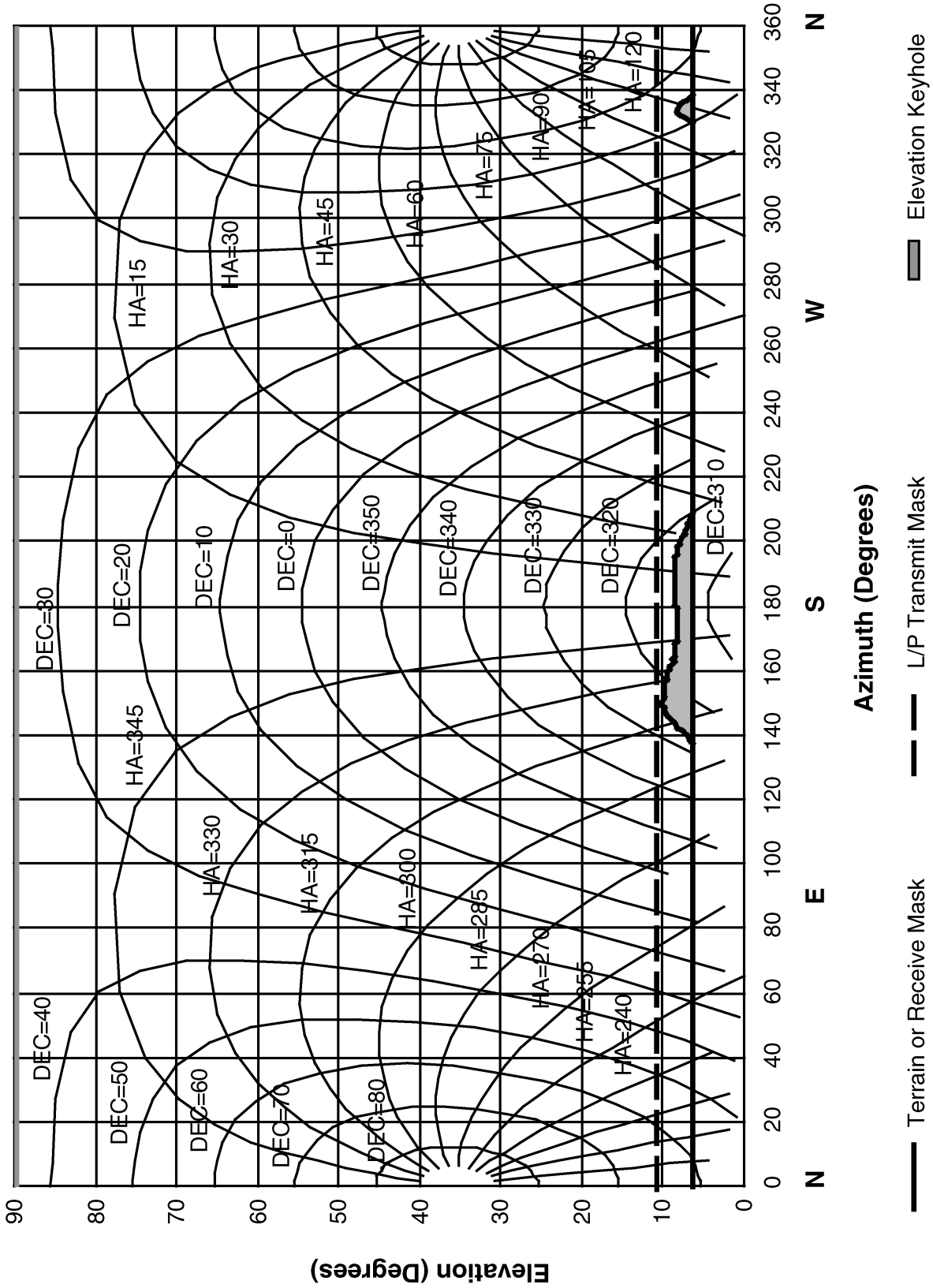
Figure 14. DSS 15 Hour-Angle and Declination Profiles and Horizon Mask
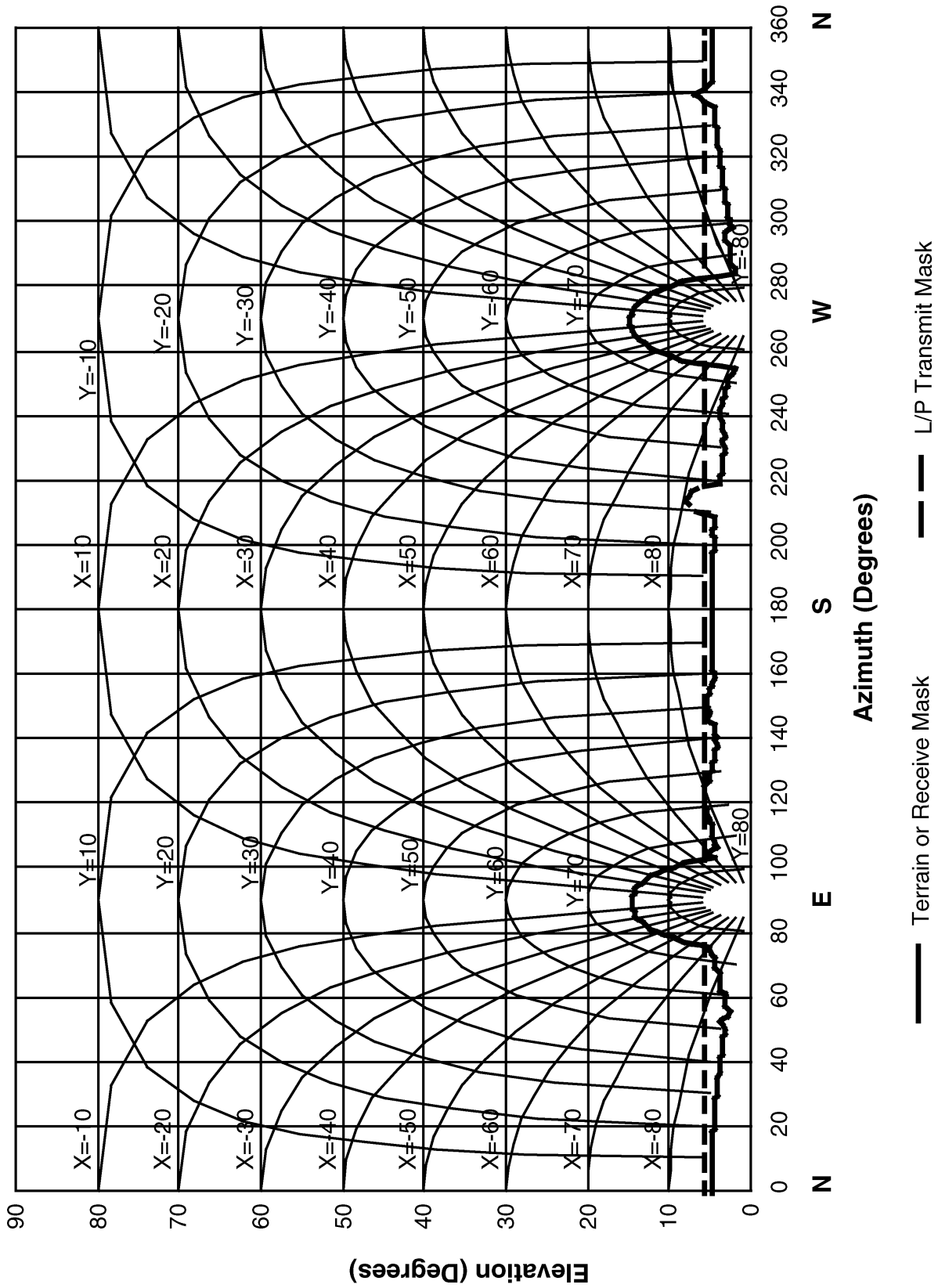
Figure 15. DSS 16 X-Y Profiles and Horizon Mask
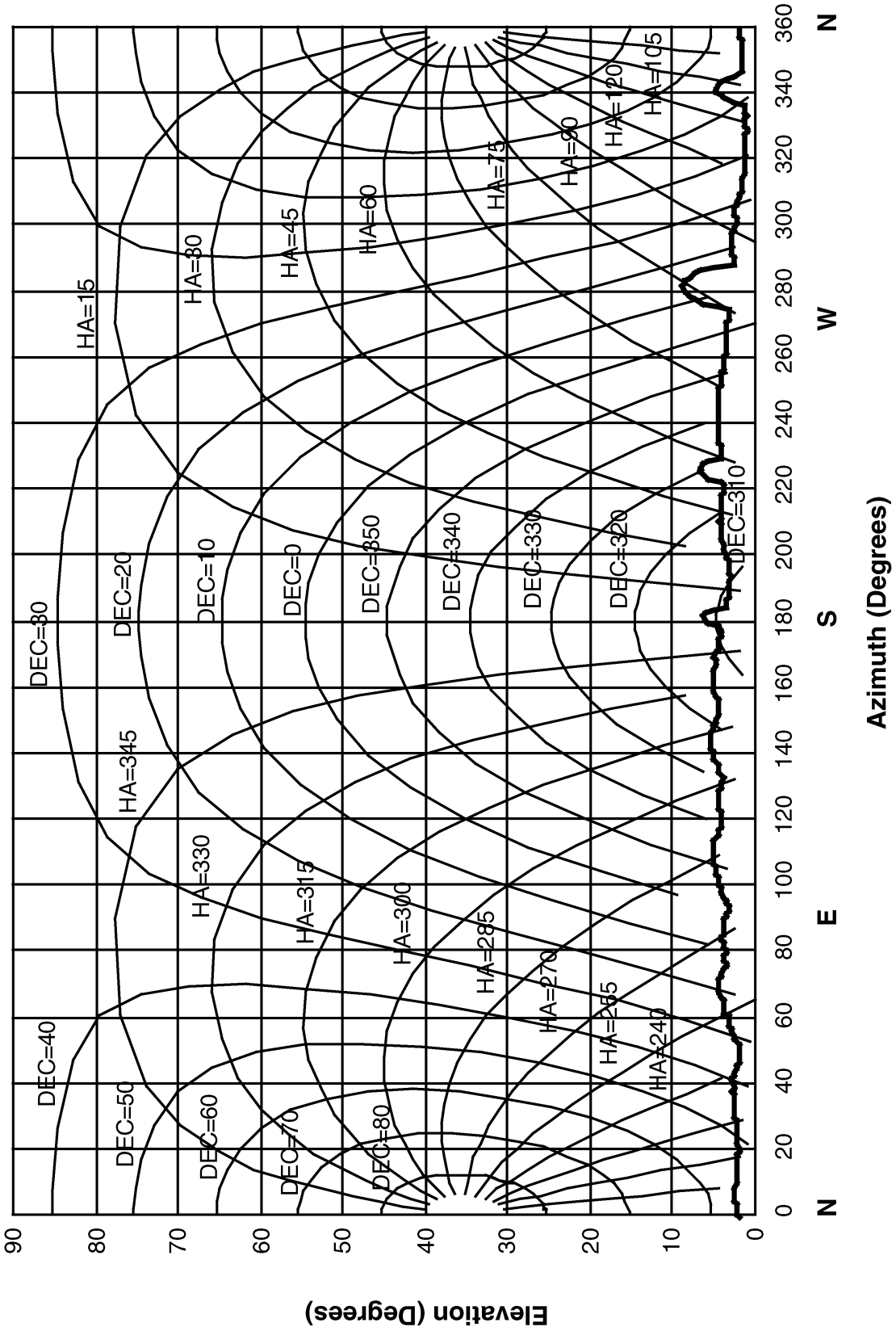
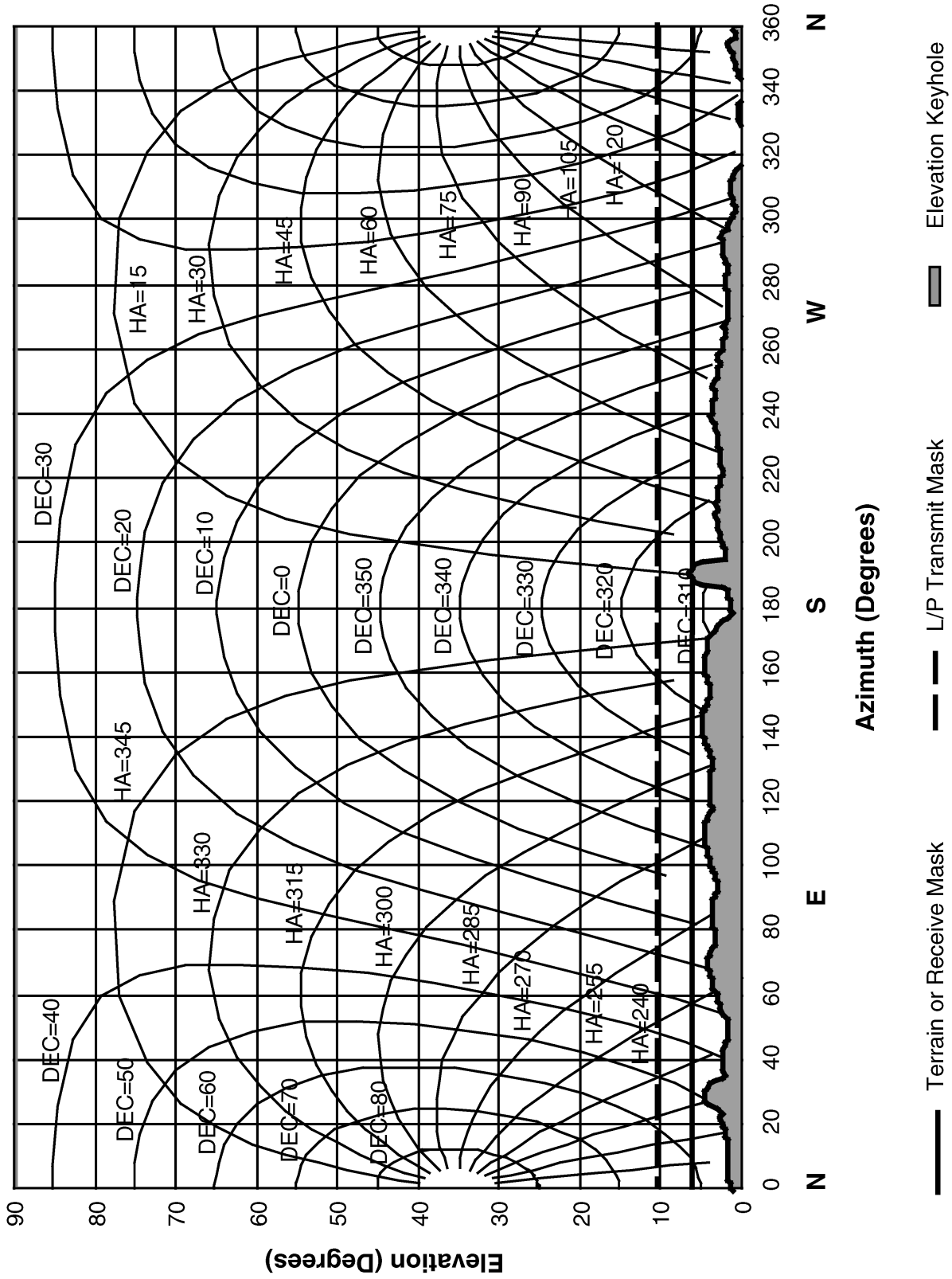Figure 16. DSS 23 Hour-Angle and Declination Profiles and Horizon Mask

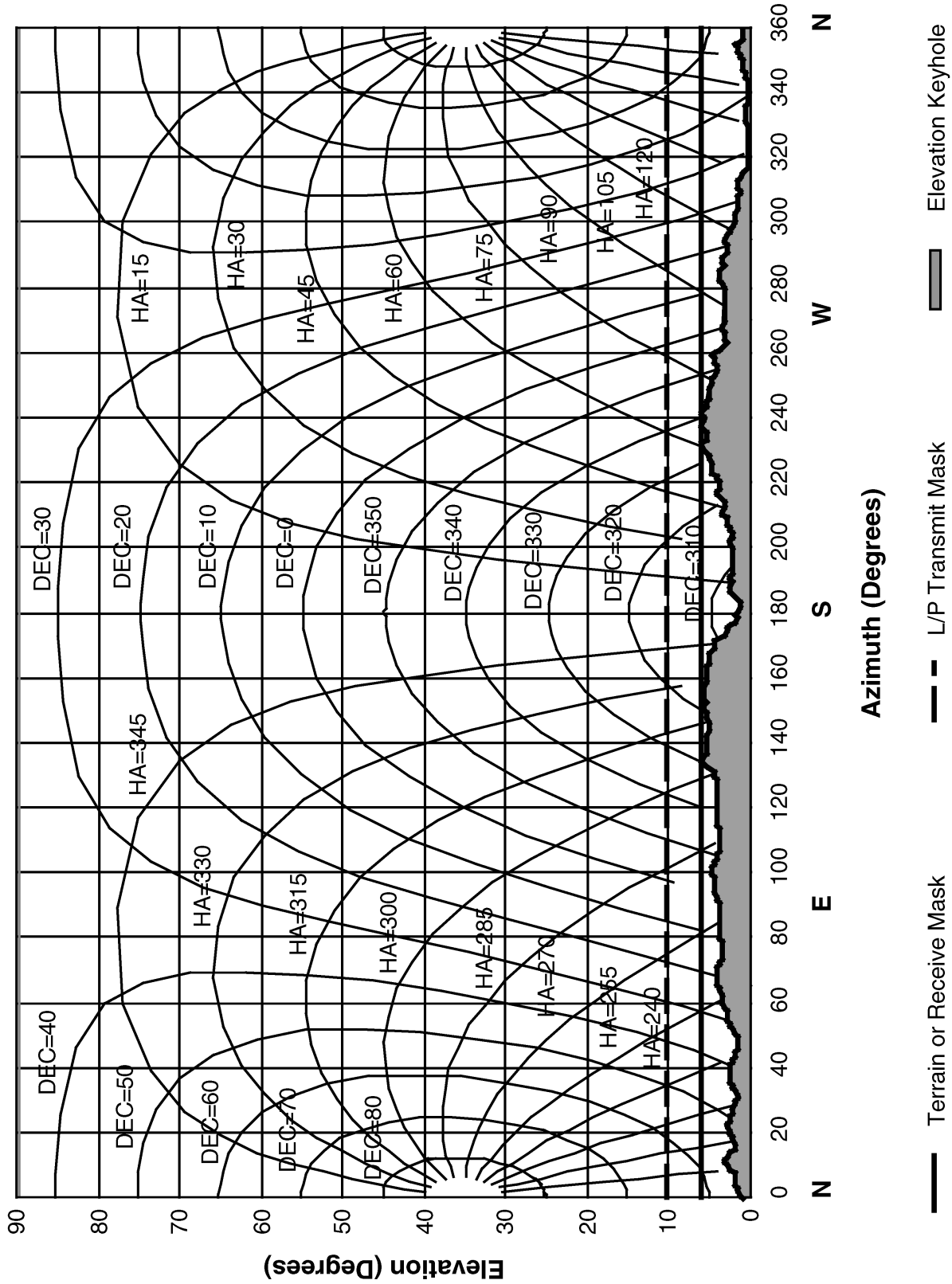Figure 17. DSS 24 Hour-Angle and Declination Profiles and Horizon Mask

Figure 18. DSS 25 Hour-Angle and Declination Profiles and Horizon Mask
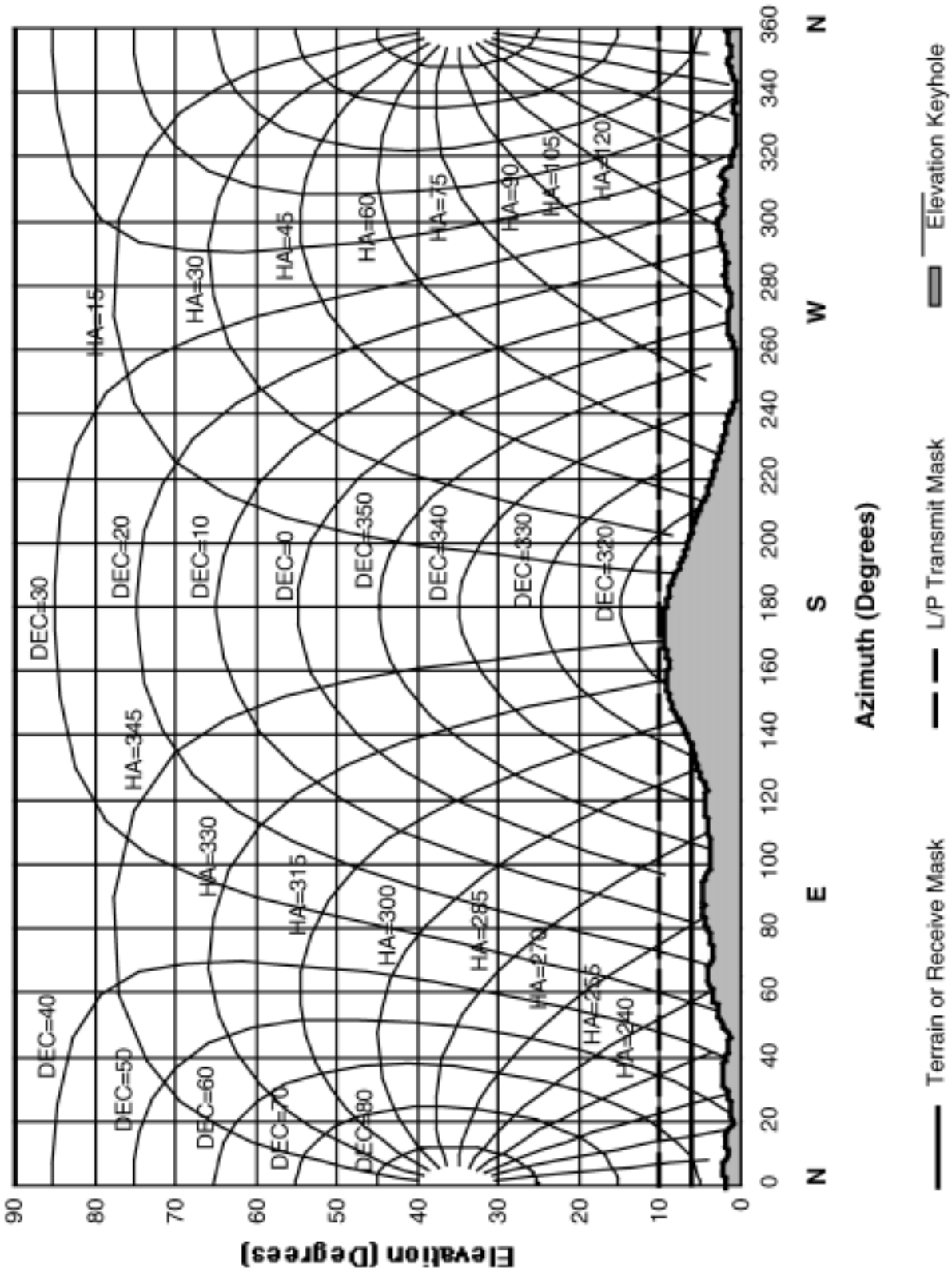
Figure 19.   DSS 26 Hour Angleñelination Profiles and Horizon Mask

Figure 20. DSS 27 Hour-Angle and Declination Profiles and Horizon Mask

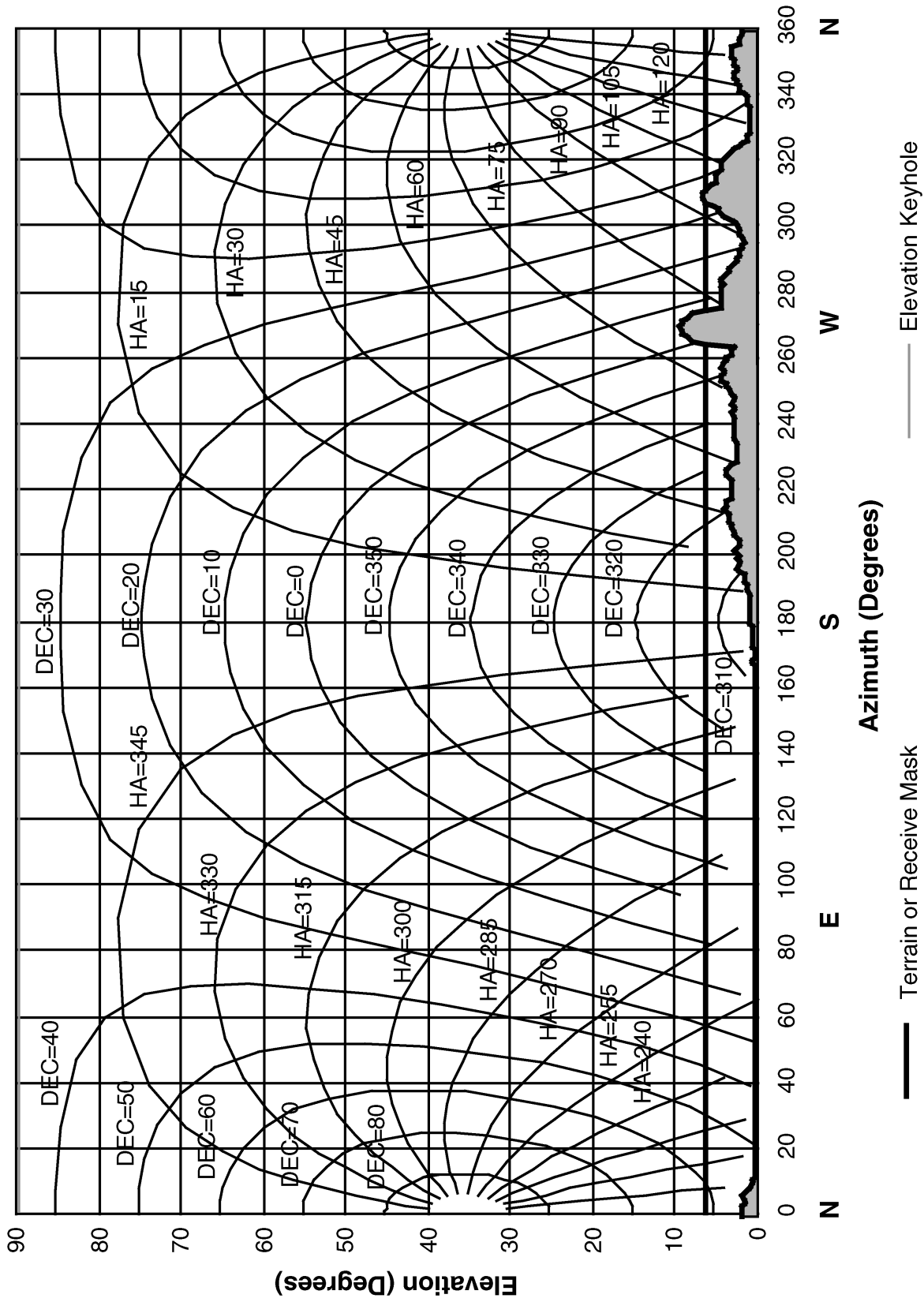—— Terrain or Receive Mask   —— Elevation Keyhole

Figure 21. DSS 33 Hour-Angle and Declination Profiles and Horizon Mask

Figure 22. DSS 34 Hour-Angle and Declination Profiles and Horizon Mask

Figure 23.   DSS 43 Hour Angleñ Declination Profiles and Horizon Mask

Figure 24. DSS 45 Hour-Angle and Declination Profiles and Horizon Mask
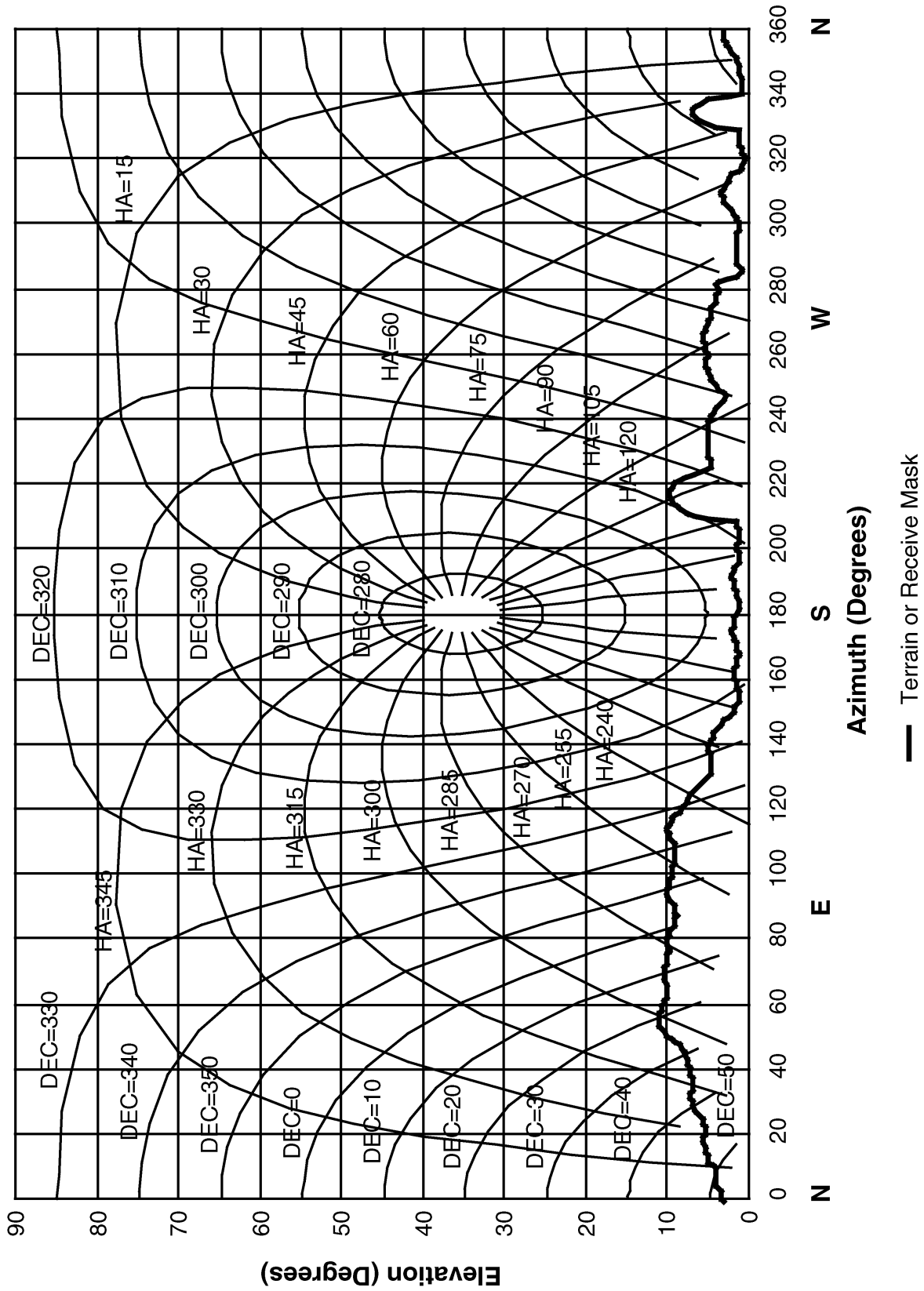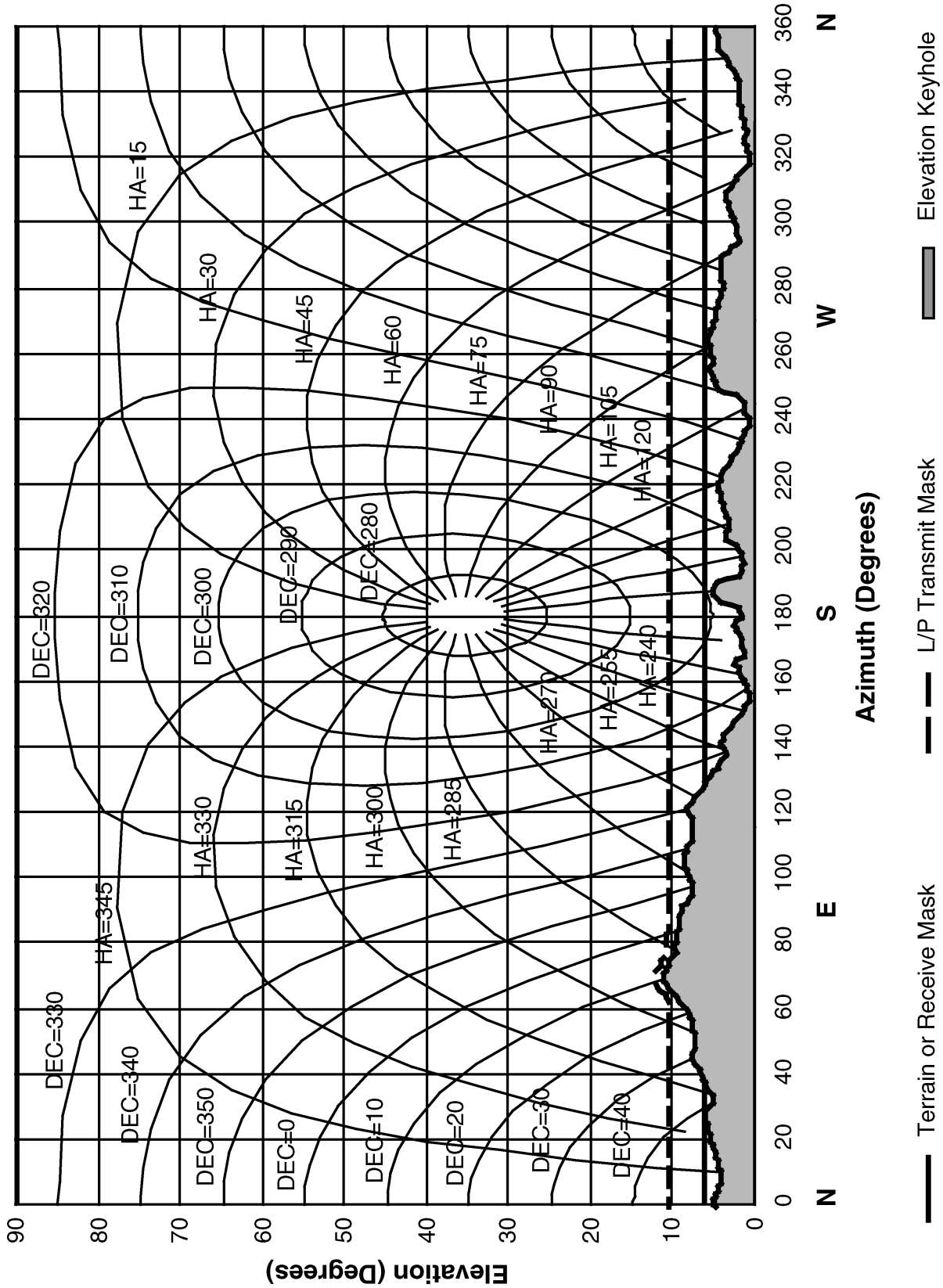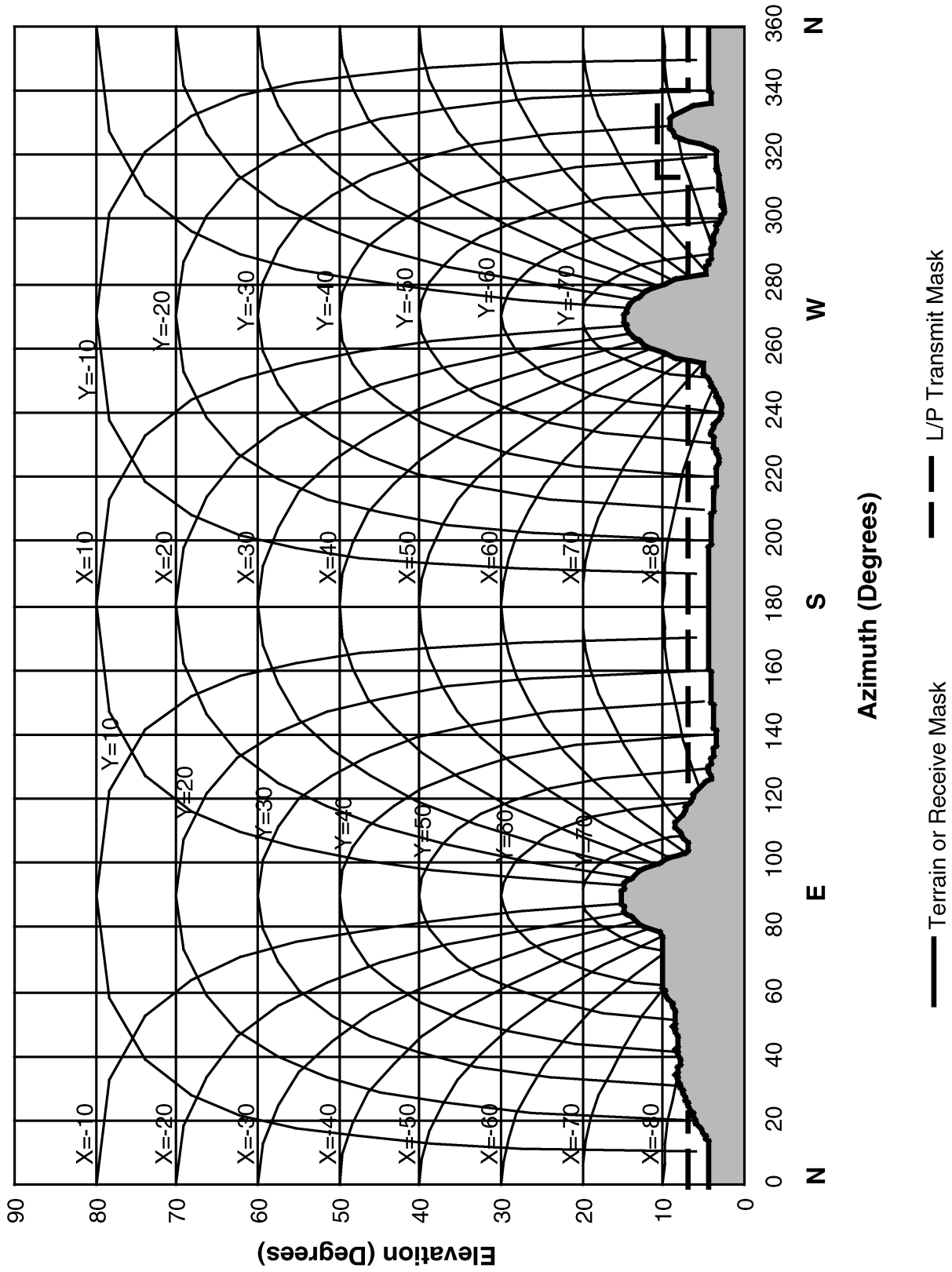
Figure 25. DSS 46 X-Y Profiles and Horizon Mask
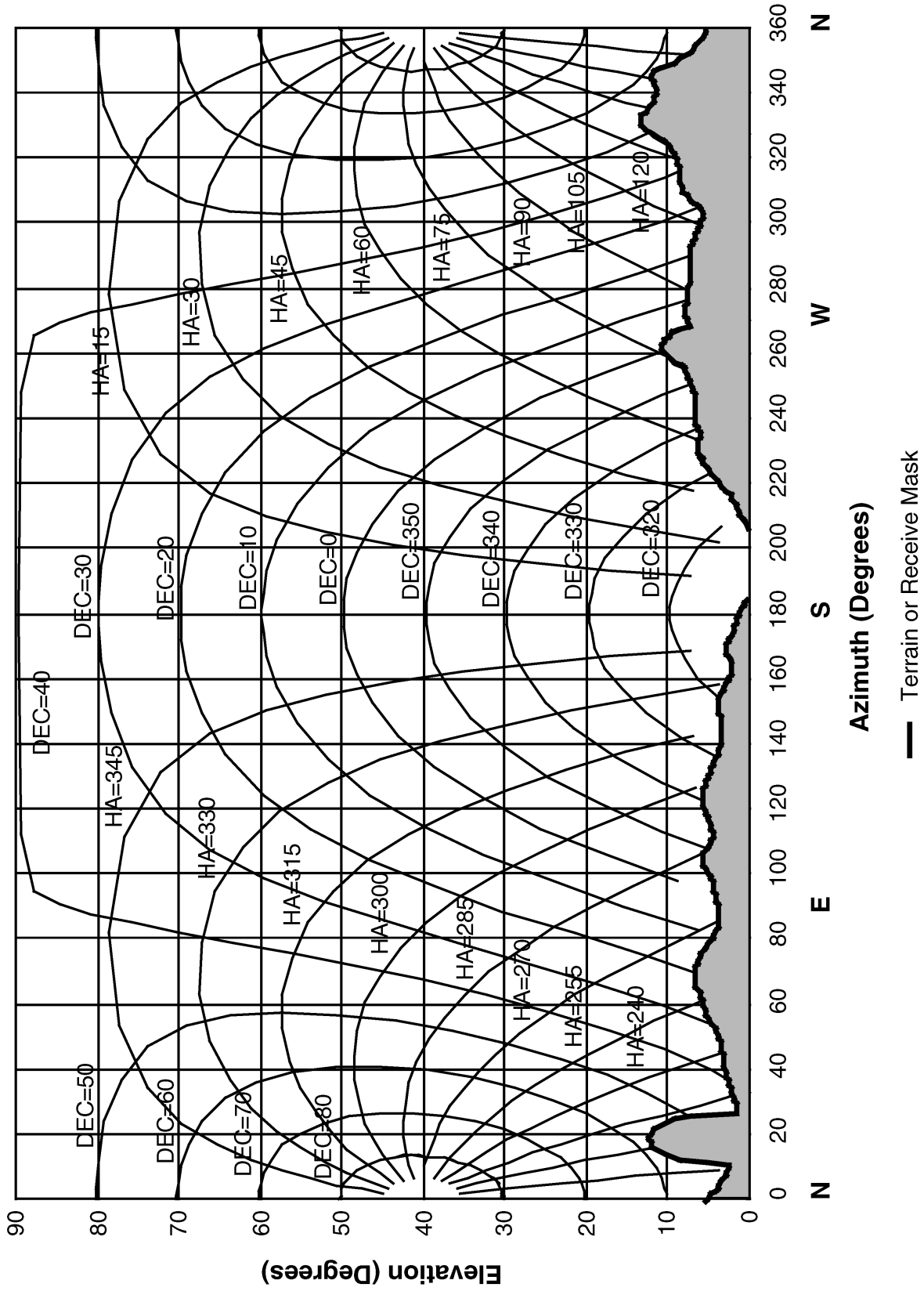
Figure 26. DSS 53 Hour-Angle and Declination Profiles and Horizon Mask

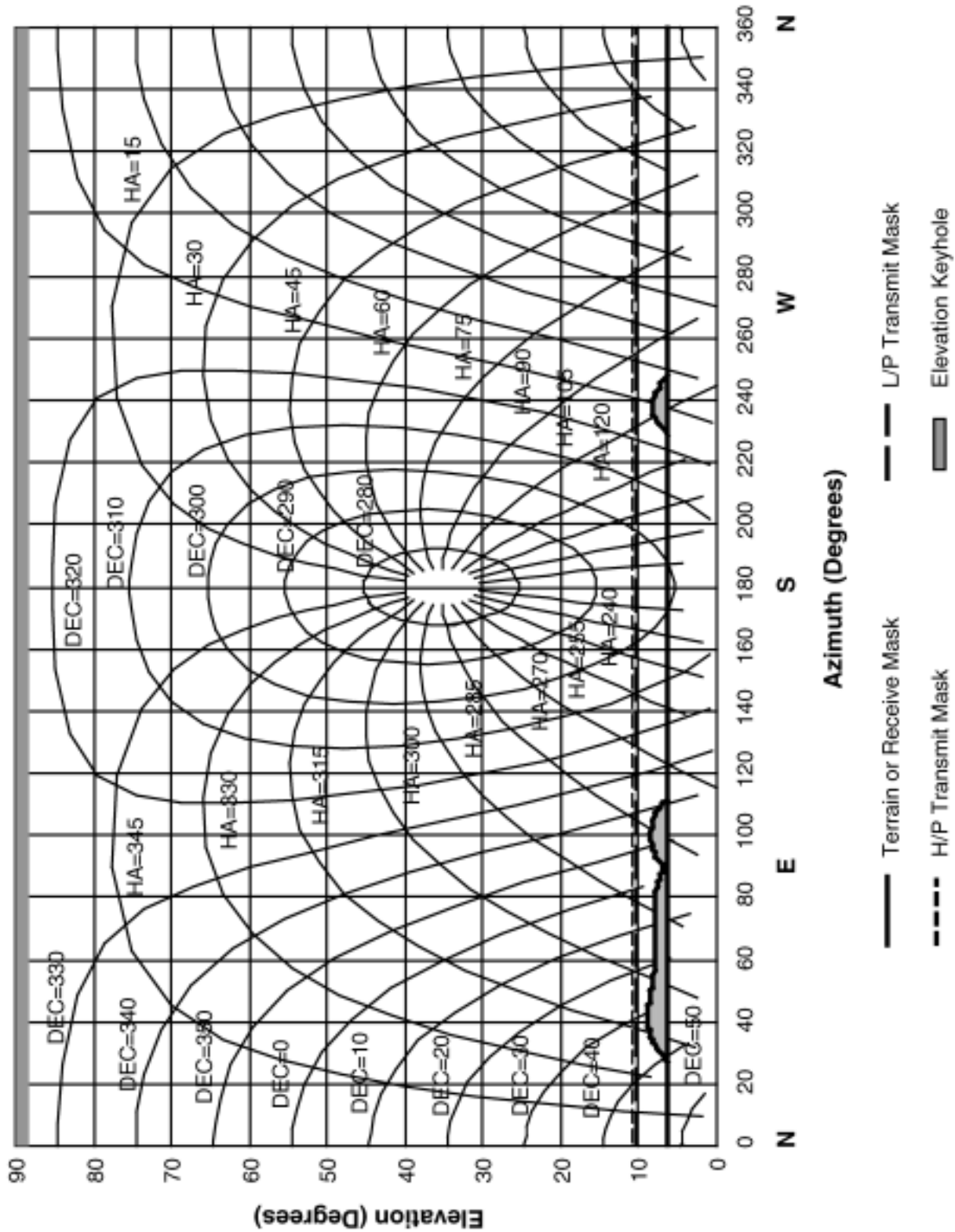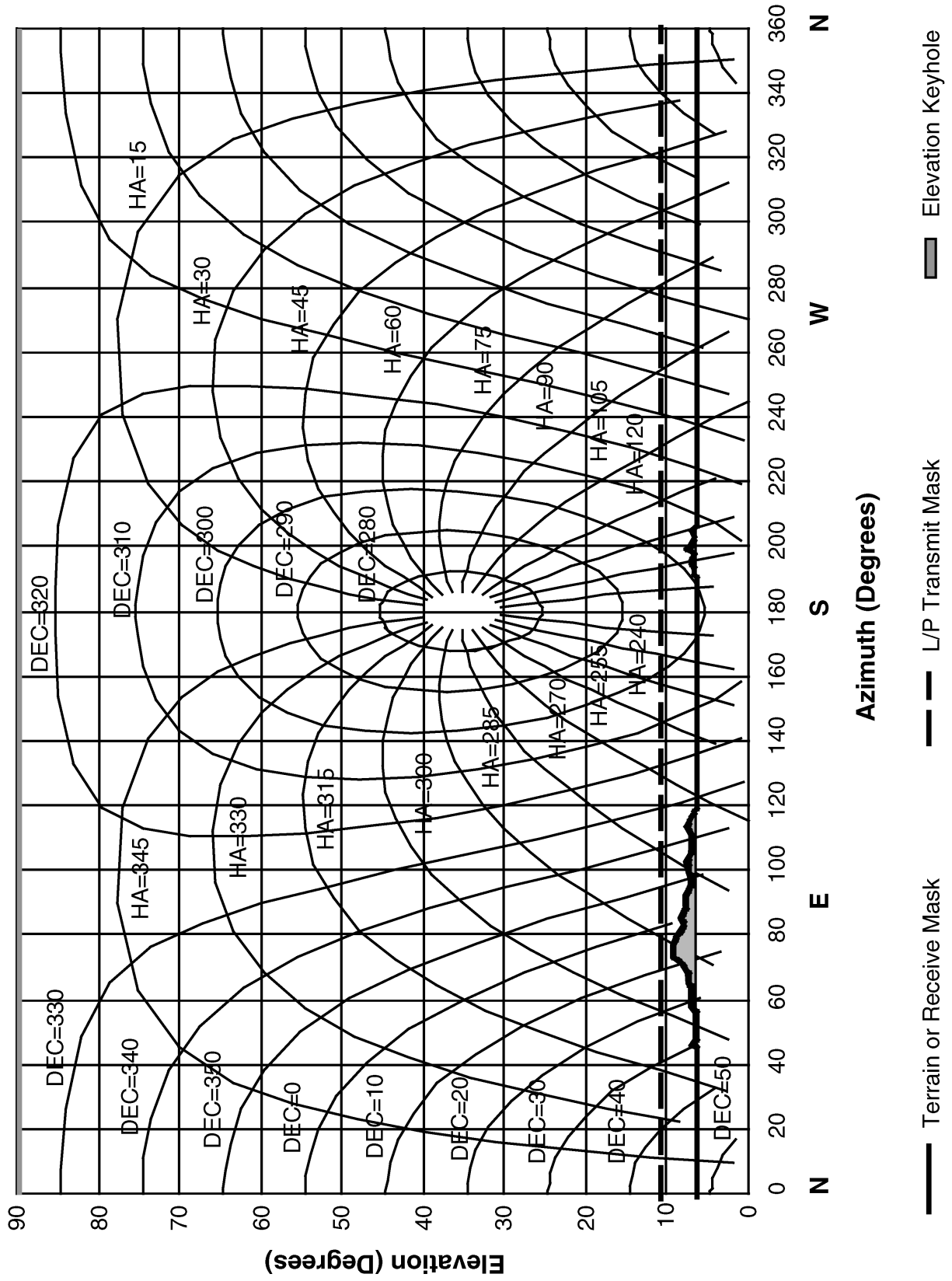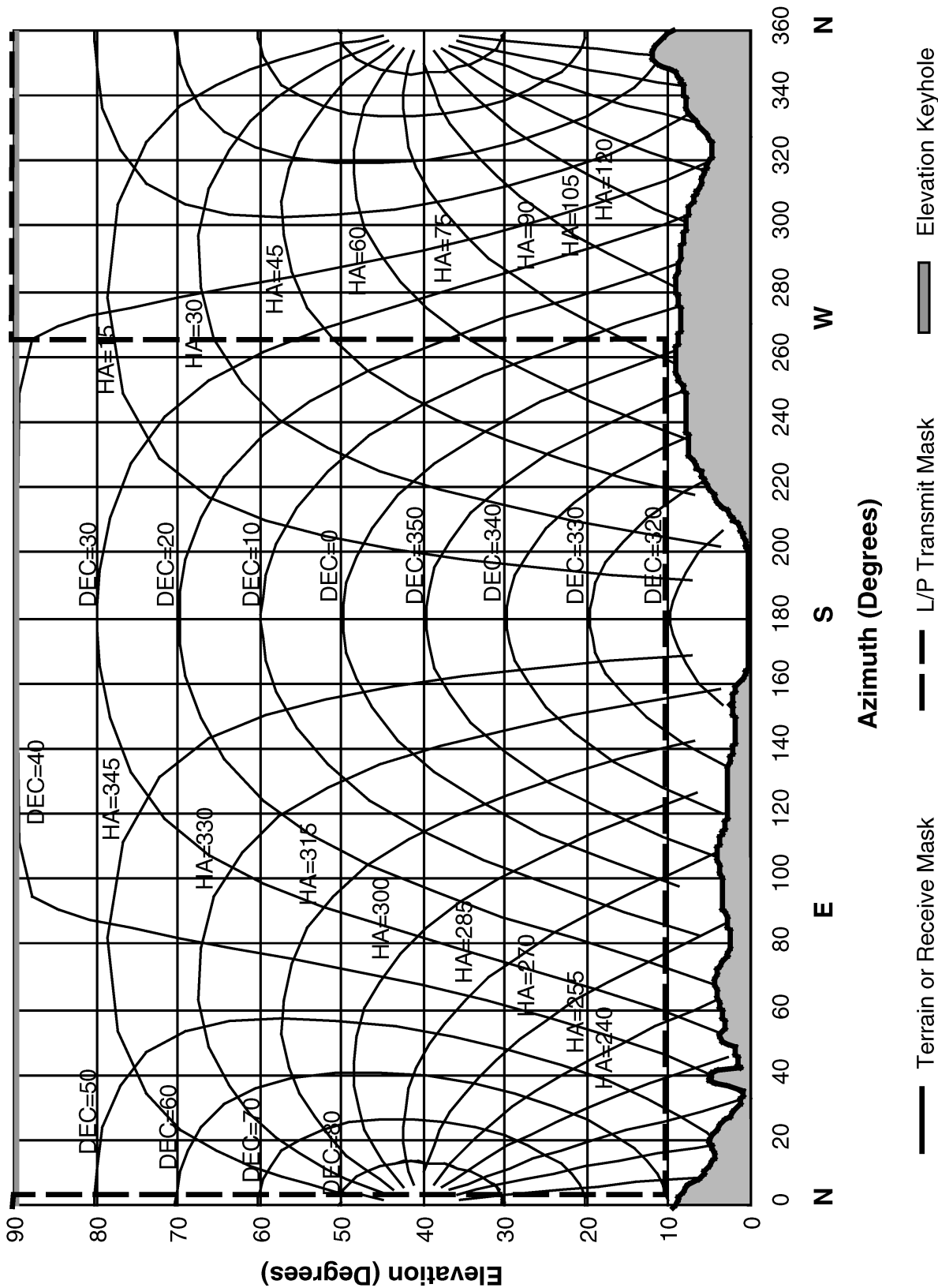Figure 27. DSS 54 Hour-Angle and Declination Profiles and Horizon Mask
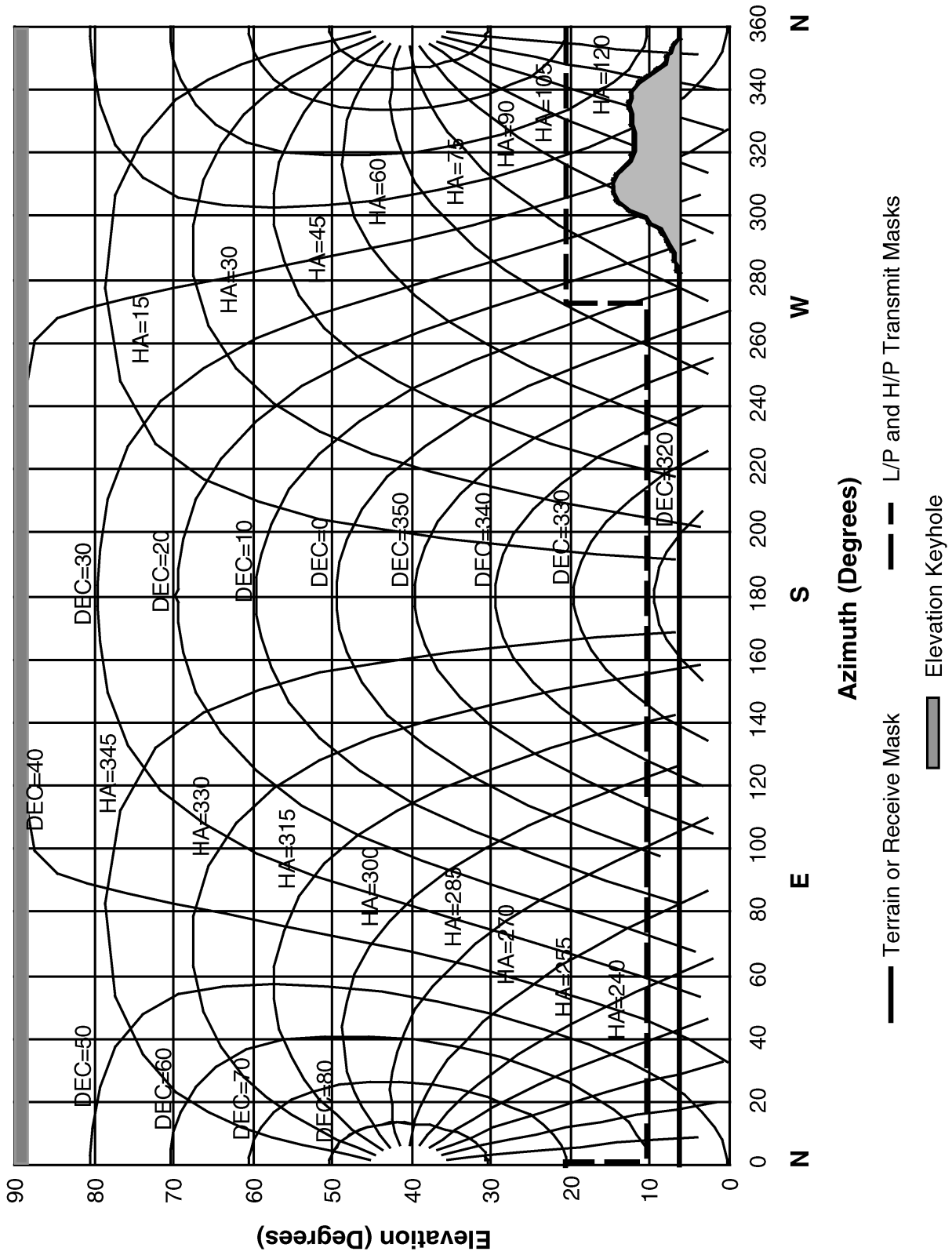
Figure 28. DSS 63 Hour-Angle and Declination Profiles and Horizon Mask
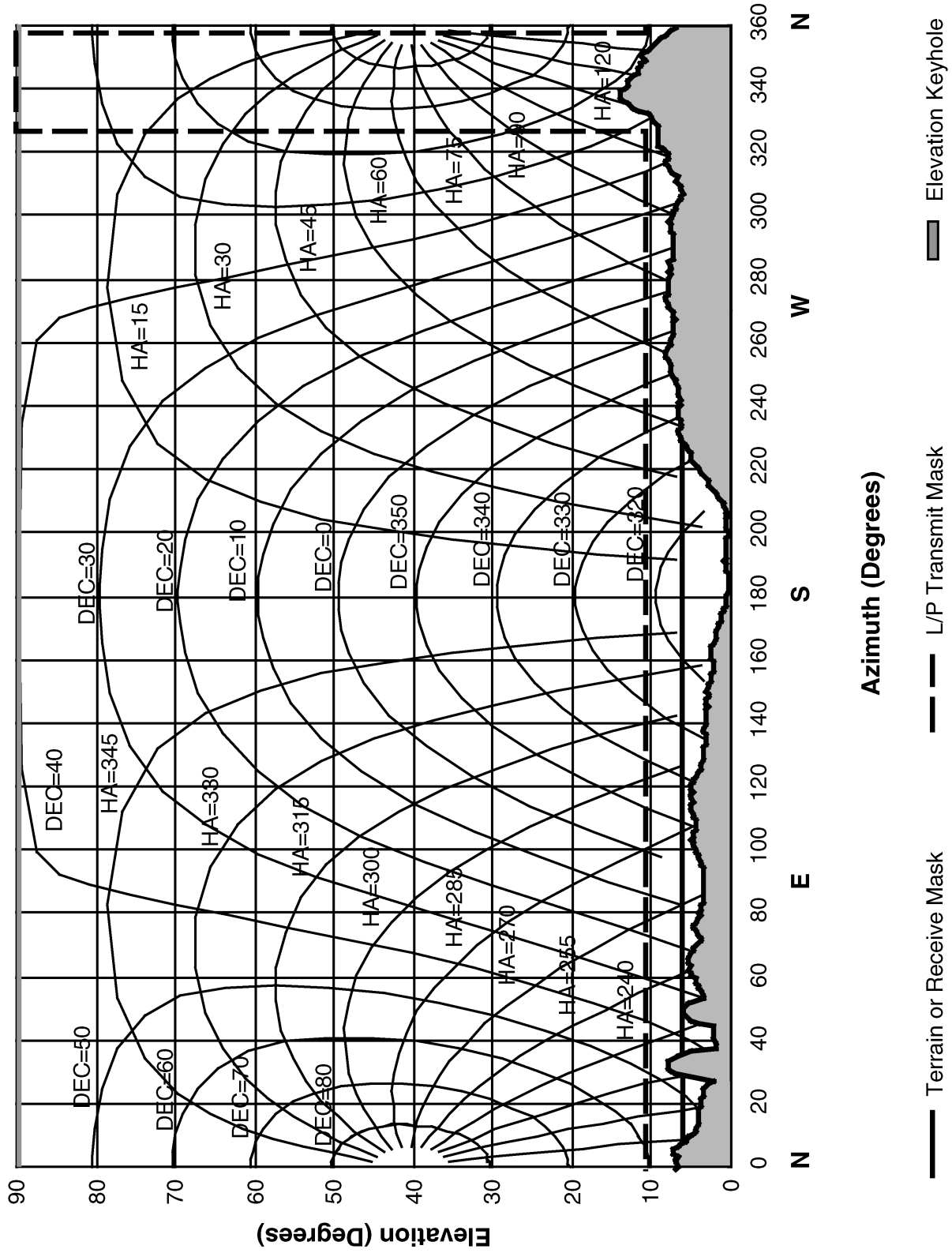
Figure 29. DSS 65 Hour-Angle and Declination Profiles and Horizon Mask
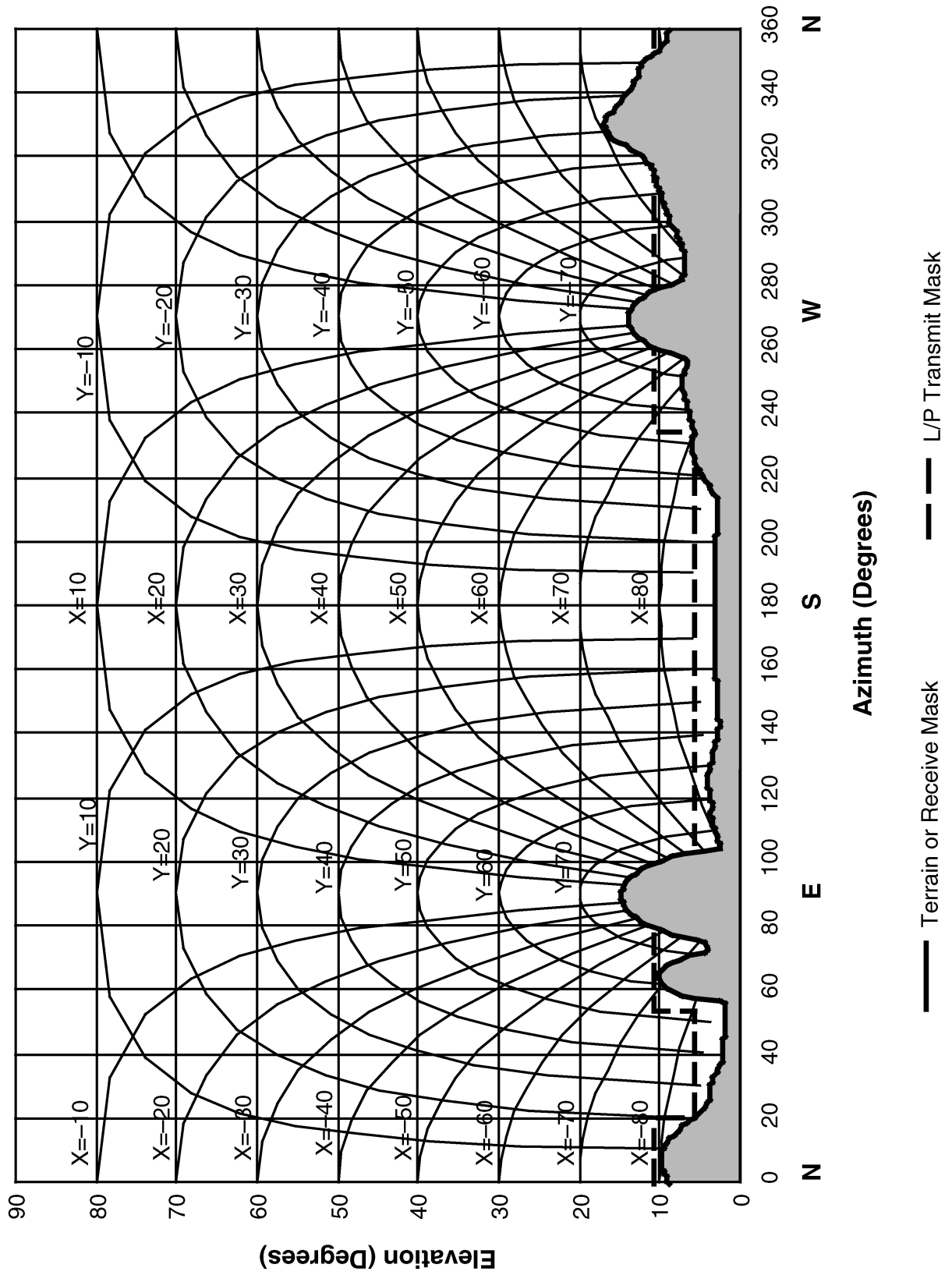
Figure 30. DSS 66 X-Y Profiles and Horizon Mask

Appendix A
References

1   C. Boucher, Z. Altamimi, and L. Duhem, *Results and analysis of the ITRF93*, IERS Technical Note 18, Observatoire de Paris, October 1994

2   B. R. Bowring, "The accuracy of geodetic latitude and height equations," *Survey Review*, 28, pp. 202-206, 1985.

303
Media Calibration

Effective November 30, 2000

Document Owner:

Approved by:

P. H. Richter,
Senior Engineer

Date 12/11/00

A. Kwok
Tracking and Navigation Service
Systems Development Engineer

Date 12/13/00

Released by:

[Signature on file at TMOD Library]

TMOD Document Release   Date

Change Log

Rev	Issue Date	Paragraphs Affected	Change Summary
Initial	1/15/2001	All	All

Note to Readers

There are two sets of document histories in the 810-005 document, and these histories are reflected in the header at the top of the page. First, the entire document is periodically released as a revision when major changes affect a majority of the modules. For example, this module is part of 810-005, Revision E. Second, the individual modules also change, starting as an initial issue that has no revision letter. When a module is changed, a change letter is appended to the module number on the second line of the header and a summary of the changes is entered in the module's change log.

This module supersedes module MED-10 in 810-005, Rev. D.

Contents

Tables

1　　　　*Introduction*

1.1　　　*Purpose*

This module describes the capabilities of the equipment used by the Deep Space Network (DSN) to obtain data from which correction factors can be determined for media effects that limit navigational accuracy. The data are forwarded from each Deep Space Communications Complex (DSCC) to the Network Operations Control Center (NOCC) where they are processed and archived.

1.2　　　*Scope*

The functional performance and data characteristics of the Deep Space Station (DSS) Media Calibration Subsystem (DMD) are described. The DMD is responsible for obtaining Global Positioning System (GPS) and ground weather data for the NOCC Tracking Subsystem (NTK) and Navigation Subsystem (NAV).

2　　　　*General Information*

The DMD provides two types of data:

- GPS data consisting of L-band carrier phase and group delay of GPS satellite signals, in addition to ephemeris and almanac data for the GPS satellites.

- Weather data, consisting of temperature, barometric pressure, relative humidity, precipitation rate, total precipitation, wind speed, and wind direction.

2.1　　　*Global Positioning System Data*

The Global Positioning System GPS Operational Constellation consists of at least 24 satellites that orbit the earth with a 12 sidereal-hour period. There are often more than 24 as new satellites are launched to replace the older ones. The orbit is such that the satellites repeat the same track and configuration over any point approximately each 24 hours (4 minutes earlier each day). There are six orbital planes (with nominally four satellites in each), equally spaced (60 degrees apart), and inclined at about fifty-five degrees with respect to the equatorial plane. This constellation provides the user with between five and eight satellites visible from any point on the Earth. A minimum of four satellite signals must be received to estimate the four unknowns of position in three dimensions and time.

The DSCC GPS Receiver/Processor Assembly (GRA), which is part of the DMD, makes use of the GPS data to provide carrier phase and group delay for the GPS signals.

These data may then be used to characterize the Earth's ionosphere and troposphere along the line of sight from a given satellite to the DSCC.

2.1.1 GPS Signal Structure

The GPS satellite signals are complex in structure, with each L-band frequency being binary biphase-modulated with two pseudo-random noise codes, the Coarse Acquisition (C/A) and Precision (P) codes, and a navigation message.

The complete signal broadcast by a satellite may be represented as:

$$s(t) = \left[A_C C(t)D(t)\sin(2\pi f_1 t) + A_P P(t)D(t)\cos(2\pi f_1 t) \right] + \left[A_P P(t)D(t)\cos(2\pi f_2 t) \right] \tag{1}$$

where the first square bracket is the L1 signal at frequency f_1, and the second square bracket is the L2 signal at frequency f_2. The terms appearing above have the following definitions:

A_c and A_p = the constant amplitudes of the Coarse Acquisition (C/A) and Precision (P) codes

$C(t)$ = the C/A-code modulation (= ±1)

$P(t)$ = the P-code modulation (= ±1)

$D(t)$ = the navigation message modulation (= ±1)

f_1 = $154 f_0$ = 1575.42 MHz

f_2 = $120 f_0$ = 1227.60 MHz.

The $C(t)$, $P(t)$, and $D(t)$ modulations are all synchronized to the fundamental clock frequency, f_0, such that they have the following frequencies:

f_0 = 10.23 MHz (Note 1)

$C(t)$ = $f_0/10$ = 1.023 Mbps

$P(t)$ = f_0 = 10.23 Mbps

$D(t)$ = $f_0/204600$ = 50 bps.

Note (1): To partially compensate for general and special relativistic effects on the satellite clock (gravitational red shift and time dilation), the actual value of f_0 is 10.23 MHz – 4.55 mHz.

The complete C/A code contains 1023 cycles (or "chips"), has a total period of 1.0 ms, and is different for each satellite.

The P-code is more complicated and consists of two code segments (X1 and X2), which differ in length by 37 chips. These are added modulo 2 and timed in such a way that

exactly 403,200 X1 code segments correspond to exactly one week, the period of the P-code. (The P-code actually has a total period of 37 weeks, with each satellite using only a single one-week segment of the total.) The duration of the X1 code segment is thus 1.5 seconds and contains exactly 15,345,000 chips at 10.23 Mbps. As is the case with the C/A code, the P-code is different for each satellite.

The navigation message also has a complex structure, with a total period of 12.5 minutes (one master frame) and is divided into frames, subframes, words, and bits. The first three subframes (lasting 6 seconds each) repeat every 30 seconds, while the last two subframes are different in each of 25 consecutive frames (pages), after which the entire message repeats.

2.1.2 *GPS Receiver/Processor Assembly (GRA)*

The GRA provides the following functional capabilities:

1) Automatically acquire and track the L1 and L2 GPS signals for specified satellites, usually all of those transiting

2) Extract and store GPS almanac and ephemeris data from the navigation message

3) Measure the differential P-code group delay between the L1 and L2 GPS signals

4) Measure the differential carrier phase between the L1 and L2 GPS signals.

The almanac data, contained in subframe 5 of the GPS navigation message, consist of approximate ephemeris data for all satellites and are used by the GRA for signal acquisition.

The ephemeris data for a specified satellite (subframes 2 and 3) provide a complete description of the orbit. When the data are combined with measured signal delays, the local position and atmospheric path that the signal has traversed can be determined.

Since the Department of Defense, which controls the GPS signal content, may elect at any time to encrypt the P-code (resulting in what is termed an anti-spoofing (A/S) mode of operation in which the encrypted, or Y-code, is unavailable to civilian users of the system) the GRA operates in two distinct modes to determine the differential group and phase delays of the satellite signals.

In the normal, coded mode, the known P-code is used to determine the carrier phase and group delay of each signal (L1 and L2) separately. The computed differences may then be used to characterize the propagation medium over the path of the signals. This provides the most precise determination due to the length of the P-code.

In the codeless mode, advantage is taken of the fact that the same unknown Y-code is transmitted on both the L1 and L2 channels with an unknown delay. The product of the two signals is formed and the differential group and phase delays are determined by cross-correlation. This method results in a somewhat reduced accuracy.

The GRA simultaneously receives and processes the signals from up to eight satellites selected to provide the longest unbroken tracks at any given time. In addition to the data described above, the system provides various status and health data on the signals being processed. Tables 1 through 4 list the GPS parameters measured, their ranges and accuracy, and the sample intervals provided.

2.1.3   *Relation of Phase and Group Delay to Atmospheric Properties*

The Earth's atmosphere may conveniently be divided into three regions according to the effects produced on the propagation of electromagnetic radiation:

(1)   troposphere, stratosphere, and lower part of mesophere — region between the Earth's surface and about 60 km altitude consisting of neutral (unionized) gases

(2)   ionosphere — region from about 60 km to between ~500 and 2000 km, depending on the extent of extraterrestrial ionizing radiation, consisting of partially ionized gases

(3)   plasmasphere — ionized region extending from ~2000 km to about four Earth radii (26,000 km), where it blends into the solar wind of the Earth's magnetosphere

At the frequencies in which the DSN operates, tropospheric dispersion may be neglected and the refractivity represented by a dry and a wet component whose approximate total zenith phase and group delays are:

$$\Delta t_D \quad \sim \quad 7.6 \text{ ns},$$

$$\Delta t_W \quad \sim \quad 0.3 \text{ ns} - 1.4 \text{ ns}.$$

The first varies linearly with pressure at the Earth's surface; the second increases as the tropospheric moisture content increases.

Since tropospheric dispersion is negligible at L-band, these delays cancel when differential delays are computed or measured between f_1 and f_2.

In the ionized portion of the Earth's atmosphere, the medium displays anomalous dispersion at microwave frequencies. This causes the phase velocity to exceed, and the group velocity to be less than, the speed of light in a vacuum, c. Specifically, to a good approximation at L-band:

$$\frac{v}{c} = 1 + \frac{x}{2} \tag{2}$$

$$\frac{v_g}{c} = 1 - \frac{x}{2}. \tag{3}$$

Table 1. GPS Metric Data, Code Mode

Parameter	Units (1)	Approximate Decimal Range
Delay Calibration	2^{-7} ns	±255 ns
Output Interval	sec	1–300 s
L1-C/A Doppler Phase	2^{-16} cycles	±2.1 x 10^9 cycles
L1-C/A Doppler Phase Noise	2^{-16} cycles	0–1 cycle
L1-P Doppler Phase	2^{-16} cycles	±2.1 x 10^9 cycles
L1-P Doppler Phase Noise	2^{-16} cycles	0–1 cycle
L2-P Doppler Phase	2^{-16} cycles	±2.1 x 10^9 cycles
L2-P Doppler Phase Noise	2^{-16} cycles	0–1 cycle
L1-C/A Group Delay	2^{-11} ns	±0.27 sec
L1-C/A Group Delay Noise	2^{-11} ns	0–32 ns
L1-P Group Delay	2^{-11} ns	±0.27 sec
L1-P Group Delay Noise	2^{-11} ns	0–32 ns
L2-P Group Delay	2^{-11} ns	±0.27 sec
L2-P Group Delay Noise	2^{-11} ns	0–32 ns
C/A SNR (1 sec)	2^{-4} volt/volt	0–4096
P1 SNR (1 sec)	2^{-4} volt/volt	0–4096
P2 SNR (1 sec)	2^{-4} volt/volt	0–4096
Receiver Clock Error	2^{-32} sec	±0.5 sec
L1-C/A Residual Phase	2^{-10} cycles	0–0.25 cycle

Note (1): Least significant bit transmitted by the GRA.

Table 2. GPS Metric Data, Non-Code Mode

Parameter	Units [1]	Approximate Decimal Range
Delay Calibration	2^{-7} ns	±255 ns
Output Interval	sec	1–300 sec
L1-C/A Doppler Phase	2^{-16} cycles	±2.1 x 10^9 cycles
L1-C/A Doppler Phase Noise	2^{-16} cycles	0–1 cycle
L1-L2 Doppler Phase	2^{-16} cycles	±2.1 x 10^9 cycles
L1-L2 Doppler Phase Noise	2^{-16} cycles	0–1 cycle
L1-C/A Group Delay	2^{-11} ns	±2.1 x 10^9 cycles
L1-C/A Group Delay Noise	2^{-11} ns	0–32 ns
P2-P1 Group Delay	2^{-9} ns	±1.1 s
P2-P1 Group Delay Noise	2^{-9} ns	0–128 ns
C/A SNR (1 s)	2^{-4} volt/volt	0–4096
P2-P1 SNR (1 s)	2^{-6} volt/volt	0–1024
Receiver Clock Error	2^{-32} s	±0.5 s
L1-C/A Residual Phase	2^{-10} cycles	0–0.25 cycle

Note (1): Least significant bit transmitted by the GRA.

Table 3. GPS Ephemeris Data

Parameter	Units (1)	Approximate Decimal Range
Sample Year (Modulo 100)	Year	0–99 yrs
Sample Day-of-Year	Days	0–366 days
Sample Hours	Hours	0–24 hrs
Sample Minutes	Minutes	0–60 minutes
Sample Seconds	seconds	0–60 s
GPS Week Number	N/A	
Satellite Number	N/A	
L2 Code Type/L2 Code On	N/A	
User Range Accuracy	N/A	
Issue of Data (Clock)	N/A	
Clock Data Reference Time (t_{oc})	2^4 s	$0–6.0 \times 10^5$ s
Time Correction Coefficient (a_{f2})	2^{-55} s/s^2	$\pm 3.6 \times 10^{-15}$ s/s^2
Time Correction Coefficient (a_{f1})	2^{-43}s/s	$\pm 3.7 \times 10^{-9}$ s/s
Time Correction Coefficient (a_{f0})	2^{-31}s	± 3.9 ms
Issue of Data (Ephemeris)	N/A	
Amplitude of Sine Harmonic Correction to the Orbit Radius (C_{rs})	2^{-5}m	± 1.0 km
Mean Motion Difference From Computed Values (Delta N)	2^{-43} semicir/s	$\pm 1.2 \times 10^{-5}$ mrad/s
Mean Anomaly at Reference Time (M_O)	2^{-31} semicir	± 180 deg
Amplitude of Cosine Harmonic Correction to the Argument of Latitude (C_{uc})	2^{-29} radians	$\pm 6.1 \times 10^{-2}$ mrad
Eccentricity (e)	2^{-33}	0–0.03
Amplitude of Sine Harmonic Correction to the Argument of Latitude (C_{us})	2^{-29} radians	$\pm 6.1 \times 10^{-2}$ mrad
Square Root of Semi-Major Axis ($A^{1/2}$)	2^{-19} m$^{1/2}$	0–8200 m$^{1/2}$
Ephemeris Reference Time (t_{0E})	2^4 s	$0–6.0 \times 10^5$ s

Note (1): Least significant bit transmitted by the GRA.

Table 3. GPS Ephemeris Data (Continued)

Parameter	Units (1)	Approximate Decimal Range
Amplitude of Cosine Harmonic Correction to Inclination (C_{ic})	2^{-29} radians	$\pm 6.1 \times 10^{-2}$ mrad
Right Ascension at Reference Time ($Omega_0$)	2^{-31} semicir	± 180 deg
Amplitude of Sine Harmonic Correction to Inclination (C_{is})	2^{-29} radians	$\pm 6.1 \times 10^{-2}$ mrad
Inclination at Reference Time (i_0)	2^{-31} semicir	± 180 deg
Amplitude of Cosine Harmonic Correction to the Orbit Radius (C_{rc})	2^{-5} m	± 1.0 km
Argument of Perigee (Omega)	2^{-31} semicir	± 180 deg
Right Ascension Rate (Omega DOT)	2^{-43} semicir/s	$\pm 3.0 \times 10^{-3}$ mrad/s
Issue of Data (Ephemeris)	N/A	
Inclination Angle Rate (IDOT)	2^{-43} semicir/s	$\pm 1.2 \times 10^{-5}$ mrad/s

Note (1): Least significant bit transmitted by the GRA.

Table 4. GPS Almanac Data

Parameter	Units [1]	Approximate Decimal Range
Sample Year (Modulo 100)	Year	0–99 yr.
Sample Day-of-Year	Days	0–366 days
Sample Hours	Hours	0–24 hrs
Sample Minutes	Minutes	0–60 minutes
Sample Seconds	s	0–60 s
GPS Week Number	N/A	
Satellite Number	N/A	
Data and Space Vehicle ID	N/A	
Eccentricity (e)	2^{-21}	0–0.03
Reference Time (t_{OA})	2^{+12} s	0–6.0×10^5 s
Delta Inclination (δ_i)	2^{-19} semicir	±11 deg
Right Ascension Rate (Omega DOT)	2^{-38} semicir/sec	$\pm 3.7 \times 10^{-4}$ mrad/s
Square Root of Semi-Major Axis ($A^{1/2}$)	2^{-11} $m^{1/2}$	0–8200 $m^{1/2}$
Right Ascension at Reference Time ($Omega_0$)	2^{-23} semicir	±180 deg
Argument of Perigee (Omega)	2^{-23} semicir	±180 deg
Mean Anomaly (M_0)	2^{-23} semicir	±180 deg
Correction Term (a_{f0})	2^{-20} s	±0.03 deg
Correction Term (a_{f1})	2^{-38} s	$\pm 1.2 \times 10^{-7}$ s/s

Note (1): Least significant bit transmitted by the GRA.

where:

$$v \qquad = \qquad \text{phase velocity} = \omega/k$$

$$v_g \qquad = \qquad \text{group velocity} = d\omega/dk$$

$$k \qquad = \qquad \textit{wave vector } (\lambda/2\pi)$$

$$x \qquad = \qquad (f_p/f)^2 \ll 1$$

$$f \qquad = \qquad \text{frequency of interest}$$

$$f_p \qquad = \qquad \text{plasma frequency} = (Ne^2/m\varepsilon_0)^{1/2}/2\pi$$

$$N \qquad = \qquad \text{electron density (electrons/m}^3)$$

$$e \qquad = \qquad \text{electronic charge}$$

$$m \qquad = \qquad \text{electronic mass}$$

$$\varepsilon_O \qquad = \qquad \text{permittivity of free space.}$$

In terms of the above, the phase (Δt) and group (Δt_g) delays at frequency f may be written:

$$\Delta t_g = -\Delta t = \left(\frac{1.345 \times 10^{-7}}{f^2} \right) \times \text{TEC} , \text{ s} \qquad (4)$$

where $\text{TEC} = \int N \, dl$ is the total electron content (TEC) along the propagation path (electrons/m^2).

The corresponding differential delays are given by:

$$\delta t_g = -\delta t = 1.345 \times 10^{-7} \left(\frac{1}{f_2^2} - \frac{1}{f_1^2} \right) \times \text{TEC} , \text{ s} \qquad (5)$$

where $\delta t_g = \Delta t_g (f_2) - \Delta t_g (f_1)$.

Since the TEC along the satellite line of sight may vary between $\sim 10^{16}$ and $4 \times 10^{18} \text{m}^{-2}$, the group and phase delays typically range between ~ 0.5 ns and 90 ns, and the differential delays between ~ 0.35 ns and 35 ns, although larger values are often observed during periods of high solar activity.

2.2 *Ground Weather Data*

The ground weather data are generated by instruments located near the Signal Processing Centers (SPC) at each DSCC. In particular, the wind speed and direction sensors are adjacent to the 34m HEF antennas.

All data are asampled once per second by the instruments, and the resulting data stream is transmitted to the Subsystem Control and Monitor Assembly (SCA) of the DMD. Here the data are packaged and transmitted to the NTK and NAV at regular intervals and stored for up to five days for later recall. Table 5 lists the weather parameters measured, their ranges and accuracy, and the interval of transmission to the NTK, NAV, and DMC.

Table 5 Weather Data Transmitted from the SCA

Parameter	Range	Accuracy	Transmission Interval	
			Default	Range
Temperature	−50 to +50°C	±0.1°C	60 s	10 s to 1 hr
Barometric Pressure	600 to 1100 mbar	1.0 mb	60 s	10 s to 1 hr
Relative Humidity[1]	0 to 100%	2%	60 s	10 s to 1 hr
Dew Point Temperature	−40 to 50°C	±0.5°C	60 s	10 s to 1 hr
Precipitation Rate	0 to 250 mm/hr	5%	60 s	10 s to 1 hr
Total Precipitation	>0 mm	5%	60 s	10 s to 1 hr
Wind Speed[2]	0 to 100 km/hr	±0.6 km/hr	60 s	10 s to 1 hr
Wind Direction[2]	0 to 360 deg	±3.6 deg	60 s	10 s to 1 hr

See notes on following page.

(1)　Relative humidity is calculated from the measured weather parameters according to the formula:

$$\text{RH} \quad = \quad 10^x \text{ percent,} \tag{6}$$

where:

$$x \quad = \quad 2 + 2300\,(1/T - 1/T_d),$$

$$T \quad = \quad \text{temperature in Kelvins}$$

$$T_d \quad = \quad \text{dew point temperature in Kelvins.}$$

(2)　Wind data are averaged over 10-s intervals by converting the polar velocity vector:

$$\mathbf{v_w} = S_w\hat{\mathbf{e}}(\theta) \tag{7}$$

where

$$S_w \quad = \quad \text{wind speed,}$$

$$\hat{\mathbf{e}}(\theta) \quad = \quad \text{wind direction unit vector,}$$

to rectangular form,

$$\mathbf{v_w} = S_x\hat{\mathbf{i}}(\theta) + S_y\hat{\mathbf{j}}(\theta) \tag{8}$$

and computing $\langle S_w \rangle$ and $\langle \theta \rangle$, where

$$\langle S_w \rangle^2 \quad = \quad \langle S_x \rangle^2 + \langle S_y \rangle^2,$$

$$\langle \theta \rangle \quad = \quad \tan^{-1}(\langle S_x \rangle / \langle S_y \rangle),$$

$$S_x \quad = \quad S_w \cos\theta,$$

$$S_y \quad = \quad S_w \sin\theta.$$

901
Handbook Glossary

Effective November 30, 2000

Document Owner::

Approved by:

R. W. Sniffin   Date

12/11/00

K. R. Kimball   Date
Manager, DSMS Implementation
Engineering

14 DEC 00

Released by:

[Signature on file at TMOD Library]

TMOD Document Release   Date

Change Log

Rev	Issue Date	Affected Paragraphs	Change Summary
Initial	1/15/2001	All	All

Note to Readers

There are two sets of document histories in the 810-005 document, and these histories are reflected in the header at the top of the page. First, the entire document is periodically released as a revision when major changes affect a majority of the modules. For example, this module is part of 810-005, Revision E. Second, the individual modules also change, starting as an initial issue that has no revision letter. When a module is changed, a change letter is appended to the module number on the second line of the header and a summary of the changes is entered in the module's change log.

This module supersedes Appendix A in 810-005, Rev. D.

Contents

1   Introduction

1.1   Purpose

The purpose of this document is to present a useful glossary of commonly used terms, abbreviations, and acronyms that are current and applicable to the Deep Space Network (DSN) and the Telecommunications and Mission Operations Directorate (TMOD) of the Jet Propulsion Laboratory.

1.2   Scope

This scope of this document is limited to providing terms, abbreviations, and acronyms that are used within Document 810-005 and especially those that may be different from usage in other organizations.

Terms, abbreviations, and acronyms are included in this document if they meet any of the following criteria:

- used within the DSN or TMOD but with a meaning that may be unique to the DSN or TMOD,

- used within 810-005 in place of equivalent terms, abbreviations, and acronyms that may be used elsewhere, or

- commonly used in the field of telecommunications engineering but not necessarily known to all users of 810-005.

1.3   Revisions

This glossary will be periodically revised with changes, improvements, or additions. Usually, these revisions will be coincident with the publication of new or revised 810-005 modules that contain new or revised terminology.

1.4   Definitions

The following paragraphs define the types of items that appear in this glossary and give general rules for their formation.

1.4.1   Terms

A *term* is any word or expression that has a precise meaning in a particular field, in this case, telecommunications engineering.

1.4.2   Abbreviations

An *abbreviation* is a shortened or contracted form of a word or phrase. In a strict sense, the letters are individually pronounced (for example, rpm or DSN) or the reader might visualize and pronounce the complete form of the word (for example, "assembly" for "assy" or "telemetry" for "TLM").

1.4.3   Acronyms

An *acronym* is a pronounceable abbreviation formed by one of two methods: (1) combining the first syllables of the key words (for example, Caltech or FORTRAN) or (2) combining the first letter and other letters, as required, from the name or key words of an organization, project, or piece of equipment (for example, AMMOS or LAN).

1.5   Controlling Documents

The terms, abbreviations, and acronyms contained in this document are intended to be consistant with those defined in JPL internal publication, DSMS Requirements and Design — DSMS Terms and Abbreviations; DSMS Document 820-062 which serves as the controlling document for this module

2   *Abbreviations and Terms*

Abbreviation or Term	*Definition*
A	
A-D	analog-to-digital
A/S	anti-spoofing mode of operation (Global Positioning System) in which the encrypted, or Y-code, is unavailable to civilian users of the system
AFC	automatic frequency control
AGC	automatic gain control
alidade	The rotating but non-tilting portion of the DSN azimuth-elevation antennas.
AM	amplitude modulation
AMP	amplifier
AMMOS	Advanced Multimission Operations System
ARC	ambiguity resolving code
ASM	attached synchronization marker
atm	atmospheric
az	azimuth
AZ-EL	azimuth-elevation
B	
B2MCD	Block II Maximum Likelihood Convolutional Decoder
B3MCD	Block III Maximum Likelihood Convolutional Decoder
B/W	bandwidth
BER	bit error rate
BET_L	lock bit error tolerance
BET_S	search bit error tolerance
Boltzmann constant	-198.6 dBW/(Hz $\cdot$ K)
BPSK	binary phase shift keying
BVR	Block V Receiver (part of DTT Subsystem)

Abbreviation or Term	Definition
BWG	Beam Waveguide (antenna or subnet)

C

c	speed of light, 299,792.5 km/s
Category A	missions within 2 million km of Earth
Category B	missions at distances greater than 2 million km from Earth
C/A	Coarse Acquisition (GPS code)
CCSDS	Consultative Committee for Space Data Systems
CCW	counter-clockwise
CD	cumulative distribution
CDSCC	Canberra (Australia) Deep Space Communications Complex
CONSCAN	conical scanning
CPA	Command Processor Assembly
cryo	cryogenic
CSS	Channel-Select Synthesizer
CV	connection vector
CW	clockwise

D

D/C	downconverter
D/L	downlink
dB	decibel(s)
dBc	decibel(s) with respect to carrier
dBi	decibel(s) with respect to isotropic
dBm	decibel(s) with respect to one milliwatt
DCC	Downlink Channel Controller
DCPC	DTT Controller Processing Cabinet
DDC	Digital Downconverter
dec	declination
deg	degree(s)
DIG	digitizer (assembly)

Abbreviation or Term	**Definition**
DLT	digital linear tape
DMC	DSS Monitor and Control
DMD	DSS Media Calibration Subsystem
DN, dn	down
DRVID	differenced range versus integrated Doppler
DSCC	Deep Space Communications Complex
DSN	Deep Space Network
DSMS	Deep Space Mission System
DSS	Deep Space Station
DSS 14	70-m antenna at Goldstone DSCC
DSS 15	34-m HEF antenna at Goldstone DSCC
DSS 16	26-m antenna at Goldstone DSCC
DSS 23	11-m antenna at Goldstone DSCC
DSS 24	34-m BWG antenna at Goldstone DSCC
DSS 25	34-m BWG antenna at Goldstone DSCC
DSS 26	34-m BWG antenna at Goldstone DSCC
DSS 27	34-m HSB antenna at Goldstone DSCC
DSS 33	11-m antenna at Canberra DSCC
DSS 34	34-m BWG antenna at Canberra DSCC
DSS 43	34-m HEF antenna at Canberra DSCC
DSS 45	34-m HEF antenna at Canberra DSCC
DSS 46	26-m antenna at Canberra DSCC
DSS 63	34-m HEF antenna at Madrid DSCC
DSS 65	34-m HEF antenna at Madrid DSCC
DSS 66	26-m antenna at Madrid DSCC
DSS 53	11-m antenna at Madrid DSCC
DSS 54	34-m BWG antenna at Madrid DSCC
DTF	Development and Test Facility
DTK	DSS Tracking (Subsystem)
DTT	Downlink Telemetry and Tracking (Subsystem)

Abbreviation or Term	**Definition**

E

EIRP	effective isotropic radiated power
el, EL, elev	elevation
EOP	Earth Orientation Parameters (of the International Earth Rotation Service [IERS])

F

F/O	fiber optic
FCD	feedback concatenated decoding
FER	frame error rate
FET	field-effect transistor
FFT	fast Fourier transform
F M	frequency modulation
FOM	figure of merit
FSK	frequency-shift keyed
FTP	file transfer protocol
FTS	Frequency and Timing Subsystem

G

G/T	(antenna) gain divided by (operating system) temperature
GCF	Ground Communications Facility
GDSCC	Goldstone (California) Deep Space Communications Complex
GPS	Global Positioning System
GRA	GPS Receiver/Processor Assembly
GSFC	Goddard Space Flight Center

H

H/P	high power
HA	hour angle
HEF	high efficiency (antenna)

Abbreviation or Term	**Definition**
HEMT	high-electron-mobility (field-effect) transistor
HPBW	half-power beamwidth
HRM	high-rate (radio loss) model
HSB	High (angular-tracking) Speed Beam Waveguide (antenna)

I

I/F	interface
IDC	IF to Digital Converter
IERS	International Earth Rotation Service
IF	intermediate frequency
ITRF	IERS Terrestrial Reference Frame
ITU	International Telecommunications Union

J-K

JPL	Jet Propulsion Laboratory

L

L/P	low power
LCP	left (-hand) circular polarization
LNA	low noise amplifier
LRM	low-rate (radio loss) model
LSB	least significant bit

M

MAP	maximum *a posteriori* probability
MASER	microwave amplification by stimulated emission of radiation
max	maximum
MB	medium bandwidth
MCD	Maximum Likelihood Convolutional Decoder
MDA	Metric Data Assembly
MDSCC	Madrid (Spain) Deep Space Communications Complex

Abbreviation or Term	*Definition*
MED	minimum error detection
MFR	Multi-function Receiver
MGC	manual gain control
min	minimum
MOCC	Mission Operations Control Center
mod	modulation
MRT	major range tone

N

NA; N/A	not applicable
NASA	National Aeronautics and Space Administration
NAV	Navigation (Subsystem)
NB	narrowband, narrow bandwidth
NCO	numerically controlled oscillator
NMC	Network Monitor and Control (Subsystem)
NOAA	National Oceanic and Atmospheric Administration
NOCC	Network Operations Control Center
NRZ	non-return to zero
NRZ-L	non-return to zero, level
NRZ-M	non-return to zero, mark
NRZ-S	non-return to zero, space
NSP	Network Simplification Plan
NTIA	National Telecommunications and Information Administration
NTK	NOCC Tracking (Subsystem)

O

OQPSK	offset quadriphase-shift keying
OVLBI	Orbiting Very-long Baseline Interferometry

P

PCG	Phase Calibration Generator (part of FTS)

Abbreviation or Term	**Definition**
PCM	pulse-code modulation
PDF	probability density function
	portable document formet (type or extension of computer file)
PDRVID	pseudo-DRVID
PLL	phase-locked loop
P M	phase modulation
PN	pseudo-random noise
POCC	Project Operations Control Center
PSK	phase-shift keyed
PTS	Precision Telemetry Simulator

Q

QPSK	quadriphase-shift keying

R

R/T	real-time
RCP	right circular polarization
rev	revision
RF	radio frequency
RH	relative humidity
RID	RF to IF Downconverter
RMDC	Radio-Metric Data Conditioner
RMS; rms	root-mean-square
RNG	range
RNS	Reliable Network Service
RRP	Receiver Ranging Processor
RS	Reed-Solomon (code), radio science
RSR	Radio Science Receiver
rss, RSS	root-sum-square
RTLT	round-trip light time
RU	range unit

Abbreviation or Term	**Definition**

S

S/C	spacecraft
SCA	Subsystem Control and Monitor Assembly
SEP	Sun-Earth-Probe (angle)
SFU	solar flux units (one SFU = 1×10^{-22} W/m^2/Hz)
SNR	signal-to-noise ratio
SPC	Signal Processing Center
SPD	S-Band Polarization Dipled (feedcone)
SRA	Sequential Ranging Assembly
stowed	With respect to an antenna, aimed near zenith for protection from the wind.
sub, subcarr	subcarrier
SYM	symbol
SYS	system

T

TBD	to be determined
TDDS	Tracking and Data Delivery Sustem
TDRSS	Tracking and Data Relay Satellite System
TEC	total vertical electron content
TLM	telemetry
TMOD	Traking and Mission Operations Directorate
T_{OP}	T sub OP (operating system temperature)
TXR	transmitter or Transmitter Subsystem

U

U/L	uplink
ULNA	ultra low-noise amplifier
UPA	Uplink Processor Assembly
URA	Uplink Ranging Assembly

Abbreviation or Term	**Definition**
USO	Ultra-Stable Oscillator
UTC	Universal Time, Coordinated
V	vacuum
VCO	voltage controlled oscillator
VLBI	very-long baseline interferometry
W	
W/B, WB	wideband
WD	waveform distortion
X	
X-EL	cross-elevation
XMIT	transmit
XRO	X-band receive only (feedcone)
XTR	X-band transmit-receive (feedcone)
Y	
yr	year
Z	
ZDD	Zero-delay Device
ZEN	zenith